Microfluidic devices with integrated biosensors for biomedical applications

César Alejandro Parra Cabrera

Universitat de Barcelona

Tesis doctoral

Microfluidic devices with integrated biosensors for biomedical applications

Memoria presentada por
César Alejandro Parra Cabrera

Para optar por el grado de **Doctor en Biomedicina**

Universitat de Barcelona
Departament d'Electrònica

Programa de doctorado de Biomedicina
2010-2014

Tesis doctoral dirigida por: **Dr.Antoni Homs Corbera**
Prof. Josep Samitier Martí

Barcelona, 2014

Not in knowledge is happiness, but in the acquisition of knowledge!

Edgar Allan Poe

The Power of Words, 1845

Why then do you try to "enlarge" your mind? Subtilize it.

Herman Melville

Moby Dick, 1851

…for strange effects and extraordinary combinations we must go to life itself.

Sir Arthur Conan Doyle

The adventures of Sherlock Holmes, 1892

A MI FAMILIA

Agradecimientos

"No llores porque ya se terminó, sonríe porque sucedió" (Gabriel García Márquez)…Seis años han pasado desde que me embarqué en está aventura y muchas cosas han pasado en este periodo de tiempo. He pasado por momentos inolvidables y algunos pasajes amargos, afortunadamente ha salido adelante gracias al apoyo y compañía de mucha gente. Quisiera empezar por agradecer a mis padres, César y Lucero, por su ayuda incondicional, por escucharme y aconsejarme en los momentos más difíciles y por estar presentes durante mis alegrías, sin ustedes este trabajo no hubiera sido posible ya que ustedes construyeron los cimientos de mi enseñanza. De igual manera, quiero agradecer a mis hermanos, Jorge y Juan Carlos, porque a pesar de la distancia siempre me acompañan y están presentes en todos los momentos importantes de mi vida, siempre permaneceremos unidos "manazos". También quiero agradecer a Carla por ser el apoyo incondicional a mi hermano, en especial cuando su hermano mayor no ha podido estar presente. Y que decir de las "pequeñas princesas", Renata y Viry, cuya compañía siempre me alegra y me llena de vida, sus sonrisas y ocurrencias hacen que las dificultades parezcan tonterías, y sus locuras siempre alegran a su tío.

Me siento afortunado de haber conocido un grupo de gente a la cual puedo llamar mi nueva familia, ellos me han brindado su amistad, me han aconsejado en todos los ámbitos de mi vida y sin ellos este viaje no hubiera sido igual, así que muchas gracias: Roberto, Sabrina, Oriol, Juan Pablo, Tere, Félix, Alida, Annamaria, Gonzalo y Barbara. De igual manera quiero a mis colegas de la UBB, con los que me he divertido en viajes y fiestas: Irina, Roland, Noelia, Victor, Juanjo, Gaby, Rocio y Tomás.

De manera especial quiero agradecer a mis asesores, Dr. Antoni Homs y Prof. Josep Samitier, por compartir sus conocimientos, por su guía a lo largo del proyecto, por su paciencia y por revivir el doctorado conmigo. Ha sido un camino largo y no siempre de fácil trayecto, sin embargo han confiado y creído en mi. Moltes gracies!

El trabajo día a día no hubiera sido igual sin los colegas del laboratorio, así que agradezco a la gente del grupo de Nanobioingeniería del IBEC, por sus recomendaciones y palabras amables. En particular, quiero agradecer a mis compañeros

y amigos del laboratorio 221 de electrónica: Anita, Juanma, Luis, Bea, Javi, Elia, Roberto, Cristina y Ziqiu, gracias por su ayuda, sus consejos, y los momentos de ocio y diversión que han hecho muy agradable el trabajo diario.

Also, I want to thank to the people of KTH, thanks for sharing your knowledge, experience and also thanks for the good times, it was a short and a bit cold time, however unforgettable. So thank you: Tommy, Wouter, Fredrik, Carlos, Fritzi, Gabriel, Simon, Floria, Chianty, Laila and Hithesh.

Finalmente quiero agradecer de manera especial a la Universitat de Barcelona (UB), al Ministerio de Asuntos Exteriores y de Cooperación (MAEC), a la Agencia Española de Cooperación Internacional para el Desarrollo (ACID), al Instituto de Bioingeniería de Cataluña (IBEC), al Parc Científic de Barcelona por todo el apoyo recibido para la realización de este trabajo.

General Index

General Index ..... **I**

List of Figures ..... **V**

Abbreviations ..... **XI**

CHAPTER 1 General Introduction **1**

1.1. Introduction **1**
1.2 State-of-the art and Rationale **9**
1.3 Objectives **13**
1.4 Dissertation Outline **14**

CHAPTER 2 Design, fabrication and fluid dynamics of the microfluidic devices. **21**

2.1. Introduction **21**
2.1.1 Microfabrication technologies for microfluidics. Theoretical background... 22
2.1.1.1 Fabrication materials *22*
2.1.1.2 Replication technologies *23*
2.1.1.3 Microelectrodes fabrication *26*
2.1.1.4 Bonding techniques *26*
2.1.2 The physics of microfluidics. Theoretical background. 27
2.1.3 Fluid dynamics 30
2.2. Materials and methods **31**
2.2.1 Fabrication of the microfluidic devices 32
2.2.1.1 Microchannels fabrication *32*
2.2.1.2 Biosensor Fabrication *35*
2.2.1.3 Lab-on-a-Chip Bonding *35*
2.3 Results and discussions **36**
2.3.1 Microfluidic devices design 36
2.3.2 Characterization of the dimensions of the fabricated devices 43
2.3.3 Fluid dynamics 46
2.4 Conclusions **49**
2.5 References **50**

CHAPTER 3 In situ selective functionalization of biosensors: Determination of optimum functionalization times **53**

3.1 Introduction **53**
3.1.1 Introduction 53
3.1.1.1 Classification by recognition principle *53*
3.1.1.2 Classification by transduction *54*
3.1.2 Surface functionalization 56
3.1.2.1 Adsorption *57*
3.1.2.2 Entrapment *57*
3.1.2.3 Cross-linking *57*
3.1. 2.4 Covalent bonding *57*
3.1.3 Chapter aim 57
3.2 Materials and methods **58**

3.2.1 Protocol for the determination of optimum functionalization times through impedance ... 58
3.2.2 Verification protocol for selective functionalization ... 59
3.2.3 Differential voltage detection protocol ... 60
3.3 Results and discussions ... 61
3.3.1 Protocol for the determination of optimum functionalization times through impedance ... 61
3.3.2 Verification protocol for selective functionalization ... 63
3.3.2.1 Optical analysis ... 63
3.3.2.2 Impedance analysis ... 64
3.3.3 Detection protocol: Optical analysis and differential voltage analysis ... 66
3.3.3.1 Optical analysis ... 66
3.3.3.2 Differential detection ... 67
3.4 Conclusions ... 69
3.5 References ... 69

CHAPTER 4 Electrochemical detection of biomarkers: proof-of-concept ... 71
4.1 Introduction ... 71
4.1.1 Electrochemical biosensors ... 71
4.1.1.1 Potentiometric biosensors ... 71
4.1.1.2 Amperometric biosensors ... 72
4.1.1.3 Impedimetric biosensors ... 72
4.1.1.4 Electrical double layer ... 73
4.1.2 Chapter aim ... 74
4.2 Materials and methods ... 75
4.2.1 Protocol for the selective functionalization of the biosensors ... 75
4.2.2 Voltage measurements ... 76
4.2.3 Impedance measurements ... 77
4.3 Results and discussions ... 80
4.3.1 Differential voltage detection protocol ... 80
4.3.2 Differential impedance detection protocol ... 81
4.4 Conclusions ... 86
4.5 References ... 86

CHAPTER 5 Application of LOC to single biomarker detection: prostate-specific antigen ... 89
5.1 Introduction ... 89
5.1.1 Cancer ... 89
5.1.2 Prostate cancer ... 90
5.1.3 Prostate-specific antigen biosensors ... 93
5.2 Materials and methods ... 93
5.3 Results and discussions ... 96
5.3.1 Determination of the blocking protocol to improve the voltage output ... 96
5.3.2 Determination of the adjustability in the detection range for PSA ... 98
5.3.3 Characterization of PSA ... 104
5.4 Conclusions ... 109
5.5 References ... 110

CHAPTER 6 Application of LOC to multiple biomarkers detection: prostate-specific antigen and Spondin-2 113
6.1 Introduction 113
6.1.1 Prostate cancer biomarkers 114
6.2 Materials and methods 116
6.3 Results and discussions 121
6.3.1 Determination of the adjustability in the detection range for Spondin-2 121
6.3.2 Detection of Spondin-2 124
6.4 Conclusions 128
6.5 References 129

General conclusions and discussion 131

Future work 134

Annex 1 Characterization of impedance spectroscope (HF2TA) 135
Annex 2 Development of custom made software 137
Annex 3 Surface characterizations of OSTE polymer measurements 149
Materials and methods 149
Results and discussions 150
Conclusions 155
References 156

List of Figures

Fig. 1. 1 The smallest movie. Today we are able to handle and image atoms. Feynman's once visionary view came to reality less than half a century later. 1
Fig. 1. 2 The first microfluidic device, a gas chromatographic analyzer developed on 1975 [5]. 2
Fig. 1. 3 Microfluidic systems. a) Gold electrode sensing, b) Liver cells patterns, c) Gradient generator, d) Cells in tiny wells. *Albert Folch's Lab.* 3
Fig. 1. 4 A complete lab-on-chip for DNA analyses [17]. 4
Fig. 1. 5 Microfluidic drug delivery systems. a) Delivery by diffusion [29], b) Delivery by pressure [32] and c) Electrokinetic forces [31]. 5
Fig. 1. 6 Microfluidic systems for cellomics [42]. 6
Fig. 1. 7 Commercially available biosensor with multiple cartridge analysis (http://www.abbottpointofcare.com/). 7
Fig. 1. 8 ELISA test. a) The plate is coated with a capture antigen; b) sample is added, and any antibody present binds to antigen; c) enzyme-linked secondary antibody is added, and binds to detecting antibody; d) substrate is added, and e) is converted by enzyme to detectable form. 10

Fig. 2. 1 Positive and negative photoresists. The positive photoresists is more soluble when is irradiated while the negative resist is less soluble. 23
Fig. 2. 2 Micromilling machine [23] and medical staple mold [24] from MAKINO, one example of micromachining technologies used for the fabrication of masters. 24
Fig. 2. 3 LIGA process. A piece of PMMA is exposed to X-ray, then with electroplating the master is created [26]. 24
Fig. 2. 4 Injection molding process. Polymer beads are heated with a screw and then push into the mold cavity [27] 25
Fig. 2. 5 Soft lithography process. A master is fabricated with a photoresist, and then PDMS is poured on the master. And once cured is peel off [29] 26
Fig. 2. 6 Microelectrode fabrication. a) Evaporation of metal [30] and b) sputtering[31] 26
Fig. 2. 7 Lamination with a PET foil. The polymer is heated and pressed against the microchannel surface [33] 27
Fig. 2. 8 Plasma bonding technique. a) Surface of substrate b) Oxygen plasma applied to the substrate surface, c) The plasma generates hydroxyl groups, d) A second substrate, also treated with plasma, can be bonded 27
Fig. 2. 9 a) Fully developed parabolic laminar flow, b) diagram of a rectangular pipe with radius element *R* in fully develop laminar flow. 29
Fig. 2. 10 a) Illustration of flow focusing and b) Analogous circuit used to design and analyze the focusing network of a). 31
Fig. 2. 11 a) Chemical baths, b) The substrates are placed on the plasma cleaner, c) Vacuum is applied to the plasma cleaner, d) The plasma is activated. 33
Fig. 2. 12 a) Pre-bake of the sample, b-c) Spinning of the photoresist on the substrate, d-e) Exposure of the samples 34
Fig. 2. 13 a) The pre-polymeric solution is weighted and mixed, b) The mixed solution is placed on vacuum to eliminate bubbles, c) The PDMS is poured over the masters, d) Vacuum is applied to the masters, e) The polymer is cured by temperature 34
Fig. 2. 14 a) The photoresist is exposed, b) The un-polymerized photoresist is rinsed, c) Metal deposition over the samples, d) Lift-off to reveal the microelectrodes 35
Fig. 2. 15 a) The microchannels and microelectrodes are aligned, b) The LOC is irreversible bonded, c) Cables are welded to each pad 36
Fig. 2. 16 Optical microscope images showing the effect of the hydrodynamic focalization [19]. 37

Fig. 2. 17 Layout of the proposed microfluidic device. We proposed a device with two microchannels with different microfluidic resistances (1x and 0.3x) to functionalize only a third of the channel. We also propose a set of microelectrodes and connect them in differential mode and use them as biosensors..... 37
Fig. 2. 18 Reynolds number for our devices at 20ºC and 40ºC. The black line represents the transition between laminar and transitional flow. The green line represents transition to turbulent flow..... 40
Fig. 2. 19 Mixing length as a function of input flow. The doted black line represents the total microchannel length of our device..... 41
Fig. 2. 20 Diffusion length for biotin solutions. Three critical zones are defined, the starting of the channel (dotted cyan line), the beginning of the smaller electrodes (dotted magenta line) and the end of the electrodes (dotted black line) 42
Fig. 2. 21 a) Microfluidic device proposed for hydrodynamic focusing and selective functionalization for single detection, b) Microfluidic device proposed for the detection of multiple analytes with hydrodynamic focusing..... 43
Fig. 2. 22 a-c) Characterization of the dimensions of the SU-8 masters with a profilometer, d-f) Characterization of the dimensions of the replicated microchannels with a profilometer. The blue line corresponds to the main channel and the green line corresponds to the lateral channel..... 44
Fig. 2. 23 Characterization of the dimensions of the SU-8 masters using an interferometer. 45
Fig. 2. 24 Characterization of the dimensions of the PDMS replicas using an interferometer..... 45
Fig. 2. 25 Microscopic images of the microelectrodes. All the pathways were checked to avoid short circuits 46
Fig. 2. 26 Simulation of a co-flow. The main input was kept constant while the lateral input flow was increased. The simulations were performed with COMSOL Multiphysics..... 47
Fig. 2. 27 Experimental analysis of the fluid dynamics. A inked solution was flowed through the lateral channel, the flows used were the same as the ones used for simulations 48
Fig. 2. 28 Fluid dynamics. Experimental (red dots), calculated (blue line) and simulated (green line). The main flow was kept constant while increasing the lateral flow 48
Fig. 2. 29 Simulation of the fluid dynamics for the second device. The red and green fluids represent the functionalization solutions. Different cases were studied a) Flow on the main channel and first lateral channel, b) Flow on the three channels with similar flow in the lateral channels, c) Flow on the three channels but different flow on the lateral channels, d) Flow only on the main channel..... 49

Fig. 3. 1 Schematic representation of a biosensor. The left column show the biosensor used for the development of this work..... 53
Fig. 3. 2 Scheme of a productive biosensor related to a catalytic reaction [3] and non-productive biosensor usually antibody-antigen or ligand-receptor interactions [4] 54
Fig. 3. 3 Biosensor classification by transduction..... 55
Fig. 3. 4 Protocol for the determination of functionalization times. a) Biotin-thiol solution flowing through the channel, b) Streptavidin solution functionalizing the biosensors. The measurements were made every 15 minutes. The images are represented in false color..... 59
Fig. 3. 5 Protocol for selective functionalization. a) Rinsing with PBS, b) First selective functionalization with biotin-thiol solution, c) Addition of a layer of streptavidin, d) Detection of the selective functionalization with quantum dots. The images are represented in false color. 60
Fig. 3. 6 Protocol for the detection of Quantum dots. a) Rinsing with PBS, b) Selective blocking with a PEG-thiol solution, c) Electrode surface modified with biotin-thiol, d) Addition of a layer of streptavidin, e) Detection of biotinylated Quantum dots. The images are represented in false color. 61
Fig. 3. 7 Analysis of the impedance drift of biotin-thiol solution. The chart of the top is the impedance measured every 15 minutes during functionalization. The spectrogram was calculated to see the evolution of the impedance along time. 62
Fig. 3. 8 Analysis of the impedance drift of SAV-TRed solution. The chart of the top is the impedance measured every 15 minutes during functionalization. The spectrogram was calculated to see the evolution of the impedance along time. 63
Fig. 3. 9 Microscopic images of the fluorescent study. A solution of PBS (1) was used to form a co-flow and focalize the functionalization solutions over e_1: a) Functionalization with Biotin - Thiol (2), b)

Functionalization with SAV – TRed (3), c) Functionalization with Biotin - QD (4), d) The asterisk is placed inside the functionalized electrode (e_1), er is the biggest electrode and it shows no signs of functionalization. 64
Fig. 3. 10 a) Impedance between top and central electrodes ($|Ze_1:e_r|$) at frequencies of interest (100 - 10000 Hz) comparing different stages of the protocol, b) Differential comparison between protocol stages compared to previously functionalized e_1. 65
Fig. 3. 11 Percentage of the differential impedance between functionalized & non-functionalized electrode pairs ($|Ze_1:e_r|$-$|Ze_2:e_r|$) in respect to the previous functionalizing step. 66
Fig. 3. 12 Microscopic images of the fluorescent study at the end of the detection protocol. a) Functionalized electrode with NAV-OregonG b) Three electrodes comparison of a), c) Functionalized electrode with Biotin-QD, d) Three electrodes comparison of c). The dotted lines reflect the edges of the electrodes. Microscopic images of the fluorescent study at the end of the detection protocol. a) Functionalized electrode with NAV-OregonG b) Three electrodes comparison of a), c) Functionalized electrode with Biotin-QD, d) Three electrodes comparison of c). The dotted lines reflect the edges of the electrodes 67
Fig. 3. 13 a, b) Voltage evolution at 500 and 1000 Hz. Calculated fitting curve is shown in black. The voltage evolution at 1000 Hz showed a more stable signal 68

Fig. 4. 1 Schematic of an ISE [2]. 72
Fig. 4. 2 Working principle of an amperometric biosensor. 72
Fig. 4. 3 Scheme of an impedimetric biosensors. The analysis can be performed with different device. 73
Fig. 4. 4 The electrical double layer of a receptor modified electrode–electrolyte interface and its associated Randles equivalent circuit 73
Fig. 4. 5 Protocol for the detection of human serum albumin. a) Rinsing with PBS, b) Selective blocking with a PEG-thiol solution, c) Electrode surface modified with biotin-thiol, d) Addition of a layer of streptavidin, e) Deposition of a layer biotinylated antibody, f) Detection of HSA. The images are represented in false color. 76
Fig. 4. 6 Schematics of the voltage measurements. Connections of the microelectrodes with the impedance spectroscope. 77
Fig. 4. 7 Electrical schematics of the voltage measurements. Voltage and impedance equivalency of the microfluidic system. 77
Fig. 4. 8 Schematics of the impedance measurements. Connections of the microelectrodes with the measurement devices. The impedance spectroscope was used to measure voltage and the transimpedance amplifier to convert the current into voltage. 78
Fig. 4. 9 Electrical schematics of the voltage measurements. Voltage and impedance equivalency of the microfluidic system. 79
Fig. 4. 10 Schematics of the noise characterization set-up. To study the noise of the measurement devices two known resistances were connected as voltage divider. 79
Fig. 4. 11 Detection range for the human serum albumin protein. Voltage measurements. The factor α was calculated and a decrease in voltage was observed after the deposition of the protein. The factor α was obtained as proposed in Parra-Cabrera et al. 80
Fig. 4. 12 The noise produced by the measurement devices was characterized. The noise limits the LOD for the detection of a biomarker. 81
Fig. 4. 13 Detection range of the microfluidic system for HSA. A linear tendency was observed between 0.05 -10 µg/ml and a fitting analysis was performed. a) Shows the results for the impedance modulus analysis, b) Represents the measurements of the differential voltage. 82
Fig. 4. 14 Detection range of the microfluidic system for HSA. A linear tendency was observed between 0.05 -10 µg/ml and a fitting analysis was performed. Corresponds to the factor α calculations. 84

Fig. 5. 1 Metastasis process of tumor cells 90
Fig. 5. 2 The anatomy of the prostate 91
Fig. 5. 3 Inflammatory process as a precursor of prostate cancer. 92

Fig. 5. 4 Protocol for the detection of prostate-specific antigen. a) Rinsing with PBS, b) Selective blocking with a PEG-thiol solution, c) Electrode surface modified with biotin-thiol, d) Addition of a layer of streptavidin, e) Deposition of a layer biotinylated antibody. f) Detection of PSA. The images are represented in false color. 95
Fig. 5. 5 Electrical schematics of the measurements. a) Connections of the microelectrodes with the measurements devices, b) Impedance equivalency of the microfluidic system..... 96
Fig. 5. 6 Effect of PEG-Thiol solution on voltage drop. Different concentrations and times of deposition. a) Concentration of 1 mg/ml for 30 minutes. b) Concentration of 1 mg/ml for 60 minutes. c) Concentration of 10 mg/ml for 30 minutes. For the latter characterization of PSA we selected the parameters of the last test (c). 97
Fig. 5. 7 Real-time monitoring of impedance change for different concentrations of PSA 98
Fig. 5. 8 Real-time monitoring. The black lines represent the smoothed signal. The noise is for all the concentrations are represented on the right..... 99
Fig. 5. 9 Unfiltered signals with its respective electronic noise..... 99
Fig. 5. 10 Filtered signals and its respective noise..... 100
Fig. 5. 11 Sigmoidal fitting of the experimental data when evaluating different concentrations of PSA and detection times 101
Fig. 5. 12 Linear behavior of the fitting in the PSA concentrations of interest interval. 102
Fig. 5. 13 Adjustability of the sensing parameters of our device. a) Exponential fitting of the sensitivity with the experimental data for different detection times. b) Fitting for LOD with experimental data and different detection times. c) Fitting for LOQ with experimental data and different detection times. 103
Fig. 5. 14 Impedance detection range of the microfluidic system for the detection of PSA (round marks). The system was tested with human serum at a known concentration (square mark) 105
Fig. 5. 15 Voltage detection range of the microfluidic system for the detection of PSA (round marks). The system was tested with human serum at a known concentration (square mark)..... 106
Fig. 5. 16 Factor α detection range of the microfluidic system for the detection of PSA (round marks). The system was tested with human serum at a known concentration (square mark) 106
Fig. 5. 17 Tests with human plasma. The impedance modulus did not changed after the flowing of plasma without PSA (black plots) while the impedance modulus increased only for the functionalized electrode (red plots) $Z_{e1:er}$ and therefore we detect PSA on plasma. 108

Fig. 6. 1 Layout of the microfluidic device the functionalization of the two sets of electrodes is performed through the three separated inlets..... 116
Fig. 6. 2 a) Layout of the microfluidic device the functionalization of the two sets of electrodes is performed through the three separated inlets. b-f) Protocol for the multiplexed fluidic detection of Spondin-2 and PSA. b) Selective blocking with a PEG-thiol solution, c) Electrodes surface modified with biotin-thiol, d) Addition of a layer of streptavidin, e) Simultaneous deposition of a layer biotinylated antibodies. f) Detection of Spondin-2 and PSA. The images are represented in false color. 118
Fig. 6. 3 a) Set-up diagram, the DG333A helps to multiplex the measurements between sensor A (red path) and B (blue path). b) DG333A functional block diagram, the chip consists in 4 analog switches independently controlled. 120
Fig. 6. 4 Electrical schematics of the voltage measurements. Voltage and impedance equivalency of the microfluidic system. 120
Fig. 6. 5 Real-time monitoring of impedance magnitude (o module) change for different concentrations of SPON2 121
Fig. 6. 6 Sensitivity adjustment of the microfluidic system. Linear behavior of the fitting in the SPON2 concentrations. 122
Fig. 6. 7 Adjustability of the sensing parameters of our device. a) Linear fitting of the sensitivity with the experimental data for different detection times. b) Exponential fitting for LOD with experimental data and different detection times. c) Exponential fitting for LOQ with experimental data and different detection times. 123

Fig. 6. 8 Detection range of impedance measurements for both biomarkers. The test 1 has a SPON2 concentration of 1 ng/ml, the test 2 had a SPON2 concentration of 5 ng/ml and the test 3 had a SPON2 concentration of 10 ng/ml. The PSA was kept at 5 ng/ml for all the tests. 126
Fig. 6. 9 Detection range of voltage measurements for both biomarkers. The test 1 has a SPON2 concentration of 1 ng/ml, the test 2 had a SPON2 concentration of 5 ng/ml and the test 3 had a SPON2 concentration of 10 ng/ml. The PSA was kept at 5 ng/ml for all the tests. 126
Fig. 6. 10 Detection range of factor α measurements for both biomarkers. The test 1 has a SPON2 concentration of 1 ng/ml, the test 2 had a SPON2 concentration of 5 ng/ml and the test 3 had a SPON2 concentration of 10 ng/ml. The PSA was kept at 5 ng/ml for all the tests. 127

Fig. A1. 1 Schematics of the characterization set-up. 135
Fig. A1. 2 Comparison between HF2TA and multimeter measurements. 135
Fig. A1. 3 Characteristic curves for the percentage error of HF2TA measurements 136
Fig. A1. 4 Corrected measurements. 136
Fig. A1. 5 Characteristic curves for the percentage error after the correction. 136

Fig. A2. 1 Custom-made software first version, voltage measurements only. 139
Fig. A2. 2 Custom-made software second version, impedance and voltage simultaneous measurements. 142
Fig. A2. 3 Custom-made software third version, multiplexed measurements. 147

Fig. A3. 1 Protocol for the fabrication of an OSTE-thiol gradient. a) The OSTE-thiol (80)+BP is spun over a glass slide, b) The polymer is UV cured, c) The second solution of OSTE-thiol (80) is poured over the first layer with a tilt and UV cured, d) After the sample is rinsed in toluene a second layer is formed on top of the first OSTE, e) The sample is cut into 4 pieces and immerse on Ellman's reagent to estimate the thiol concentration. 150
Fig. A3. 2 OSTE-thiol samples immersed in Ellman's reagent. a) Each sample was immerse in 30 ml, b) Different concentrations were characterized, c) The absorbance of the reacted solution was measured. 151
Fig. A3. 3 a) Relative absorbance of the OSTE-thiol samples, b) Absolute absorbance. 152
Fig. A3. 4 Calibration curve for different OSTE-thiol concentrations. 152
Fig. A3. 5 First test with a gradient. a) Absorbance of the three sections, b) Absorbance of each section at 412 nm. 153
Fig. A3. 6 a) Diagram of the first gradient, b) Concentration as a function of distance. 153
Fig. A3. 7 Second test, an allyl solution was used as second layer. 154
Fig. A3. 8 a) Diagram of the first gradient, b) Concentration as a function of distance. 154
Fig. A3. 9 Third test of fabrication. The height of the tilt was increased. 154
Fig. A3. 10 a) Diagram of the first gradient, b) Concentration as a function of distance. 155

Abbreviations

MEMS	Micro-Electro-Mechanical Systems
μTAS	Micro Total-chemical Analysis System
LOC	Lab-on-a-Chip
ELISA	Enzyme-Linked Immuno-Sorbent Assay
PCa	Prostate Cancer
PSA	Prostate Specific Antigen
EIS	Electrochemical Impedance Spectroscopy
SPON2	Spondin-2
PDMS	Poly(dimethylsiloxane)
PBS	Phosphate Buffer Saline
Biotin-thiol	Biotinylated alkyl thiol
SAV-TRed	Streptavidin-Texas red
QD	Quantum Dots
PEG-thiol	Polyethyleneglycol-thiol
NAV-OGreen	Neutravidin-OregonGreen
SAM	Self-Assembled Monolayer
HSA	Human Serum Albumin
AHSA	Anti-Human Serum Albumin antibody
LOD	Limit of Detection
LOQ	Limit of Quantification

APSA	Anti-Prostate Specific Antigen antibody
ASPON2	Anti-Spondin-2 antibody
OSTE	Off-Stoichiometric Thiol-Ene

CHAPTER 1 General Introduction

1.1. Introduction

"There's Plenty of Room at the Bottom" ... a simple rather powerful statement that was done in 1959 by Richard Feynman while giving a visionary speech during the American Physical Society at Caltech. Feynman, a once Nobel price in Physics, was proposing to explore new and revolutionary fields: *Nano and micro technologies* [1]. Feynman's talk, five years after the development of the first working silicon transistor by Morris Tanenbaum at Bell Labs [2], is often referred to as the beginning of the application of the science of the small to improve technologies. He proposed to write an Encyclopedia into the head of a needle, build tiny machines with tools, or even work with biological systems from the engineering point of view.

Fig. 1. 1The smallest movie. Today we are able to handle and image atoms. Feynman's once visionary view came to reality less than half a century later.

As he pointed out giving a first glimpse on biotechnology: Many of the cells are very tiny, but they are very active; they manufacture various substances; they walk around; *they wiggle; and they do all kinds of marvelous things – all on a very small scale* [1]. Feynman set the wheels in motion and, since then, breakthroughs on creating miniaturized devices, first in the micro and then in the nano scale, have not ceased (Fig. 1. 1). Advances in, complementary disciplines, such as microfluidics, transducers, microelectronics and molecular assemblies, have made it possible to conceive our novel devices by exploiting synergies in these fields.

Miniaturization impact on Analytical sciences

The miniaturization of the chemical reaction chambers and the evolution of Micro-electro-mechanical systems (MEMS) fabrication techniques along with silicon technology gave birth to use microfluidics [3] for analytical chemists. The first microfluidic device was fabricated around 1975; a silicon-based gas chromatographic analyzer (Fig. 1. 2). The gas chromatograph consisted on microchannels etched in silicon and was able to separate compounds in just a few seconds [4, 5]. However, the separation-science community didn't pay much attention to that novel device, probably due to the lack of experience with silicon fabrication technology or the language and discussion forums distance between the microfabrication and the analytical chemistry scientific communities.

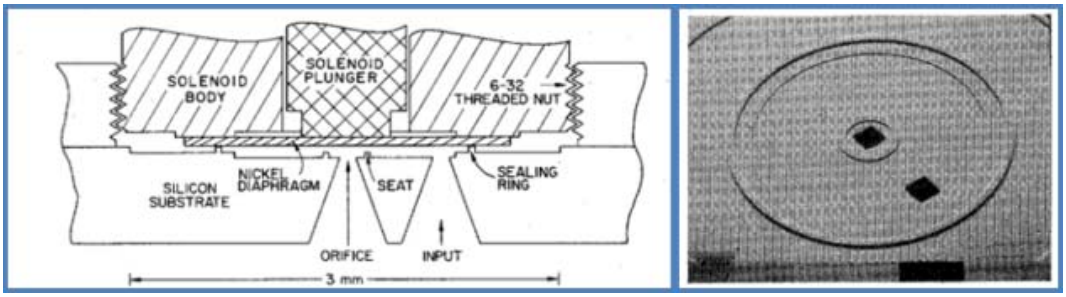

Fig. 1. 2 The first microfluidic device, a gas chromatographic analyzer developed on 1975 [5].

It was not until 15 years later, in 1990, when an attempt to miniaturize a liquid chromatograph fabricated on silicon was done. Chemists became fully aware of the advantages that miniaturization could bring to their field: "*micro total chemical analysis system"* (μTAS) concept was born [6]. These microdevices had a great impact in the years to come on analytical sciences giving rise to the exploitation of microfluidics, and their combination with micro actuators and sensors, to improve, or create, a great extent of applications such as: electrophoretic separation systems [7], electro-osmotic pumping systems [8], diffusive separation systems [9], micromixers [10], DNA amplifiers [11], cytometers [12], and chemical microreactors [3], just to mention a few (Fig. 1. 3). These microfluidic systems can analyze and work with small volumes of complex fluids in sealed environments making the analysis cheaper in terms of reagents and reducing waste while automating some operations [13]. The small sample quantity can also improve the sensitivity and decrease the reaction times for a detection [14]. The possibility to miniaturize a whole analytical lab on a small chip, or Micro Electro Mechanical System

(MEMS), had become more feasible and these devices started being referred alternatively as Lab-on-a-Chip (LOC).

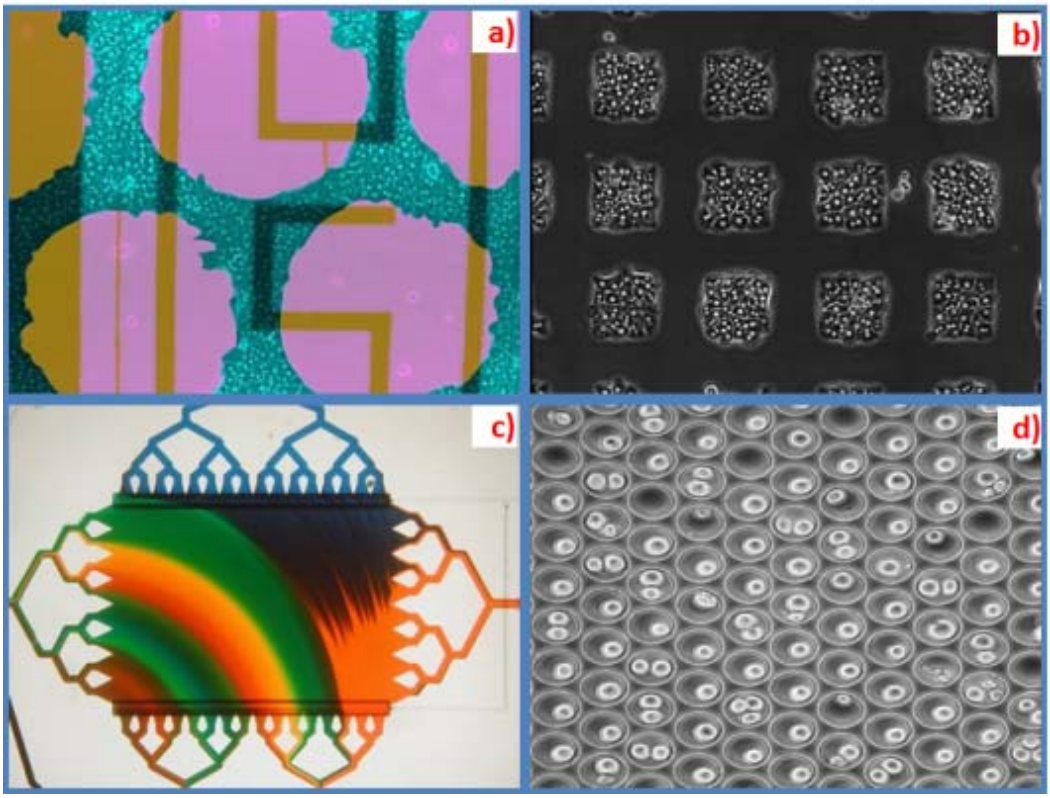

Fig. 1. 3 Microfluidic systems. a) Gold electrode sensing, b) Liver cells patterns, c) Gradient generator, d) Cells in tiny wells. *Albert Folch's Lab.*

However, the main goal, or Holy Grail, of LOC or μTAS devices, has remained to analyze a raw sample with a single chip, performing sample extraction, conditioning, and analytes quantification, or detection, in a simple use and completely automated microchip. Several attempts to accomplish the complete integration of all the steps on a single chip have been made with more or less success: i-STAT corporation developed a silicon microchip for the monitoring of several analytes (Na, K, Cl, Ca, HCO, Glucose, Urea, pH, pO_2, pCO_2, and Hct). The analyzer is fully automatic with a pre-functionalized biosensor array, the sample (whole blood or urine) is treated in the device, with a fluid handling by capillarity and electrochemical signal detection [15].

Daktari diagnostics designed a microfluidic cell chromatograph for CD4 cell counting, It uses whole blood as a sample and after lysis, measures the cell chemical content by impedance spectroscopy [16].

Burns et al developed one of the first fully integrated LOC; they fabricated a device with microfluidic channels, heaters, temperature sensors and fluorescent

detectors to analyze DNA samples. The system was totally closed and the mixing, amplifying and digestion of the DNA were performed inside the cartridge [17] (Fig. 1. 4). Van Heirstraeten et al developed a fully integrated DNA and RNA extractor from bacterial and viral pathogen. The device had a module for sample treatment, lysis of the sample, purification and concentration of nucleic acids and recovery of the sample. Using this device they proved that the miniaturization helped to reduce the costs, the sample consumption and the time of analysis [11].

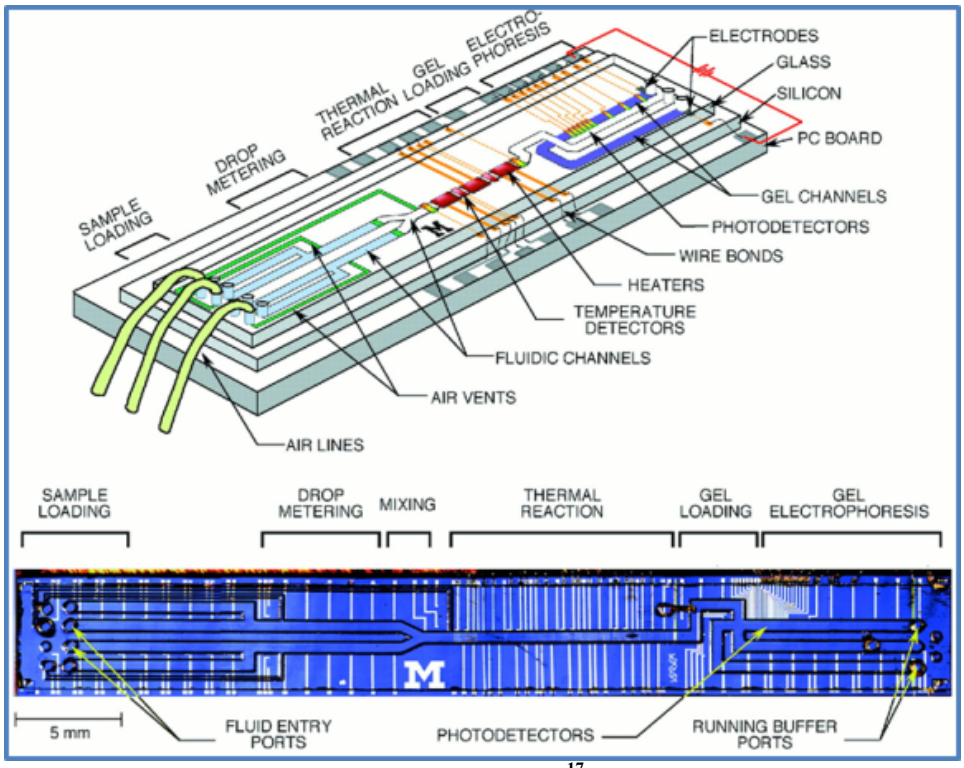

Fig. 1. 4 A complete lab-on-chip for DNA analyses [17].

Only a few examples reported were able to perform all operations from sample preparation to analyte quantification. Most of the commercial ones had limited quantification capabilities and restricted sensitivities and limits of detection. Furthermore, the lifetime of these devices was compromised by the biological components of the sensors. This also restricted their mass production, since the biocomponents are present on the LOC device before it's sealing. Also, many of those devices use optical read-out, increasing the cost and complexity of the whole device [18].

Biomedical applications of LOC Devices

In recent years, the LOC community has focused most of its research in the biomedical and biotechnology fields, due to the need of portable, low power consumption and low cost theranostics microdevices. Some developing countries do not have suitable medical

diagnostics technologies and the supply and storage of the reagents is in many cases limited as well as the access to energy. Furthermore, developed countries are experimenting population aging needing novel low cost efficient disease-screening technologies. The introduction of LOC and microfluidics allow the integration of complex functions that could lead to the developing of more accurate, cheap and reliable theranostic tools. Current focus of application is focused mostly in drug delivery [19], cellular analysis [20], and disease diagnosis [21].

Drug delivery methods aim to administer a pharmaceutical compound in a controlled manner to achieve a therapeutic effect on disease. Most drugs are administrated orally or by injection. However, these types or dosage are non-local and could affect healthy organs or cells. Ideally, the drug delivery should be focalized and dose specific. With microfabrication technologies, some devices have been developed to achieve drug delivery more efficiently, with a more controlled treatment and local drug release to minimize toxicity. Most of the commercially available devices are based on a microreservoir and the delivery can be achieved by different triggers: electrochemical dissolution [22, 23], temperature [24, 25], polymer degradation [26, 27], and magnetic force [28]. However, the delivery could be done by a microfluidic method and the drug can be introduced by diffusion [29, 30] (Fig. 1. 5a), pressure injection [31] (Fig. 1. 5b) or electrokinetic force [32-34] (Fig. 1. 5c). The main advantages of these devices are that they are controllable platforms able to do a precise drug delivery, including drug concentration more stable, minimizing drug degradation, and providing a sustained drug release.

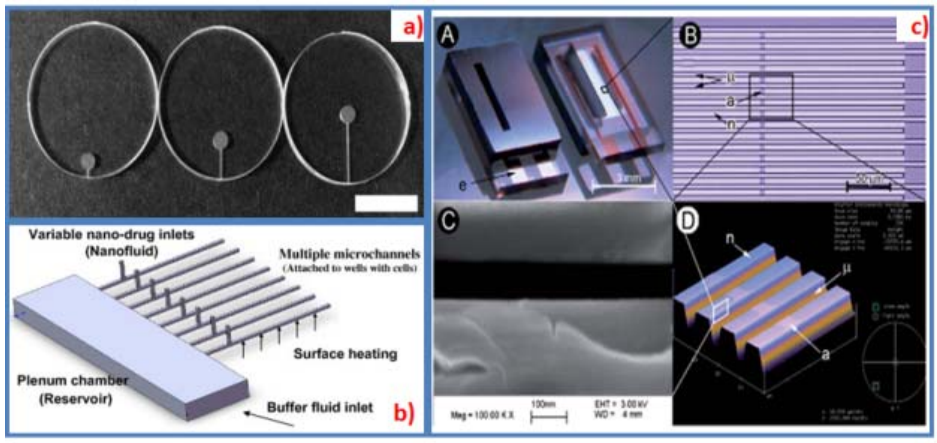

Fig. 1. 5 Microfluidic drug delivery systems. a) Delivery by diffusion [29], b) Delivery by pressure [32] and c) Electrokinetic forces [31].

Another important life science application of microfluidics is cell analysis and handling (Fig. 1. 6). Microfluidic devices for the trapping, treatment or characterization of cells were developed. The cell trapping and sorting can be done by an electrical [35] or mechanical [36] mechanism. The integration is one of the most important characteristics of the microfluidics systems; therefore cell treatment (lysis [37], electroporation [38] or even cell fusion [39]) plays a key role in a lab-on-chip development. The cell analysis has the advantages of reduce cell consumption, automated reagent addition and reproducible mixing of the reagents [20]. Some analytical applications include the transport of cells and generation of gradients [40], manipulation of cells for the detection of specific antibodies [41] or monitoring of cellular metabolic reactions [20].

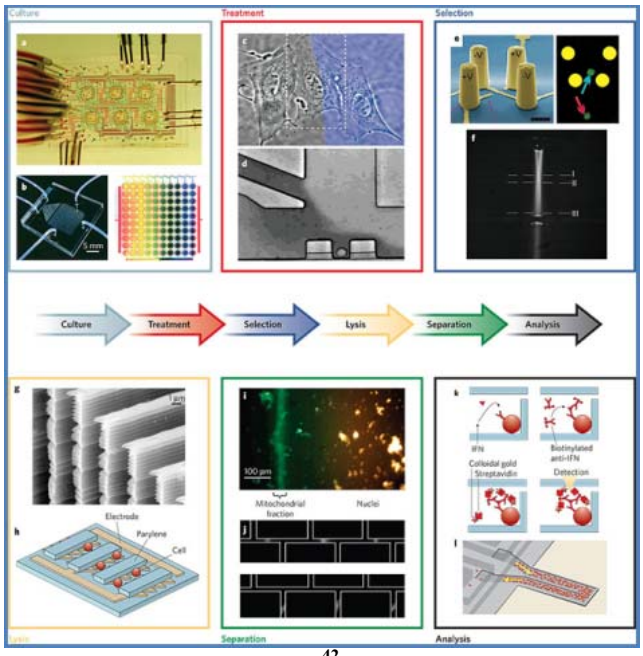

Fig. 1. 6 Microfluidic systems for cellomics [42].

For disease diagnosis, the most used techniques are small molecules monitoring [43], immunoassays [44], nucleic-acid amplification [14] and cells analysis [45]. These techniques look for a specific antibody, protein, biomolecule or cell in body fluids. The major class of currently commercially available tests is based on the lateral flow or immunochromatographic strip (ICS); these test use a membrane or paper strip to indicate the presence of a specific biomarker. The lateral flow tests are widely used to diagnose infections diseases such as HIV or flu; another example is the pregnancy tests and the blood glucose test [16].

On the other hand, for the detection of small molecules the most successful example is the iSTAT developed by Abbott. The device was fabricated with the

integration of microfluidics and microfabrication technologies. The integrated biosensors are able to detect blood chemistries, and coagulation and cardiac biomarkers. A potentiometric module performs the direct measurements of sodium, potassium, pH or pCO_2. And the reagents are stored on a disposable plastic test cartridge, which contains a pre-functionalized silicon microelectrodes array [46] (Fig. 1. 7).

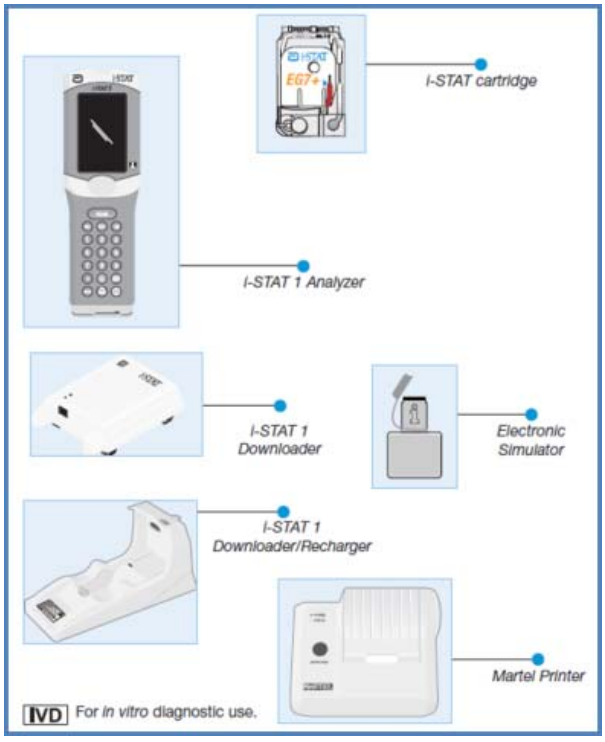

Fig. 1. 7 Commercially available biosensor with multiple cartridge analysis (http://www.abbottpointofcare.com/).

Furthermore, in developing countries, several companies are working in devices for the monitoring and diagnose of HIV. The novel microfluidic systems are focused on the counting of CD4+ T-cells. Alere employs an image analysis based on flow cytometry. While Daktari Diagnostics uses affinity chromatography to selectively capture of the cells [47], with impedance spectroscopy to simplify the read-out. The systems are mainly qualitative.

There is a great interest for detection of DNA and RNA for diagnose and monitoring due to its specificity. However, these test are the most challenging to develop since they have to integrate a sample pre-treatment, signal amplification and target contamination and instability [16]. One of the firsts companies working on this field was Handylab. They developed a device with disposable cartridges with pre-functionalized reagents, and instrument with heating, fluid control and fluorescence

detection. However, some procedures are performed outside the chip and the cost of these devices is relatively high.

The development of immunoassays as point-of-care devices is limited by their low sensitivity, poor quantification of the sample and inability to detect multiple targets. However, several companies are working to improve and overcome such drawbacks, so far with limited success. Biosite developed a test to detect cardiac disease biomarkers by fluorescence signals. Philips is working with nanoparticles to optically detect protein analytes at low concentrations (pM at most). And Claros Diagnostics uses an absorbance reader to measure the optical density of the biomarkers. The devices presented are pre-functionalized and only the Claros test approach includes a multiple detection [16].

Microfluidics is improving the developing of novel point-of-care devices, but there are some challenges that are slowing down the massive production of these LOC. These areas include new methods for sample collection, world-to-chip interfaces, sample pre-treatment, improvement of long-term stability of reagents, working with complex sample specimens, multiple detection of biomarkers and simplify the read-out [16].

The main aim of this thesis work was to create novel, cheap and with a high degree of automatization miniaturized biosensing devices with the objective to facilitate Point-of-Care diagnostics in the near future. Our efforts have been focused into developing a LOC system with electrochemical sensing capabilities adjustable to any biomarker, depending only on sample volumes and required analysis times. The devices integrate low-cost label-free biosensors exploiting microfluidics-based self-functionalization, or specialization. The biosensor functionalization takes place in situ and selectively, just before the sensing, and their area keeps dry and inactive until the test starts. The reagents and the sensing parts are kept separated and brought into contact just before the test, avoiding the need of complex fabrication and storage methods to guarantee functionalization integrity. The novel design reduces the cost of the final instrumentation, by simplifying the measurements, while keeping sensitivities and LODs relevant for the application. Furthermore, since the interaction of antibody and protein is time and concentration dependent, our device has the capability to adjust its sensitivity. We have tuned and characterized our system sensitivity using different

biomarkers. The development of our novel devices was possible by exploiting synergies in disciplines previously studied in our group. Particularly, in fields such as microfluidics [48-51], surface functionalization [52-57] and electrochemical biosensors [58-62].

1.2 State-of-the art and Rationale

As previously stated, the biosensors research tends to be an important tool for clinicians for the rapid diagnosis of diseases, such as cancer. Some of the advantages of this tool are the reduced costs for a single test, the capability of performing measurements on real-time, automated and rapid diagnose, and some devices are able to detect multiple analytes [14]. The study and discovery of new biomarkers related to a specific disease had increased to potential and development of novel biosensors [63]. Some of the most promising biosensors monitor the mutation of DNA or the expression of specific proteins biomarkers related to an early diagnostic. Also, the integration of biosensors to a microfluidic system or lab-on-chip, introduces new advantages towards point of care diagnose. LOC devices developed lately usually need less reagents, use less time for the detection of analytes, allow multiplexed detections, and are small and portable [64].

DNA based biosensors offer the advantage of identifying highly specific disease markers. However, these systems are highly complex, since they have to integrate all the tools for hybridization assays. A different approach is the protein-based biosensors. These biosensors are easy to implement and have the advantage of a greater selectivity; since one gene can express multiple proteins but each protein could be related to a specific biological function [14]. For that specific characteristic, we propose novel microfluidic devices with integrated biosensors for the detection of protein biomarkers related to prostate cancer.

Nowadays, the most used technique for immunoassays is the Enzyme-Linked Immuno-Sorbent Assay (ELISA), which is a very reliable technique. However, the long incubation times (on the order of days) and long diffusion, and the need of fluorophores that do not affect the antigen-antibody interaction are some of the drawbacks of this technique [65]. The ELISA test is based on the reaction inside a chamber and therefore there is no fluidic system involved on the detection (Fig. 1. 8). A microfluidic immunoassay can reduce the costs, and improve sensitivity and time of detection in comparison with classical ELISA test [66].

In this thesis, we are proposing a novel microfluidic device with integrated biosensors that can be functionalized in-situ and selectively. We wanted to design a microfluidic immunosensor with a biomedical application; to improve the sensitivity, reduce the time of detection, reduce costs and avoid complex fabrication techniques. We desired to develop a system with an adjustable sensitivity and range of detection, to adapt our device to a specific biomedical application. By performing an in-situ surface modification, we were hoping to simplify the fabrication process. The method of fabrication should help us to decrease the costs of production. The time of detection could be adapted and reduced, by changing the concentrations of the functionalization solutions.

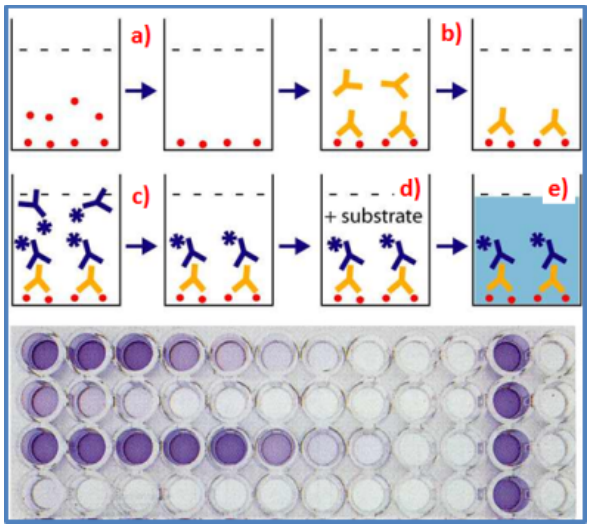

Fig. 1. 8 ELISA test. a) The plate is coated with a capture antigen; b) sample is added, and any antibody present binds to antigen; c) enzyme-linked secondary antibody is added, and binds to detecting antibody; d) substrate is added, and e) is converted by enzyme to detectable form.

As biomedical application we chose prostate cancer (PCa). Since PCa is the second most diagnosed cancer on men worldwide [67]. On 2008, a prediction of 890,000 new cases per year was reported in the project GLOBOCAN [68]. In USA, the American Cancer Society (ACS) estimated more than 238,000 new cases as for 2013, being PCa the most diagnosed cancer type in men. A prediction of deaths by PCa was also estimated to be 30,000 cases that same year in the USA [69]. In Europe, PCa is the third most common cause of death by cancer, with an estimation of more than 70,000 new deaths in 2013 [70]. As first proof-of-concept we selected Prostate Specific Antigen (PSA) for detection of PCa, since it is used in oncology as an unspecific biomarker for prostate cancer pre-screening [71].

There are some commercially available tests for PSA determination in serum. Manufacturers, such as Roche, Bayer or Beckman Coulter, have developed assays for accurate and fast detection of PSA. They can reach detection limits ranging from 5 or 50 pg/ml up to 100 ng/ml, over covering the current cut off value for serum PSA evaluation in medical practice that is 4 ng/ml, and have a turnaround time lower than 1 hour [72]. However, their main drawback is the need of specialized laboratories, to do the analysis and to maintain these machines, which increases costs and delays diagnosing.

Different signal transduction methods have been extensively investigated to develop alternative point of care detection methods for PSA, being mainly of optical, electrical or mechanical nature [73]. In many cases, these biosensors are based on labeling methods that incorporate fluorescent nanoparticles [74], generate biobarcode assays [75] or produce electrochemical reactions [76], in order to achieve higher limits of detection and sensitivities. However, the main issues of these label-based biosensors are their test complexity, their associated cost intensive mass-production, their non-specificity, in some cases, and their far from optimal turnaround times, that could ease their generalized use for other biomarkers and applications. Due to all these issues the alternative use of label-free methods is preferred for potential commercial applications [77]. However, these methods are sometimes limited due to their lack of sensing tuning mechanisms and limited sensitivities. Electrochemical biosensors are the choice of preference when a label-free method is selected due to their sensitivity, selectivity, fast response, small packaging and low power requirements [44]. Different types of electrochemical biosensors had been developed for the detection of PSA in the last years depending on the measuring method: field-effect transistor biosensors [78, 79], voltammetry [80] and Electrochemical Impedance Spectroscopy (EIS) [81]. The electrochemical biosensors usually need to be embedded into controlled microfluidic systems or LOC devices. These platforms show several advantages such as low reagent and sample consumption, fast analysis times, automation and flexibility [73].

Therefore, we have developed a LOC system with electrochemical sensing capabilities adjustable to any biomarker, depending only on sample volumes and required analysis times. The device is a low-cost label-free biosensor exploiting microfluidics-based self-functionalization, or specialization.

We also know that the use of prostate-specific antigen test as a screening tool in diagnosing prostate cancer is controversial. The Prostate, Lung, Colorectal and Ovarian Cancer Screening Trial (PLCO), in the United States, claim that PSA test plus a digital rectal examination has no mortality benefit [82]. In contrast, the European Randomize Study of Screening for Prostate Cancer (ERSPC), in Europe, says that the PSA screening had reduced the mortality in a 20% [83]. Therefore, novel biomarkers are being studied for diagnose, staging and treatment of prostate cancer. Also, when developing LOC systems certain demands must be fulfilled such as high sensitivity, detection of multiple biomarkers, high selectivity, fast response, small, cheap and easy integration of the system. Therefore, as second application we selected two cancer biomarkers for the screening of PCa.

Since an early and precise diagnose of PCa is desirable; therefore, a series of biomarkers had been reported to improve the detection of the disease. The new biomarkers could help to develop more personalized treatments. The biomarkers used for the study of PCa can be divided taking into account the matrix where they are present in serum, urine and tissue. Spondin-2 (SPON2) is a relatively novel biomarker that seems to have the ability to avoid some of the drawbacks presented during PSA tests. SPON2 is expressed in cancerous and non-cancerous cells, plays a key role in the initiation of the immune response and is a recognition molecule for microbial pathogens [84].

Due to the low specificity of PSA, a simultaneous and multiple detection of biomarkers is desirable for diagnosing PCa. There had been several attempts to detect multiple prostate cancer biomarkers towards developing point-of-care devices. A multiplex suspension array technology with microbeads was developed to detect simultaneously PSA, prostate stem cell antigen, prostatic acid phosphatase and prostate-specific membrane antigen; the biomarkers levels were quantified by fluorescent intensities showing no significant cross-talk among biomarkers [85]. Another approach was the development of a piezoelectric biosensor, two ceramic resonators were connected in parallel for the multiplexed detection of PSA and α-fetoprotein, showing high sensitivity and fast detection [86]. Also, microfluidics had helped to developed devices for detection of cancer biomarkers. An electrochemiluminescence immunoarray with a microfluidic module was developed for the detection of PSA along with IL-6, the technology used a ultrasensitive approach by using silica nanoparticles [87]. However, the

main issues of these devices are that they use a label to improve the sensitivity of their system. That characteristic increases the complexity of the test as well as its cost. Also, they don't have a tuning mechanism that can be adapted for different applications. As the best knowledge of the authors, is the first attempt to detect simultaneously and in real-time PSA and SPON2, for an early diagnose of PCa.

Summarizing, we are proposing novel microfluidic devices with integrated biosensors. The systems are based on the principle of laminar co-flow in order to perform an on-chip selective surface bio-functionalization of LOC integrated biosensors. This method has the advantage of performing the surface modification protocols "in situ" before the detection. The system can be easily scaled to incorporate several sensors with different biosensing targets in a single chip. We are proposing a novel voltage and impedance differential measurements; that allow us to simplify the read-out. As biomedical application we focus our attention on the detection of prostate cancer biomarkers.

1.3 Objectives

Main objective:

- To study and exploit microfluidics physics, self-assembled molecular monolayers, proteins interactions and electronic detection techniques to design, develop and fabricate a versatile biosensing novel lab-on-a-chip device suitable for point of care applications with multiplexing capabilities, and adjustable sensitivity and range of detection depending on the application

Specific objectives:

- To fabricate and characterize lab-on-a-chip microdevices, using photolithographic and molding techniques.
- To characterize and adjust the fluid dynamics of novel microfluidic LOC devices using simulations and experimentation.
- To develop an on-chip self-functionalizing protocol for the detection of a biomolecules of interest for biomedical applications and improve the long-term storage capabilities of the device prior of its use.

- To study the self-functionalizing capabilities of the device, by means of laminar co-flow phenomena, and study the impedance changes of the integrated biosensors after the deposition of a monolayer.
- To study the impedance changes produced by the interaction between biotin and streptavidin on the formation of different monolayers over the surface of the integrated biosensors.
- To perform an optical analysis, by means of fluorescence, of quantum dots after its selective deposition and detection to verify the behavior of the device.
- To proof the equivalence of impedance changes monitoring of the biosensors in front of previous optical studies.
- To detect optically and electrically quantum dots, with a self-functionalized biosensor, for comparison purposes and test the correct self-blocking of the remaining integrated biosensors.
- To develop custom made software to do the voltage and impedance measurements, and characterize the impedance spectroscope in order to avoid errors.
- To characterize the novel device for the detection of human serum albumin, by a real time voltage and impedance measurements.
- To improve the blocking protocol to get a better response with the voltage measurements.
- To characterize the microfluidic LOC for the detection of prostate-specific antigen, as a biomedical application.
- To fabricate and test a device with multiple biosensors for the detection of two cancer biomarkers as a biomedical application.

1.4 Dissertation Outline

The present thesis entitled "***Microfluidic devices with integrated biosensors for biomedical applications***" aims to contribute in the field of Biomedical Engineering. This work presents novel microfluidic devices with integrated biosensors for the detection of a biomolecule of interest, in particular prostate cancer biomarkers. The functionalization was done "in situ" after bonding, and so simplifying the fabrication process. The devices were fabricated and characterized for the detection of PSA and SPONDIN-2 as biomedical applications. The thesis is divided on the next chapters:

In **Chapter 2**, In this chapter a state of the art of microfluidics and fabrication techniques is presented in the context of this work. Different fabrication techniques are presented and the selection of materials and techniques for our device are justified. The novel analytical devices were designed, and the physics involved in the microfluidic behavior were studied, using mathematical models and simulations, to support the designs and create a new device exploiting these phenomena in an efficient mean.

In **Chapter 3**, an overview of the different biosensors is presented. The different functionalization techniques are described. The first protocol used for the determination of optimum functionalization times is shown; the measurements helped to choose the most suitable working frequencies. An improved second protocol, for the selective functionalization is presented; the analysis is performed optically and electronically. Finally in this chapter, the results for the first protocol for detection are discussed, using optical and voltage characterization.

In **Chapter 4**, an electrochemical detection of single biomarkers is presented as a proof-of-concept. The protocol selected for the detection is presented. The measurements are performed by voltage and impedance analysis

In **Chapter 5**, the first biomedical application of LOC for the detection of a single biomarker is explored. The state-of-the-art biosensors for detection of prostate cancer are explained. We reported a device with self-functionalized and integrated biosensors for the detection of prostate-specific antigen (PSA) for diagnosing prostate cancer. The detection parameters of the device were characterized with impedimetric and voltage measurements. And the system was tested with human serum.

In **Chapter 6**, we present the second designed device, to demonstrate the capability of multiple biomarkers detection. The device was functionalized for the detection of prostate cancer as biomedical application. By increasing the number of biomarkers to be detected the device gains specificity and reliability. Therefore, we tested our device with two biomarkers and checked that the integrated biosensors had no cross talk.

In **Chapter 7**, the general conclusions are presented, focusing on the contribution of this thesis. Also, we are proposing a future work, since we think that the results obtained so far could be useful to in a near future develop a device for point-of-care.

In **Annex 1**, the characterization of the measurement device is explained, and how a correction was performed in order to reduce the percentage error. The analysis and detection of the biomolecules used in this thesis was performed once the error was reduced.

In **Annex 2**, we programmed several versions of custom-made software. Each version of the software was adapted to the corresponding test. The first electrical analysis was done by studying the voltage changes, and so the software was programmed to acquire and save the data from measurements. An update of the software was necessary when the complexity of functionalization protocols increased. Therefore, we developed a version for the impedance and voltage measurements and a version for the multiplexed system.

In **Annex 3**, a novel method for the fabrication of thiol gradients in polymers is explained as a part of a stage done at the Kungliga Tekniska Högskolan (KTH, Stockholm). The study was performed with a polymer developed at the KTH and a protocol for the detection of thiol concentrations was also developed and explained.

1.5 References

1. R. P. Feynman, *Microelectromechanical Systems, Journal of*, 1992, **1**, 60-66.
2. M. Tanenbaum, L. B. Valdes, E. Buehler and N. B. Hannay, *Journal of Applied Physics*, 1955, **26**, 686-692.
3. P. Tabeling, *Introduction to microfluidics*, Oxford University Press, 2005.
4. S. C. Terry, 1975.
5. S. C. Terry, J. H. Jerman and J. B. Angell, *Electron Devices, IEEE Transactions on*, 1979, **26**, 1880-1886.
6. A. Manz, N. Graber and H. M. Widmer, *Sensors and Actuators B: Chemical*, 1990, **1**, 244-248.
7. I. Mitra, S. P. Marczak and S. C. Jacobson, *ELECTROPHORESIS*, 2014, **35**, 374-378.
8. D. Piwowar, M. E. Tawfik and F. J. Diez, *Microfluidics and Nanofluidics*, 2013, **15**, 859-870.
9. O. Ymbern, N. Sandez, A. Calvo-Lopez, M. Puyol and J. Alonso-Chamarro, *Lab on a Chip*, 2014, **14**, 1014-1022.
10. J.-N. Kuo and L.-R. Jiang, *Microsystem Technologies*, 2014, **20**, 91-99.
11. L. Van Heirstraeten, P. Spang, C. Schwind, K. S. Drese, M. Ritzi-Lehnert, B. Nieto, M. Camps, B. Landgraf, F. Guasch, A. Homs Corbera, J. Samitier, H. Goossens, S. Malhotra-Kumar and T. Roeser, *Lab on a Chip*, 2014.
12. Y. Chen, A. A. Nawaz, Y. Zhao, P.-H. Huang, J. P. McCoy, S. J. Levine, L. Wang and T. J. Huang, *Lab on a Chip*, 2014, **14**, 916-923.
13. P. Yager, T. Edwards, E. Fu, K. Helton, K. Nelson, M. R. Tam and B. H. Weigl, *Nature*, 2006, **442**, 412-418.

14. S. Choi, M. Goryll, L. Sin, P. Wong and J. Chae, *Microfluidics and Nanofluidics*, 2011, **10**, 231-247.
15. N. Peled, *Pure and applied chemistry*, 1996, **68**, 1837-1841.
16. C. D. Chin, V. Linder and S. K. Sia, *Lab on a Chip*, 2012, **12**, 2118-2134.
17. M. A. Burns, B. N. Johnson, S. N. Brahmasandra, K. Handique, J. R. Webster, M. Krishnan, T. S. Sammarco, P. M. Man, D. Jones, D. Heldsinger, C. H. Mastrangelo and D. T. Burke, *Science*, 1998, **282**, 484-487.
18. M. Mir, A. Homs and J. Samitier, *ELECTROPHORESIS*, 2009, **30**, 3386-3397.
19. I. U. Khan, C. A. Serra, N. Anton and T. Vandamme, *Journal of Controlled Release*, 2013, **172**, 1065-1074.
20. H. Andersson and A. Van den Berg, *Sensors and Actuators B: Chemical*, 2003, **92**, 315-325.
21. M. J. Cima, *Annual Review of Chemical and Biomolecular Engineering*, 2011, **2**, 355-378.
22. J. T. Santini, M. J. Cima and R. Langer, *Nature*, 1999, **397**, 335-338.
23. G. Voskerician, R. S. Shawgo, P. A. Hiltner, J. M. Anderson, M. J. Cima and R. Langer, *Biomedical Engineering, IEEE Transactions on*, 2004, **51**, 627-635.
24. M. Kohl and K. D. Skrobanek, *Sensors and Actuators A: Physical*, 1998, **70**, 104-111.
25. N. M. Elman, B. C. Masi, M. J. Cima and R. Langer, *Lab on a Chip*, 2010, **10**, 2796-2804.
26. A. Müller, Z. Ni, N. Hessler, F. Wesarg, F. A. Müller, D. Kralisch and D. Fischer, *Journal of Pharmaceutical Sciences*, 2013, **102**, 579-592.
27. A. C. R. Grayson, I. S. Choi, B. M. Tyler, P. P. Wang, H. Brem, M. J. Cima and R. Langer, *Nat Mater*, 2003, **2**, 767-772.
28. F. N. Pirmoradi, J. K. Jackson, H. M. Burt and M. Chiao, *Lab Chip*, 2011, **11**, 2744-2752.
29. S. H. Lee, M. Park, C. G. Park, J. E. Lee, M. R. Prausnitz and Y. B. Choy, *AAPS PharmSciTech*, 2012, **13**, 211-217.
30. E. Garcia, J. R. Kirkham, A. V. Hatch, K. R. Hawkins and P. Yager, *Lab Chip*, 2004, **4**, 78-82.
31. D. Fine, A. Grattoni, E. Zabre, F. Hussein, M. Ferrari and X. Liu, *Lab Chip*, 2011, **11**, 2526-2534.
32. C. Kleinstreuer, J. Li and J. Koo, *International Journal of Heat and Mass Transfer*, 2008, **51**, 5590-5597.
33. S. L. Tao, M. W. Lubeley and T. A. Desai, *J Control Release*, 2003, **88**, 215-228.
34. D. Fine, A. Grattoni, S. Hosali, A. Ziemys, E. De Rosa, J. Gill, R. Medema, L. Hudson, M. Kojic, M. Milosevic, L. Brousseau Iii, R. Goodall, M. Ferrari and X. Liu, *Lab Chip*, 2010, **10**, 3074-3083.
35. A. Y. Fu, C. Spence, A. Scherer, F. H. Arnold and S. R. Quake, *Nat Biotechnol*, 1999, **17**, 1109-1111.
36. R. H. Carlson, C. V. Gabel, S. S. Chan, R. H. Austin, J. P. Brody and J. W. Winkelman, *Physical Review Letters*, 1997, **79**, 2149-2152.
37. M. T. Taylor, P. Belgrader, B. J. Furman, F. Pourahmadi, G. T. Kovacs and M. A. Northrup, *Anal Chem*, 2001, **73**, 492-496.
38. Y. Huang and B. Rubinsky, *Sensors and Actuators A: Physical*, 2003, **104**, 205-212.
39. A. Stromberg, A. Karlsson, F. Ryttsen, M. Davidson, D. T. Chiu and O. Orwar, *Anal Chem*, 2001, **73**, 126-130.

40. M. Yang, C.-W. Li and J. Yang, *Analytical Chemistry*, 2002, **74**, 3991-4001.
41. L. J. Kricka, O. Nozaki, S. Heyner, W. T. Garside and P. Wilding, *Clin Chem*, 1993, **39**, 1944-1947.
42. J. El-Ali, P. K. Sorger and K. F. Jensen, *Nature*, 2006, **442**, 403-411.
43. V. Srinivasan, V. K. Pamula and R. B. Y. Fair, - *Lab on a Chip*, - 310.
44. Y. Wan, Y. Su, X. Zhu, G. Liu and C. Fan, in *Biosens Bioelectron*, 2013 Elsevier B.V, England, 2013, vol. 47, pp. 1-11.
45. T. D. Chung and H. C. Kim, *ELECTROPHORESIS*, 2007, **28**, 4511-4520.
46. K. A. Erickson and P. Wilding, *Clin Chem*, 1993, **39**, 283-287.
47. X. Cheng, D. Irimia, M. Dixon, K. Sekine, U. Demirci, L. Zamir, R. G. Tompkins, W. Rodriguez and M. Toner, *Lab on a Chip*, 2007, **7**, 170-178.
48. R. Rodriguez-Trujillo, C. A. Mills, J. Samitier and G. Gomila, *Microfluidics and Nanofluidics*, 2007, **3**, 171-176.
49. R. Rodriguez-Trujillo, O. Castillo-Fernandez, M. Garrido, M. Arundell, A. Valencia and G. Gomila, *Biosensors and Bioelectronics*, 2008, **24**, 290-296.
50. O. Castillo-Fernandez, R. Rodriguez-Trujillo, G. Gomila and J. Samitier, *Microfluidics and Nanofluidics*, 2014, **16**, 91-99.
51. J. Comelles, V. Hortigüela, J. Samitier and E. Martínez, *Langmuir*, 2012, **28**, 13688-13697.
52. E. Prats-Alfonso, F. García-Martín, N. Bayo, L. J. Cruz, M. Pla-Roca, J. Samitier, A. Errachid and F. Albericio, *Tetrahedron*, 2006, **62**, 6876-6881.
53. J. Vidic, M. Pla-Roca, J. Grosclaude, M.-A. Persuy, R. Monnerie, D. Caballero, A. Errachid, Y. Hou, N. Jaffrezic-Renault, R. Salesse, E. Pajot-Augy and J. Samitier, *Analytical Chemistry*, 2007, **79**, 3280-3290.
54. Y. Hou, S. Helali, A. Zhang, N. Jaffrezic-Renault, C. Martelet, J. Minic, T. Gorojankina, M.-A. Persuy, E. Pajot-Augy, R. Salesse, F. Bessueille, J. Samitier, A. Errachid, V. Akimov, L. Reggiani, C. Pennetta and E. Alfinito, *Biosensors and Bioelectronics*, 2006, **21**, 1393-1402.
55. S. Rodríguez Seguí, M. Pla, J. Minic, E. Pajot-Augy, R. Salesse, Y. Hou, N. Jaffrezic-Renault, C. A. Mills, J. Samitier and A. Errachid, *Analytical Letters*, 2006, **39**, 1735-1745.
56. A. Lagunas, J. Comelles, E. Martínez and J. Samitier, *Langmuir*, 2010, **26**, 14154-14161.
57. A. Lagunas, J. Comelles, S. Oberhansl, V. Hortigüela, E. Martínez and J. Samitier, *Nanomedicine: Nanotechnology, Biology and Medicine*, 2013, **9**, 694-701.
58. M. Castellarnau, N. Zine, J. Bausells, C. Madrid, A. Juárez, J. Samitier and A. Errachid, *Materials Science and Engineering: C*, 2008, **28**, 680-685.
59. M. Castellarnau, N. Zine, J. Bausells, C. Madrid, A. Juárez, J. Samitier and A. Errachid, *Sensors and Actuators B: Chemical*, 2007, **120**, 615-620.
60. M. Kuphal, C. A. Mills, H. Korri-Youssoufi and J. Samitier, *Sensors and Actuators B: Chemical*, 2012, **161**, 279-284.
61. D. Caballero, E. Martinez, J. Bausells, A. Errachid and J. Samitier, *Analytica Chimica Acta*, 2012, **720**, 43-48.
62. M. Barreiros dos Santos, J. P. Agusil, B. Prieto-Simón, C. Sporer, V. Teixeira and J. Samitier, *Biosensors and Bioelectronics*, 2013, **45**, 174-180.
63. J. Wang, *Biosensors and Bioelectronics*, 2006, **21**, 1887-1892.
64. S. Choi and J. Chae, *Microfluidics and Nanofluidics*, 2009, **7**, 819-827.
65. R. M. Lequin, *Clinical Chemistry*, 2005, **51**, 2415-2418.

66. K. Sato, M. Tokeshi, T. Odake, H. Kimura, T. Ooi, M. Nakao and T. Kitamori, *Anal Chem*, 2000, **72**, 1144-1147.
67. M. Dean and H. Lou, *Asian J Androl*, 2013, **15**, 309-313.
68. J. Ferlay, H. R. Shin, F. Bray, D. Forman, C. Mathers and D. M. Parkin, *Int J Cancer*, 2010, **127**, 2893-2917.
69. R. Siegel, D. Naishadham and A. Jemal, *CA: A Cancer Journal for Clinicians*, 2013, **63**, 11-30.
70. M. Malvezzi, P. Bertuccio, F. Levi, C. La Vecchia and E. Negri, *Annals of Oncology*, 2013.
71. S. P. Balk, Y.-J. Ko and G. J. Bubley, *Journal of Clinical Oncology*, 2003, **21**, 383-391.
72. D. A. Healy, C. J. Hayes, P. Leonard, L. McKenna and R. O'Kennedy, in *Trends Biotechnol*, England, 2007, vol. 25, pp. 125-131.
73. K. N. Han, C. A. Li and G. H. Seong, *Annu Rev Anal Chem (Palo Alto Calif)*, 2013, **6**, 119-141.
74. J. H. Choi, H. S. Kim, J.-W. Choi, J. W. Hong, Y.-K. Kim and B.-K. Oh, *Biosensors and Bioelectronics*, 2013, **49**, 415-419.
75. C. S. Thaxton, R. Elghanian, A. D. Thomas, S. I. Stoeva, J.-S. Lee, N. D. Smith, A. J. Schaeffer, H. Klocker, W. Horninger, G. Bartsch and C. A. Mirkin, *Proceedings of the National Academy of Sciences*, 2009, **106**, 18437-18442.
76. J. Wang, *Analyst*, 2005, **130**, 421-426.
77. X. Luo and J. J. Davis, *Chem Soc Rev*, 2013, **42**, 5944-5962.
78. A. Kim, C. S. Ah, H. Y. Yu, J.-H. Yang, I.-B. Baek, C.-G. Ahn, C. W. Park, M. S. Jun and S. Lee, *Applied Physics Letters*, 2007, **91**, -.
79. C. Li, M. Curreli, H. Lin, B. Lei, F. N. Ishikawa, R. Datar, R. J. Cote, M. E. Thompson and C. Zhou, *Journal of the American Chemical Society*, 2005, **127**, 12484-12485.
80. J. Okuno, K. Maehashi, K. Kerman, Y. Takamura, K. Matsumoto and E. Tamiya, *Biosensors and Bioelectronics*, 2007, **22**, 2377-2381.
81. M. S. Chiriaco, E. Primiceri, A. Montanaro, F. de Feo, L. Leone, R. Rinaldi and G. Maruccio, *Analyst*, 2013, **138**, 5404-5410.
82. G. L. Andriole, E. D. Crawford, R. L. Grubb, S. S. Buys, D. Chia, T. R. Church, M. N. Fouad, E. P. Gelmann, P. A. Kvale, D. J. Reding, J. L. Weissfeld, L. A. Yokochi, B. O'Brien, J. D. Clapp, J. M. Rathmell, T. L. Riley, R. B. Hayes, B. S. Kramer, G. Izmirlian, A. B. Miller, P. F. Pinsky, P. C. Prorok, J. K. Gohagan and C. D. Berg, *New England Journal of Medicine*, 2009, **360**, 1310-1319.
83. F. H. Schröder, *New England Journal of Medicine*, 2011, **365**, 1953-1955.
84. X. Qian, C. Li, B. Pang, M. Xue, J. Wang and J. Zhou, *PLoS ONE*, 2012, **7**, e37225.
85. N. Liu, W. Liang, X. Ma, X. Li, B. Ning, C. Cheng, G. Ou, B. Wang, J. Zhang and Z. Gao, *Biosensors and Bioelectronics*, 2013, **47**, 92-98.
86. L. Su, L. Zou, C.-C. Fong, W.-L. Wong, F. Wei, K.-Y. Wong, R. S. S. Wu and M. Yang, *Biosensors and Bioelectronics*, 2013, **46**, 155-161.
87. N. Sardesai, K. Kadimisetty, R. Faria and J. Rusling, *Analytical and Bioanalytical Chemistry*, 2013, **405**, 3831-3838.

CHAPTER 2 Design, fabrication and fluid dynamics of the microfluidic devices

2.1. Introduction

Due to their small size, in the order of 10 – 100 μm; and slow flow rates, a few μl/min; flows in microfluidic systems are generally dominated by viscous effects. The main characteristics in microfluidics, laminar flow and small Reynolds number, had helped to develop microfluidic devices for various applications, including inkjet printing, blood analysis, biochemical detection, chemical synthesis, drug screening/delivery, protein analysis, DNA sequencing, and so on. Microfluidics technologies could be divided into two main categories: continuous (often referred to as analogical) and droplet-based (digital) microfluidics. The droplet-based devices can be used for synthesis of materials on the micron scale for health care and pharmacy [1], synthesis of spheres, liposomes [2] and polymersomes [3, 4], or even self-assembled nanostructures [5]. Continuous-flow microfluidics is suitable for simple surface modification applications, such as generation of gradients for cell studies [6]. Within this microfluidic systems, the use of a co-flow allowed the controlled transport of chemical or biological substances, or even cells along the microchannels [7-10], the production of micro or nanostructures [1-5], detection of a biomolecule or cell of interest [11, 12], measurement of pressure [13] or droplet formation [14], among other applications.

The use of microfluidic devices that manipulate particles, biological or synthetic, had increased in last years, due to the reduced sample and reagent used, enhanced efficiency, shorter processing times, and various other advantages. Particles can be focused in either two-dimensional or three-dimensional. A 2D co-flow focusing normally indicates the horizontal focusing of particles to the center plane of a microchannel, where particles still scatter over the channel depth [15]. The translocation of two or more particles, in micro-flow cytometers, is the mayor problem when using two-dimensional focusing. These problems are not encountered in 3D focusing, where particles are focused simultaneously in both the horizontal and the vertical directions [16-18].

Our group had developed several applications in the field of microfluidics. Rodriguez-Trujillo et al developed a low-cost micro-Coulter counter; they incorporated hydrodynamic focusing, which provides high versatility and they were able to probe particles with a wide range of sizes with this novel device [19]. Afterwards, they modify the original design and proposed a micro-Coulter counter with a two-dimension and adjustable aperture; this modification enhanced the sensitivity and versatility of the system [20]. Castillo-Fernandez et al developed a high-throughput impedance flow cytometer; the system was used the count red blood cells and white blood cells, demonstrating an excellent discrimination performance under high-throughput conditions [10]. In the field of biomaterials and microfluidics, Castillo-Fernandez et al, studied the DNA transport through gels or polymers inside a microfluidic channel [21]. In our group the modification of substrates was also studied in order to generate gradients, Comelles et al used a microfluidic approach to obtain linear protein gradients relevant at the single-cell levels [6]. All the knowledge and experience gained along the past years, allow us to propose novel microfluidic devices with integrated biosensors for biomedical applications. And we are proposing lab-on-chip systems that exploit the co-flow phenomena to selectively modify the surface of biosensors in order to detect a biomolecule of interest. The co-flow and fluid dynamics allow us to control the surface that we are going to modify, as well as the detection range that we want to detect. Our goal is to develop a system easy to fabricate and use.

In this chapter, the design, fabrication and characterization of our novel microfluidic devices are explained. As theoretical background, the commonly used fabrication techniques are showed. As well as the physics involved in the development of microfluidic systems. Using the proposed dimensions of our devices, we calculated the most important fluidic characteristics: laminar flow regime, diffusion and fluid dynamics. We used these parameters to design and later improve the behavior of our device. Simulations were done in order to perform minor corrections. Finally, we characterized the fluidic performance of the fabricated devices;

2.1.1 Microfabrication technologies for microfluidics. Theoretical background.

2.1.1.1 Fabrication materials

Polymers.- Are the commonly used materials in microfluidics, since they can be employed along with replication technologies. Each polymer has different optical

characteristics, mechanical properties, biocompatibility and resistance against chemicals. The light, pressure, temperature or addition of a substance starts the polymerization process. The most popular polymer for microfluidic applications are polymethylmethacrylate (PMMA), polycarbonate (PC) and polydimethylsiloxane (PDMS) [22].

Photoresists.- The photoresists are a subclass of polymers used in the photolithographic technologies. A photochemical reaction of the resist material is triggered with irradiation, with electrons, ions, X-rays, UV or visible light. The photoresists can be used as a coating material, as sacrificial layer or as a master. There are two types of photoresists positive and negative. The positive photoresists are more soluble when they are irradiated; contrary in negative photoresist the polymer is less soluble (Fig. 2. 1). The irradiated or non-irradiated areas are removed with a developer [22]. There is also special type of photoresist with the capability of image reversal. These photoresists are commonly used in lift-off techniques and depending on the needed wall profile, they can be used as positive or negative.

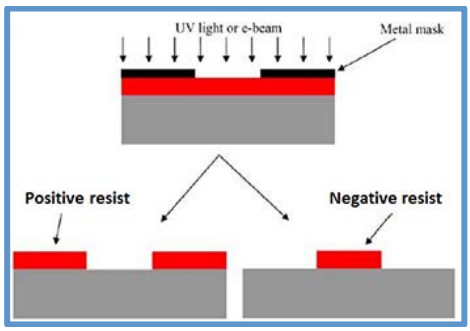

Fig. 2. 1 Positive and negative photoresists. The positive photoresists is more soluble when is irradiated while the negative resist is less soluble.

2.1.1.2 Replication technologies

The main advantage of using a replication technique in microfluidics is the low cost of fabrication. A master is usually fabricated once, being the most expensive part of the process, and then different polymer replicas can be done. The master could be fabricated with different technologies, allowing various geometries designs.

Master fabrication

Different techniques had been used for the fabrication of microfluidic masters; however we only focused on the more relevant for this field.

Micromachining.- Sawing, cutting, milling and turning, are some of the modern micromachining technologies, and are capable of producing molds with a minimum motif size of 10 µm [22] (Fig. 2. 2). One of the advantages is the wide range of materials, which can be machined. Silicon micromachining was one of the first techniques to be applied in microfluidics. However, silicon is not an ideal material for microfluidic devices, due to its optical opacity, cost and lack of biocompatibility. Nevertheless, silicon could be used perfectly as a master to replicate polymer substrates.

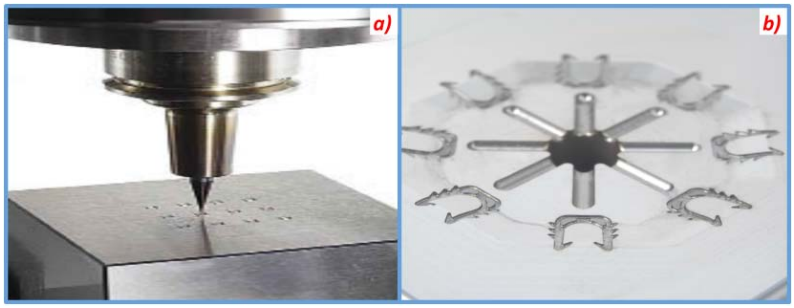

Fig. 2. 2 Micromilling machine [23] and medical staple mold [24] from MAKINO, one example of micromachining technologies used for the fabrication of masters.

Electroplating.- A photolithographic process, where a nickel or nickel alloy layer is coated with a photoresist, except for the areas to be electroplated. The structure is placed into a galvanic bath, and the metallic master starts to grow in the structure. Another fabrication technology to create high aspect ratio is the LIGA process, which is a type electroplating develop in early 1980s in the Karlsruhe Institute [25] (Fig. 2. 3). Sensitive Polymer photoresists are exposed to either a synchrotron radiation or a pulsed UV-light followed of a chemical removal of exposed (or unexposed) photoresist results in a three-dimensional structure which can be filled by the electroplating of a metal layer and finally separating the polymer from metal to get the master.

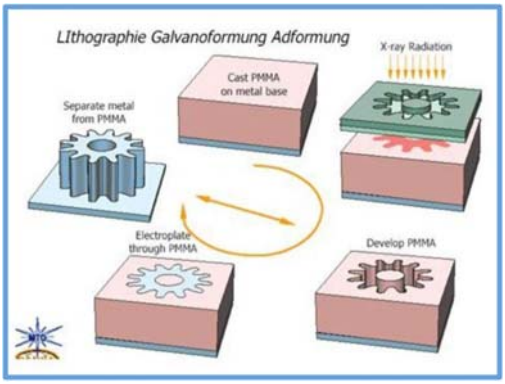

Fig. 2. 3 LIGA process. A piece of PMMA is exposed to X-ray, then with electroplating the master is created [26]

Injection molding

Polymer material in granular form is placed inside a cylinder; a screw is heated and starts melting the pellets (Fig. 2. 4). The polymer is push across the cylinder and at high pressure is injected into the cavity that contains the master structure. Two cooling process could be use; the mold could be kept below the solidification temperature of the polymer allowing a rapid fabrication technique. However, for smaller structures with high aspect ratio, the molding cavity with the master is also heated and the cooled separately, the main drawback is the time needed in this fabrication process due to the thermal cycles [22].

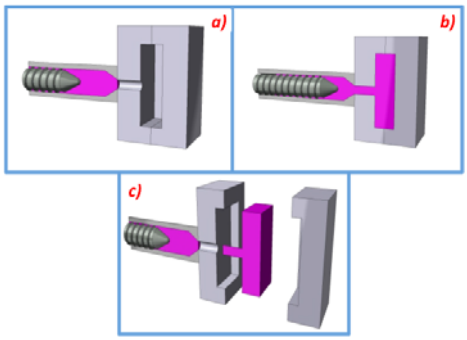

Fig. 2. 4 Injection molding process. Polymer beads are heated with a screw and then push into the mold cavity [27]

Soft lithography

Soft lithography is a technique widely used in microfluidics and spread by Whiteside's group [28]. The process is fast, less expensive and the material used is biocompatible. An elastomer and its curing agent, typically polydimethylsiloxane (PDMS), are mixed and then poured into a master. Usually, the master is a photoresist fabricated by a photolithographic technique. Once the liquid solution is cured, the polymer is peel-off revealing the replicated geometry (Fig. 2. 5). The replica could be bonded to a glass, silicon, or a electronic board [28].

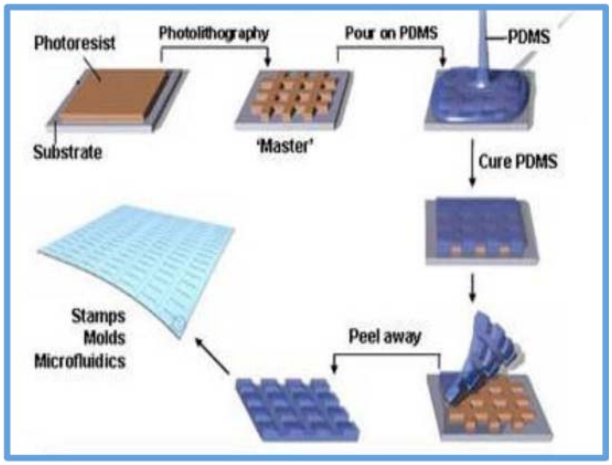

Fig. 2. 5 Soft lithography process. A master is fabricated with a photoresist, and then PDMS is poured on the master. And once cured is peel off [29]

2.1.1.3 Microelectrodes fabrication

Several microfluidic applications have the need to add microelectrodes to the final device. The commonly used fabrication methods include sputtering and thermal or electron beam evaporation (Fig. 2. 6). A photolithography process is performed prior the deposition, and a sacrificial layer is fabricated over a non-conducting substrate. Once the electrodes geometry is defined the metal deposition starts Finally, a lift-off technique is use to dissolve the sacrificial layer revealing the metal electrodes [22].

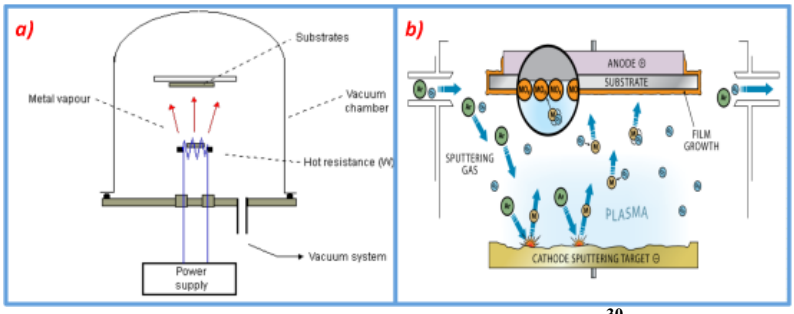

Fig. 2. 6 Microelectrode fabrication. a) Evaporation of metal [30] and b) sputtering[31]

2.1.1.4 Bonding techniques

Once the microchannels are fabricated on a substrate material a bonding process is necessary to close the open structures. Attention must be paid to avoid the closing of the channel or the modification of its geometry. Several methods can be used to close a microfluidic device.

Lamination.- A PET foil sheet with an adhesive layer is bonded to the microchannel with a heated roller (Fig. 2. 7). The adhesive layer melts to the replicated structure and then closing the channel. This technique is mainly used in the macroworld, since the adhesive, with a typical thickness of 5-10 μm, could close small channels. Besides

lamination, commercially available glue could be used to seal the channels, but this technique also has the problem of randomly blocking them [32].

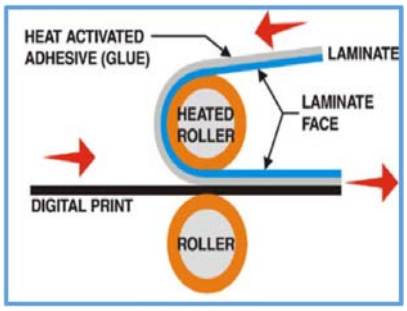

Fig. 2. 7 Lamination with a PET foil. The polymer is heated and pressed against the microchannel surface [33]

Plasma bonding.- By exposing a surface of a substrate to air or oxygen plasma, it became hydrophilic. The process starts by forming a superficial layer of oxygen, which increases the concentration of hydroxyl groups. These groups can react with a wide range of silanes. If two surfaces are treated with plasma then both reactive surfaces can be bonded irreversible [22] (Fig. 2. 8).

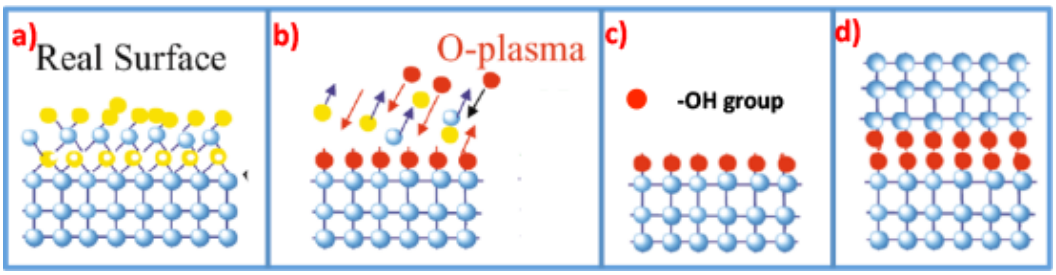

Fig. 2. 8 Plasma bonding technique. a) Surface of substrate b) Oxygen plasma applied to the substrate surface, c) The plasma generates hydroxyl groups, d) A second substrate, also treated with plasma, can be bonded

2.1.2 The physics of microfluidics. Theoretical background.

The design and fabrication of microfluidic devices is greatly affected by certain fluid phenomena presented at the microscale. The physical phenomena of the device must be perfectly understood and we must be aware of the dominant and most relevant laws in microfluidics: laminar flow, diffusion, fluidic resistance, surface area to volume ratio and surface tension are the more dominant effects in microfluidics [34].

Reynolds Number and Laminar flow

The transition from laminar to turbulent flow depends on different factors (geometry, surface, flow velocity, etc.). However, the relation between inertial and viscous forces has the greatest impact when characterizing the flow regime. The relation between both forces is called the Reynolds number [35]:

$$\mathrm{Re} = \frac{V_{avg} D_h}{\nu} = \frac{\rho V_{avg} D_h}{\mu} \qquad \text{(Eq. 2. 1)}$$

Where V_{avg} is the average flow velocity [m/s], D_h is the hydraulic diameter and depends on the geometry of the channel [m], $\nu = \rho/\mu$ is the kinematic viscosity [m^2/s], ρ is the fluid density [kg/m3] and μ is the fluid viscosity [kg/m·s]. Being the Reynolds number a dimensionless quantity. The hydraulic diameter can be obtained using the equation [35]:

$$D_h = \frac{4A}{P} \qquad \text{(Eq. 2. 2)}$$

Where A is the area of a cross section of the channel and P is the wetted perimeter. The most common types of geometries are circular, square or rectangle. For a circular channel the hydraulic diameter is equal to the diameter of the channel:

$$D_h = \frac{4A}{P} = \frac{4 \cdot \pi \cdot r^2}{\pi \cdot d} = \frac{4 \cdot (d/2)^2}{d} = d \qquad \text{(Eq. 2. 3)}$$

For a square microchannel, with a height equal to l, the hydraulic diameter can be obtained with:

$$D_h = \frac{4A}{P} = \frac{4 \cdot l^2}{4 \cdot l} = l \qquad \text{(Eq. 2. 4)}$$

And for a rectangular pipe, with a cross section with a length a and a height of b, the hydraulic diameter is:

$$D_h = \frac{4A}{P} = \frac{4 \cdot a \cdot b}{2 \cdot (a+b)} = \frac{2 \cdot a \cdot b}{a+b} \qquad \text{(Eq. 2. 5)}$$

In microfluidics systems the Reynolds number must be small, to work in laminar flow regime [36]. A laminar flow is obtained when the Reynolds number is smaller than 2300, a transition behavior between laminar and turbulent flow can be observed with a Reynolds number between 2300 and 4000. A totally turbulent flow regime is predicted when the Reynolds number is higher than 4000 [34].

The characteristics of a laminar flow are, smooth streamlines and a highly ordered motion [35]. The velocity profile in laminar flow is parabolic with a maximum at the centerline and minimum at the walls (Fig. 2. 9a), and can be expressed as:

$$u(r) = 2V_{avg}\left(1 - \frac{r^2}{R^2}\right) \qquad \text{(Eq. 2. 6)}$$

Where, R is the radio of the channel and r is the axis along the radio (Fig. 2. 9b). When working with a laminar co-flow the streams flow in contact with each other, and they only mix by diffusion.

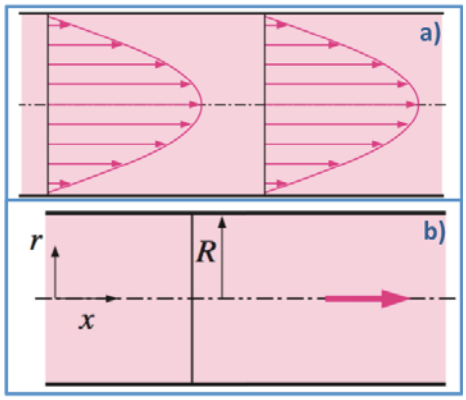

Fig. 2. 9 a) Fully developed parabolic laminar flow, b) diagram of a rectangular pipe with radius element *R* in fully develop laminar flow.

Diffusion in microfluidic systems

Diffusion is the process, by which a concentrated group of particles in a volume will, by Brownian motion, spread out over time so that the average concentration of particles throughout the volume is constant [34]. The distance that a particle diffuses into a less concentrated solution is given by the expression:

$$x^2(t) = 2Dt \qquad \text{(Eq. 2. 7)}$$

Where D is the diffusion coefficient of the particle and t is the time. Diffusion is important at the microscale due to the fact that the distance varies to the square power. The diffusion coefficient could be obtained practically, and some coefficients for typically used particles could be found on literature. However, this coefficient can be calculated by the Stokes-Einstein equation:

$$D = \frac{kT}{6\pi r\mu} \qquad \text{(Eq. 2. 8)}$$

Where T is the absolute temperature, r is the radius of the particle and μ is the fluid viscosity.

The diffusive mixing time of a co-flow microchannel, is given by the equation:

$$\tau \approx \frac{w^2}{D} \qquad \text{(Eq. 2. 9)}$$

Where w is the width of a cross section of the channel and D is the diffusion coefficient. The mixing of two fluids as a function of the channel length can be also predicted too. The length necessary for a complete mixing, considering a cross section of width w, height h, flow rate Q and a diffusion coefficient D, is [36]:

$$L \approx \frac{Qw}{hD} \qquad \text{(Eq. 2. 10)}$$

Hydrodynamic resistance

Since the microfluidic devices usually have complex geometries, it is rather useful to know the resistance in order to determine the behavior of the flow in each branch. The flow rate in a microchannel is given by the expression:

$$Q = \frac{\Delta P}{R} \qquad \text{(Eq. 2. 11)}$$

Where, Q is the total flux, ΔP is the pressure drop across the channel and R is the channel resistance. The resistance of a circular pipe can be calculated using [35]:

$$R = \frac{8\mu L}{\pi r^4} \qquad \text{(Eq. 2. 12)}$$

Where, μ is the fluid viscosity, L is the length of the channel and r is the radio of the channel. For a rectangular microchannel with a low aspect ratio (h≈w), the resistance is [35]:

$$R = \frac{12\mu L}{wh^3}\left[1 - \frac{h}{w}\left(\frac{192}{\pi^5}\sum_{n=1,3,5}^{\infty}\frac{1}{n^5}\tanh\left(\frac{n\pi w}{2h}\right)\right)\right] \qquad \text{(Eq. 2. 13)}$$

Where, w is the channel width and h is the height. For a rectangular microchannel with a high aspect ratio (h<<w) the expression is reduced to [35]:

$$R = \frac{12\mu L}{wh^3} \qquad \text{(Eq. 2. 14)}$$

2.1.3 Fluid dynamics

Analysis and prediction of focusing behavior using the fluidics equivalent of Ohm's law, $\Delta P = QR$, dependent on the fluid velocity profile [37].

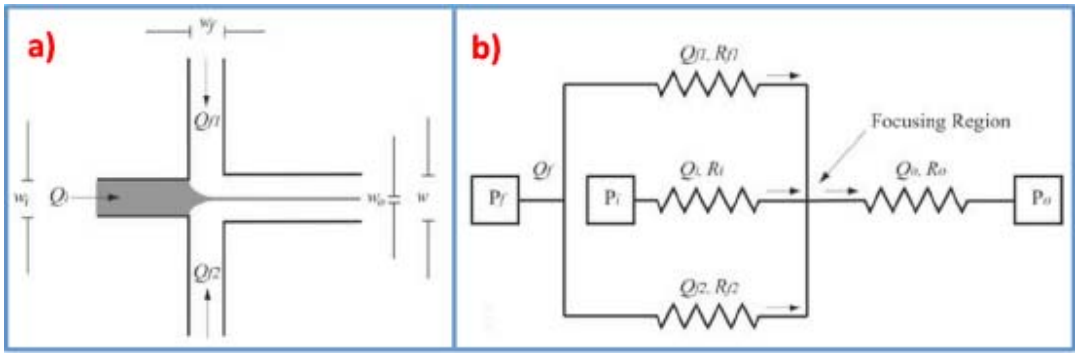

Fig. 2. 10 a) Illustration of flow focusing and b) Analogous circuit used to design and analyze the focusing network of a).

The width of the focused fluid can be predicted when the inlet flow rates are fixed and it can be approximated by a ratio between both flows [37]:

$$\frac{w_0}{w} = \frac{1}{g(\lambda)} \frac{Q_i}{Q_i + Q_f} \qquad \text{(Eq. 2. 15)}$$

Where w is the width of the channel, w_0 is the focused width, Q_i is the focused flow rate and Q_f is the focusing flow rate. The $g(\lambda)$ is a correction factor, when using a square channel, and it is dependent of the channels' dimensions. This factor should be used only when $h<<w$, otherwise $g(\lambda)$ is equal to 1. The factor depends on the ratio $\lambda=h/w$, where h is the height of the channel, and it can be obtained as [38]:

$$g(\lambda) = (1+\lambda^2)(1-1.3553\lambda+1.9467\lambda^2-1.7012\lambda^3+0.9564\lambda^4-0.2537\lambda^5) \qquad \text{(Eq. 2. 16)}$$

2.2. Materials and methods

The first microfluidic device or lab-on-chip was designed by us to do an "in-situ" selective functionalization of its microelectrodes, by exploiting laminar co-flow. The co-flow and fluid dynamics allow us to control the surface that we are going to modify. We desired to develop a system easy to fabricate and use, with surface modification capabilities and a simplified read-out system.

The second device was designed to do multiple sensing, also selectively functionalizing the electrodes with different biomolecules using a laminar co-flow. We wanted to do a microfluidic control and multiplexing in order to study the interaction and cross talk between biomarkers. Nowadays, several biomarkers are being studied for different diseases, and we wanted to prove that with our device we were able to detect simultaneously more than one biomarker for a biomedical application.

The device design process starts with the calculation of the Reynolds number for both devices to determine the range for working in laminar flow regime. We calculated first the hydraulic diameter. The next parameter is the velocity profile. Finally, to calculate the Reynolds number we need the kinematic viscosity, several studies had been performed on this subject. And for a water-based solution, like the ones used in our protocols, we have a value depending on the temperature: $1.004x10^{6}$ [m^2/sec] @ 20ºC, $0.658x10^{-6}$[m^2/sec] @ 40ºC [39].

Another phenomenon that we had to consider was the diffusion, since we are working with a laminar co-flow. The diffusion could affect the performance of our device by contaminating the surface of the electrodes that we do not want to functionalize. Two parameters about diffusion where studied: the necessary length to achieve mixing of two solutions, and the diffusion length of one solution into another as a function of time.

2.2.1 Fabrication of the microfluidic devices

With the devices already designed, according with the specific physics requirements, then we proceeded to the fabrication of the devices. The fabrication process of the devices can be divided in three main steps: microchannels molding, electrodes fabrication and LOC bonding. First a photolithographic technique was used to build a mold on top of a glass substrate and poly dimethylsiloxane (PDMS) was cast molded to fabricate the microchannels. For the fabrication of the microelectrodes a lift-off process was applied, after the evaporation of gold over a glass surface. Finally to seal to channels with the biosensor a plasma bonding technique was used. Detailed description of the different steps follows.

2.2.1.1 Microchannels fabrication

The masters were fabricated on top of glass slides (Deltalab) using a negative photoresist (SU-8 10, Microchem). A cleaning protocol based on chemical baths was performed on the slides, starting with an acetone treatment, followed by an isopropanol, ethanol and finally pure water rinsing; each treatment lasted 5 minutes (Fig. 2. 11). A posterior cleaning stage, consisting in a surface activation of the glass with plasma cleaner (PDC-002, Harrick Scientific Corporation), was also applied. The slides were placed over the vacuum chamber, with the clean surface facing upwards (Fig. 2. 11). Vacuum was applied for 2 minutes, with all valves perfectly closed. The oxygen valve

is open and closed several times, once vacuum is completed, so the oxygen enters correctly. This step lasted 1 minute. The glass surface was subjected to 10.15W of plasma power for 10 minutes to improve photoresist adhesion. Finally, the slides out of the chamber were heated for 30 minutes at 200 ºC in a final step before placing the photoresist on top of the glass.

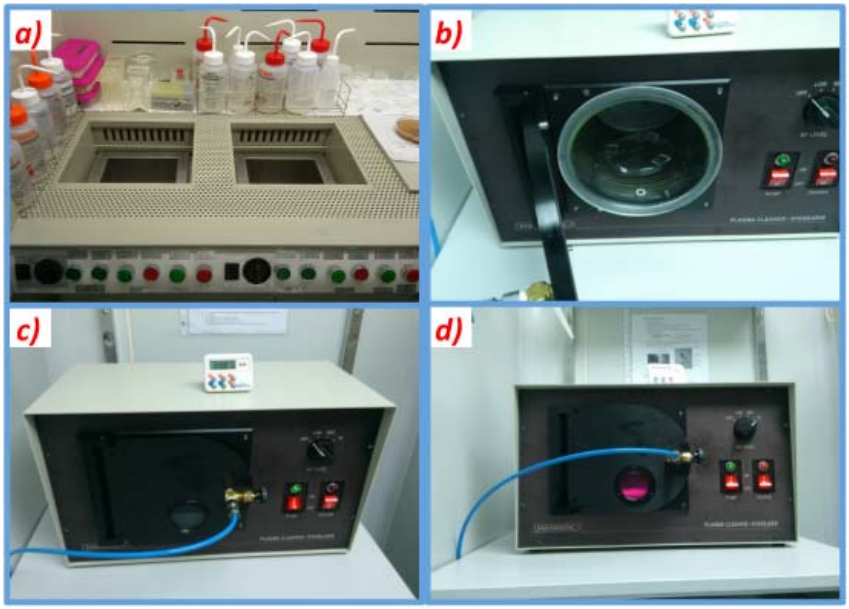

Fig. 2. 11 a) Chemical baths, b) The substrates are placed on the plasma cleaner, c) Vacuum is applied to the plasma cleaner, d) The plasma is activated.

With the slides all cleaned a photolithographic process were performed, a 30-µm high SU-8 10 (MicroChem) was spun over the glass slides. Starting by pouring 1 ml of the photoresist onto the slides and following with a two-step spinning protocol. The slides were spun for 5 seconds at 500 rpm and then at 1200 rpm for 30 seconds. They were subsequently placed on a hot plate at 95 ºC for 5 minutes. The selective exposure of the SU-8 was made with a MJB4 aligner from SÜSS Microtec. The slides were subjected to 345 nm illumination with 21 mW/cm^2 power for 5 seconds (Fig. 2. 12). They were then post-baked at 95 ºC for 5 minutes and left to cool for up to 2 hours before developing. The desired microchannel mold was finally obtained using a SU-8 developer from MicroChem (Fig. 2. 12).

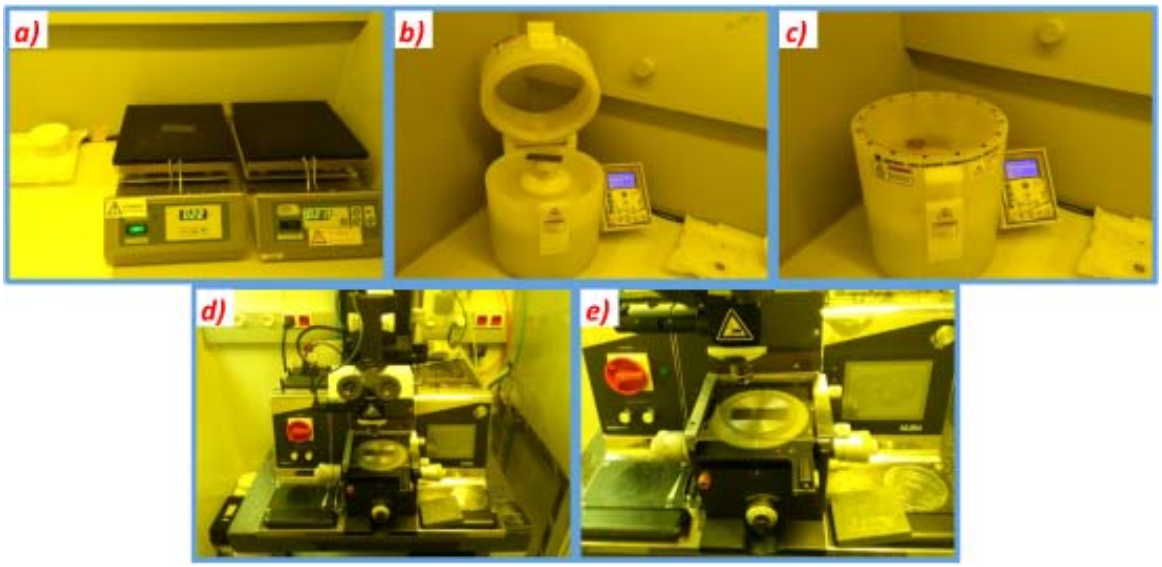

Fig. 2. 12 a) Pre-bake of the sample, b-c) Spinning of the photoresist on the substrate, d-e) Exposure of the samples

With the masters fabricated is time to replicate them, with a polymeric solution, in order to get the microchannels. The PDMS pre-polymeric solution was mixed with its curing agent (Sylgard®184, Dow Corning) at a ratio of 10:1. The mix was placed in a desiccator and vacuum was applied in order to remove bubbles. Later, 20 g of PDMS was poured onto the SU-8 master and placed under vacuum for 15 minutes. Placing the masters with PDMS inside an oven at 75 ºC for 30 minutes performed curing (Fig. 2. 13). The casted PDMS was peeled off from the master and inlet and outlet holes were made using a Harris Uni-Core 0.8-mm puncher (Ted Pella).

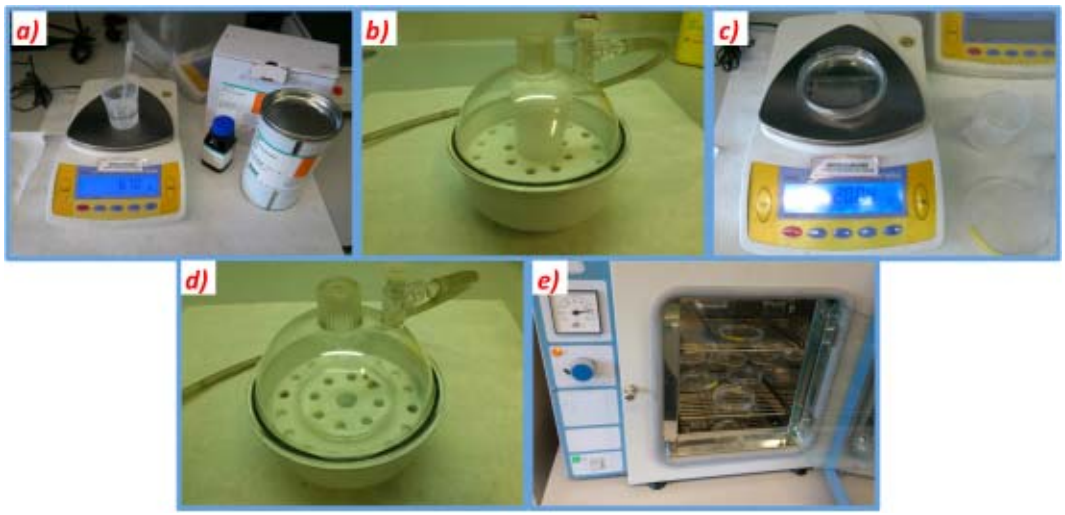

Fig. 2. 13 a) The pre-polymeric solution is weighted and mixed, b) The mixed solution is placed on vacuum to eliminate bubbles, c) The PDMS is poured over the masters, d) Vacuum is applied to the masters, e) The polymer is cured by temperature

2.2.1.2 Biosensor Fabrication

The biosensors were fabricated over a glass slides. Glass substrates were cleaned with Piranha solution. The slides were placed on a glass petri dish with piranha and were cleaned by immersion for 15 minutes. After, the slides were rinsed with water and placed on a vertical staining jar full with water. Finally, the substrates were dehydrated in an oven for 30 minutes at 200ºC.

The AZ 1512 (AZ Electronic Materials) photoresist was chosen to act as a sacrificial layer and, as in the case of the SU-8 10, it was spun in order to achieve a thickness of 1µm. The protocol consisted of three spinning steps: 3 seconds at 300 rpm, 6 seconds at 600 rpm, and finally 30 seconds at 4000 rpm. A baking step followed and the spun AZ 1512 was heated at 95ºC for 1 minute and 10 seconds using a hotplate. Patterning of the sacrificial layer was performed by aligning the corresponding electrode mask to the spun glass slides and applying 26mW/cm^2 of UV light for 10 seconds (Fig. 2. 14). One hour later, the glass substrates were immersed in an AZ developer (AZ 726, AZ Electronic Materials) pool for 10 seconds and rinsed with pure water. After exposure and first development of the AZ 1512, two metal layers were vapor-deposited onto the surface. An initial layer of titanium with a height of 10 nm was covered by a second layer of 80 nm gold. The photoresist sacrificial layer and the metal deposited over it were removed in a final sonicating step in the presence of AZ 100 Remover (AZ Electronic Materials). After this lifting-off process, the final design of the biosensor electrodes was unveiled.

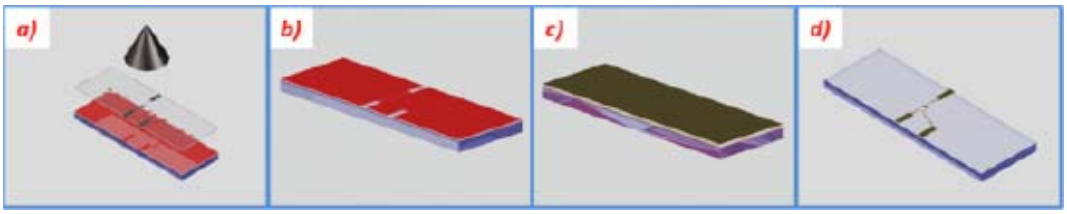

Fig. 2. 14 a) The photoresist is exposed, b) The un-polymerized photoresist is rinsed, c) Metal deposition over the samples, d) Lift-off to reveal the microelectrodes

2.2.1.3 Lab-on-a-Chip Bonding

Once the PDMS replica and the microelectrodes had been produced, the LOC microfluidic channels were sealed and defined by means of a bonding process. As in previous processes, a deep cleaning procedure was initially applied to both parts: the cover and the microchannels. This procedure again comprised a combination of chemical rinses and oxygen plasma. Oxygen plasma surface activation was applied for

15 seconds at a power of 10.15 W. PDMS channels were finally aligned and attached by contact to the glass substrate containing the electrodes to form an irreversible bond (Fig. 2. 15). The complete LOC device was finished by connecting and cold-soldering a cable to each pad. The welding of cable and pad was achieved by applying conductive silver paint (RS 186-3593, RS Components), which acted as a connective soldering glue. The soldered pads were left to dry at room temperature for 30 minutes. An epoxy glue mix (RS 406-9592, RS Components) was also applied later and left to cure at room temperature for a further 60 minutes to increase the mechanical properties of the bond.

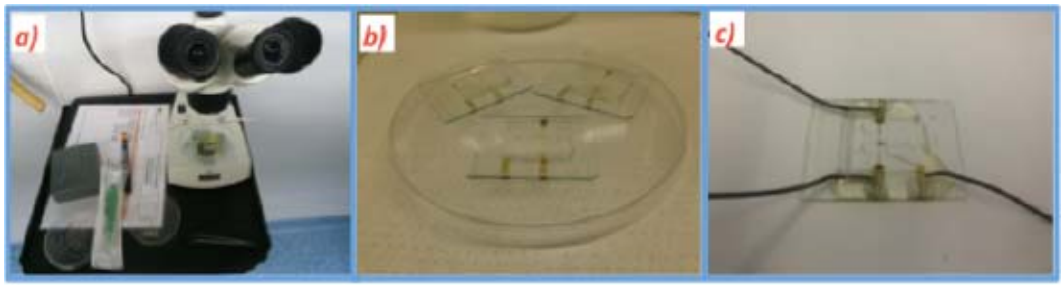

Fig. 2. 15 a) The microchannels and microelectrodes are aligned, b) The LOC is irreversible bonded, c) Cables are welded to each pad

2.3 Results and discussions

2.3.1 Microfluidic devices design

To design our device we studied the devices developed in our group, in order to understand the microfluidic behavior and adapt the previous knowledge in our application.

We started with the work presented by Rodriguez-Trujillo et al, where they developed a micro-Coulter counter with hydrodynamic focusing [19]. They fabricated their microchannel in PDMS with a height of 50 μm and a width of 190 μm for all the channels. They fix the inlet flow from the lateral channels at 10 μl/min and changed the main flow between 0.1 and 20 μl/min (Fig. 2. 16).

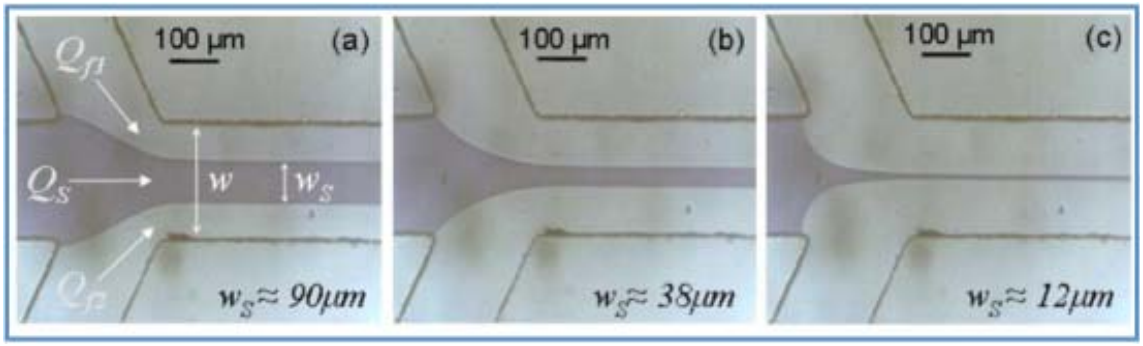

Fig. 2. 16 Optical microscope images showing the effect of the hydrodynamic focalization [19].

We wanted to propose a novel device with similar hydrodynamic behavior but with an easier set-up for a biomedical application. And instead of having a central focusing we wanted a lateral focusing, to modify only a specific region of the channel. Like the device presented by Rodriguez-Trujillo et al, we wanted to incorporate microelectrodes, changing their layout and use them as biosensors.

Therefore we thought in reducing the inlets, we also wanted to give flexibility to the system and use it with either two pumps or only one pump. With two pumps we need to "push" the fluid in the inlets and we could characterize the hydrodynamic behavior of the device and the width of the focalization like the work presented by Rodriguez-Trujillo. And with the use of one pulling single pump we depend on the geometry of the channels; the channels must have different resistance in order to functionalize only one region of the channel, like the work proposed by Stiles et al [37]. The novel device proposed is shown of Fig. 2. 17.

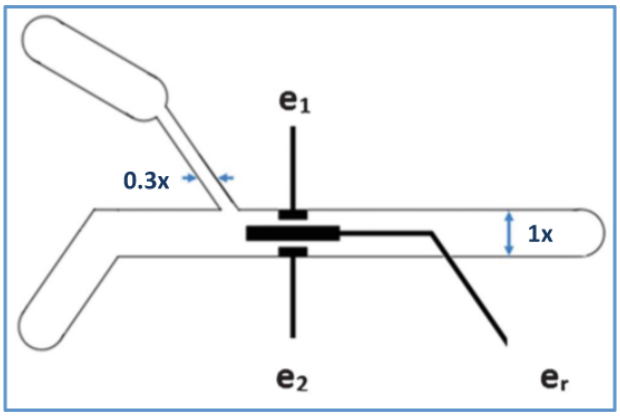

Fig. 2. 17 Layout of the proposed microfluidic device. We proposed a device with two microchannels with different microfluidic resistances (1x and 0.3x) to functionalize only a third of the channel. We also propose a set of microelectrodes and connect them in differential mode and use them as biosensors.

Our set-up was designed to work on laminar flow regime and the Reynolds number was calculated to get the suitable working flow rates. However, we need to get

the variables needed to calculate the Reynolds number, starting with the hydraulic diameter. Since we used the fabrication protocols use in our group [20, 38], for a height we assume 30 μm, and we propose a width of 1000 μm in order the fit the set of microelectrodes. Substituting the values of our device in Eq.2.2:

$$D_h = \frac{4A}{P}$$
$$D_h = \frac{4 * Width_{channel} * Height_{channel}}{2(Width_{channel} + Height_{channel})}$$
$$D_h = \frac{4 * (1x10^{-3}) * (30x10^{-6})[m^2]}{2 * (1x10^{-3} + 30x10^{-6})[m]}$$
$$D_h = 5.8x10^{-5}[m]$$

We had a hydraulic diameter of 58 μm. The next step is to calculate the velocity profile with the simplified equation (Eq.2.6). Reaching a maximum velocity at the centerline r = 0:

$$u(r = 0) = 2V_{avg} \qquad \text{(Eq. 2. 17)}$$

For our device, we assume that a bio-particle travels in the centerline and reaches maximum velocity (Eq. 2.17). The bio-particle is suspended usually in a water solution, and the liquid should flow and fill the whole channel when introduced with a syringe pump. With a given input flow we could obtain the needed time to fill the channel and therefore the time needed for the particle to reach the end. With the time and the length of the whole channel we could approximate a maximum velocity and after get the average velocity. And with the kinematic viscosity we could get the Reynolds number for each flow and even get the limits for laminar and turbulent flow with our device.

As an example let's assume that a solution of water is introduced in our microfluidic system with an input flow of 10 μl/min, let's calculate the Reynolds number under these conditions and determine if the device is working in laminar or turbulent flow regime. First we need to know the volume of the device, and the approximated value is:

$$V = 4.8x10^{-10}[m^3]$$

Then we can express our flow in cubic meters per second:

$$Q = 10[\mu l/\min] = 1x10^{-8}[m^3/\min]$$
$$Q = 1.7x10^{-10}[m^3/seg]$$

The time needed to fill the whole channel is easily calculated with:

$$t = \frac{V}{Q} \qquad \text{(Eq. 2. 18)}$$

$$t = \frac{4.8x10^{-10}[m^3]}{1.7x10^{-10}[m^3/seg]}$$
$$t = 2.9[seg]$$

We know that the total length of the channel is 0.01144 [m]. Thus, we can get the maximum and average velocities, by substituting in equation 2.17:

$$u = \frac{d}{t} \qquad \text{(Eq. 2. 19)}$$

$$u = \frac{1.1x10^{-2}[m]}{2.9[seg]}$$
$$u = 3.9x10^{-3}[m/seg]$$
$$V_{avg} = 1.9x10^{-3}[m/seg]$$

Finally, to calculate the Reynolds number we need the kinematic viscosity, several studies had been reported in the literature about this subject. For water we have a value depending on the temperature: $1.004x10^{6}$ [m^2/sec] @ 20ºC, $0.658x10^{-6}$[m^2/sec] @ 40ºC [39]. By substituting the values calculated so far on equation 2.1, the Reynolds number for our device, for a water solution at 20ºC:

$$\mathrm{Re}(t = 20^{o}C) = \frac{V_{avg} * D_h}{\nu_{water}(t = 20^{o}C)}$$
$$\mathrm{Re}(t = 20^{o}C) = \frac{(1.9x10^{-3}[m/seg]) * (5.8x10^{-5}[m])}{1.004x10^{-6}[m/s]}$$
$$\mathrm{Re}(t = 20^{o}C) = 0.115$$

And for a temperature of 40ºC:

$$\mathrm{Re}(t = 40^{o}C) = \frac{V_{avg} * D_h}{\nu_{water}(t = 40^{o}C)}$$

$$\mathrm{Re}(t = 40^{o}C) = \frac{(1.9x10^{-3}[m/seg]) * (5.8x10^{-5}[m])}{0.658x10^{-6}[m/s]}$$

$$\mathrm{Re}(t = 40^{o}C) = 0.176$$

For both temperatures at flow rate of 10 µl/min our device works on a laminar flow regime. It is interesting to know the limits of our LOC, when working in laminar flow. For that reason, we calculated the Reynolds number as a function of input flow. Later we will explain the different solutions used for the functionalization protocols, and most of them are water-based solutions, and for that reason we used the dynamic viscosity of water when calculating the Reynolds number. Since the devices are designed for a biomedical application, we considered the temperature range between 20 and 40 ºC. The Reynolds number as a function of input flow is showed on Fig. 2. 18.

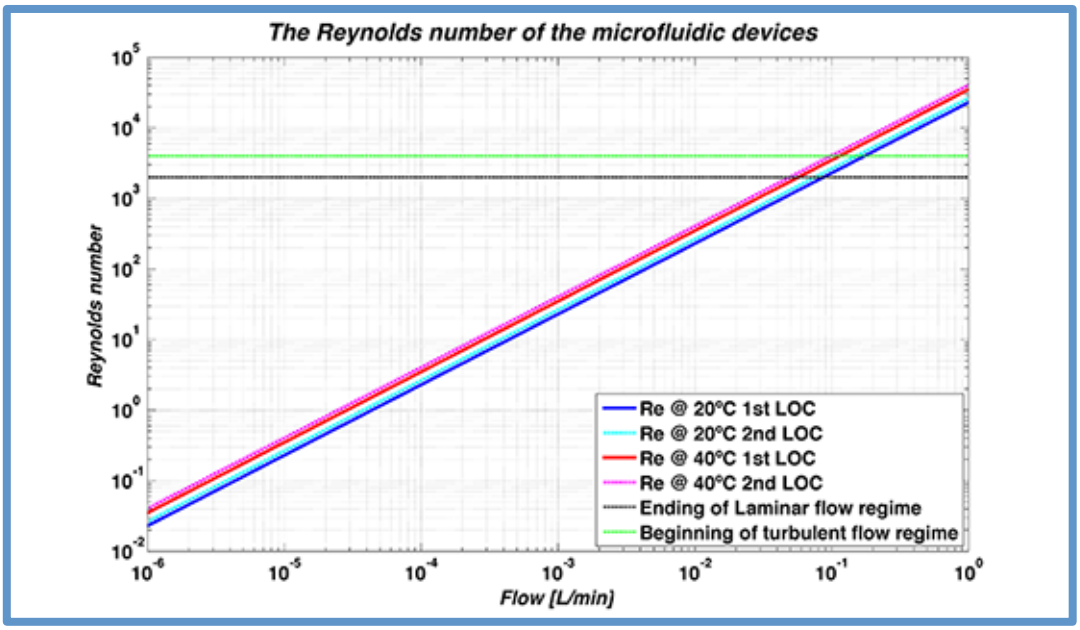

Fig. 2. 18 Reynolds number for our devices at 20ºC and 40ºC. The black line represents the transition between laminar and transitional flow. The green line represents transition to turbulent flow

The flow rates selected for all detection and characterization protocols are between 3 and 20 µl/min, the device has a laminar regime behavior according with the Reynolds number in that range (Fig. 2. 18). In order to change into a turbulent regime the input flow must be higher than 100 ml/min. One of the advantages of using low input flows is that the solution needed for detection is reduced. With our protocols, the

functionalizing solutions usually flow at 6 µl/min; with a maximum time of 60 minutes. Therefore, the maximum amount of reagents needed was 360 µl.

Two parameters about diffusion were studied: the necessary length to achieve mixing of two solutions, and the diffusion length of one solution into another as a function of time. We are proposing an "in-situ" surface modification protocol of the active area of the electrodes. The protocol is based on the interaction between biotin and avidin molecules; in order to form a self assembled monolayer on top of a conducting surface. The protocol selected is going to be explained in more detail on the next chapters. However, since we chose that deposition method, we are going to study the diffusion of biotin and streptavidin solutions into water-based solutions. Now considering the dimensions of our LOC, w = 1mm and h = 30 µm, and the diffusion coefficient of biotin and streptavidin, the length necessary for mixing is calculated by changing the input flow (Fig. 2. 19) in equation 2.10.

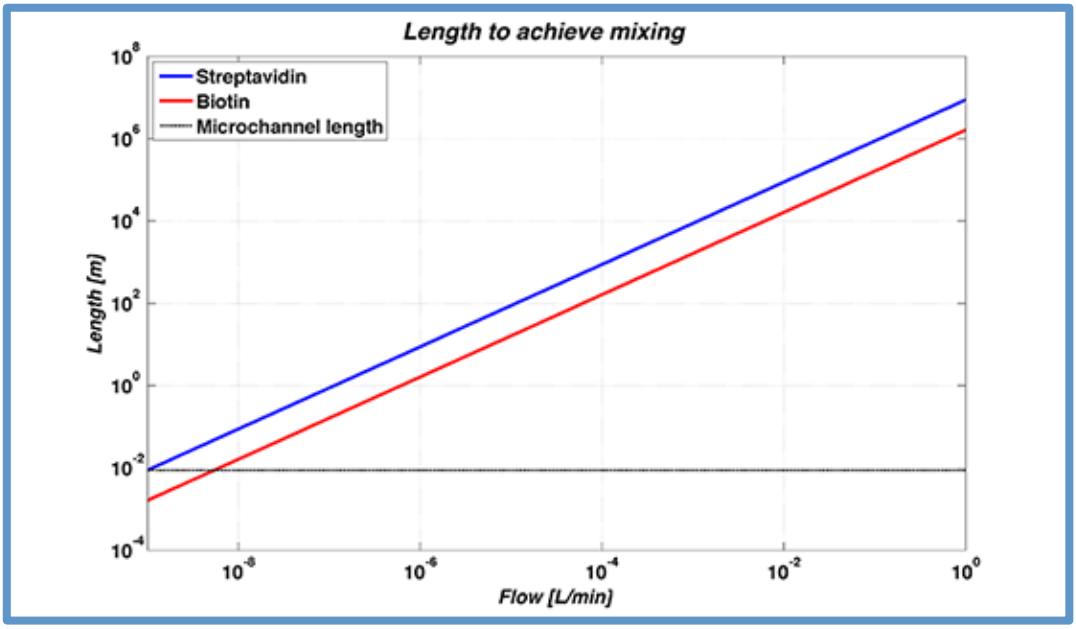

Fig. 2. 19 Mixing length as a function of input flow. The doted black line represents the total microchannel length of our device.

Once again let's focus on the flows proposed for our experimentation. At 20 µl/min, the length necessary to achieve mixing must be at least 1 meter for a biotin solution and 10 meters for a streptavidin solution. And since our device has a total length of 8.8 mm, with the selected flows we won't get a mixing between the buffer and the functionalizing solution. However, with the geometry of our device we can get a mixing between solutions and that can be done by decreasing the input flow. For a solution of biotin and buffer the mixing is reached with flows around 5 nl/min and for

streptavidin with flow lower than 1 nl/min. The diffusion is a phenomenon that depends on the time, we can't achieve a complete mixing with the selected flow for experimentation, but we could get a partial mixing or regions were the biomolecule starts to diffusing into the other solution.

To study the partial mixing of a biomolecule as a function of time, we used the Brownian motion equation related to diffusion length (equation 2.7). To calculate this length we used the average velocity from our Reynolds number calculations, and we related the velocity with the length of the channel and the time. For a given input flow, we know the theoretical diffusion length at a specific distance of the channel length (Fig. 2. 20).

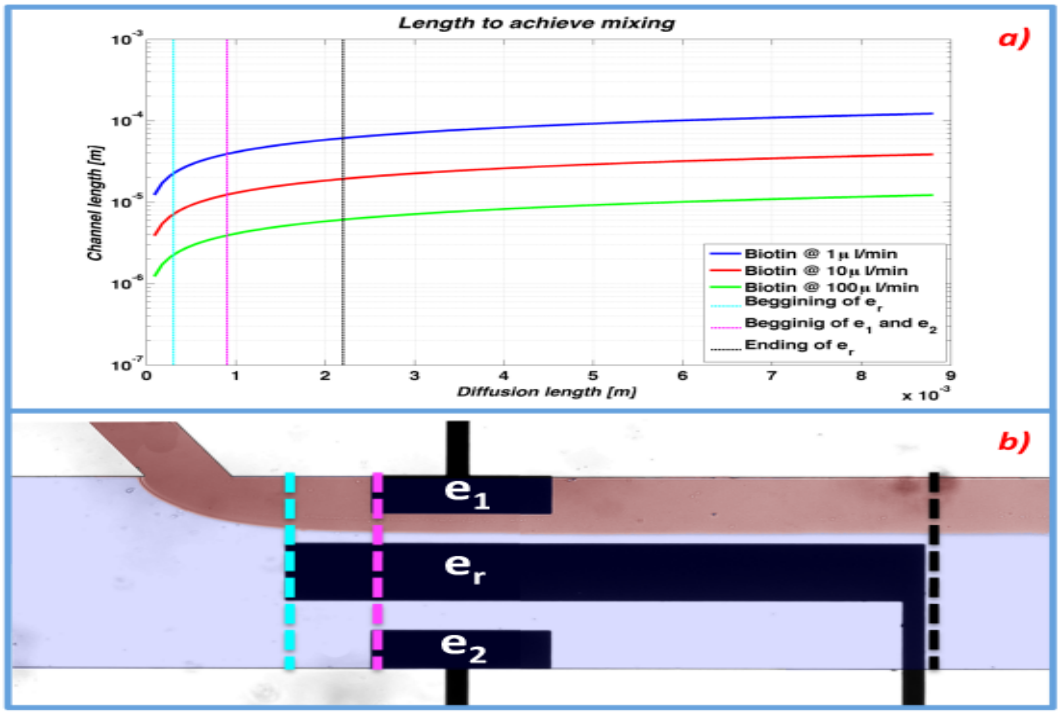

Fig. 2. 20 Diffusion length for biotin solutions. Three critical zones are defined, the starting of the channel (dotted cyan line), the beginning of the smaller electrodes (dotted magenta line) and the end of the electrodes (dotted black line)

As the diffusion coefficient depends on the size of the particle, the smaller the particle the greater the diffusion length, and for that reason we only calculated the length for a biotin solution, since is smaller than streptavidin. Biotin solution could give us the minimum requirements for our set-up. As expected the lower the flow the greater the diffusion length, that is explained because the solutions are more time in contact.

With a flow of 1 µl/min we had a diffusion length of 122 µm at the end of the channel, therefore with the selected flows we don't expect to have a contamination due

to diffusion phenomena. The input flow is the addition of the lateral and the main flow, to achieve the selective functionalization a characterization of the fluid dynamics were also performed, and will be explained later on this chapter.

All the theoretical analysis helped to select the dimensions of our devices as well as the flows. On Fig. 2. 21 the layouts of the novel microfluidic devices are shown.

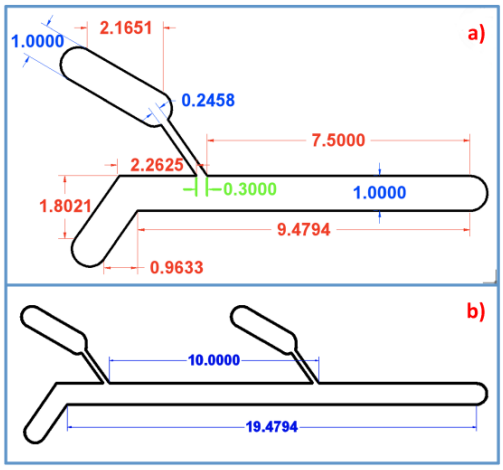

Fig. 2. 21 a) Microfluidic device proposed for hydrodynamic focusing and selective functionalization for single detection, b) Microfluidic device proposed for the detection of multiple analytes with hydrodynamic focusing.

2.3.2 Characterization of the dimensions of the fabricated devices

A profilometer (DEKTAK 6M, Veeco Instruments) was used to characterize the dimensions of microchannels replicas and masters, and microelectrodes, the height and width was measured. However, when doing the measurements for the electrodes, we must be very careful with the applied force to avoid scratching the gold from glass. An interferometer (WYKO NT1100, Veeco Instruments) was also used to measure the dimensions of the channels (masters and replicas). Finally, for the electrodes a microscopic (Eclipse L150, Nikon Instruments Inc.) image was acquired.

With the profilometer we focused on two different places, the main channel and the lateral channel. The widths of both places were measured as well as the height. We characterized a batch of 10 fabricated devices and measurements were performed. SU-8 masters and PDMS replicas were analyzed. The data acquired was processed with Matlab and the results are shown on Fig. 2. 22.

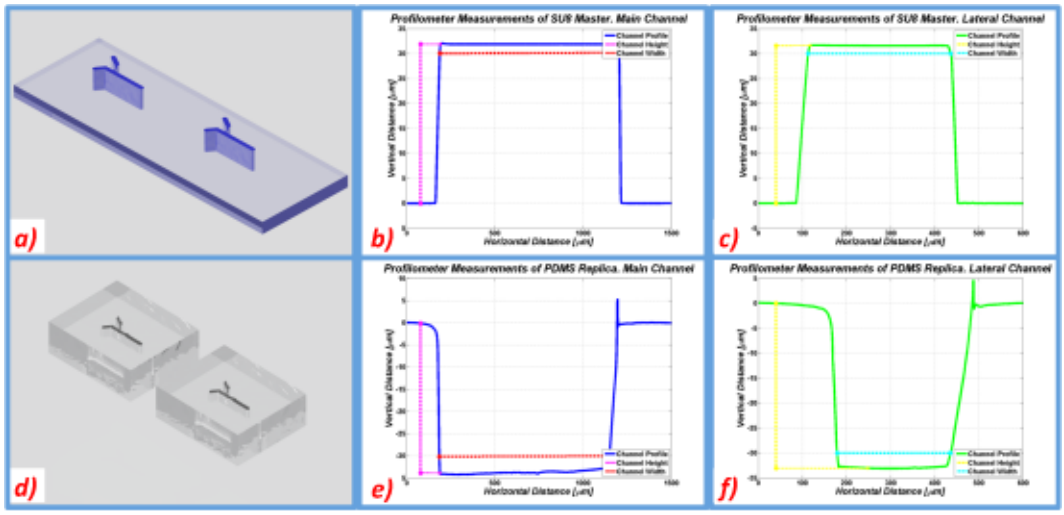

Fig. 2. 22 a-c) Characterization of the dimensions of the SU-8 masters with a profilometer, d-f) Characterization of the dimensions of the replicated microchannels with a profilometer. The blue line corresponds to the main channel and the green line corresponds to the lateral channel.

The results are summarized on the Table 2. 1.

Table 2. 1 Dimensions of the characterized devices

Sample	Lateral Channel		Main Channel	
	Height [µm]	Width [µm]	Height [µm]	Width [µm]
SU-8 Master	26.9 ± 4	300.1 ± 6	26.5 ± 2	1058.2 ± 3
PDMS Replica	27.7 ± 5	274.7 ± 5	27.5 ± 2	1014.5 ± 6

The height in both, master and replica, are similar and had a medium error of approximately 10%, according with the desired height of 30 µm. The width of the SU-8 is greater than the width of the PDMS replicas, that‘s because the PDMS is a polymer and when cured show shrinkage. The SU-8 masters were also characterized with the interferometer. This characterization was performed to corroborate the results obtained with the profilometer, and as expected the results were very similar. However, with the interferometer we can get a 3D image of a given surface of the masters or replicas. The measurements performed with the interferometer for the SU-8 master are shown on Fig. 2. 23.

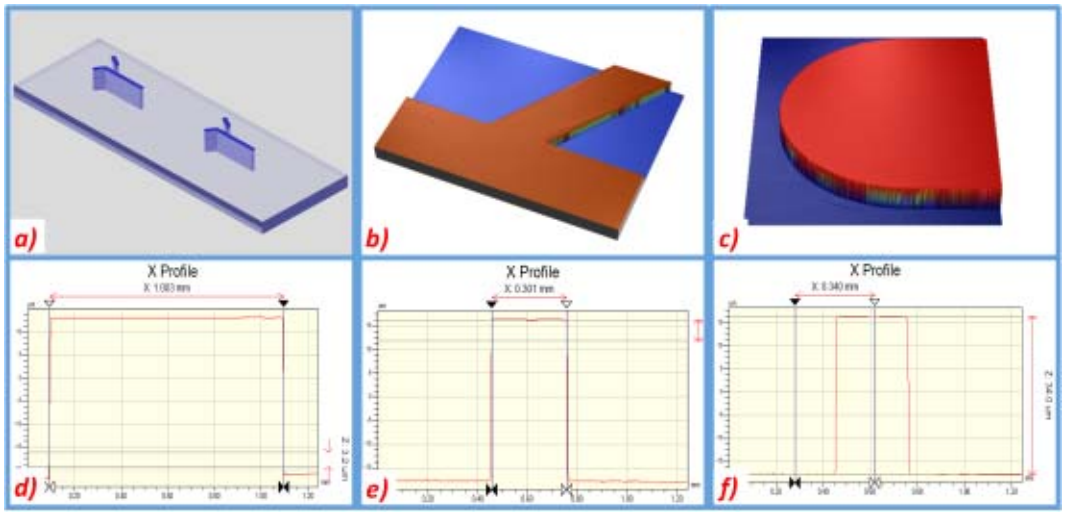

Fig. 2. 23 Characterization of the dimensions of the SU-8 masters using an interferometer.

As mention before, due to the PDMS shrinkage, the replicas were smaller in width than the masters. Nevertheless, the geometry of the channel wasn't affected as it can be seen on Fig. 2. 24. Despite the shrinkage, the microchannels kept a rectangular structure (Fig. 2. 24).

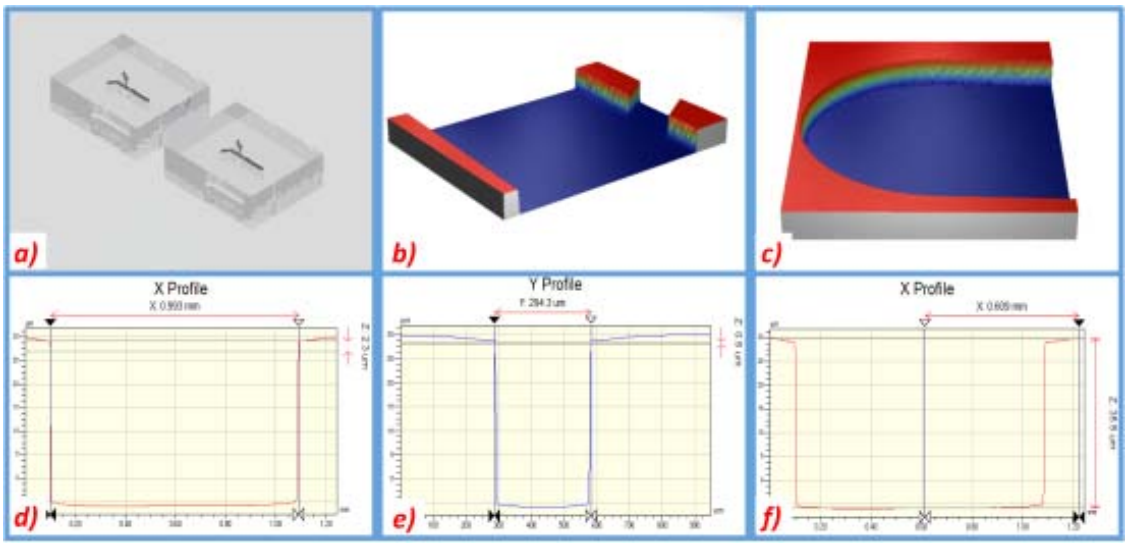

Fig. 2. 24 Characterization of the dimensions of the PDMS replicas using an interferometer.

The characterization of the electrodes was done optically. The electrodes were placed on a microscope and the connections were observed. During the lift-off process is common to damage the electrodes paths and a short circuit could be presented. Therefore, this characterization helped to discard to electrodes that were damage during the fabrication process, which approximately were a 10 % of every fabricated batch (Fig. 2. 25).

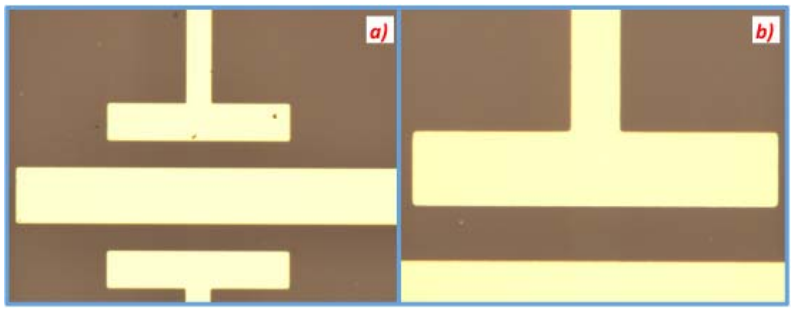

Fig. 2. 25 Microscopic images of the microelectrodes. All the pathways were checked to avoid short circuits

2.3.3 Fluid dynamics

The behavior of the fluid dynamics in the first device was characterized by modifying the input flows. Two solutions were used, an un-dyed and a red-dyed phosphate buffered saline solutions (PBS, Sigma Aldrich, P4417). A clear difference between both liquids could be observed by optical inspection. In the set-up a flow was maintained in the main channel input (10, 20 and 40 µl/min) while a swept flow was applied to the lateral channel. Different ratios between both flows were defined (30, 25, 20, 15, 10, 5, 3 and 2) and lateral flow was applied accordingly. A simulation was done, prior the experimental characterization, with COMSOL multiphysics (COMSOL Inc, Palo Alto, CA, USA) using the values defined for the layouts. The results, simulation and experimental, were compared with theoretical values. The fluid dynamics of the second device was also characterized.

The devices used to control the microfluidic flow at the inlets and to perform the fluid dynamics characterization were two syringe pumps: KDS-101 from Kd Scientific. For the practical measurements and image acquisition, an inverted microscope from Olympus (IX71) with an integrated CCD camera was employed.

In order to characterize the width of the co-flow the inlet flow rate on the main channel was kept steady while increasing the lateral flow. The overall main to lateral flow ratio was subsequently decreased changing the corresponding width of the focused fluid. The experimental data was measured through microscope images (Fig. 2. 27). Prior experimental analysis a simulation was performed, using the same flow conditions as in experimentation (Fig. 2. 26).

Using the analytical description and rewriting the hydrodynamic focusing equation (Eq. 2.20) that predicts the width of the focused fluid [37]:

$$\frac{w_0}{w} = \frac{1}{g(\lambda)} \frac{Q_i}{Q_i + Q_f}$$

And the correction factor $g(\lambda)$, where $\lambda = h/w$ and h is the height of the channel and w is the width, can be obtained as [38]:

$$g(\lambda) = (1+\lambda^2)(1 - 1.3553\lambda + 1.9467\lambda^2 - 1.7012\lambda^3 + 0.9564\lambda^4 - 0.2537\lambda^5)$$

The width of our microchannel was 1000 µm while the height was 30 µm. We kept the main channel flow fix (Q_f) at 10, 20 and 40 µl/min while a swept flow was applied to the lateral channel (Q_i). Different ratios between both flows were defined (30, 25, 20, 15, 10, 5, 3 and 2) and lateral flow was applied accordingly. The results were plotted and compared with the simulations and experimental analysis (Fig. 2. 28).

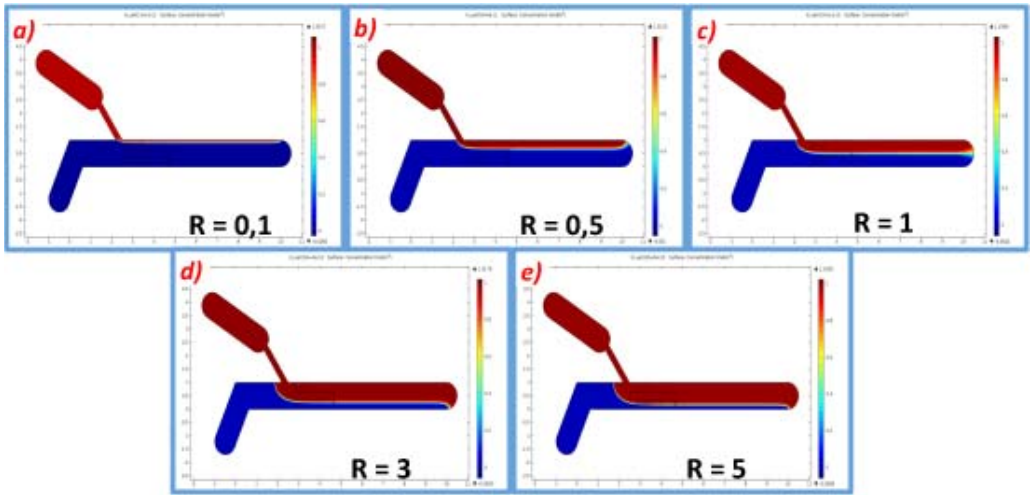

Fig. 2. 26 Simulation of a co-flow. The main input was kept constant while the lateral input flow was increased. The simulations were performed with COMSOL Multiphysics

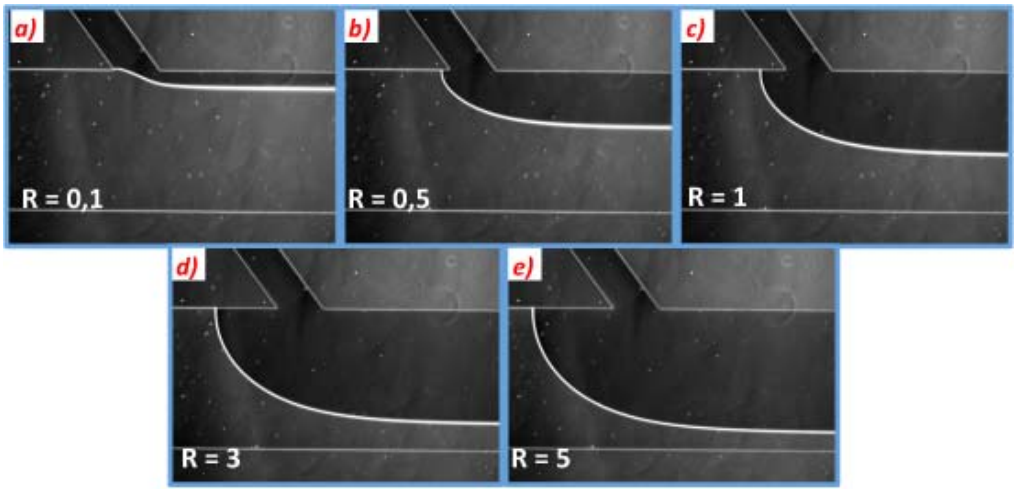

Fig. 2. 27 Experimental analysis of the fluid dynamics. A inked solution was flowed through the lateral channel, the flows used were the same as the ones used for simulations

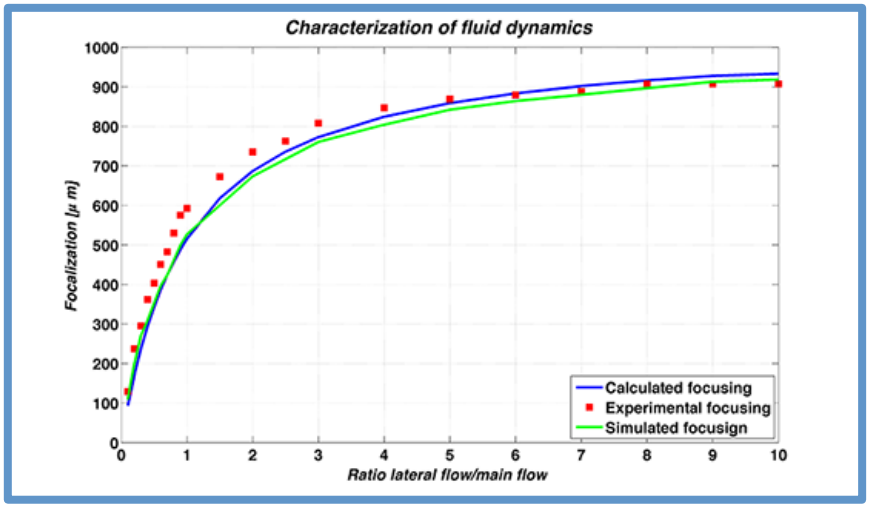

Fig. 2. 28 Fluid dynamics. Experimental (red dots), calculated (blue line) and simulated (green line). The main flow was kept constant while increasing the lateral flow

The experimental results showed only a small deviation when compared to theoretical and simulated values (Fig. 2. 28). An estimation of the width of the lateral fluid could be made with the used equations having maximum fit errors of 20.5±9μm at flow rates higher than 10 μl/min. Selective flowing of the compounds injected on the lateral microchannel, to functionalize only the e_1 electrode was achieved by using the predictions of the fluid dynamics equations [37].

The fluid dynamics of the second device was also characterized (Fig. 2. 29).

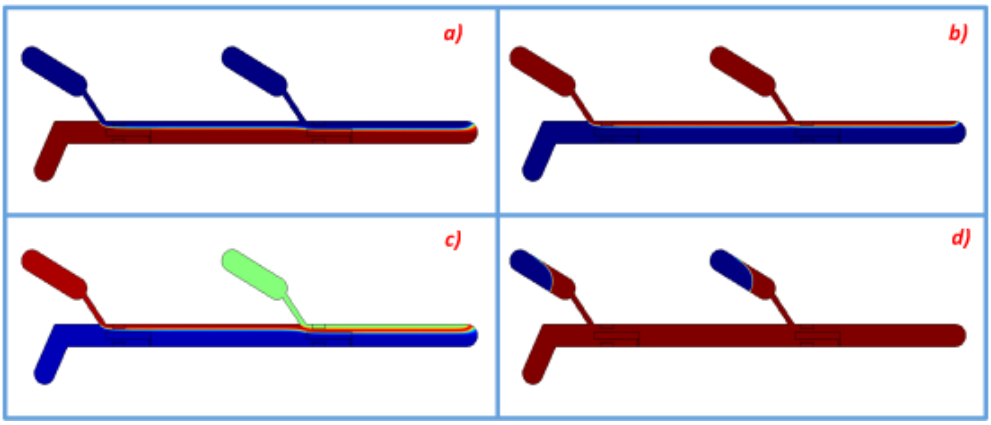

Fig. 2. 29 Simulation of the fluid dynamics for the second device. The red and green fluids represent the functionalization solutions. Different cases were studied a) Flow on the main channel and first lateral channel, b) Flow on the three channels with similar flow in the lateral channels, c) Flow on the three channels but different flow on the lateral channels, d) Flow only on the main channel.

After simulations, we concluded that the hydrodynamic focusing equation (Eq. 2.20) that predicts the width of the focused fluid [37] can be used for the selection of our flows:

$$\frac{w_0}{w} = \frac{1}{g(\lambda)} \frac{Q_i}{Q_i + Q_f}$$

But since we have three inlets $Q_f = Q_{f1} + Q_{f2}$ [19], where Q_{f1} is the inflow applied to the main channel, Q_i is the inflow in the first lateral channel and Q_{f2} is the input applied to the second lateral channel.

2.4 Conclusions

In this chapter, we have presented how two different lab-on-chip systems for biodetection purposes were designed. The microfluidic part consisted on microchannels exploiting the laminar co-flow principle. A set of electrodes was thought as integrated biosensing element. The physics involved in microfluidic devices were studied prior the fabrication of the devices.

We used a soft lithography and casting technique for the fabrication of the microchannels. The masters of the microchannels were fabricated with a SU-8 10 photoresist; we selected that resist since is very resistant to solvents, acids and bases and have excellent thermal and mechanical stability, making them well suited for fabricating permanent structures. Then, the microchannels were replicated in polydimethylsiloxane (PDMS), since this polymer has great optical properties, is biocompatible, the replicas can be reproduced with high fidelity and its surface can be oxidized to do a sealing. The

microelectrodes were fabricated by a photolithography technique followed by a metal evaporation technique. Gold was selected since it's one of the least reactive metal, with high malleability, ductility, resistance to corrosion and conductivity. Also, a self-assembled monolayer with a thiol termination can be easily formed on top of a gold surface.

The masters of the microchannels were fabricated over a glass surface using a negative photoresist (SU-8 10). The selected photoresists allow us to obtain a height of 27μm along the whole microchannels. The width of the main channel had a maximum error of 5.8% while the lateral channel had an error of at most 2%. The microchannels were casted using PDMS but some undesired 10% dimensional shrinkage was detected. The microelectrodes were then characterized by optical analysis

The study of the physics involved in our microfluidic devices help us to select the flows that let us work under laminar flow regime. The diffusion phenomenon was also minimized by selecting the appropriated flows. The fluid dynamics was simulated and results were compared with experimental tests according theoretical calculations. The comparison between the fluid dynamics data gave us a maximum fitting error of 20 μm. The study of the laminar co-flow was useful to select the most suitable inflows for developing a functionalization protocol. We selected a lateral inflow of 6 μl/min and a main flow of 20 μl/min for every selective functionalization step, since the physics and fluidic study predicts that only one electrode is functionalized and the diffusion is diminished. This ratio between lateral and main channel of 0.3 can be extrapolated and used to choose the inflows for the blocking step in the functionalization protocol.

2.5 References

1. A. M. Gañán-Calvo, J. M. Montanero, L. Martín-Banderas and M. Flores-Mosquera, *Advanced Drug Delivery Reviews*, 2013, **65**, 1447-1469.
2. G. T. Vladisavljević, A. Laouini, C. Charcosset, H. Fessi, H. C. H. Bandulasena and R. G. Holdich, *Colloids and Surfaces A: Physicochemical and Engineering Aspects*.
3. A. Perro, C. l. Nicolet, J. Angly, S. b. Lecommandoux, J.-F. o. Le Meins and A. Colin, *Langmuir*, 2010, **27**, 9034-9042.
4. A. N. Mitropoulos, G. Perotto, S. Kim, B. Marelli, D. L. Kaplan and F. G. Omenetto, *Advanced Materials*, 2014, **26**, 1105-1110.
5. J. Castillo-León, R. Rodriguez-Trujillo, S. Gauthier, A. C. Ø. Jensen and W. E. Svendsen, *Microelectronic Engineering*, 2011, **88**, 1685-1688.
6. J. Comelles, V. Hortigüela, J. Samitier and E. Martínez, *Langmuir*, 2012, **28**, 13688-13697.

7. X. Mao, A. A. Nawaz, S.-C. S. Lin, M. I. Lapsley, Y. Zhao, J. P. McCoy, W. S. El-Deiry and T. J. Huang, *Biomicrofluidics*, 2012, **6**, -.
8. S.-C. Lin, P.-W. Yen, C.-C. Peng and Y.-C. Tung, *Lab on a Chip*, 2012, **12**, 3135-3141.
9. R. Rodriguez-Trujillo, C. A. Mills, J. Samitier and G. Gomila, *Microfluidics and Nanofluidics*, 2007, **3**, 171-176.
10. O. Castillo-Fernandez, R. Rodriguez-Trujillo, G. Gomila and J. Samitier, *Microfluidics and Nanofluidics*, 2014, **16**, 91-99.
11. G. A. Justin, A. K. Denisin, M. Nasir, L. C. Shriver-Lake, J. P. Golden and F. S. Ligler, *Sensors and Actuators B: Chemical*, 2012, **166–167**, 386-393.
12. C. Parra-Cabrera, C. Sporer, I. Rodriguez-Villareal, R. Rodriguez-Trujillo, A. Homs-Corbera and J. Samitier, *Lab on a Chip*, 2012.
13. K. Xu, C. P. Tostado, J.-H. Xu, Y.-C. Lu and G.-S. Luo, *Lab on a Chip*, 2014, **14**, 1357-1366.
14. J. Sivasamy, T.-N. Wong, N.-T. Nguyen and L.-H. Kao, *Microfluidics and Nanofluidics*, 2011, **11**, 1-10.
15. X. Xuan, J. Zhu and C. Church, *Microfluidics and Nanofluidics*, 2010, **9**, 1-16.
16. A. A. Nawaz, X. Zhang, X. Mao, J. Rufo, S.-C. S. Lin, F. Guo, Y. Zhao, M. Lapsley, P. Li, J. P. McCoy, S. J. Levine and T. J. Huang, *Lab on a Chip*, 2014, **14**, 415-423.
17. S. Carlotto, I. Fortunati, C. Ferrante, P. Schwille and A. Polimeno, *Microfluidics and Nanofluidics*, 2011, **10**, 551-561.
18. Y.-J. Chiu, S. H. Cho, Z. Mei, V. Lien, T.-F. Wu and Y.-H. Lo, *Lab on a Chip*, 2013, **13**, 1803-1809.
19. R. Rodriguez-Trujillo, C. Mills, J. Samitier and G. Gomila, *Microfluidics and Nanofluidics*, 2007, **3**, 171-176.
20. R. Rodriguez-Trujillo, O. Castillo-Fernandez, M. Garrido, M. Arundell, A. Valencia and G. Gomila, *Biosensors and Bioelectronics*, 2008, **24**, 290-296.
21. O. Castillo-Fernandez, G. B. Salieb-Beugelaar, J. W. van Nieuwkasteele, J. G. Bomer, M. Arundell, J. Samitier, A. van den Berg and J. C. T. Eijkel, *ELECTROPHORESIS*, 2011, **32**, 2402-2409.
22. H. Becker and C. Gartner, in *Electrophoresis*, Germany, 2000, vol. 21, pp. 12-26.
23. K. Hanson, Micromilling, http://www.micromanufacturing.com/content/micromilling-vs-wire-edming-steel-molds, 2013.
24. Makino, Medical staple mold, http://www.makino.com/resources/case-studies/medical-staple-mold/423/, 2013.
25. E. Backer, W. Ehrfeld, D. Münchmeyer, H. Betz, A. Heuberger, S. Pongratz, W. Glashauser, H. Michel and R. v. Siemens, *Naturwissenschaften*, 1982, **69**, 520-523.
26. LIGA Process, http://asu.ieee.org.eg/liga-process/.
27. Rutland, Injection molding process, http://www.rutlandplastics.co.uk/moulding_process.shtml, 2013.
28. Y. Xia and G. M. Whitesides, *Annual review of materials science*, 1998, **28**, 153-184.
29. Nanoterra, Soft lithography, http://www.nanoterra.com/soft_lithography.asp.
30. CSIC, Thermal evaporation in vacuum, http://www.icmm.csic.es/fis/english/evaporacion_resistencia.html, Accessed 2013.

31. C. Metals, Sputtering, http://clearmetalsinc.com/technology/, 2013.
32. M. A. Roberts, J. S. Rossier, P. Bercier and H. Girault, *Analytical Chemistry*, 1997, **69**, 2035-2042.
33. D. Keegan, The art of laminating, http://www.signindustry.com/finishing/articles/2002-07-13-DK-laminatingPT1.php3, Accessed 2013.
34. D. J. Beebe, G. A. Mensing and G. M. Walker, in *Annu Rev Biomed Eng*, United States, 2002, vol. 4, pp. 261-286.
35. Y. A. Çengel, *Fluid Mechanics*, Tata McGraw Hill Education Private, 2010.
36. P. Tabeling, *Introduction to microfluidics*, Oxford University Press, 2005.
37. T. Stiles, R. Fallon, T. Vestad, J. Oakey, D. W. M. Marr, J. Squier and R. Jimenez, *Microfluidics and Nanofluidics*, 2005, **1**, 280.
38. A. I. Rodriguez-Villarreal, M. Arundell, M. Carmona and J. Samitier, *Lab on a Chip*, 2010, **10**, 211-219.
39. J. Kestin, H. E. Khalifa and R. J. Correia, *Tables of the dynamic and kinematic viscosity of aqueous NaCl solutions in the temperature range 20-150 C and the pressure range 0.1-35 MPa*, American Chemical Society and the American Institute of Physics for the National Bureau of Standards, 1981.

CHAPTER 3 In situ selective functionalization of biosensors: Determination of optimum functionalization times

3.1 Introduction

3.1.1 Introduction

Biosensors are defined as analytical devices incorporating a biological material (tissue, microorganisms, organelles, cell receptors, enzymes, antibodies, nucleic acids, natural products etc.), a biologically derived material (e.g. recombinant antibodies, engineered proteins, aptamers, etc.) or a biomimic (e.g. synthetic receptors, biomimetic catalysts, combinatorial ligands, imprinted polymers etc.) intimately associated with or integrated within a physicochemical transducer or transducing microsystem (Fig. 3. 1), which may be optical, electrochemical, thermometric, magnetic or mass-sensitive [2]. Biosensors can be classified according to the recognition principle or the physics of the transduction process.

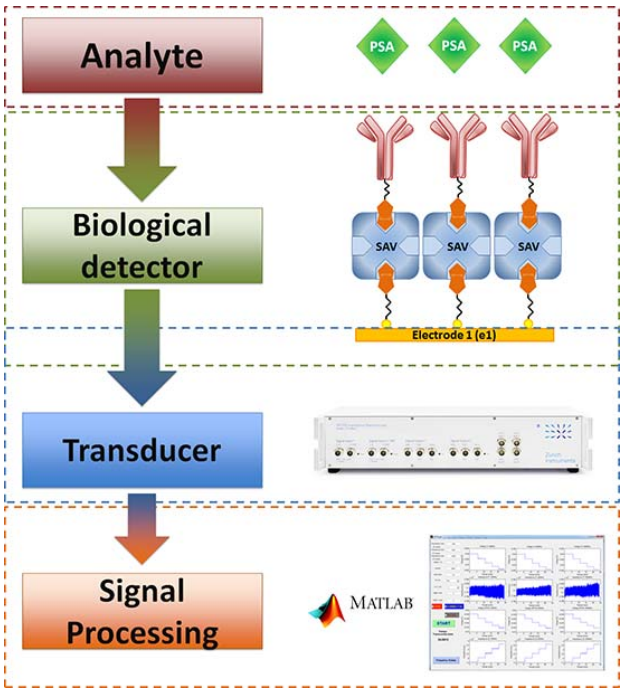

Fig. 3. 1 Schematic representation of a biosensor. The left column show the biosensor used for the development of this work.

3.1.1.1 Classification by recognition principle

The interaction of the analyte with the biological detector can have affinity interactions or non-affinity interactions (Fig. 3. 2). A productive interaction is related to a catalytic reaction produced between the biological detector and the specific analyte. And it is

usually represented by an enzyme or enzyme cascade. The interaction can be done with a sample solution or with cells. Antibody-antigen, ligand-receptor interactions, DNA-DNA hybridization give a non-productive recognition, also referred as affinity interactions.

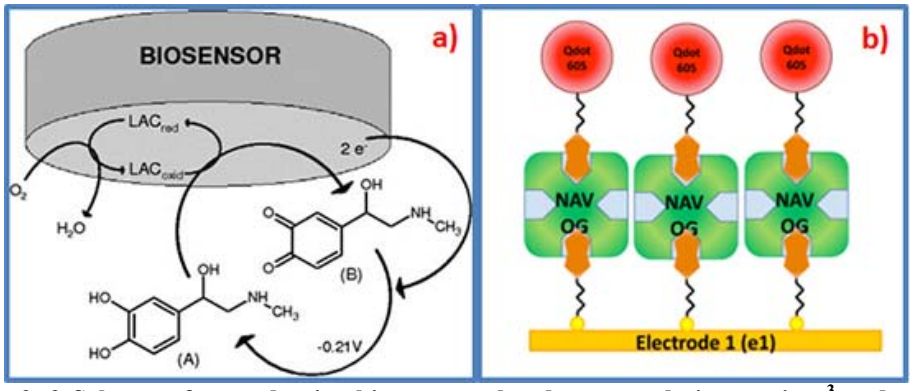

Fig. 3. 2 Scheme of a productive biosensor related to a catalytic reaction [3] and non-productive biosensor usually antibody-antigen or ligand-receptor interactions [4]

3.1.1.2 Classification by transduction

Biosensors can be classified by the transduction process. The most common transducers are: electrochemical, thermal, magnetic, optical or mass-sensitive (Fig. 3. 3).

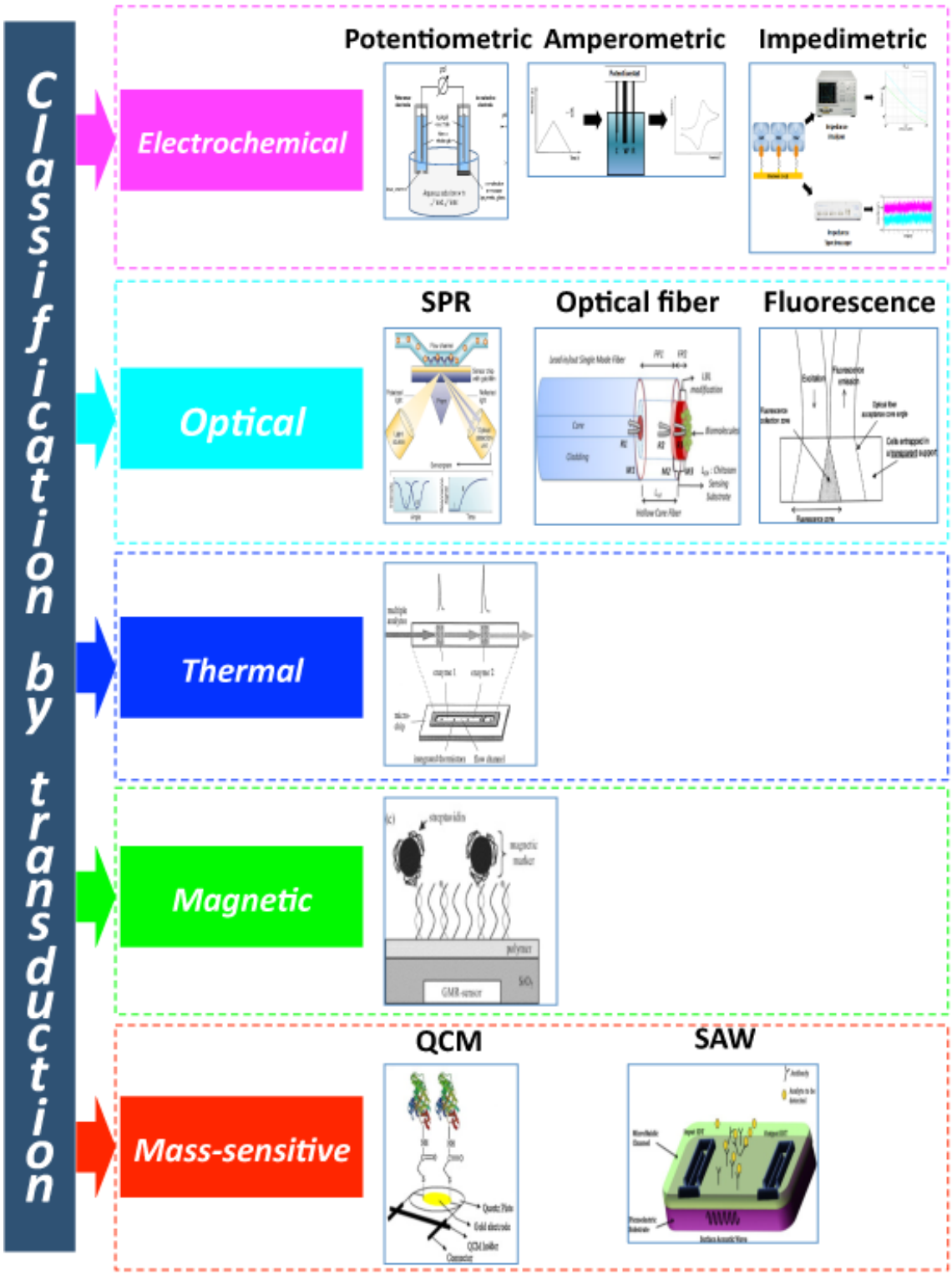

Fig. 3. 3 Biosensor classification by transduction.

Electrochemical biosensors

Electrochemical biosensors are able to convert a biological event into an electronic signal. The transduction principle of these biosensors can be potentiometric [5, 6], amperometric [7] or impedimetric [8]. In particular, electrochemical transduction is widely used in biosensors since this process is easily integrated into LOC devices and

simplifies the read-out equipment [9].

Optical biosensors

The principle of optical biosensors is based on the change in the characteristics of the medium in contact with the light produced by stimuli. The variations can be in its emission, adsorption properties or refractive index. The most commonly used optical biosensors include surface plasmon resonance (SPR) biosensors [10], optical fiber biosensors [11] and fluorescence based [12].

Thermal biosensors

Absorption or evolution of heat produced by a biological reaction is the principle of thermal biosensors. The reaction medium suffers a change in temperature. The thermometric devices measure the changes in temperature of the circulating fluid, which is due to the reaction of immobilized enzymes to a specific substrate. The commonly used methods are calorimetry, enzyme catalysis, immobilization and flow injection; and several devices had been developed in past years [13, 14].

Magnetic biosensors

A super-paramagnetic particle is conjugated to the antibody or biomolecule of interest; then with magneto resistive sensors integrated in silicon detection is done. The magnetic markers can be used also to manipulate the sample with the help of electromagnets [15].

Mass-sensitive biosensors

The micromechanical biosensors transduce a physical o mechanical change into electrical energy and vice versa. Acoustic sensors can also measure the mass change by the binding of antigen/antibody complexes. The most common mass-sensitive biosensors are the quartz crystal microbalance (QCM) [16] and the based on surface acoustic waves (SAV) [17].

3.1.2 Surface functionalization

The biological detector in a biosensor must be attached to the transducer in order to develop a biosensor; this process is known as immobilization or functionalization. The main methods to attached biomolecules to the transducer are: adsorption, entrapment, cross-linking and covalent bonding.

3.1.2.1 Adsorption

This method is the simplest approach with minimal preparation; the biosensor should be used in a short period of time since the binding is weak. Enzymes are adsorbed by many substances and there is no need of reagents. There are two main types of adsorption, physical and chemical. The main difference is the force of interaction. The physisorption is based on van der Waals forces and the chemisorption is based on covalent bonds; therefore the chemical adsorption is much stronger. A disadvantage of this method is that the adsorbed biomaterial is very sensitive to changes in pH, temperature or ionic strength.

3.1.2.2 Entrapment

The material is trapped by mixing it with a monomer solution and polymerizing it into a gel. The main problem of this system is the diminished transport by diffusion which affects the time response of the biosensor. Also, the porosity of the gel reduces the enzyme activity but this problem could be fixed with a cross-linking.

3.1.2.3 Cross-linking

A chemical bonding is performed between the biomolecule and the transducer surface. Some problems with this method are the diffusion limitations, and the weak mechanical strength. Although, the cross-linking method is useful when used simultaneously with adsorbed method, since it stabilize the immobilized biomolecules.

3.1. 2.4 Covalent bonding

A functional group is covalently bonded to the transducer. The nucleophilic groups for coupling used in covalent bonding are: NH_2, CO_2H, OH, C_6H_4OH and SH. The reactions are limited in a range of pH, temperature and ionic strength. With this method is possible to form self-assembled monolayers of biomolecules on the surface of the transducer.

3.1.3 Chapter aim

In previous chapters we explained the methodology followed for the design, fabrication and microfluidic behavior of our lab-on-a-chip. For that reason, in this chapter we focused our attention in the development of a functionalization protocol and the determination of the optimum times for in-situ selective functionalization.

We took advantage of the knowledge acquired in our group on last years for the functionalization of surfaces. Prats-Alfonso et al first synthesized biotinylated alkyl thiols to develop self-assembled monolayers on gold surfaces; this biotinylated thiols had the capacity to graft avidin proteins [18]. Some approaches included the gold surface functionalization with self-assembled monolayers for the detection of specific olfactory receptors [19], using electrochemical impedance spectroscopy [20, 21] or quartz crystal microbalance [22].

Lagunas et al adapted these first protocols and they developed chemical gradients based on the biotin-streptavidin interaction [23]. They developed a universal platform for biological applications and latter they tested the gradients with continuous bone morphogenetic protein-2 for the study of C2C12 cells [24]. The surface modification method was based on the formation of self-assembled monolayers.

Here we present a system based on laminar co-flow to perform an on-chip selective surface bio-functionalization of LOC-integrated sensors. We adapted the protocols developed in our group and first characterized the functionalization times in order to achieve a robust surface modification process.

3.2 Materials and methods

3.2.1 Protocol for the determination of optimum functionalization times through impedance

The monitoring of impedance evolution along time served to control the functionalization protocol and define the most suitable adsorption times for each biomolecular deposition process.

For the impedance analysis the Agilent 429A was used. A frequency logarithmic swept was programmed from 40 Hz to 110 MHz with an input of 50 mV peak to peak. Impedance spectra was recorded each 15 minutes during a total period of time of 90 minutes while a continuous input flow rate of 20µl/min was introduced into the chip. This protocol was repeated for each functionalization step and different solutions in order to characterize electrically the electrodes surface changes over time. Tested solutions included: biotinylated alkyl thiols with a polyethylene glycol linker (biotin-thiol), prepared as reported by E. Prats-Alfonso et al [18] and dissolved in ethanol at a concentration of 10^{-3} M, Streptavidin–Texas red conjugate 17 µg/ml in phosphate buffer saline (PBS) (Fig. 3. 4).

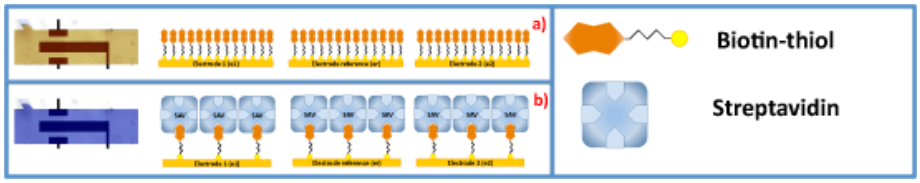

Fig. 3. 4 Protocol for the determination of functionalization times. a) Biotin-thiol solution flowing through the channel, b) Streptavidin solution functionalizing the biosensors. The measurements were made every 15 minutes. The images are represented in false color.

3.2.2 Verification protocol for selective functionalization

The selective functionalization consisted on forming layer of biomolecules on top of one electrode (e_1). And keeping the remaining electrodes surfaces (e_2, e_r) with bare gold. PBS was applied through the LOC in order to deeply clean the microchannels and the electrodes prior to their use after being fabricated. The buffer was driven into the channels at 20 µl/min during 15 minutes (Fig. 3. 5a). This was enough to eliminate particles as well as any substances previously left.

The first performed selective functionalization started depositing a self-assembled monolayer of biotin-thiol groups over the surface of the electrode e1 (Fig. 3. 5b). The biotin-thiol solution was introduced at 6µl/min through the lateral microchannel. Simultaneously, PBS buffer through the main channel was kept at a rate of 20µl/min. This process lasted 45 minutes and served as an in-between layer for the next deposited biomolecules. Immediately after the biotin-thiol deposition, the chip was rinsed by flowing PBS at 20 µl/min for 15 minutes through both channels. At the end of the process the remaining thiols should be attached to the electrodes surface and their associated biotin pointing up to the solution.

The second functionalization step is meant to form a Streptavidin-Texas red (SAV-TRed conjugate, Invitrogen, S872) layer on top of the biotin layer (Fig. 3. 5c). Again, a 20 µl/min PBS is flowed into the chip through the main channel while the functionalizing solution is laterally introduced at 6µl/min. The process lasts 30 minutes to guarantee the complete functionalization of e_1. A 15 minutes PBS rinsing process followed to remove unattached SAV molecules

Finally, SAV-TRed layer formation was also verified by monitoring its attachment to quantum dots (QD) functionalized with biotin. The previous functionalization step was repeated using PBS buffer with 0.3nM of QD 605-biotin conjugate (Invitrogen, Q10301MP) (Fig. 3. 5d). After the PBS rinsing step, optical and

electrical measurements were performed. An inverted optical microscope (Olympus IX71) with an integrated CCD Hamamatsu camera was used for this purpose. Images were acquired through a fluorescence filter. Optical measurements were complemented with impedance studies. Impedance measurements were performed after each functionalizing step by applying a logarithmic frequency swept from 40 Hz to 110 MHz and an input voltage of 50 mV.

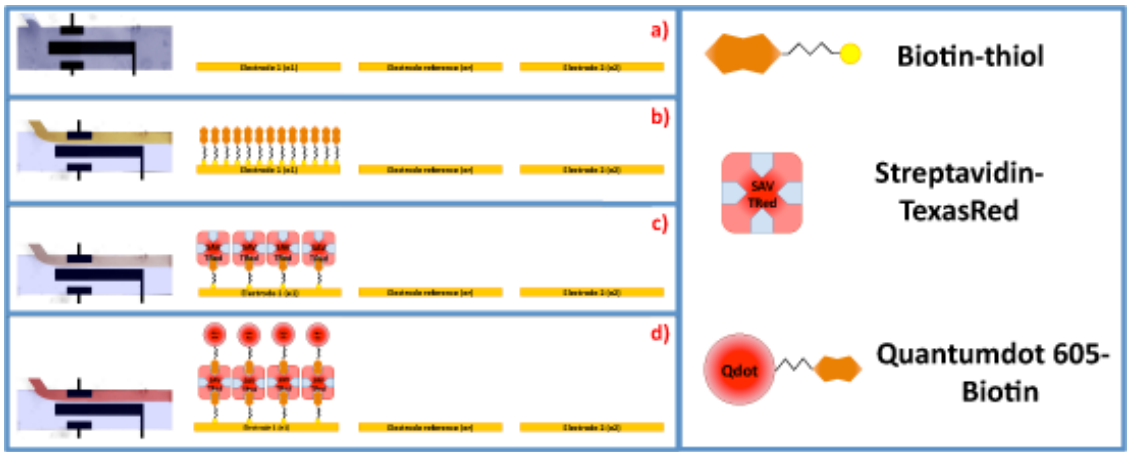

Fig. 3. 5 Protocol for selective functionalization. a) Rinsing with PBS, b) First selective functionalization with biotin-thiol solution, c) Addition of a layer of streptavidin, d) Detection of the selective functionalization with quantum dots. The images are represented in false color.

3.2.3 Differential voltage detection protocol

Avoiding non-specific adsorption on the electrodes acting as a reference (e_r and e_2) is strongly important for the differential impedance detection. In order to make these electrodes inert to biomolecules and the sensing part (e_1) sensitive to the specific target a protocol was developed and executed in situ in the LOC device. The first step lasted 30 minutes and involved selective blocking of electrodes e_2 and e_r to avoid unspecific adsorption (Fig. 3. 6b). A lateral 4.5 µl/min PBS co-flow was combined with main channel triethylene glycol mono-11-mercaptoundecyl ether (PEG3-Thiol, Sigma Aldrich) in ethanol solution (10^{-3}M) at 6 µl/min.

The next stages were the same as the two first steps in the functionalization verification protocol. However, Neutravidin-Oregon Green (NAV-OGreen) conjugated (NeutrAvidin Oregon Green 488, Invitrogen A6374) in PBS solution (10 ng/ml), replaced the SAV-TRed (Fig. 3. 6d). NAV is very similar to SAV regarding to its affinity to biotin (also with four binding sites) but with neutral charge.

The overall system performance as a sensing device was checked. Biotin-QD solution (0.3nM in PBS) was injected along the two channels during a period of 30 minutes (Fig. 3. 6e). The measurements were done optically and electrically with the inverted microscope and with the Impedance Spectroscope respectively.

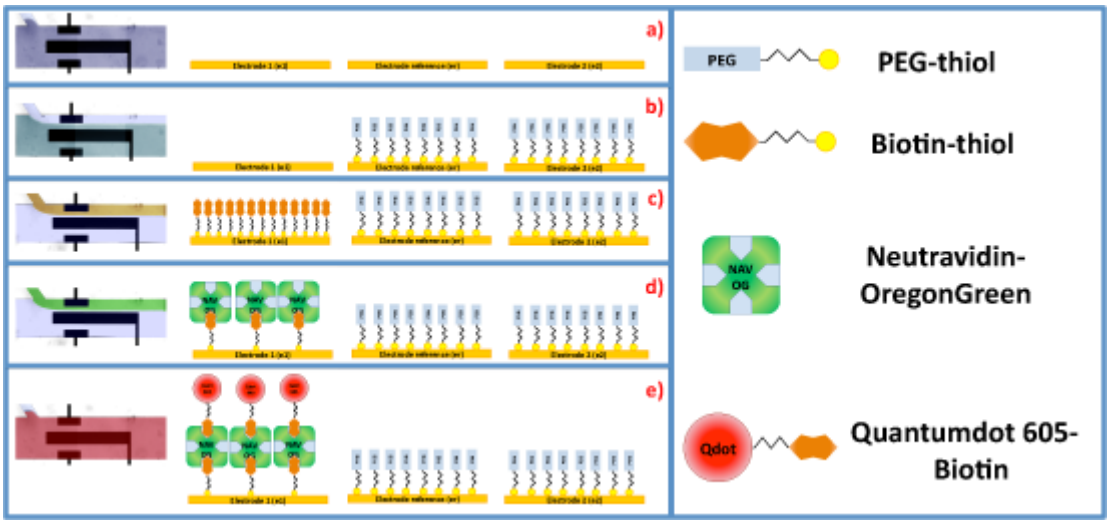

Fig. 3. 6 Protocol for the detection of Quantum dots. a) Rinsing with PBS, b) Selective blocking with a PEG-thiol solution, c) Electrode surface modified with biotin-thiol, d) Addition of a layer of streptavidin, e) Detection of biotinylated Quantum dots. The images are represented in false color.

3.3 Results and discussions

3.3.1 Protocol for the determination of optimum functionalization times through impedance

The objective of this set-up was to select stabilization times for the chosen functionalization processes. The analysis was done by selectively applying the different protocol steps through the lateral channel during 90 minutes and monitoring impedance changes. The electrical analysis was performed each 15 minutes between the top and bottom electrodes (e_1-e_2). After acquiring all the data, a posterior impedance comparison was performed. The evolution in time of these parameters was used to determine the times needed to guarantee optimum surface covering through limited drift. The first solution to be analyzed was the biotin-thiol one.

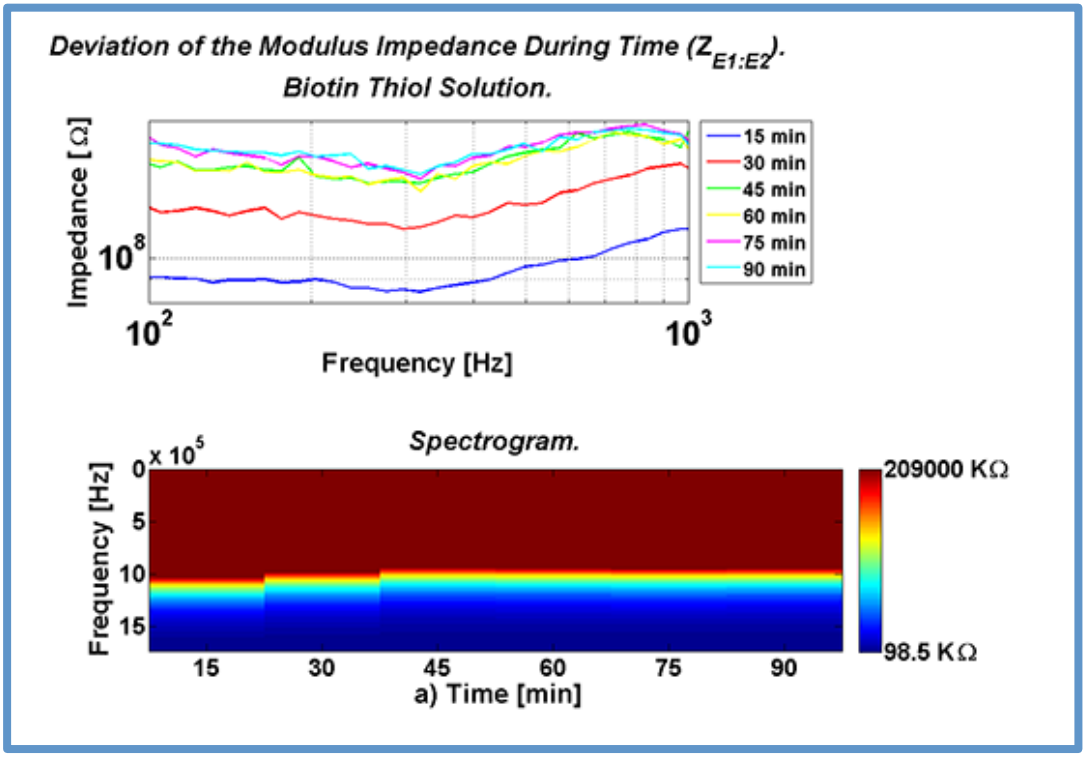

Fig. 3. 7 Analysis of the impedance drift of biotin-thiol solution. The chart of the top is the impedance measured every 15 minutes during functionalization. The spectrogram was calculated to see the evolution of the impedance along time.

The impedance change is related to the formation of the new layer over the surface of the electrode. The impedance modulus will increase until the electrode is totally saturated. Once the impedance is stabilized, we selected the most suitable times for every functionalization protocol. The time selected for the functionalization with biotin-thiol was 45 minutes, since after those times the impedance value is stable (Fig. 3. 7). After, we analyzed the impedance drift for the streptavidin solution.

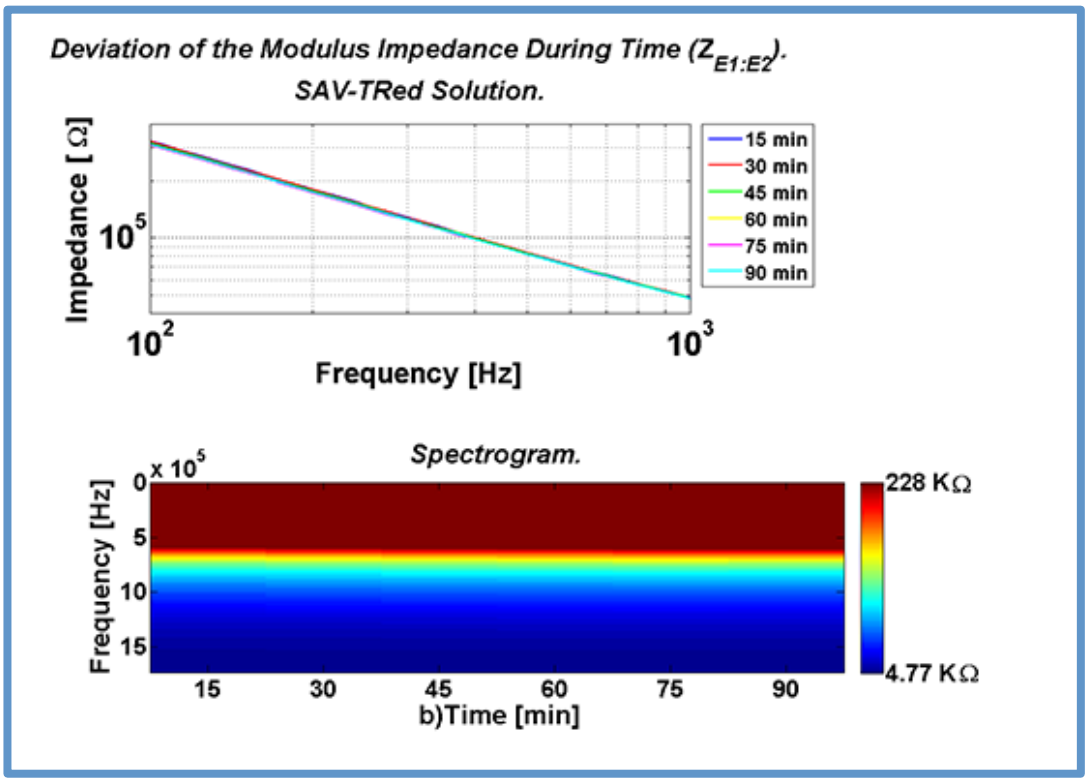

Fig. 3. 8 Analysis of the impedance drift of SAV-TRed solution. The chart of the top is the impedance measured every 15 minutes during functionalization. The spectrogram was calculated to see the evolution of the impedance along time.

The streptavidin protein interacted with the first biotin layer and formed a second layer over the electrodes. With this new layer, the impedance modulus changed again, and the time selected for this functionalization depends on the saturation. After evaluating the results (Fig. 3. 8), the selected times for the functionalization was: 30 minutes for the selective functionalization stage with SAV and NAV. Chosen times ensured that the impedance had a stable value at the different frequencies and remaining drifts were minimal. The times were selected considering the concentrations chosen on this chapter, however by increasing the concentration the deposition times can be reduced.

3.3.2 Verification protocol for selective functionalization

The selective functionalization was evaluated with two methods simultaneously: an optical and an impedance analysis in order to further validate the obtained results.

3.3.2.1 Optical analysis

Optical measurements were used to guarantee formation of the different layers over the electrode during functionalization on top of the electrical characterization. Particles on the different solutions were labeled to achieve this objective. An optical microscope

with a fluorescent filter was used to monitor electrode surface changes after each rinsing step. The SAV was conjugated with a Texas red fluorochrome having an excitation wavelength of 596 nm and emission at 615 nm. The biotin layer was conjugated with quantum dots with an emission wavelength of 605 nm, to perform simultaneously optical and electrical detection.

The LOC with the fluorescent solution flowing continuously was observed at the beginning of the experiment (Fig. 3. 9a-c). This served to check that the co-flow was guaranteed from the beginning and functionalization was selective as predicted. In Fig. 3. 9 it can be seen that only the top electrode is in contact with the dyed solution forming a new layer on its surface.

Initially, a self-assembled monolayer of Biotin-Thiol forms onto the electrode surface. In a second step, SAV-TRed binds with biotin. Finally, biotin-QDs form a third layer on top of the SAV-TRed, increasing its emission on the red spectra. At the end of the protocol, only e_1 is functionalized with SAV-TRed (Fig. 3. 9d).

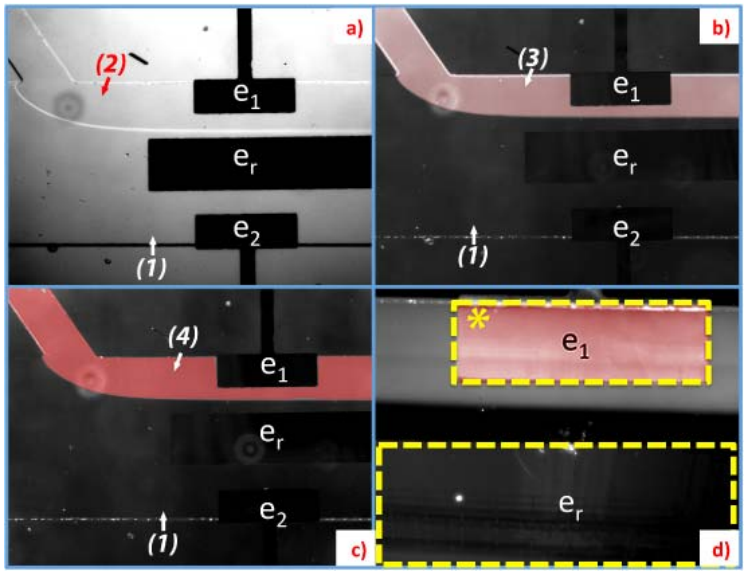

Fig. 3. 9 Microscopic images of the fluorescent study. A solution of PBS (1) was used to form a co-flow and focalize the functionalization solutions over e_1: a) Functionalization with Biotin - Thiol (2), b) Functionalization with SAV – TRed (3), c) Functionalization with Biotin - QD (4), d) The asterisk is placed inside the functionalized electrode (e_1), er is the biggest electrode and it shows no signs of functionalization.

3.3.2.2 Impedance analysis

An impedance analysis was also done in parallel to the optical results. Impedance measurements were performed after reaching previously defined times for layers deposition stabilization. Two-point measurements of both e_1:e_r and e_r:e_2 were obtained

in order to compare between them. The analysis was performed on low frequencies since previous experiments showed a larger sensitivity during the functionalization processes.

After initial cleaning with PBS, the basal impedance value was determined. Subsequent measurements were made following the formation of the biotin-thiol, the SAV-TRed, and the biotin-QD, layers on top of e_1. It is well known the interaction and strong affinity between biotin and SAV, NAV and AV. Also it is known that the SAV is a tetrameric protein, having four biotin binding spots. The biotin-QD complex will therefore also attach to the previously anchored SAV.

Variations on the impedance modulus value of the functionalized electrode ($|Ze_1{:}e_r|$) showed the effect of the formed biomolecular layer (Fig. 3. 10).

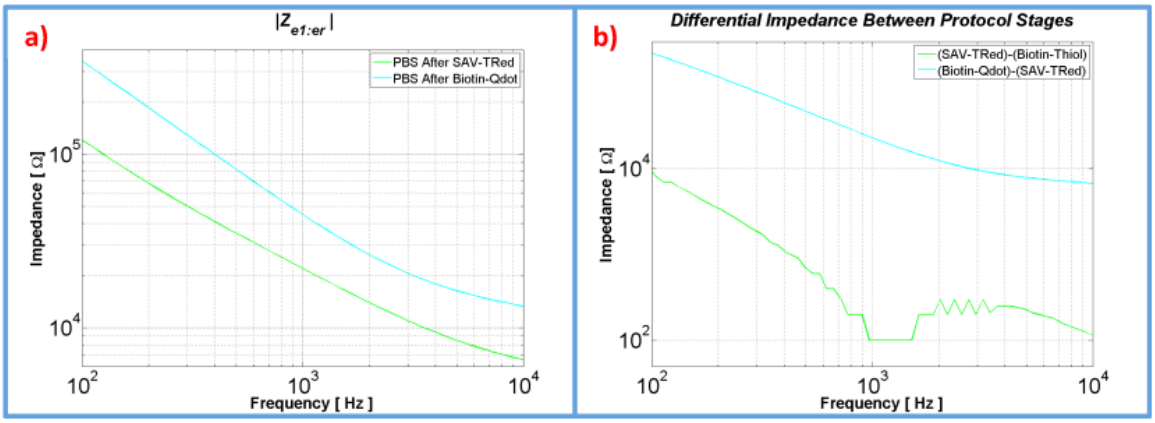

Fig. 3. 10 a) Impedance between top and central electrodes ($|Ze_1{:}e_r|$) at frequencies of interest (100 - 10000 Hz) comparing different stages of the protocol, b) Differential comparison between protocol stages compared to previously functionalized e_1.

Subtraction values between $|Ze_1{:}e_r|$ and $|Ze_2{:}e_r|$ were also evaluated (Fig. 3. 11). $Ze_2{:}e_r$ corresponds to the impedance between the electrodes that were not surface treated. Calculated differential values served to further support that selective in situ functionalization was correctly achieved. These were also useful to prove that a differential measurement between functionalized and non-functionalized electrodes, acting as a reference, could be used as a sensitive biosensor. Real-time differential impedance measurements are proposed as the method for electronic detection for these in situ functionalizing electrodes. Slow signal drifts along time, that could dramatically modify the electrical detection, are reduced by this method.

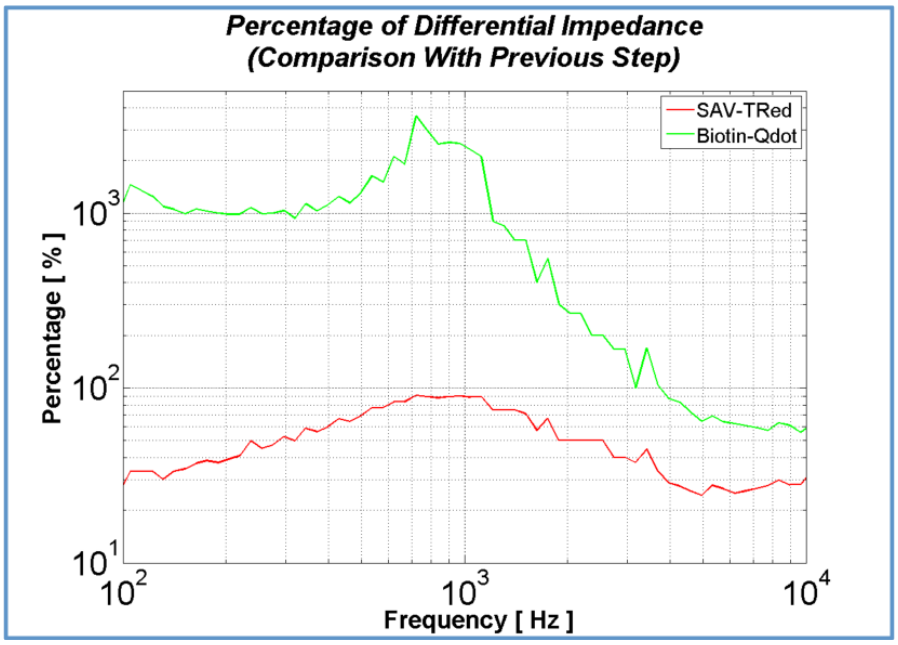

Fig. 3. 11 Percentage of the differential impedance between functionalized & non-functionalized electrode pairs ($|Ze_1:e_r|$-$|Ze_2:e_r|$) in respect to the previous functionalizing step.

With the differential analysis the most suitable range frequency was selected (600-1200 Hz). This was because impedance changed between 83% and 90% for SAV (Fig. 3. 11 red line); and 21 to 25 times greater after QDs in this range (Fig. 3. 11 green line). This was the higher impedance change of all the studied frequencies. The impedance modulus $|Ze_1:e_r|$ is sensitive to the biochemical layers being added to e_1; while $|Ze_2:e_r|$ remains immune due to the selective electrodes functionalization.

3.3.3 Detection protocol: Optical analysis and differential voltage analysis

The detection protocol was also evaluated with two methods simultaneously: an optical and a differential voltage analysis in order to further validate the obtained results.

3.3.3.1 Optical analysis

Fluorescent images of the electrodes were taken at the end of the whole test using the inverted microscope. In order to monitor these experiments, NAV-OGreen was used in the final functionalization step and Biotin-QD was chosen to be detected. The fluorescence of every molecule was selected to have different wavelengths of excitation and emission. Emission wavelengths are 526 and 605 nm for NAV-OGreen and Biotin-QD respectively. NAV was chosen instead of SAV in order to change the electrical characteristics of the layer without modifying its affinity to Biotin. Selective blocking of electrodes e_2 and e_r with PEG-thiol was performed.

To acquire the images different fluorescence filters were applied in order to identify the biomolecules correctly. This was helpful to avoid false positive results and identifying the correct deposition of the layers. Fig. 3. 12 shows the functionalized electrode as well as the three biosensors electrodes. The intensities were observed with the different filters; green for NAV (Fig. 3. 12 a & b) and red for QD (Fig. 3. 12 c & d). The intensities demonstrated the correct absorption and detection of the biomolecules.

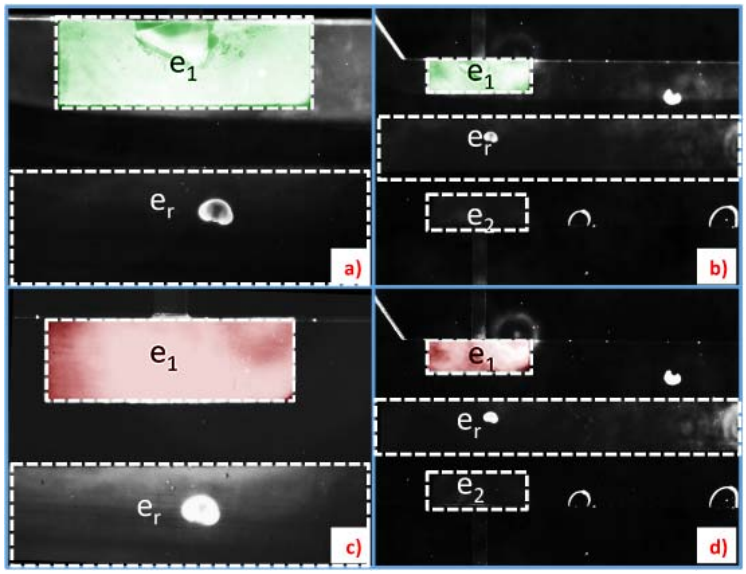

Fig. 3. 12 Microscopic images of the fluorescent study at the end of the detection protocol. a) Functionalized electrode with NAV-OregonG b) Three electrodes comparison of a), c) Functionalized electrode with Biotin-QD, d) Three electrodes comparison of c). The dotted lines reflect the edges of the electrodes. Microscopic images of the fluorescent study at the end of the detection protocol. a) Functionalized electrode with NAV-OregonG b) Three electrodes comparison of a), c) Functionalized electrode with Biotin-QD, d) Three electrodes comparison of c). The dotted lines reflect the edges of the electrodes.

3.3.3.2 Differential detection

An impedance Spectroscope (HF2IS, Zurich Instruments) was used for the differential measurements. In the final experiments, the device was connected to the chip electrodes and a 3mV at 1 kHz signal was applied. The analysis was performed in real time, measuring the output voltage continuously during the whole test and keeping each protocol stage for up to 15 minutes. The input signal was applied between e_1 and e_2 (symmetrical electrodes) and the output was taken between e_r and the ground. Voltage drop was measured between e_1 and e_r. This measure should be equivalent to a relative change on the impedance of these electrodes (Ze_1:e_r) in respect to the impedance (Ze_2:e_r). In fact, if these impedances were the same, the measured value should be half of the applied voltage. The relative change was calculated with the voltage divider (equation 3.1) [4].

$$\alpha = \frac{Z_{e1:er}}{Z_{e2:er}} = \frac{V_{e1:er}}{V_{e2:er}} \quad {}^{4} \qquad \text{(Eq. 3. 1)}$$

The analysis of the results obtained when evaluating the modulus of the impedance, section 3.3, suggested that working at frequencies in the 500 to 1.2 kHz range could improve the detection. Differences between the impedances of the functionalized and non-functionalized electrodes showed to be larger in this range. An analysis was performed with the Zurich instrument showing optimum results at 1 kHz (Fig. 3. 13). The obtained results showed a more distinguishable, stable signal and a higher response at 1 kHz with this setup.

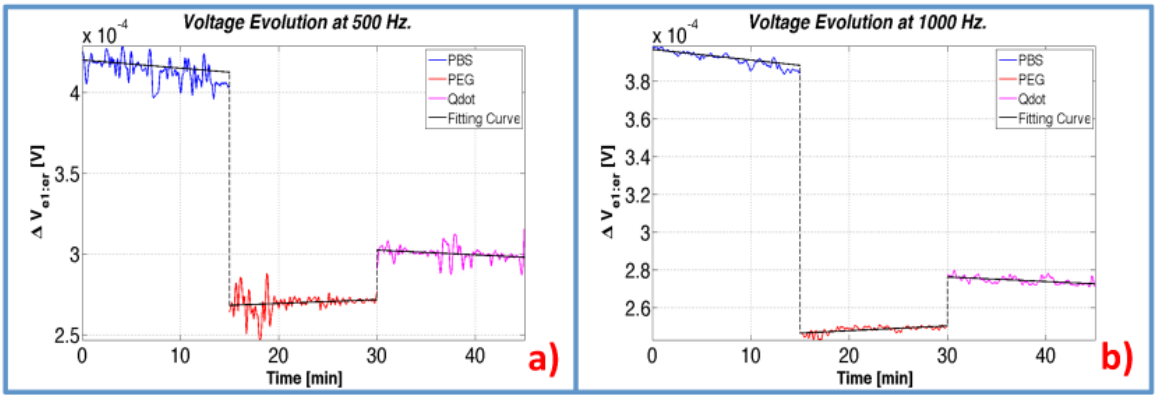

Fig. 3. 13 a, b) Voltage evolution at 500 and 1000 Hz. Calculated fitting curve is shown in black. The voltage evolution at 1000 Hz showed a more stable signal

Table 3. 1 Summarizes the percentage change factor α. Three different chips were tested at 1 kHz, and the α values were obtained after deposition of each layer. The layers of functionalizing biomolecules (biotin-thiol and NAV-OGreen) tend to increase the impedance between e_1 and e_r, as it can be deduced from the increment on the percentage of the factor α (Table 3. 1). The hypothesis used for the observation is that PEG surfaces will remain unaltered and the new depositions will change only $Z_{e1:er}$. The variation of $Z_{e1:er}$ is then reflected on the factor α.

Table 3. 1 Percentage change of α at 1 kHz for 3 different chips after 15 minutes of PBS cleaning.

Layer	Mean [%]
Biotin	2.55 ± 0.9
Neutravidin	4.09 ± 0.37
QDs	-1.40 ± 0.55

However, QDs used during the detection step seem to be the exception to the rule. This seems initial a contradiction with the results obtained during the impedance

analysis. However, it has been previously reported that QDs have a charge transfer when they are excited at green and blue wavelengths [25]. This could explain why the impedance drops during the detection of QDs, since NAV-OGreen conjugates have an emission wavelength in this particular range.

3.4 Conclusions

The microfluidic device tested included a sensing concept based on real-time direct monitoring impedance changes due to biomolecules deposition. To define a useful protocol a characterization of the device was performed. The tests helped to select the suitable times for a complete saturation of the electrode surface with biotin-thiol and streptavidin solutions. The tests also were useful to analyze the impedance drift.

The biotin solution was conjugated with a thiol termination, and as we explained before, the electrodes were fabricated with gold; therefore a self-assembled monolayer (SAM) of biotin was deposited on the surface of the electrodes. The thiol termination has a high affinity with gold surfaces. Streptavidin and biotin are two well-known biomolecules, and they interact with each other. Streptavidin is a tetrameric protein that has four binding spots for biotin. We used these biomolecules to form our first layers on the biosensor surface and we measured the impedance changes.

Electrical and optical methods were successfully used to study and proof the selective functionalization “in situ” of the biosensor parts on the chip. Different biomolecules, biotin, streptavidin and quantum dots were selectively deposited onto electrode surface and the layers formed could be monitored and detected using the two methods.

A novel differential voltage measurement was done with the chip, which also included a real time analysis. Depositions of different biomolecules were monitored by the voltage changes, and the electrical analysis was verified by an optical method.

3.5 References

1. A. A. Karyakin, M. Vuki, L. V. Lukachova, E. E. Karyakina, A. V. Orlov, G. P. Karpachova and J. Wang, *Analytical Chemistry*, 1999, **71**, 2534.
2. A. P. F. Turner, *Biosensors*, 1987, **3**, 313-315.
3. D. Brondani, C. W. Scheeren, J. Dupont and I. C. Vieira, *Sensors and Actuators B: Chemical*, 2009, **140**, 252-259.
4. C. Parra-Cabrera, C. Sporer, I. Rodriguez-Villareal, R. Rodriguez-Trujillo, A. Homs-Corbera and J. Samitier, *Lab on a Chip*, 2012.
5. B. R. Eggins, *Chemical Sensors and Biosensors*, Wiley, 2002.

6. K. Wojciechowski, *Current Opinion in Colloid & Interface Science*, 2011, **16**, 601-606.
7. C.-L. Wu, J.-C. Chou, W.-Y. Chung, T.-P. Sun and S.-K. Hsiung, *Materials Chemistry and Physics*, 2000, **63**, 153-156.
8. T. R. J. Holford, F. Davis and S. P. J. Higson, *Biosensors and Bioelectronics*, 2012, **34**, 12-24.
9. M. Mir, A. Homs and J. Samitier, *ELECTROPHORESIS*, 2009, **30**, 3386-3397.
10. E. Wijaya, C. Lenaerts, S. Maricot, J. Hastanin, S. Habraken, J.-P. Vilcot, R. Boukherroub and S. Szunerits, *Current Opinion in Solid State and Materials Science*, 2011, **15**, 208-224.
11. L. H. Chen, C. C. Chan, R. Menon, P. Balamurali, W. C. Wong, X. M. Ang, P. B. Hu, M. Shaillender, B. Neu, P. Zu, Z. Q. Tou, C. L. Poh and K. C. Leong, *Sensors and Actuators B: Chemical*, 2013, **188**, 185-192.
12. H. Nguyen-Ngoc and C. Tran-Minh, *Analytica Chimica Acta*, 2007, **583**, 161-165.
13. K. Ramanathan and B. Danielsson, *Biosensors and Bioelectronics*, 2001, **16**, 417-423.
14. B. Xie, K. Ramanathan and B. Danielsson, *TrAC Trends in Analytical Chemistry*, 2000, **19**, 340-349.
15. J. Schotter, P. B. Kamp, A. Becker, A. Pühler, G. Reiss and H. Brückl, *Biosensors and Bioelectronics*, 2004, **19**, 1149-1156.
16. W. C. Su, W. G. Zhang, S. Zhang, J. Fan, X. Yin, M. L. Luo and S. C. Ng, *Biosensors and Bioelectronics*, 2009, **25**, 488-492.
17. I. Voiculescu and A. N. Nordin, *Biosensors and Bioelectronics*, 2012, **33**, 1-9.
18. E. Prats-Alfonso, F. García-Martín, N. Bayo, L. J. Cruz, M. Pla-Roca, J. Samitier, A. Errachid and F. Albericio, *Tetrahedron*, 2006, **62**, 6876-6881.
19. J. Vidic, M. Pla-Roca, J. Grosclaude, M.-A. Persuy, R. Monnerie, D. Caballero, A. Errachid, Y. Hou, N. Jaffrezic-Renault, R. Salesse, E. Pajot-Augy and J. Samitier, *Analytical Chemistry*, 2007, **79**, 3280-3290.
20. Y. Hou, S. Helali, A. Zhang, N. Jaffrezic-Renault, C. Martelet, J. Minic, T. Gorojankina, M.-A. Persuy, E. Pajot-Augy, R. Salesse, F. Bessueille, J. Samitier, A. Errachid, V. Akimov, L. Reggiani, C. Pennetta and E. Alfinito, *Biosensors and Bioelectronics*, 2006, **21**, 1393-1402.
21. J. Minic, J. Grosclaude, J. Aioun, M.-A. Persuy, T. Gorojankina, R. Salesse, E. Pajot-Augy, Y. Hou, S. Helali, N. Jaffrezic-Renault, F. Bessueille, A. Errachid, G. Gomila, O. Ruiz and J. Samitier, *Biochimica et Biophysica Acta (BBA) - General Subjects*, 2005, **1724**, 324-332.
22. S. Rodríguez Seguí, M. Pla, J. Minic, E. Pajot-Augy, R. Salesse, Y. Hou, N. Jaffrezic-Renault, C. A. Mills, J. Samitier and A. Errachid, *Analytical Letters*, 2006, **39**, 1735-1745.
23. A. Lagunas, J. Comelles, E. Martínez and J. Samitier, *Langmuir*, 2010, **26**, 14154-14161.
24. A. Lagunas, J. Comelles, S. Oberhansl, V. Hortigüela, E. Martínez and J. Samitier, *Nanomedicine: Nanotechnology, Biology and Medicine*, 2013, **9**, 694-701.
25. S. Pradhan, S. Chen, S. Wang, J. Zou, S. M. Kauzlarich and A. Y. Louie, *Langmuir*, 2005, **22**, 787-793.

CHAPTER 4 Electrochemical detection of biomarkers: proof-of-concept

4.1 Introduction

Electrochemical transduction is widely used in biosensors since this process is easily integrated into microfluidic devices, simplifies the read-out equipment and has played an important role in the transition towards point-of-care diagnostics. Some of the advantages of electrochemical biosensors are their robustness, easy miniaturization, excellent detection limits, small analyte volumes, and ability to be used in biofluids. The main drawback of these biosensors is long-term stability and reliability. Also, non-specific adsorption reactions can be a problem since it can limit the sensitivity of these sensors.

4.1.1 Electrochemical biosensors

Electrochemical biosensors are able to convert a biological event into an electronic signal. The transduction principle of these biosensors can be potentiometric, amperometric or impedimetric.

4.1.1.1 Potentiometric biosensors

A potential change, logarithmically proportional to a particular ion activity, is measured. The samples that take place in the reaction are neither destroy nor consumed. The principle of these devices is based on Nernst equation [1]. The most used methodologies for developing these sensors are: transmembrane potential, electrode potential and field-effect transistor.

A transmembrane potential is based on the accumulation of a potential on a sensitive membrane. The membrane is usually ion-selective and generates a charge between the sensor and the surface; these electrodes are referred as ion-selective electrodes (ISE). The transmembrane potential could be changed by the binding of antigen or antibodies on the membrane surface. There is a similar approach to ISE; but instead of a membrane, the surface of the electrode reacts with the solution, and the potential changes according to the concentration of the analyte.

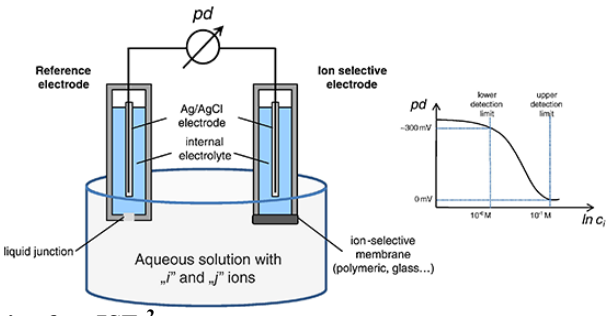

Fig. 4. 1 Schematic of an ISE [2].

The ISE can be integrated with a field-effect transistor (FET), forming an ISFET. The ion-selective electrode works as the *gate* of the FET device. The analyte concentration changes the surface potential between *source* and *drain*.

4.1.1.2 Amperometric biosensors

A voltage is applied, usually in cycles, and the current flow change is measured due to the electrochemical reaction, during the measurement a small percentage of analyte is consumed due to a redox reaction. Since proteins don't produce a redox reaction, they have to be labeled with enzyme to produce the necessary electrochemical reaction. The most commonly used sensors are oxygen and H_2O_2. These devices have three electrodes named: working, reference and counter. The working electrodes used for the sensing are commonly fabricated with platinum, gold or carbon; while the reference electrodes are fabricated with Ag/AgCl and the counter with platinum. The current is typically between some micro and nanoampers.

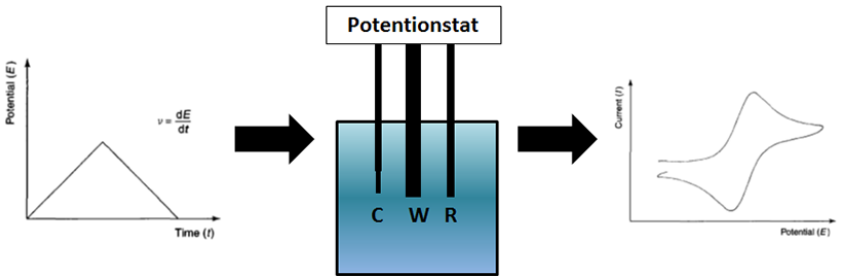

Fig. 4. 2 Working principle of an amperometric biosensor.

4.1.1.3 Impedimetric biosensors

The deposition of different layers of antibody-antigen over a surface electrode generates a change in the dielectric layer thickness and therefore in the capacitance/impedance; the change is related to the concentration of biomolecules and is the basic principle of impedimetric biosensor [3]. A fixed voltage is applied between the functionalized electrodes and the impedance change is measured, usually by an impedance spectroscope or analyzer.

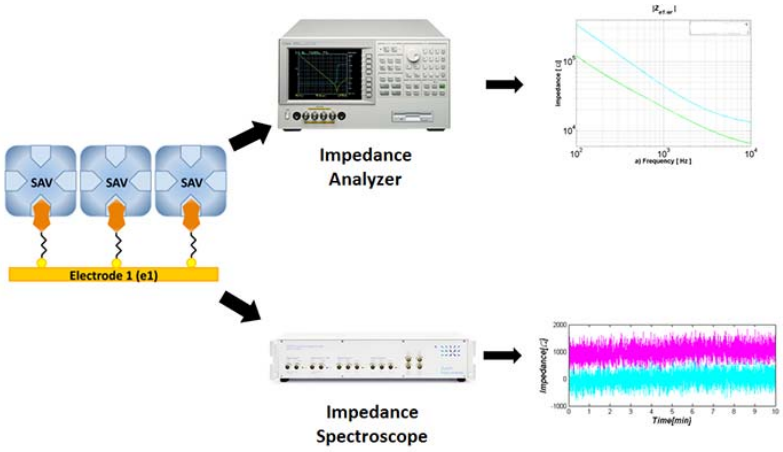

Fig. 4. 3 Scheme of an impedimetric biosensors. The analysis can be performed with different device.

4.1.1.4 Electrical double layer

When working with electrochemical biosensors an electrical double layer will be formed on the electrode–electrolyte interface (Fig. 4. 4). Several models have been proposed, being the Randles equivalent circuit the most popular. In Randles' model R_s is the solution resistance, unaffected by the presence or recognition of biological targets, R_{ct} the charge transfer resistance, Z_w the Warburg impedance, and C_{DL} the double layer capacitance. The Warburg impedance Z_w can be observed at low frequencies and it represents the delay arising from the diffusion of redox species to the electrode; therefore is important for Faradaic biosensors. R_{ct} is the resistance of the charge transfer across the interface [4].

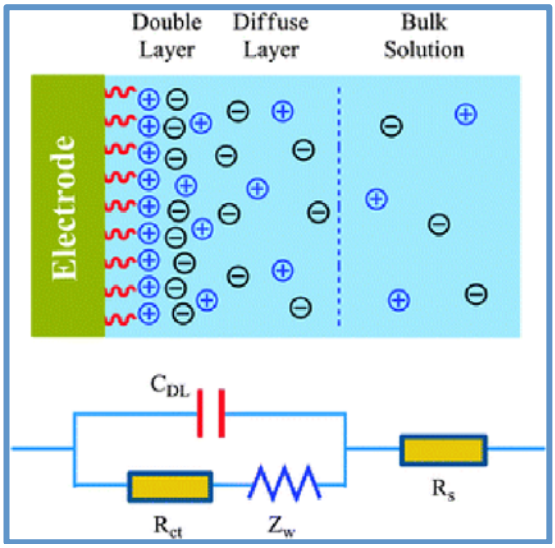

Fig. 4. 4 The electrical double layer of a receptor modified electrode–electrolyte interface and its associated Randles equivalent circuit.

4.1.2 Chapter aim

In this chapter we focused our attention in testing our device as electrochemical biosensor; we developed a selective functionalization protocol for the detection of human serum albumin as a proof of concept. We are proposing two different analyses for the detection of HSA by measuring the voltage and impedance change produced by the immobilization of the protein.

We took advantage of the knowledge acquired in our group on last years for the development of electrochemical biosensors. Castellarnau et al designed and tested an electrochemical biosensor based on ion-selective electrodes integrated with a field-effect transistor (ISFET). Bacterial metabolism was detected by monitoring pH variations. The biosensor could be used on bacteriological applications or even on food analysis [5, 6].

Kuphal et al develop a polymer-based platform for electrochemical sensing with gold electrodes. The novel process can ease the mass production and lower the costs. The electrodes were tested with impedance spectroscopy and cyclic voltammetry showing a stable response and reproducibility [7].

Several electrochemical biosensors were developed with a specific application. An impedimetric immunosensor for detection of human serum albumin was designed and tested by Caballero et al, the functionalization was done over a silicon nitride surface and the measurement were done with a electrochemical impedance spectroscope [8]. For food analysis, a label-free immunosensor was developed by Barreiros dos Santos et al for the detection of pathogenic E. coli, the pathogenic bacteria were detected by electrochemical impedance spectroscopy [9]. The immunosensors produced by our group showed to be stable and reproducible, however we wanted to use the expertise acquire with all the investigation and design a microfluidic-based biosensor in order to move towards point-of-care diagnostics.

Here we present, a lab-on-a-chip with integrated electrochemical biosensors with differential voltage and impedance analysis. The biosensors were connected as a voltage divider, therefore when a new layer was formed over the surface, the impedance changed and so the voltage potential distribution. The electrical changes were compared after the deposition of several biomolecules. And as a first proof-of-concept a protocol

for the detection of human serum albumin (HSA) was tested. This test gave us a first glimpse of the behavior of the device and helped us to analyze the effectiveness of the proposed protocols. For simplicity we analyzed the impedance modulus change in the frequency where the effect of the double layer was diminished. Also, we studied the noise component of our measurement system, since we wanted to know the limitations due to the electronic measurement.

4.2 Materials and methods

4.2.1 Protocol for the selective functionalization of the biosensors

The biosensors were characterized to the detection of Human Serum Albumin (HSA, Abcam ab8030). As in previous protocols, a selective functionalization was performed on top of one electrode (e_1) and selective blocking was done on the two remaining ones (e_2 and e_r). After each functionalization, PBS was flown into the channels at 20 µl/min during 30 minutes, and electrical measurements were performed. This allowed direct comparison of impedance and voltage values after the deposition of each layer.

The protocol started with the selective blocking of the electrodes e_2 and e_r. (Fig. 4. 5b). After the PEG-thiol deposition, the chip was rinsed by flowing PBS at 20 µl/min through both channels for 30 minutes while performing voltage and impedance measurements. The next stages were the same as the two first steps in the functionalization verification protocol, explained previously on chapter 3. However, a solution of streptavidin (Streptavidin from Streptomyces avidinii, SAV, Sigma Aldrich 85878) was introduced through the lateral channel at 6 µl/min, while PBS was introduced through the main channel at 20 µl/min, for 30 minutes. A rinsing step with PBS was performed also.

Before sensing, a layer of biotinylated HSA-specific antibody (Anti-HSA antibody, AHSA, Abcam ab81426) at a concentration of 0.5 mM was deposited selectively over the SAV layer, as a third functionalization step. The AHSA solution was kept and introduced at 6 µl/min through the lateral channel, while introducing PBS at 20 µl/min through the main channel (Fig. 4. 5e). This last functionalization lasted 30 minutes and a rinsing with PBS was performed later.

Finally, the detection of HSA was characterized by flowing different concentrations of this analyte (50 ng/ml, 1 µg/ml, 10 µg/ml and 50 µg/ml) at 6 µl/min during 30 minutes through the microchannels (Fig. 4. 5f).

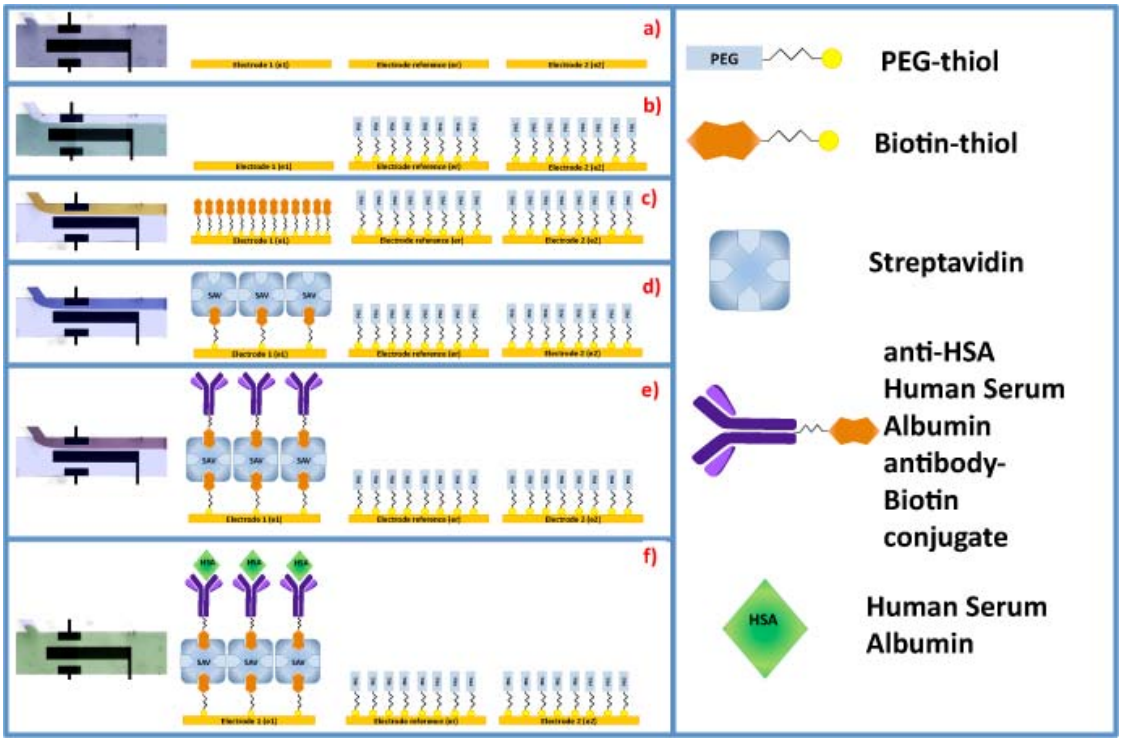

Fig. 4. 5 Protocol for the detection of human serum albumin. a) Rinsing with PBS, b) Selective blocking with a PEG-thiol solution, c) Electrode surface modified with biotin-thiol, d) Addition of a layer of streptavidin, e) Deposition of a layer biotinylated antibody, f) Detection of HSA. The images are represented in false color.

4.2.2 Voltage measurements

For the experimental set-up, the microfluidic flow at the inlets was controlled with two syringe pumps, both from KD Scientific (KDS-101) in order to control the laminar fluids co-flow, thus the selective surface functionalization inside the chip. The differential analysis of voltage was done with an Impedance Spectroscope (HF2IS by Zurich Instruments). The device was connected to the chip electrodes and an input voltage signal (V_{in}) was applied. The analysis was performed in real time, measuring the output voltage continuously during the whole test and keeping each protocol stage for up to 15 minutes. The input signal was applied between e_1 and e_2 (symmetrical electrodes) and the output was taken between e_r and the ground. Voltage drop was measured between e_1 and e_r ($V_{e1:er}$) (Fig. 4. 6).

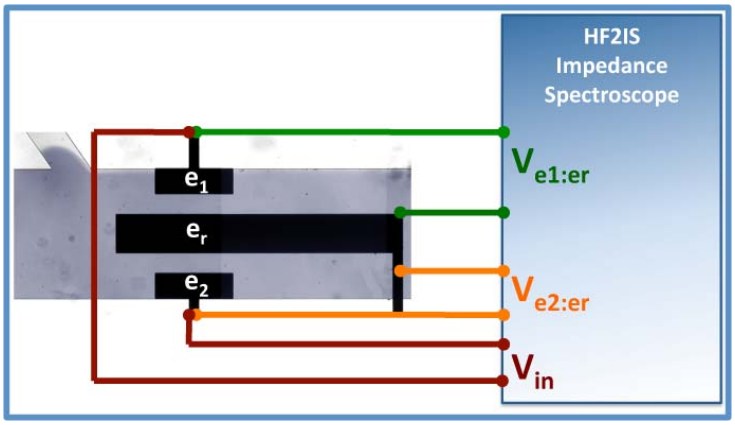

Fig. 4. 6 Schematics of the voltage measurements. Connections of the microelectrodes with the impedance spectroscope.

The voltage measured should be equivalent to a relative change on the impedance of these electrodes ($Z_{e1:er}$) in respect to the impedance ($Z_{e2:er}$) (Fig. 4. 7).

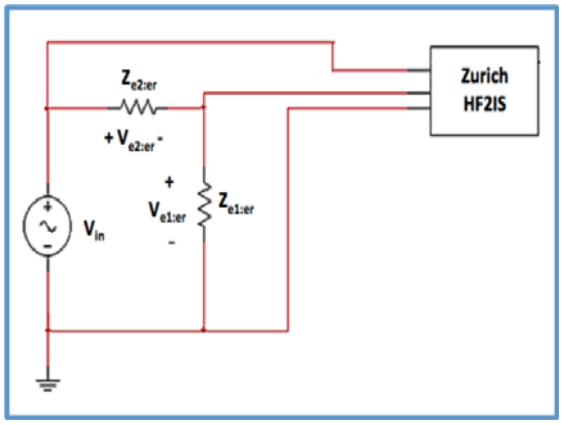

Fig. 4. 7 Electrical schematics of the voltage measurements. Voltage and impedance equivalency of the microfluidic system.

In fact, if these impedances were the same, the measured value should be half of the applied voltage. The relative change was calculated with the voltage divider as proposed in Parra-Cabrera et al (Eq. 4.1) [10].

$$\alpha = \frac{Z_{e1:er}}{Z_{e2:er}} = \frac{V_{e1:er}}{V_{e2:er}} \qquad \text{(Eq. 4. 1)}$$

4.2.3 Impedance measurements

For the experimental set-up we used the same syringe pumps from KD Scientific for the control of the microfluidic flow. The differential analysis of voltage was done with the Impedance Spectroscope (HF2IS) on real-time. A Transimpedance Current Amplifier (HF2TA by Zurich Instruments) was used to get the impedance measurements.

A diagram of the performed measurements is presented on Fig. 4. 8. The input voltage (V_{in}) is applied between e_2 and e_1. The differential voltage of the functionalized

electrode ($V_{e1:er}$), is measured directly with the HF2IS. The transimpedance current amplifier, convert an input current into output voltage. Therefore, with the HF2TA we get the current flowing across the circuit ($I_{e1:e2}$).

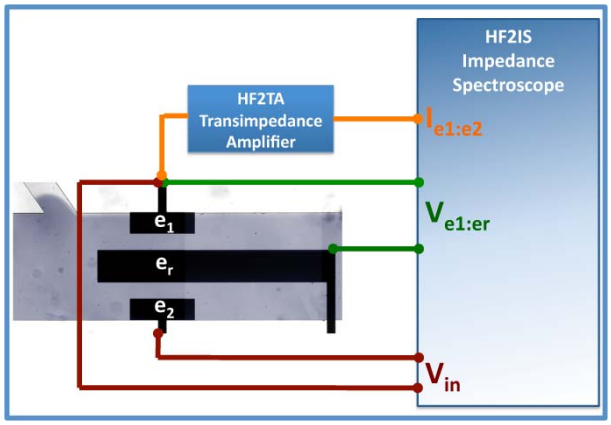

Fig. 4. 8 Schematics of the impedance measurements. Connections of the microelectrodes with the measurement devices. The impedance spectroscope was used to measure voltage and the transimpedance amplifier to convert the current into voltage.

Since we have a system that behaves as a voltage divider (Fig. 4. 9), the differential voltage of the blocked electrode ($V_{e2:er}$), is obtained indirectly:

$$\mathbf{V_{e2:er} = V_{in} - V_{e1:er}} \qquad \text{(Eq. 4. 2)}$$

With the transimpedance current amplifier (HF2TA), we get the current of the circuit ($I_{e1:er} \approx I_{e2:er} \approx I_{e1:e2}$). With the current and voltages measured, by Ohm's Law, we can get the value of the functionalized impedance ($|Z_{e1:er}|$) and the blocked impedance ($|Z_{e2:er}|$). The analysis is performed "in situ" and on real-time using a custom-made MatLab program. The impedance modulus of e_1 could be obtained directly:

$$\left|Z_{e1:er}\right| = \frac{V_{e1:er}}{I_{e1:e2}} \qquad \text{(Eq. 4. 3)}$$

The impedance modulus of e_2 is obtained indirectly:

$$\left|Z_{e2:er}\right| = \frac{V_{in} - V_{e1:er}}{I_{e1:e2}} \qquad \text{(Eq. 4. 4)}$$

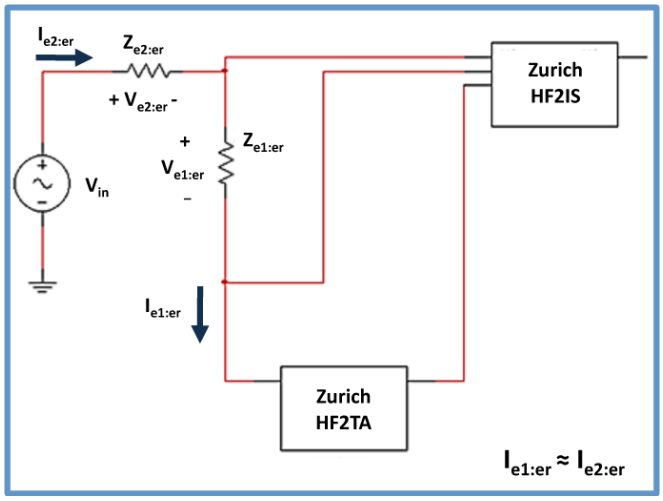

Fig. 4. 9 Electrical schematics of the voltage measurements. Voltage and impedance equivalency of the microfluidic system.

Characterization of the noise in the impedance measurements

Since we could expect small changes in impedance when detecting biomarkers, we wanted to characterize the intrinsic noise associated with the circuit elements and measurement devices; in order to get the limits of our system. The noise of the measurement can be obtained and compared with the anticipated signal levels to determine if impedance pre-amplification is required for a biomarker. The noise response of the transimpedance current amplifier (HF2TA) was characterized and the RMS of the signal was calculated. For this characterization, two resistances were connected as a voltage divider (instead of our chip) and the value of the resistance was measured with the Zurich's devices Fig. 4. 10. The resistance number 2 (Z_2) was fixed while the resistance number 1 changed (Z_1). The values of the impedance were swept between 120Ω and 100 kΩ.

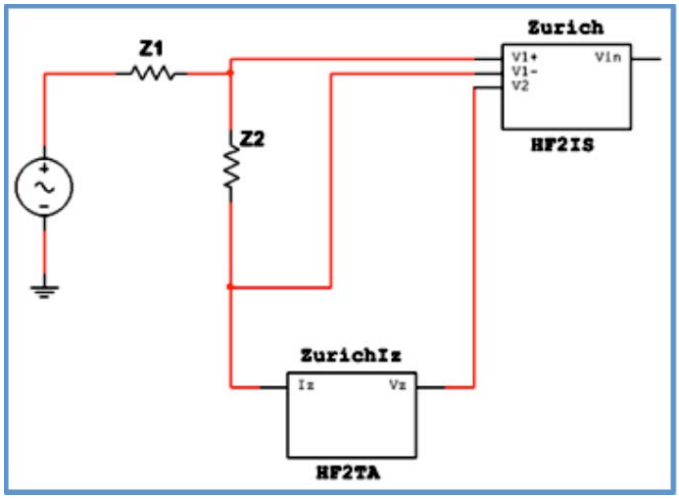

Fig. 4. 10 Schematics of the noise characterization set-up. To study the noise of the measurement devices two known resistances were connected as voltage divider.

4.3 Results and discussions

4.3.1 Differential voltage detection protocol

In the final experiments, the device was connected to the chip electrodes and a 3mV at 1 kHz signal was applied, the input was chosen after a complete characterization of the frequency spectrum (Chapter 3). As a proof-of-concept we selected human serum albumin as biomarker. The new HSA layer changed the impedance modulus of $|Ze_1:e_r|$ while keeping the impedance of $|Ze_2:e_r|$ unaffected. This was reflected on the measured output voltage ($V_{e1:er}$), and thus on the relative impedance.

To characterize the detection range, voltage drop was measured between e_1 and e_r and the percentage of change was calculated (α). Re-writing Eq. 4.1

$$\alpha = \frac{Z_{e1:er}}{Z_{e2:er}} = \frac{V_{e1:er}}{V_{e2:er}}$$

The results were obtained with three concentrations of HSA: 17 µg/ml, 85 µg/ml and 170 µg/ml (Fig. 4. 11).

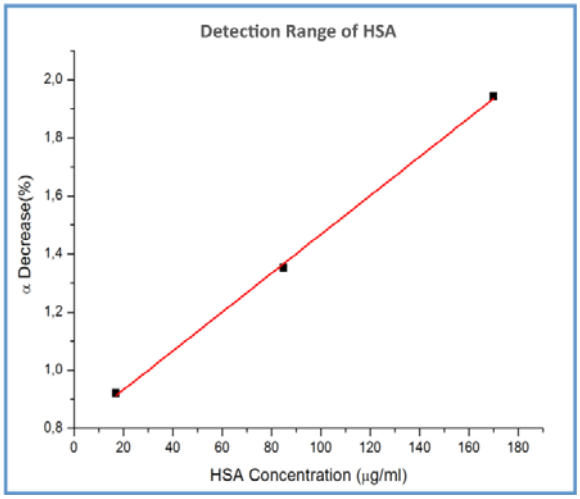

Fig. 4. 11 Detection range for the human serum albumin protein. Voltage measurements. The factor α was calculated and a decrease in voltage was observed after the deposition of the protein. The factor α was obtained as proposed in Parra-Cabrera et al.

With the three points, a linear fitting analysis was performed to predict the percentage change in relation with the concentration of protein for the system that is related to the sensitivity of the system.

$$\Delta\alpha = (0.00669 * HSA(x) + 0.799)\% \qquad \text{(Eq. 4. 5)}$$

The impedance dropped after the deposition of the HSA. This seems contradictory since albumin is a big protein (~69kDa). However, the interaction between HSA and its antibody can increase the polarity of the antigen layer, due to conformational changes of antigen-antibody [8, 11]. At this point, and with the available information this was our hypothesis to justify the result. The results obtained during this proof-of-concept of the device served as the base for the first peer-reviewed publication related to this thesis [10].

4.3.2 Differential impedance detection protocol

Characterization of the noise in the impedance measurements

The noise response of the measurement devices was characterized and the RMS of the signal was calculated. The value of RMS can limit and affect the LOD and LOQ of our system. With the characterization of the noise we can predict the limits of our device depending on the impedance values for a given application. A fitting analysis was performed in order to know the noise related to the measurement device (Fig. 4. 12).

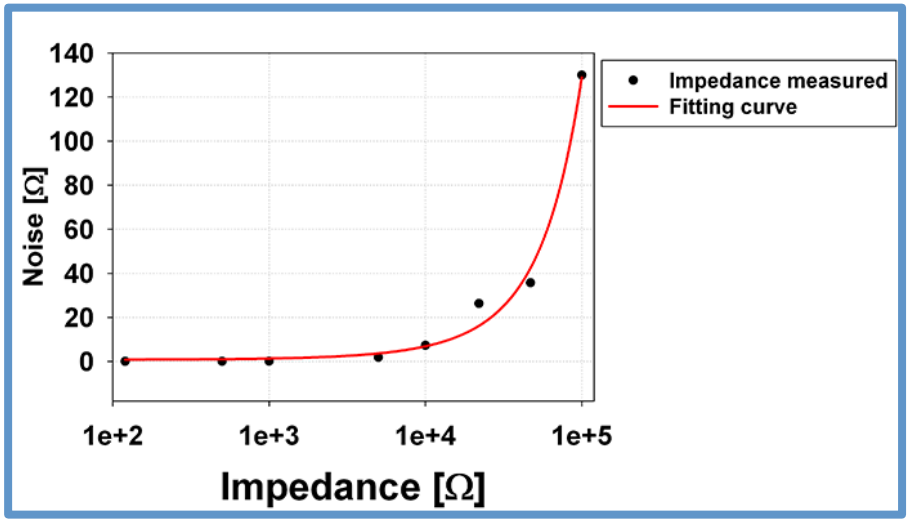

Fig. 4. 12 The noise produced by the measurement devices was characterized. The noise limits the LOD for the detection of a biomarker.

The noise response can be characterized by the next quadratic equation:

$$Noise(Z) = -7.47x10^{-9} * Z^2 - 5x10^{-4} * Z - 0.78 \qquad \text{(Eq. 4. 6)}$$

Where Z is the value of the measured impedance. In order to get the correct values of LOD and LOQ for our device, we can't differentiate between an impedance change produce by a biomarker that is smaller than 40 Ω.

Impedance measurements

A voltage input (V_{in}) of 0.1V at 1 kHz was applied between e_1 and e_2; the analysis was performed at this frequency since previous experiments showed a larger differential signal for this band (Chapter 3).

With the impedance and voltage analysis we characterized the sensor detection range, sensitivity, limit of detection (LOD), limit of quantification (LOQ) and p-values of our device for different concentrations of human serum albumin (50 ng/ml, 1 µg/ml, 10 µg/ml and 50 µg/ml). We measured both, impedance and voltage after the deposition of the antibody (AHSA) and after the detection of the protein (HSA). We expected an increase of impedance and voltage after the deposition of HSA and we calculated the increment to later plot the results (Fig. 4. 13).

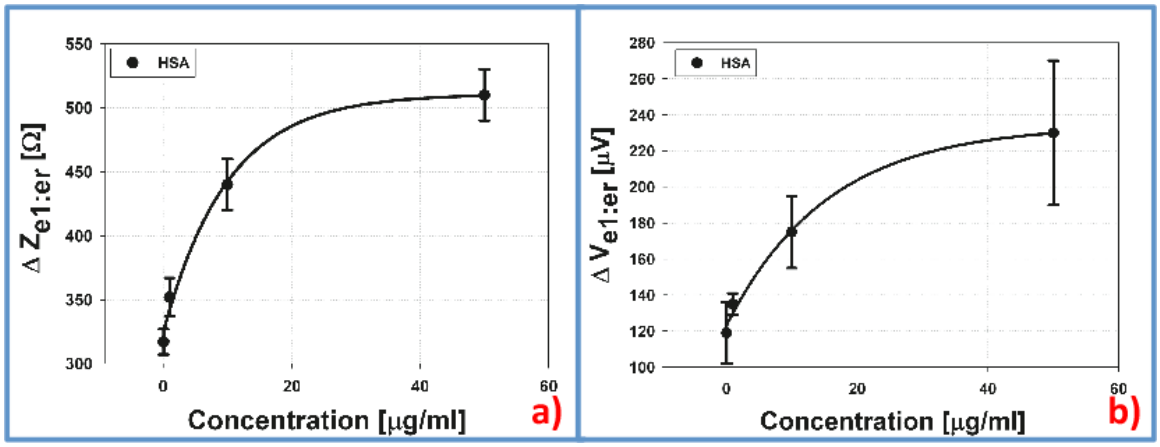

Fig. 4. 13 Detection range of the microfluidic system for HSA. A linear tendency was observed between 0.05 -10 µg/ml and a fitting analysis was performed. a) Shows the results for the impedance modulus analysis, b) Represents the measurements of the differential voltage.

We focused the analysis to the electrode e_1 since e_2 was blocked with PEG and we were expecting no significant change in its impedance. The equations related to the measurements can be expressed as:

$$\Delta|Z_{e1:er}| = |Z_{e1:er}(HSA)| - |Z_{e1:er}(AHSA)| \quad \text{(Eq. 4. 7)}$$

$$\Delta|V_{e1:er}| = |V_{e1:er}(HSA)| - |V_{e1:er}(AHSA)| \quad \text{(Eq. 4. 8)}$$

The impedance detection range chart shows a linear tendency for concentrations between 50 ng/ml and 10 µg/ml, for impedance and voltage differential measurements. The slope of the linear regression represents the sensitivity of the system.

$$\Delta|Z_{e1:er}| = (11.33 * HSA(x) + 327.9)\Omega \quad \text{(Eq. 4. 9)}$$

$$\Delta|V_{e1:er}| = (5.154 * HSA(x) + 124)\mu V \quad \text{(Eq. 4. 10)}$$

As proposed on the previous section and reported in Parra-Cabrera et al, we suggested that any change on the voltage drop is equivalent to a change in the impedance modulus:

$$\alpha = \frac{Z_{e1:er}}{Z_{e2:er}} = \frac{V_{e1:er}}{V_{e2:er}} \quad \text{(Eq. 4. 11)}$$

The factor α was defined considering an ideal performance: same electrodes area, totally blocked surface on the reference electrodes, zero non-specific adsorption. We also calculated the percentage of increment of factor α after the deposition of HSA. First we started by getting the value of α for the antibody deposition:

$$\alpha(AHSA) = \frac{|V_{e1:er}(AHSA)|}{|V_{e2:er}(AHSA)|} \quad \text{(Eq. 4. 12)}$$

After the deposition of HSA, we also calculated the value of α:

$$\alpha(HSA) = \frac{|V_{e1:er}(HSA)|}{|V_{e2:er}(HSA)|} \quad \text{(Eq. 4. 13)}$$

And finally we plotted the percentage increment of α (Fig. 4. 14) and we got the equation for the linear regression:

$$\Delta\alpha = \frac{\alpha(HSA)}{\alpha(AHSA)} * 100\%$$
$$\Delta\alpha = (0.05523 * HSA + 1.117)[\%] \quad \text{(Eq. 4. 14)}$$

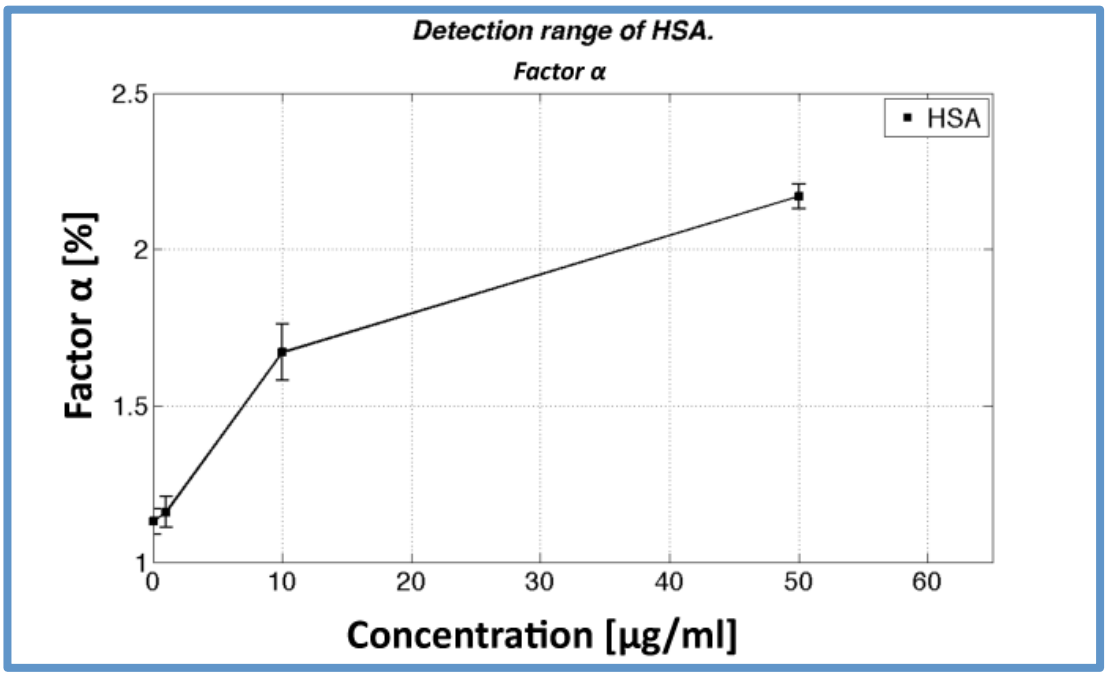

Fig. 4. 14 Detection range of the microfluidic system for HSA. A linear tendency was observed between 0.05 -10 µg/ml and a fitting analysis was performed. Corresponds to the factor α calculations.

The LOD is the lowest analyte concentration likely to be reliably distinguished between each sample, while LOQ is the lowest concentration at which the analyte can not only be reliably detected but at which some predefined goals for bias and imprecision are met [12]. Both parameters can be obtained with a linear regression with the next equations [13]:

$$LOD = \frac{3.3 * SD}{b} \qquad \text{(Eq. 4. 15)}$$

$$LOQ = \frac{10 * SD}{b} \qquad \text{(Eq. 4. 16)}$$

Where, SD is the standard deviation of the linear regression and *b* is the slope of the linear regression. Table 4. 1 summarizes the results obtained.

Table 4. 1 LOD, LOQ and sensitivity for the different electrical measurements

Measurement	LOD [µg/ml]	LOQ [µg/ml]	Sensitivity
$\Delta \mid Z_1 \mid$	0.77	2.33	11.3 [Ω*(µg/ml)$^{-1}$]
$\Delta \mid V_1 \mid$	0.77	2.35	5.2 [µV*(µg/ml)$^{-1}$]
Factor α	0.87	2.66	0.05 [%*(µg/ml)$^{-1}$]

We also calculated the p-value, using a standard t-student test, among the concentrations measured in order to compare if the samples were statistically different.

Table 4. 2 Comparison among the different concentration: p-values

Measurement	p-value: 50ng/ml - 1µg/ml	p-value: 1µg/ml - 10µg/ml	p-value: 10µg/ml - 50µg/ml
$\Delta \mid Z_1 \mid$	0.028	0.004	0.013
$\Delta \mid V_1 \mid$	0.199	0.029	0.100
Factor α	0.672	0.002	0.002

Ohm's law directly relates impedance modulus and voltage, and therefore the slope or sensitivity of both tendency graphs should be similar. However, the voltage drop on e_1 ($V_{e1:er}$) depends on the voltage drop on e_2 ($V_{e2:er}$), and vice versa. If the surface of e_2 is not totally blocked, after detection, the impedance of e_2 could increase and therefore the voltage $V_{e2:er}$. This change on $|Z_{e2:er}|$ explains why the sensitivity on the voltage tendency graph is almost 2.2 times smaller than the sensitivity of the impedance. We have a small amount of unspecific adsorption that affect the sensitivity of the voltage measurements and factor alpha, however the impedance modulus ($|Z_{e1:er}|$) is not affected by this effect, since the impedance of e_1 is directly measured by a 4 point technique, and the changes of e_2 also modify the current keeping the measures of $|Z_{e1:er}|$ without any significant change.

The LOD and LOQ for voltage and impedance are practically the same, and we are proving that our novel differential voltage measurement system can simplify the read-out with a similar response but with a smaller sensitivity. The voltage and impedance analysis is performed directly with $|Z_{e1:er}|$, while the factor α relates directly the measurement of both impedances ($|Z_{e1:er}|$ and $|Z_{e2:er}|$). Therefore, the increment of 10% of the LOD and LOQ from the factor α leads us to think that both impedance are changing and so the blocking protocol is not the best and could be improve.

In order to verify the results obtained so far, we performed the t-student statistical test. As expected the impedance measurements have a statistically significant difference between all the tested concentrations and therefore are the most reliable data that we can get. The voltage analysis showed that there is not statistically significant difference between concentrations, so the data overlaps, also due to the blocking. However, to overcome the voltage problems, the factor α was proposed, and we are now able to analyze samples that have a statistically significant difference.

4.4 Conclusions

The microfluidic device tested included a sensing concept based on real-time direct monitoring impedance changes due to biomolecules deposition. A differential voltage and impedance measurements were done with the chip, which also included a real time analysis. This first results helped to publish the proof-of-concept of our device [10].

The sensitivity of the system was characterized by means of HSA detection by electrical changes measurements. A sensitivity of 11.33[$\Omega*(\mu g/ml)^{-1}$] for impedance, and 5.15 [$\mu V*(\mu g/ml)^{-1}$] for voltage were obtained for HSA proof-of-concept experiment.

The LOD and LOQ were obtained for both types of measurements. For impedance we had a LOD = 0.77 [μg/ml] and a LOQ = 2.33 [μg/ml]. For the voltage measurements the LOD = 0. 77 [μg/ml] and LOQ = 2.35 [μg/ml]. The factor α showed an increment of 10% in both LOD and LOQ. The difference in the factor α showed that the blocking of the electrodes could be improved.

The statistical analysis told us that the impedance measurements are the most reliable samples due to its differences in p-values. The voltage showed no significant difference among samples, but by improving the blocking and changing the protocol we could solve that challenge.

The factor α was proposed to overcome the difference between the geometry of electrodes and problems on the blocking, and with the characterization of HSA, that factor showed its usefulness. With the increment of its limits of detection we realized that we had an issue with the blocking. It also was helpful to work with statistically different samples, since error was diminished because we were using the data of both pair of electrodes. However, further work was necessary in order to improve the sensitivity of the system. With the noise we are limited to detect changes smaller than 40Ω or in our proof-of-concept to 2 μg/ml of HSA (LOQ). Therefore, on the next chapter we are going to explain the changes and results that helped us to improve the sensitivity for a given biomedical application.

4.5 References

1. B. R. Eggins, Chemical Sensors and Biosensors, Wiley, 2002.
2. K. Wojciechowski, Current Opinion in Colloid & Interface Science, 2011, **16**, 601-606.

3. T. R. J. Holford, F. Davis and S. P. J. Higson, Biosensors and Bioelectronics, 2012, **34**, 12-24.
4. R. N. Vyas, K. Li and B. Wang, The Journal of Physical Chemistry B, 2010, **114**, 15818-15824.
5. M. Castellarnau, N. Zine, J. Bausells, C. Madrid, A. Juárez, J. Samitier and A. Errachid, Sensors and Actuators B: Chemical, 2007, **120**, 615-620.
6. M. Castellarnau, N. Zine, J. Bausells, C. Madrid, A. Juárez, J. Samitier and A. Errachid, Materials Science and Engineering: C, 2008, **28**, 680-685.
7. M. Kuphal, C. A. Mills, H. Korri-Youssoufi and J. Samitier, Sensors and Actuators B: Chemical, 2012, **161**, 279-284.
8. D. Caballero, E. Martinez, J. Bausells, A. Errachid and J. Samitier, Analytica Chimica Acta, 2012, **720**, 43-48.
9. M. Barreiros dos Santos, J. P. Agusil, B. Prieto-Simón, C. Sporer, V. Teixeira and J. Samitier, Biosensors and Bioelectronics, 2013, **45**, 174-180.
10. C. Parra-Cabrera, C. Sporer, I. Rodriguez-Villareal, R. Rodriguez-Trujillo, A. Homs-Corbera and J. Samitier, Lab on a Chip, 2012.
11. C. Berggren and G. Johansson, Analytical Chemistry, 1997, **69**, 3651-3657.
12. D. A. Armbruster and T. Pry, Clin Biochem Rev, 2008, **29**, S49-52.
13. A. Shrivastava and V. B. Gupta, Chronicles of Young Scientists, 2011, **2**, 21.

CHAPTER 5 Application of LOC to single biomarker detection: prostate-specific antigen

5.1 Introduction

In this chapter, an overview of prostate cancer is presented (PCa). The state-of-the-art devices developed for prostate cancer detection are presented too. We also present the lab-on-chip fabricated and tested for the detection of prostate-specific antigen, the characterization of the device, and the flexibility of the system.

As biomedical application, we selected the detection of prostate cancer. There are different biomarkers for this disease, however we chose prostate-specific antigen (PSA) for the characterization of our novel microfluidic device. We opted for PSA since is the protein that clinicians commonly use to diagnose PCa. The measurements were performed with the same novel real-time voltage and impedance differential analysis. The previous work helps us to overcome the geometric differences between electrodes, therefore once again the parameter α was calculated and the detection range was characterized. The limits of detection as well as the sensitivity of the system were calculated. The novel microfluidic device was fully characterized for its biosensing capabilities and a statistical test was used to validate to results obtained.

5.1.1 Cancer

The unregulated growth of cell and their spread, over different parts of the body, are the main characteristics that define a cancer disease. Therefore, cancer is a group of diseases; that have similar cell behavior. The treatment of cancer must be personalized, since each type of cancer spreads differently and the sensitivity to treatment differs on every case [1].

A cancer cell started as a normal cell, but several cellular processes changed its characteristics and evolution. To avoid an excess of cells on the body; there is a programmed mechanism for cell death called apoptosis. The programmed apoptosis kill the cell and cleans the derivate products without an inflammatory process. However, in almost all tumors, the cell mutates and the apoptosis mechanism seems to be disabled, leading to an overproduction of cell in the damage tissue.

A tissue with a large population of stem cells (breast, prostate, lungs, etc.); is the most suitable place for the development of cancer. The rare population of proliferating stem cells replicate themselves in an endless cycle called self-renewal, giving rise to intermediate and eventually mature cells [2].

The antigens in a cancer cell and the biologic behavior are the main differences in comparison with normal cells. The mutation of a cell is preceded by a defect in DNA, especially in the repair system of the tumor cell [3]. A new genetic sequence is the result of the few hundred of mutations of cancer cell genome. The mutations affect the intracellular proteins and the production of antigens and they differ from a normal cell; therefore the antibodies in the patient are unspecific for the new production of cancer related antigens [4].

When a tissue is having a great production of cancer cells a metastasis process is likely to happen. Starting by an invasion of tumor cells to the surrounding tissue. The cells intravasate and enter the circulatory or lymph system. The interaction with the blood produces a new mutation on the cells, so they can survive in this environment. Then the cells are extravasated into a new tissue, where they proliferate and develop a vascular system to help their growth [4] (Fig. 5. 1).

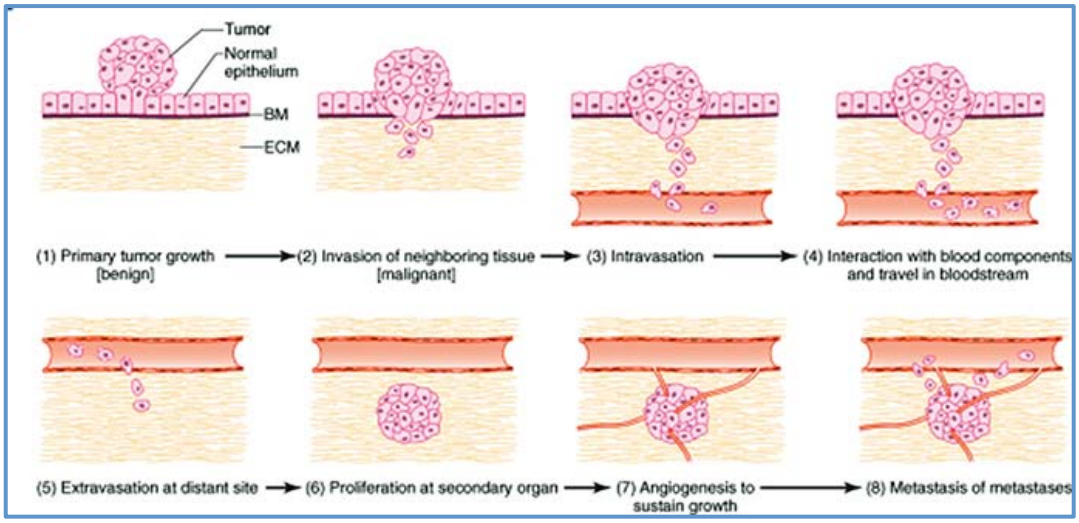

Fig. 5. 1 Metastasis process of tumor cells

5.1.2 Prostate cancer

On 2008, a prediction of 890,000 new cases per year was reported in the project GLOBOCAN [5]. In USA, the American Cancer Society (ACS) estimated more than 238,000 new cases for 2013, being prostate cancer the most diagnosed cancer type in men. A prediction of deaths by prostate cancer was also estimated for 2013, reaching

almost 30,000 cases [6]. In Europe, prostate cancer is the third most common cause of death by cancer, with an estimation of more than 70,000 new deaths for 2013 [7].

The prostate

The prostate is a gland that surrounds the urethra and is lying down to the bladder. The main function of the prostate is to secrete an alkaline fluid with citric and phosphate acid, calcium, a clotting enzyme and a profibrinolysin; the fluid increases the quantity of semen and is secreted during ejaculation [8].

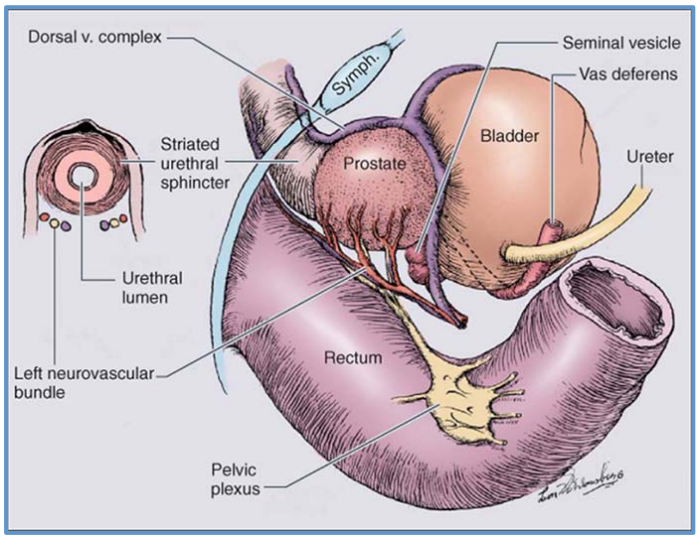

Fig. 5. 2 The anatomy of the prostate

Disorders of the prostate

The disorders presented on the prostate are inflammation or prostatitis, benign prostatic hyperplasia (BPH) and prostate cancer. These disorders can elevate the concentration of prostate-specific antigen in serum.

Prostatitis.- Is an inflammatory disorder, chronic or recurrent, of the prostate gland. Some studies propose that a recurrent inflammation might help to the development of prostate cancer [9] (Fig. 5. 3).

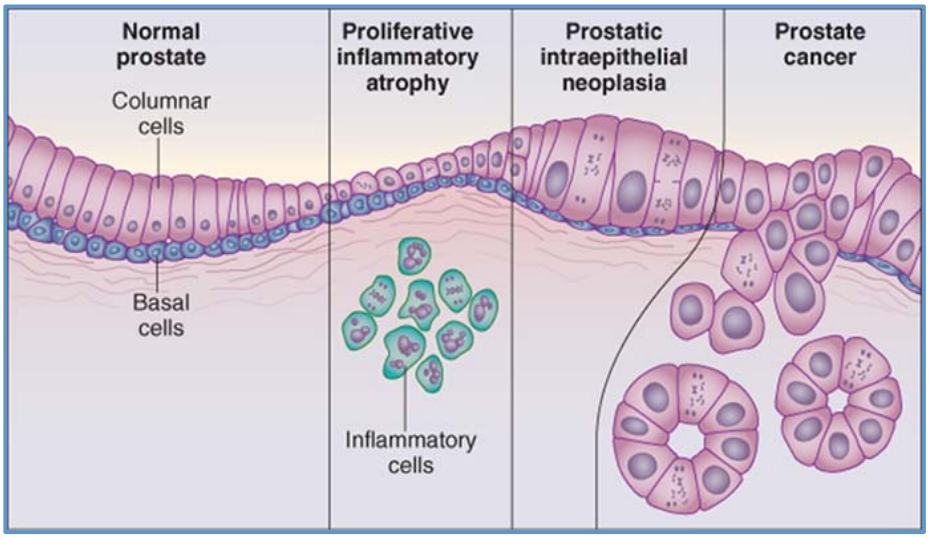

Fig. 5. 3 Inflammatory process as a precursor of prostate cancer.

Benign prostatic hyperplasia.- Is an enlargement of the prostate, related to the age and is nonmalignant. Nodular lesions are formed in the periurethral region in comparison with the lesions formed in the peripheral zone that are related to prostate cancer.

Prostate cancer.- A series of genome alterations are presented in prostate cancer cells, which include gene mutations or deletion, changes in DNA or chromosomal rearrangements, among others. The alterations can happen in many decades and be influenced by lifestyle [4]. Since the damage of prostate cancer is developed on the periphery of the gland, the disease rarely shows some kind of symptoms. When the damage touches the urethra, the symptoms start to develop. However, that can be a sign of an advance of the disease or a metastatic process. A digital rectal examination (DRE) as well as a prostate-specific antigen measurement helps to detect early stages of prostate cancer. A biopsy is usually performed to confirm a PCa diagnose.

Prostate-specific antigen (PSA) is a 33 KDa serin protease produced by the prostate epithelium that is used in oncology as a biomarker to detect early stages of prostate cancer [10]. Levels of PSA in serum lower than 4 ng/ml had been used as a reference in healthy men [11]. Elevated levels of PSA in serum could help to detect patients with prostatic epithelial changes, especially PCa. PSA concentration in serum usually increases with age [12] and the cut-off value depend on the age of the patient and the initial PSA levels [13]. Since almost all diagnosed patients are 50 years or older, the risk of death by PCa increases with the age [14]. Therefore, for an early detection of PCa, it is desirable to have a device easy to use, fast, disposable, cheap and capable of perform the analysis in situ. Furthermore, evolution of PSA levels is by far more

relevant for diagnosis than a single point analysis and a methodology suitable for Point-of-Care analysis could make a big difference in the diagnosis and follow up of PCa.

5.1.3 Prostate-specific antigen biosensors

Different signal transduction had been used for the detection of PSA, and depending on the transduction these biosensors can be classified in: optical, electrical or mechanical. Some of these biosensors had being labeled, and the labeling could be done by a fluorescent nanoparticle [15], in a biobarcode assays [16] or in an electrochemical immunoassays [17], sensing concentrations as low as 1 pg/ml in a matter of hours . However, the main issues of the label-base biosensors are the time and cost consuming, and in some cases non-specificity, therefore increasing the use of label-free methods [18].

Electrochemical biosensors are the choice of preference when a label-free method is selected, due to their sensitivity, selectivity, fast response, small packaging and low power requirements [19]. Different types of biosensors had been developed for the detection of PSA in the last years depending on the electrical method of measurement: field-effect transistor biosensors [20, 21], voltammetry [22] and Electrochemical Impedance Spectroscopy (EIS) [23]. The electrochemical biosensors usually are embedded in a microfluidic system or lab-on-chip. Some of the advantages of the microfluidic platforms are the low reagent and sample consumption, fast analysis times, automatization and flexibility [24].

5.2 Materials and methods

Determination of the blocking protocol

The results presented on previous chapters showed that the blocking on the reference electrodes (e_2 and e_r) should be improved. Then, previously the characterization of the detection of PSA, we studied the effect of the blocking solution to improve the voltage output. We tested the effect of deposition time and concentration of the blocking solution, and then we selected the most suitable parameters in order to improve the blocking step in the detection protocol.

The first test started by blocking the reference electrodes with a solution of 11-Mercaptoundecyl tetra(ethylene glycol) (PEG-Thiol, Sigma Aldrich 674508) in ethanol, at a concentration of 1 mg/ml during 30 minutes. As second test, we increased the time of PEG-Thiol deposition up to 60 minutes and kept the concentration at 1 mg/ml.

Finally, we increased the concentration of PEG-Thiol to 10 mg/ml and kept the solution flowing until 30 minutes. The voltage output was measured for the different tests, and the response was analyzed. For each test we used a new chip. The parameters obtained helped to modify the protocol for the detection of PSA.

Determination of the adjustability of the sensitivity for PSA

The device was characterized for the detection of PSA protein (PSA, Abcam ab78528) and to adjust the sensitivity of the system. A selective functionalization was performed on top of one electrode (e_1) and selective blocking was done on the two remaining ones (e_2 and e_r). After each functionalization, phosphate buffered saline (PBS) was flown into the channels at 20 µl/min during 30 minutes, and electrical measurements were performed. This allowed direct comparison of impedance and voltage values after the deposition of each layer.

The protocol started with the selective blocking of the electrodes e_2 and e_r. This was accomplished by introducing a solution of 11-Mercaptoundecyl tetra(ethylene glycol) (PEG-Thiol, Sigma Aldrich 674508) in ethanol, at a concentration of 10 mg/ml, at 6 µl/min, through the main channel (Fig. 5. 4b). Simultaneously, PBS buffer was kept at a rate of 4 µl/min through the lateral channel. This process lasted 30 minutes and served to set the electrodes e_2 and e_r as a reference. After the PEG-thiol deposition, the chip was rinsed by flowing PBS at 20 µl/min through both channels for 30 minutes while performing voltage and impedance measurements.

A first selective functionalization of e_1 was performed with a solution of biotinylated alkyl thiols with a polyethylene glycol linker (biotin-thiol), prepared as reported by Prats-Alfonso et al [25], and dissolved in ethanol at a concentration of 10^{-3} M. The biotin-thiol layer was deposited selectively on top of the e_1 by controlling the microfluidic co-flow. This solution was flowed through the lateral channel (6 µl/min) while PBS flowed simultaneously through the main channel (25 µl/min). The functionalization time was 60 minutes followed by a PBS rinsing procedure of 30 minutes (Fig. 5. 4c).

The second selective functionalization consisted on forming a layer of streptavidin on top of the biotin layer, this step helped as a connector between the monolayer formed over the gold surface and the antibody of interest. A solution of

streptavidin (Streptavidin from Streptomyces avidinii, SAV, Sigma Aldrich 85878) was introduced through the lateral channel at 6 µl/min, while PBS was introduced through the main channel at 20 µl/min, for 30 minutes. A rinsing step with PBS was performed also (Fig. 5. 4d).

Before sensing, a third selective functionalization was done with Anti-Prostate Specific Antigen antibody (APSA, Abcam ab77310). The APSA solution at a concentration of 100 µg/ml was flown through the lateral channel at 3 µl/min while PBS buffer solution was flown at 10 µl/min through the main channel. The deposition of the antibody lasted 90 minutes (Fig. 5. 4e).

Finally a detection of PSA was performed. The PSA was introduced through the two channels at a flow rate of 6 µl/min during 60 minutes (Fig. 5. 4f). The concentrations characterized were 1ng/ml, 5 ng/ml, 10 ng/ml and 50 ng/ml. After each functionalization and blocking step, a rinsing was done with PBS at 20 µl/min for 30 minutes; then measurements were performed.

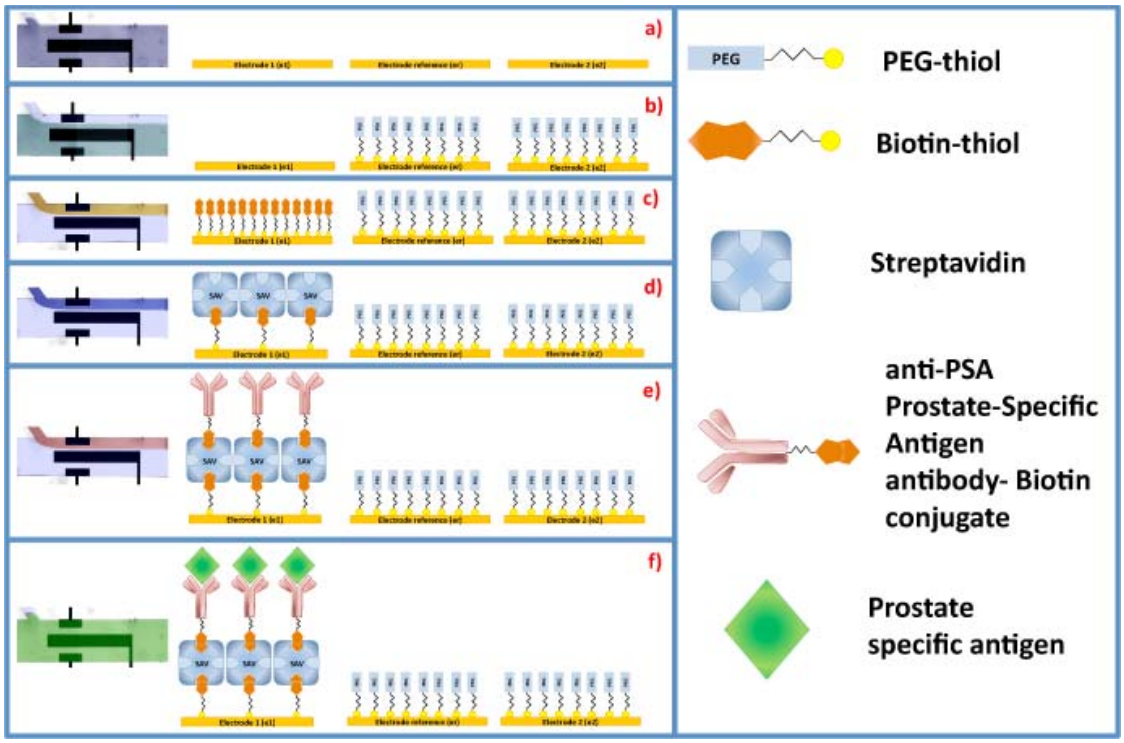

Fig. 5. 4 Protocol for the detection of prostate-specific antigen. a) Rinsing with PBS, b) Selective blocking with a PEG-thiol solution, c) Electrode surface modified with biotin-thiol, d) Addition of a layer of streptavidin, e) Deposition of a layer biotinylated antibody. f) Detection of PSA. The images are represented in false color.

Impedance and Voltage measurements

A diagram of the performed measurements is presented on Fig. 5. 5. The input voltage (V_{in}) is applied between e_2 and e_1, the input is 0.1 V at a frequency of 1kHz, the input was chosen after a complete characterization of the frequency spectrum.

The differential voltage of the functionalized electrode ($V_{e1:er}$), is measured directly with the HF2IS. Since we have a system that behaves as a voltage divider (Fig. 5. 5b), the differential voltage of the blocked electrode ($V_{e2:er}$), is obtained indirectly, $V_{e2:er} = V_{in} - V_{e1:er}$.

The transimpedance current amplifier, convert an input current into output voltage. Therefore, with the HF2TA we get the current flowing across the circuit ($I_{e1:e2}$). With the current and voltages measured, by Ohm's Law, we can get the value of the functionalized impedance ($|Z_{e1:er}|$) and the blocked impedance ($|Z_{e2:er}|$). The analysis is performed "in situ" and on real-time.

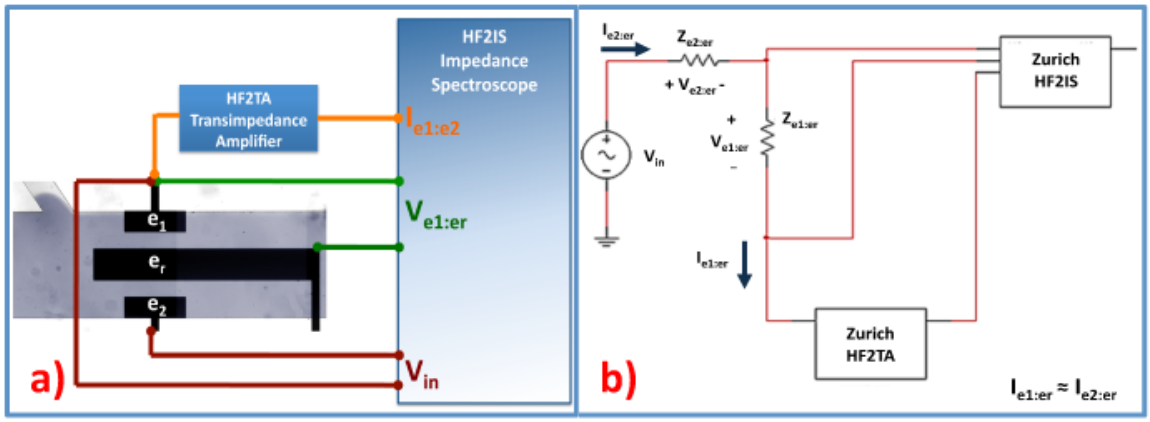

Fig. 5. 5 Electrical schematics of the measurements. a) Connections of the microelectrodes with the measurements devices, b) Impedance equivalency of the microfluidic system.

5.3 Results and discussions

5.3.1 Determination of the blocking protocol to improve the voltage output

In order to test the effect of the blocking solution over the reference electrodes, we detected PSA at a concentration of 1 ng/ml. We measured the voltage drop ($V_{e1:er}$) and analyzed the voltage increment after the detection of PSA in comparison with the functionalization of the antibody (APSA).

The undesired deposition of PSA on e_2 could affect directly the voltage drop on both microelectrodes ($V_{e1:er}$ and $V_{e2:er}$), and thus the sensitivity of the voltage could be

diminished. We expected an increment in the voltage drop of the functionalized electrode ($V_{e1:er}$), after the detection of PSA. However, with the PEG-Thiol solution at a concentration of 1 mg/ml and a deposition time of 30 minutes, we observed a decrement on $V_{e1:er}$ of almost 100 µV (Fig. 5. 6a).

The blocking had to be improved after the results of the first test. And so, the deposition time was changed in order to increase the blocked surface. The voltage drop of the functionalized electrode ($V_{e1:er}$) was improved in comparison with the previous test (Fig. 5. 6b). However, there is not a significant difference in voltage when comparing the deposition of antibody (APSA) and protein (PSA). So, a greater improvement must be performed before the complete characterization of the sensitivity of PSA.

Consequently, we tested the PEG-Thiol solution at a concentration of 10 mg/ml during a deposition time of 30 minutes and observed that the voltage drop on e_1 was improved dramatically. We got a voltage increment of almost 75 µV after the detection of PSA at a concentration of 1 ng/ml (Fig. 5. 6c).

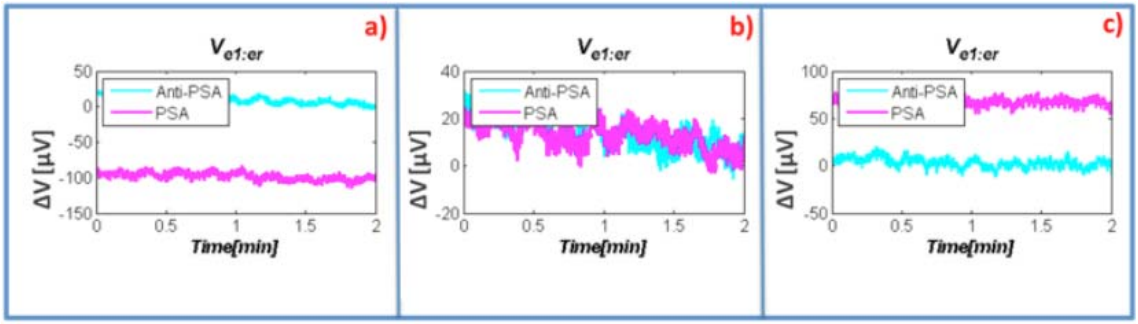

Fig. 5. 6 Effect of PEG-Thiol solution on voltage drop. Different concentrations and times of deposition. a) Concentration of 1 mg/ml for 30 minutes. b) Concentration of 1 mg/ml for 60 minutes. c) Concentration of 10 mg/ml for 30 minutes. For the latter characterization of PSA we selected the parameters of the last test (c).

With the results obtained we chose a concentration of 10 mg/ml of PEG-Thiol and a deposition time of 30 minutes. After selecting these parameters we started the determination of the adjustability in the detection range for PSA. And as explained previously, only the sensitivity of the voltage measurements is affected by a surface not totally blocked. Since the impedance measurements were done directly the effects of non-specific adsorption are disregarded.

5.3.2 Determination of the adjustability in the detection range for PSA

The device was then characterized for different concentrations of PSA (1 ng/ml, 5 ng/ml, 10 ng/ml and 50 ng/ml) for a real-time monitoring. The voltage input applied was 0.1 V at 1 kHz, between e_1 and e_2. Impedance measurements were performed with the Zurich devices (HF2IS and HF2TA). The impedance modulus ($|Z_{e1:er}|$ and $|Z_{e2:er}|$) was obtained by following the acquisition method used for the detection of HSA, as explained previously on Chapter 4. Each concentration was tested with three devices. The test lasted 60 minutes since at this point we noticed that the change of sensitivity of the system was slowing down. The results of the noisiest tests performed on the real-time monitoring of the impedance are shown on Fig. 5. 7.

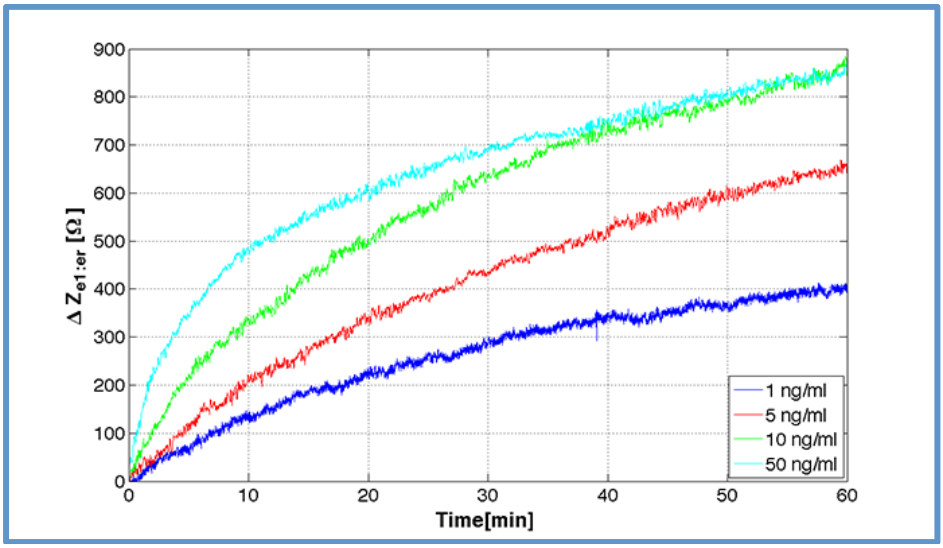

Fig. 5. 7 Real-time monitoring of impedance change for different concentrations of PSA

The noise was analyzed in order to compare it with the sensitivity of the system. The noisy signal was smoothed with a Savitzky–Golay filter, the filtered signal was subtracted to the original signal and the noise was obtained. In order to get the worst-case scenario, the noisiest signal was selected for each concentration (Fig. 5. 8).

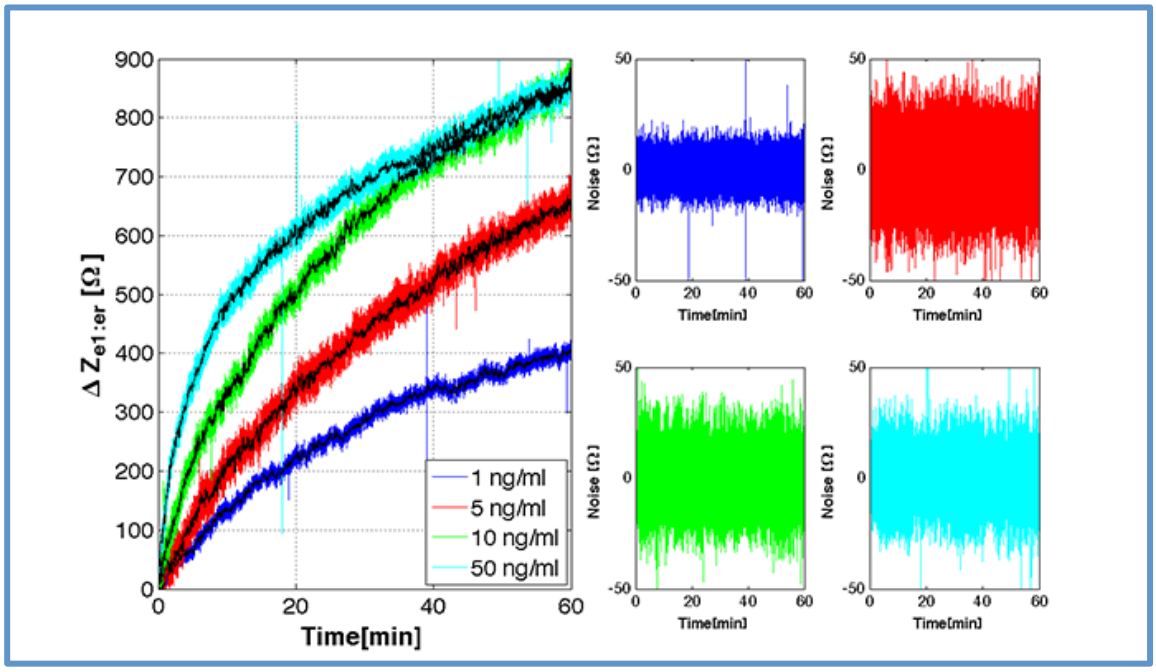

Fig. 5. 8 Real-time monitoring. The black lines represent the smoothed signal. The noise is for all the concentrations are represented on the right.

The extracted noise or RMS was of 12.91 Ω for a concentration of 1 ng/ml, while the noise in the range of 5 ng/ml – 50 ng/ml was between 20.30 Ω to 23.10 Ω, with a mean value of 21.50Ω. Filtering the signal after the measurement can reduce the noise. However, if the application requires an in-situ real-time analysis and measurement without post-filtering of the signal, a higher sensitivity is needed to overcome the noise. The three tests of concentration 1 ng/ml are shown on Fig. 5. 9. We are going to show how the filtering of the signal can improve the detection by reducing the electronic noise.

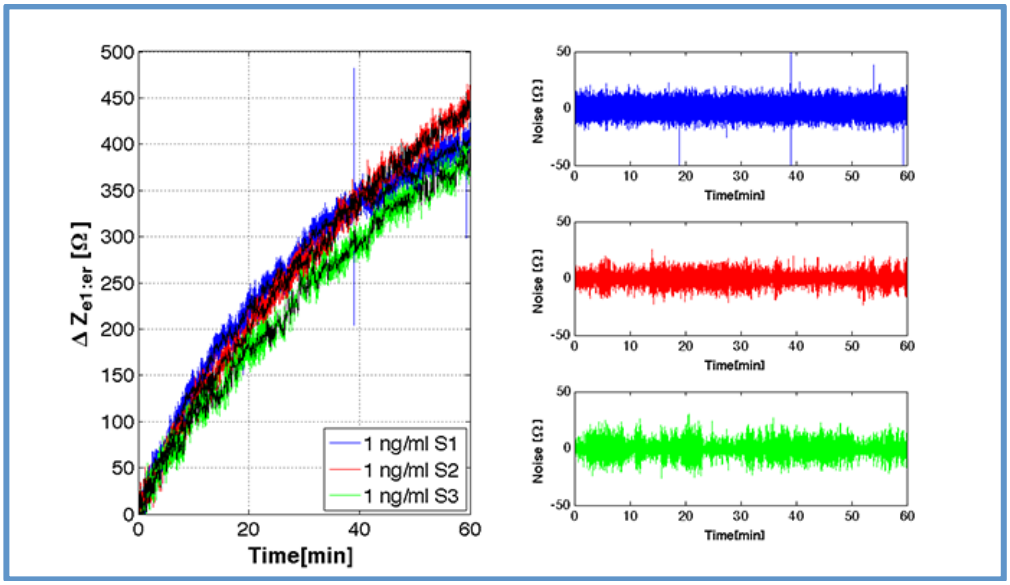

Fig. 5. 9 Unfiltered signals with its respective electronic noise.

The filtering of the signal helps us to reduce the noise and so we could use a smaller sensitivity. As mention before the amplitude of the noise affects the LOD and LOQ. The filtered signals are shown on Fig. 5. 10.

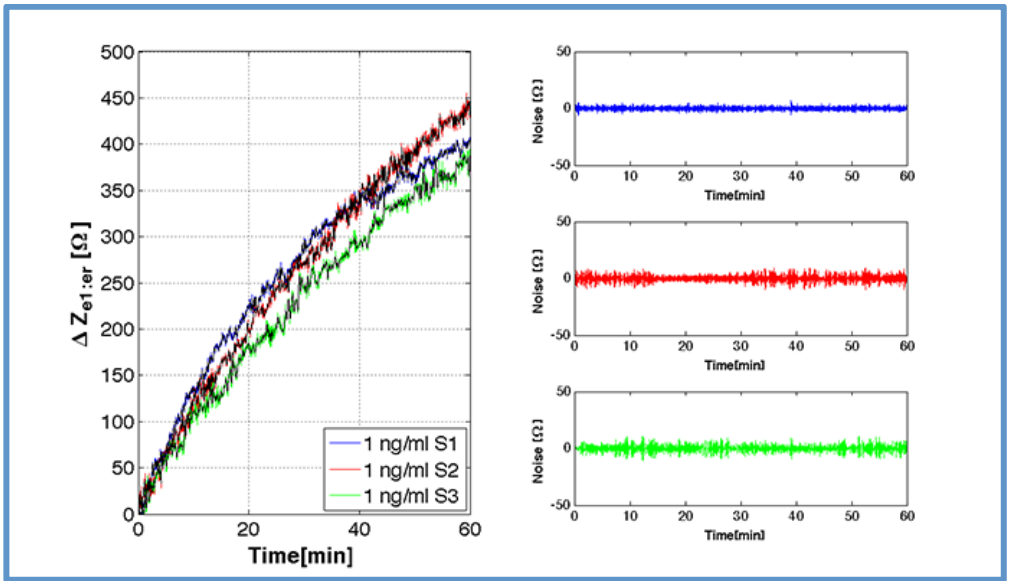

Fig. 5. 10 Filtered signals and its respective noise.

With the Savitzky–Golay filter we were able to reduce the noise from 12.91 Ω to 4.84 Ω almost 2.7 times. If we compare the results obtained, with the noise analysis performed on the previous chapter, we realized that neither the PBS nor the PSA solution increment the noise. Therefore, the noise component is given by the instrumentation.

After filtering all the signals, for the different concentrations, we took the value of the impedance modulus for every 10 minutes. With this analysis we wanted to characterize the adjustability of our device and select the most suitable time to start the detection with the differential voltage analysis. The values were plotted and a fitting analysis was performed (Fig. 5. 11). The standard deviation was taken under consideration when the fitting was done.

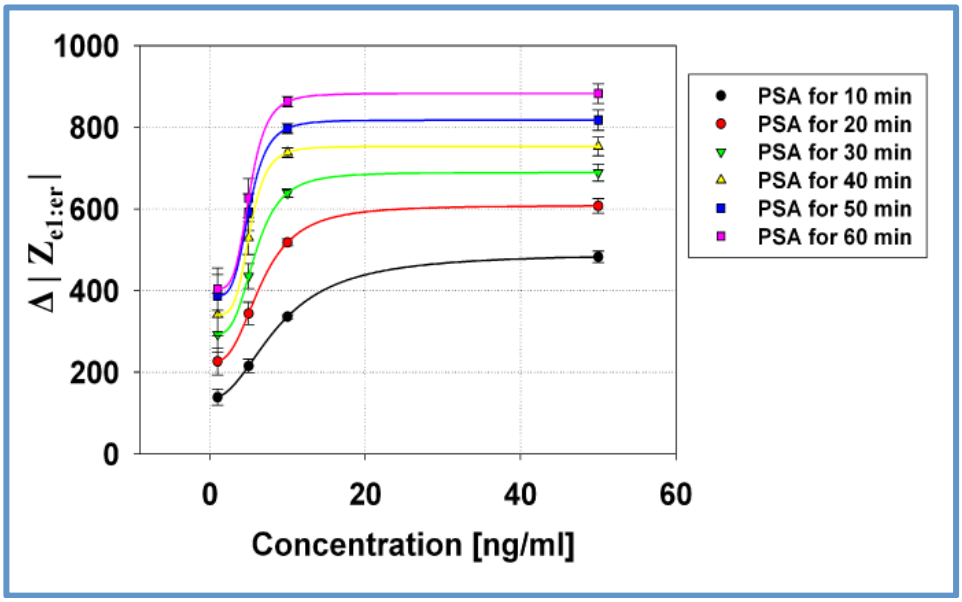

Fig. 5. 11 Sigmoidal fitting of the experimental data when evaluating different concentrations of PSA and detection times

The equation that had a perfect fitting in almost all the calibration curves was the sigmoid 4 parameter logistic:

$$y = y_0 + \frac{a}{1 + \left(\frac{x}{x_0}\right)^b} \qquad \text{(Eq. 5. 1)}$$

Where x is the concentration in ng/ml and y is the impedance in Ω. With the sigmoid fitting we had a perfect model for the behavior of our device at different times. However, this model is not useful to get the sensitivity of the system as well as the LOD and LOQ. All the curves had a linear behavior in the range between 1 ng/ml and 10 ng/ml; therefore we were able to obtain the biosensing parameters to characterize our novel microfluidic device. The linear phase for every calibration curve was plotted and a linear regression analysis was applied (Fig. 5. 12).

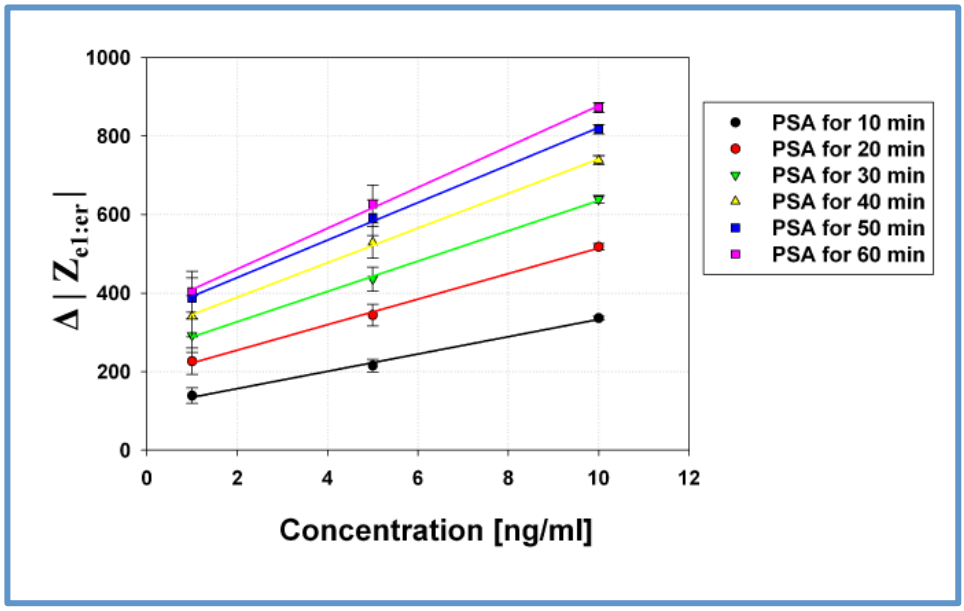

Fig. 5. 12 Linear behavior of the fitting in the PSA concentrations of interest interval.

The linear regression analysis follows the simple formula:

$$y = y_0 + b * x \qquad \text{(Eq. 5. 2)}$$

Where b is the slope of the linear regression and represent the sensitivity of the system, also with the slope and the standard deviation of the fitting we obtained the LOD and LOQ for each calibration curve.

A t-student test was performed to compare the different concentrations at specific experiment running times. Significant differences ($p<0.01$) were found in almost all the cases between 1ng/ml and 5ng/ml or 5ng/ml and 10ng/ml. Slightly less significant differences were found ($p<0.05$) after 30 minutes flow when comparing the 1ng/ml and the 5ng/ml samples. For the 10ng/ml and 50ng/ml samples comparison, at times larger than 30 minutes, no statistic differences were found ($p>0.1$). This result indicated a point of inflection were the sensor surface was saturated by the attaching proteins arriving through the solution at high concentrations.

The LOD is the lowest analyte concentration likely to be reliably distinguished between each sample, while LOQ is the lowest concentration at which the analyte can not only be reliably detected but at which some predefined goals for bias and imprecision are met [26]. Both parameters can be obtained with a linear regression with the next equations [27]:

$$LOD = \frac{3.3 * SD}{b} \qquad \text{(Eq. 5. 3)}$$

$$LOQ = \frac{10 * SD}{b} \qquad \text{(Eq. 5. 4)}$$

Where, SD is the standard deviation of the linear regression and *b* is the slope of the linear regression. With all the processed data now we can obtain the sensitivity, LOD and LOQ of our system for different times, and having an adjustable method for the detection of a biomolecule of interest, in our case PSA.

The sensitivity, LOD and LOQ of the system were plotted and a fitting analysis was performed in order to characterize the adjustability of this parameter. The sensitivity increases with time as shown on Fig. 5. 13a and has an exponential behavior rising to a maximum. The LOD (Fig. 5. 13b) and LOQ (Fig. 5. 13c) have an exponential behavior decreasing to a minimum.

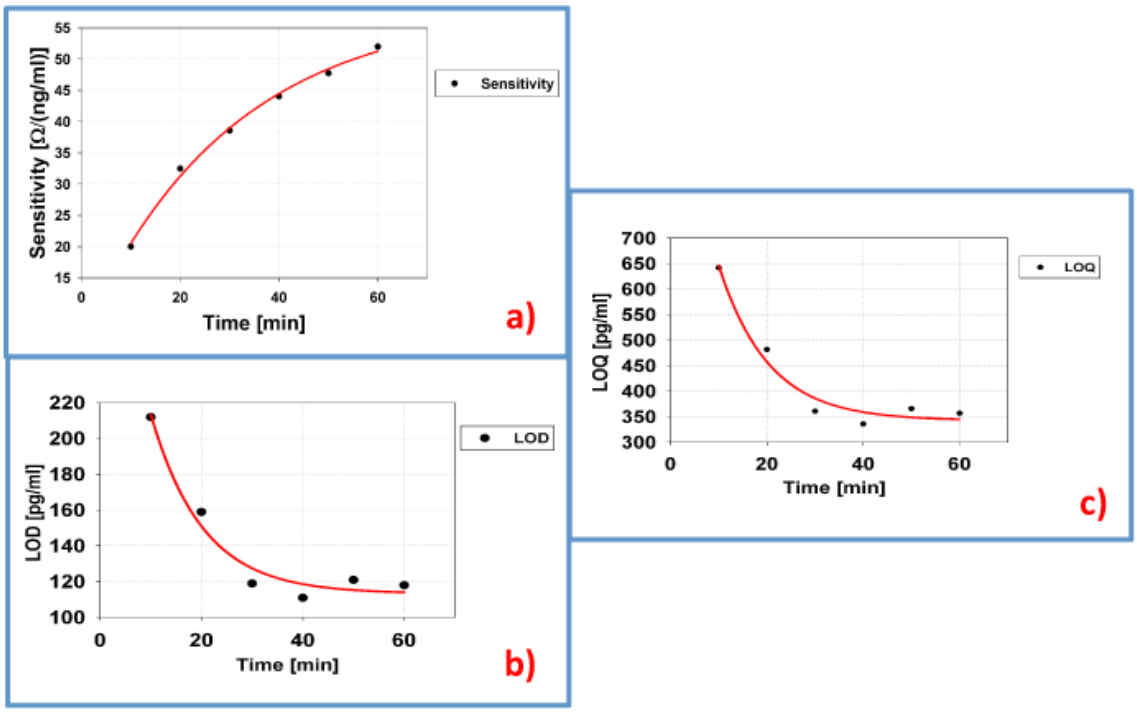

Fig. 5. 13 Adjustability of the sensing parameters of our device. a) Exponential fitting of the sensitivity with the experimental data for different detection times. b) Fitting for LOD with experimental data and different detection times. c) Fitting for LOQ with experimental data and different detection times.

The characteristic equations for our microfluidic system are:

$$Sensitivity(t) = 5.48 + 52.86 * \left(1 - e^{(-0.0335t)}\right)\left[\Omega / (ng / ml)\right] \qquad \text{(Eq. 5. 5)}$$

$$LOD(t) = \left(113.29 + 266.58 * e^{(-0.0978t)}\right)\left[pg / ml\right] \qquad \text{(Eq. 5. 6)}$$

$$LOQ(t) = \left(342.68 + 802.92 * e^{(-0.0971t)}\right)\left[pg / ml\right] \qquad \textbf{Eq. 5. 7}$$

As we increase the deposition time we get a better sensitivity, at the end of the test (60 minutes) the sensitivity is almost 2.5 times larger than the sensitivity at the beginning (10 minutes) and is almost 1.5 times bigger than at 30 minutes. On the other side, the LOD and LOQ have better results when we deposited the protein after 30 minutes, and then no significant change is observed. And the worst response for LOD and LOQ happens when the PSA is detected for up to 10 minutes.

Our system sensitivity overcomes many of the drawbacks previously reported for these types of biosensors by combining microfluidic control of the sample flow with the sensing principle. The sensitivity, LOD and LOQ are adjustable. Since LOD and LOQ improved when the deposition time increased; then we choose 60 minutes as deposition times since we are proposing a device with simplify read-out and real-time measurement, and also a higher sensitivity.

5.3.3 Characterization of PSA

With the tests performed previously, we defined a more refined protocol for the detection of PSA. The device was then characterized for different concentrations of PSA (1 ng/ml, 5 ng/ml, 10 ng/ml and 50 ng/ml). The voltage input applied was 0.1 V at 1 kHz, between e_1 and e_2. Impedance and voltage measurements were performed with the Zurich devices (HF2IS and HF2TA). Each concentration was tested with three devices. Also, we performed a test with human serum at a concentration of 5 ng/ml PSA (Fig. 5. 15 Square mark).

Impedance and voltage analysis were performed after the functionalization and detection, during the rinsing step with PBS. A voltage input (V_{in}) of 0.1V at 1 kHz was applied between e_1 and e_2, the analysis was performed at this frequency since previous experiments showed a larger differential signal around this frequency value. . The voltage change between the functionalized electrode (e_1) and the electrode acting as reference (e_r) was measured ($V_{e1:er}$); since the input is fixed at 100 mV the voltage on the blocked electrode (e_2) could be calculated:

$$V_{e2:er} = V_{in} - V_{e1:er} = \left(100 - V_{e1:er}\right)\left[mV\right] \qquad \text{(Eq. 5. 8)}$$

We measured both, impedance (Fig. 5. 14) and voltage (Fig. 5. 15), after the deposition of the antibody (APSA) and after the detection of the protein (PSA). We

expected an increase of impedance and voltage after the deposition of PSA and we calculated the increments:

$$\Delta\left|Z_{e1:er}\right| = \left|Z_{e1:er}(PSA)\right| - \left|Z_{e1:er}(APSA)\right| \quad \text{(Eq. 5. 9)}$$

$$\Delta\left|V_{e1:er}\right| = \left|V_{e1:er}(PSA)\right| - \left|V_{e1:er}(APSA)\right| \quad \text{(Eq. 5. 10)}$$

Considering ideal behavior of the device any change on the voltage drop is equivalent to a change in the impedance modulus [28]:

$$\alpha = \frac{V_{e1:er}}{V_{e2:er}} \approx \frac{Z_{e1:er}}{Z_{e2:er}}$$
$$\Delta\left|Z\right| \cong \left(\left|Z'_{e1:er}\right| - \left|Z''_{e1:er}\right|\right) \cong \left(\alpha' - \alpha''\right)\left|Z_{e2:er}\right| = \Delta\alpha\left|Z_{e2:er}\right| \quad \text{(Eq. 5. 11)}$$

The factor α (Fig. 5. 16) was defined considering an ideal performance: same electrodes area, totally blocked surface on the reference electrodes, zero non-specific adsorption.

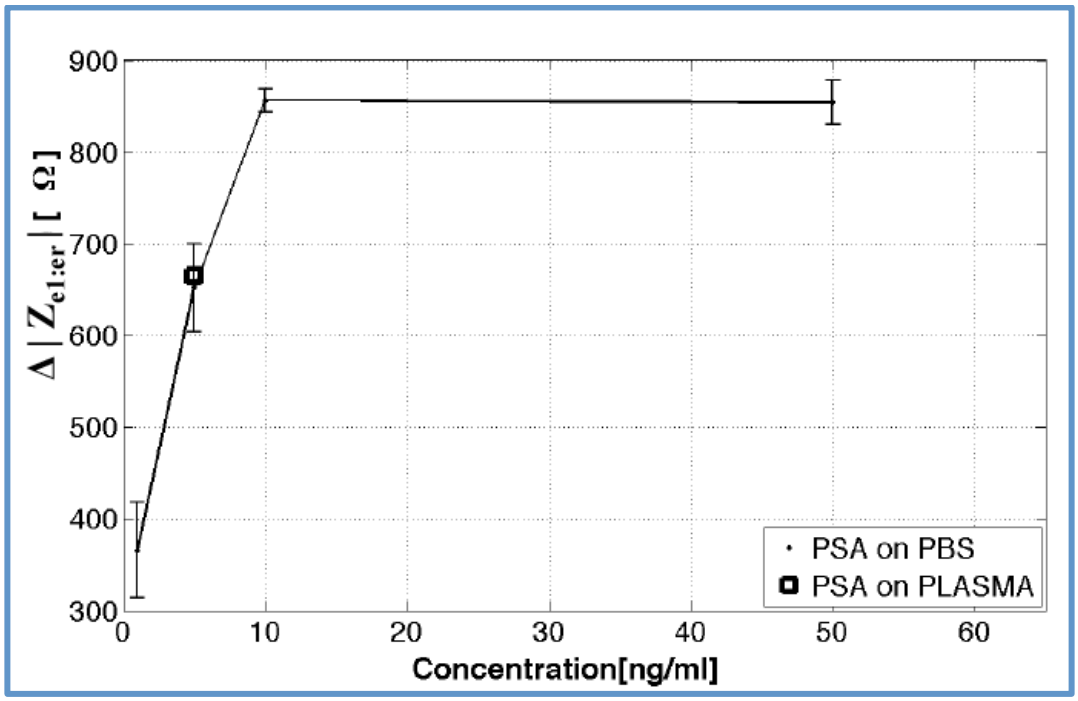

Fig. 5. 14 Impedance detection range of the microfluidic system for the detection of PSA (round marks). The system was tested with human serum at a known concentration (square mark)

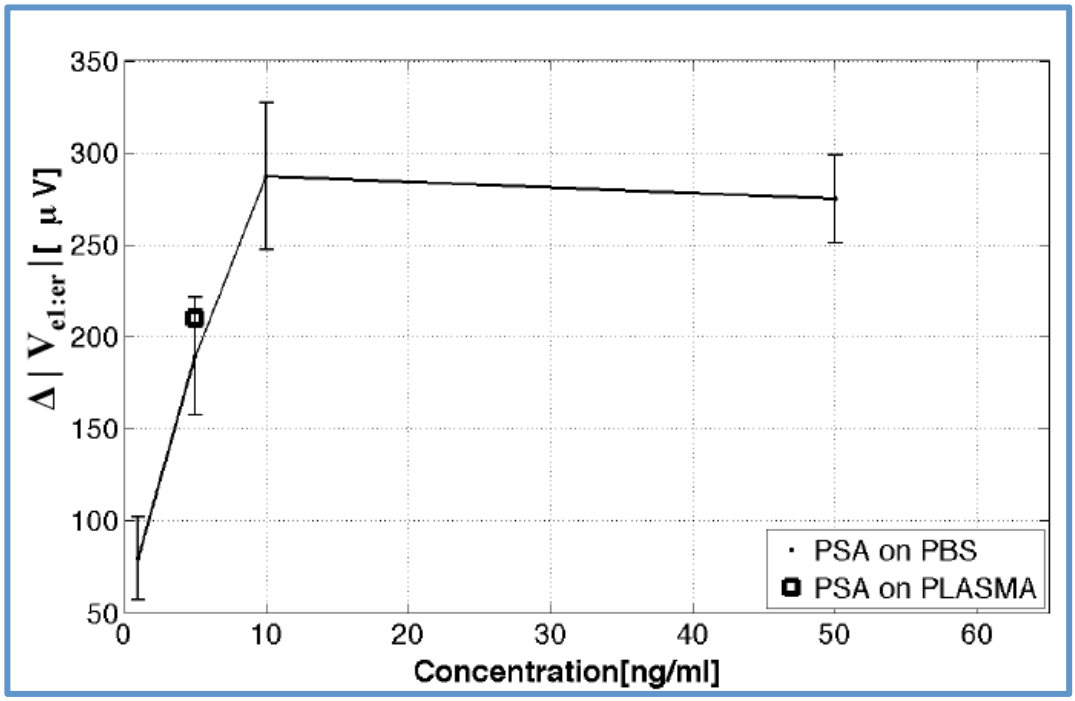

Fig. 5. 15 Voltage detection range of the microfluidic system for the detection of PSA (round marks). The system was tested with human serum at a known concentration (square mark)

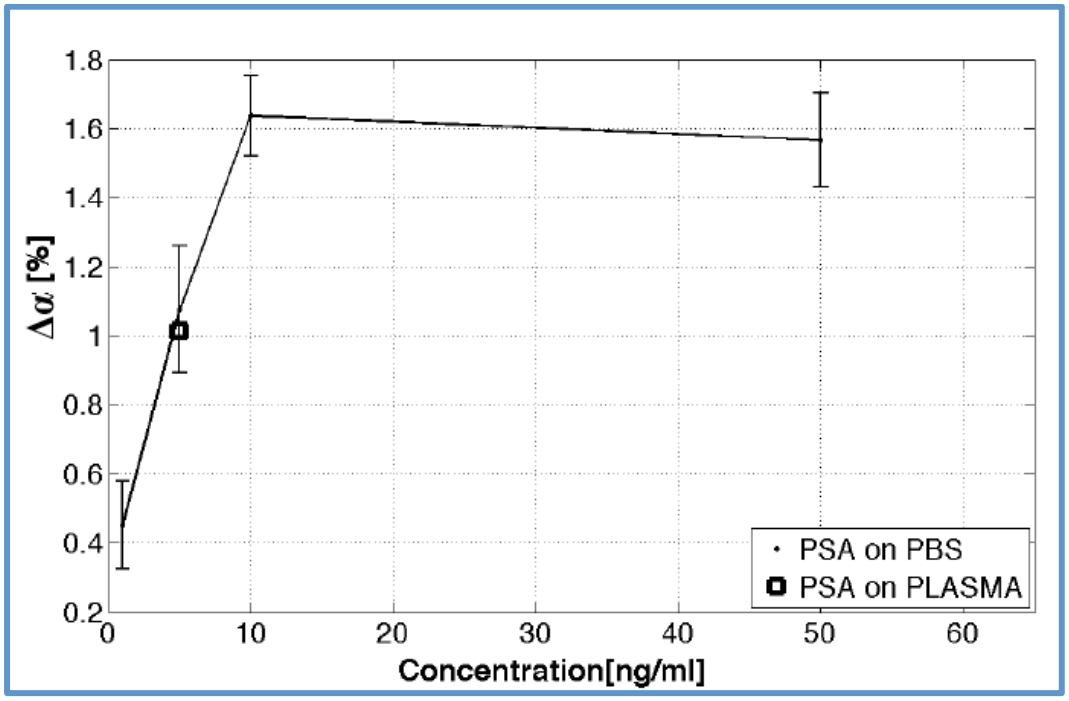

Fig. 5. 16 Factor α detection range of the microfluidic system for the detection of PSA (round marks). The system was tested with human serum at a known concentration (square mark)

The detection range graphs show a linear tendency for concentrations between 1 ng/ml and 10 ng/ml, for impedance and voltage differential measurements.

$$\Delta|Z_{e1:er}| = \left(53.96 * PSA(x) + 337.1\right)[\Omega] \qquad \text{(Eq. 5. 12)}$$

$$\Delta|V_{el:er}| = (22.9 * PSA(x) + 63.26)[\mu V] \quad \text{(Eq. 5. 13)}$$

$$\Delta\alpha = (0.1309 * PSA(x) + 0.3572)[\%] \quad \text{(Eq. 5. 14)}$$

As mention before on this chapter, the LOD and LOQ depend on the standard deviation and slope of the linear regression, re-writing the equations 5.3 and 5.4:

$$LOD = \frac{3.3 * SD}{b}$$

$$LOQ = \frac{10 * SD}{b}$$

With all the processed data now we can obtain the sensitivity, LOD and LOQ of our system for different times, and having an adjustable method for the detection of a biomolecule of interest, in our case PSA. Table 4. 1 summarizes the results obtained.

Table 5. 1 LOD, LOQ and sensitivity for the different electrical measurements for PSA

Measurement	LOD [pg/ml]	LOQ [pg/ml]	Sensitivity
$\Delta \mid Z_1 \mid$	118	357	51.1 [Ω*(ng/ml)$^{-1}$]
$\Delta \mid V_1 \mid$	383	1200	23.8 [μV*(ng/ml)$^{-1}$]
Factor α	376	1100	0.13 [%*(ng/ml)$^{-1}$]

We also calculated the p-value, using a standard t-student test, among the concentrations measured in order to compare if the samples were statistically different.

Table 5. 2 Comparison among the different concentration: p-values

Measurement	p-value: 1ng/ml – 5ng/ml	p-value: 5ng/ml – 10ng/ml	p-value: 10ng/ml – 50ng/ml
$\Delta \mid Z_1 \mid$	P<0.01	P<0.01	P>0.05
$\Delta \mid V_1 \mid$	P<0.01	P<0.05	P>0.05
Factor α	P<0.01	P<0.05	P>0.05

The device was also tested with human plasma. Two tests were performed, one with the plasma as a control (Fig. 5. 17 black plots) and the second with a fixed concentration of PSA at 5 ng/ml (Fig. 5. 17 red plots). The results were compared with the previous characterization of PSA and are represented as a black square in (Fig. 5. 14, Fig. 5. 15 and Fig. 5. 16). Impedance and voltage measurements were done.

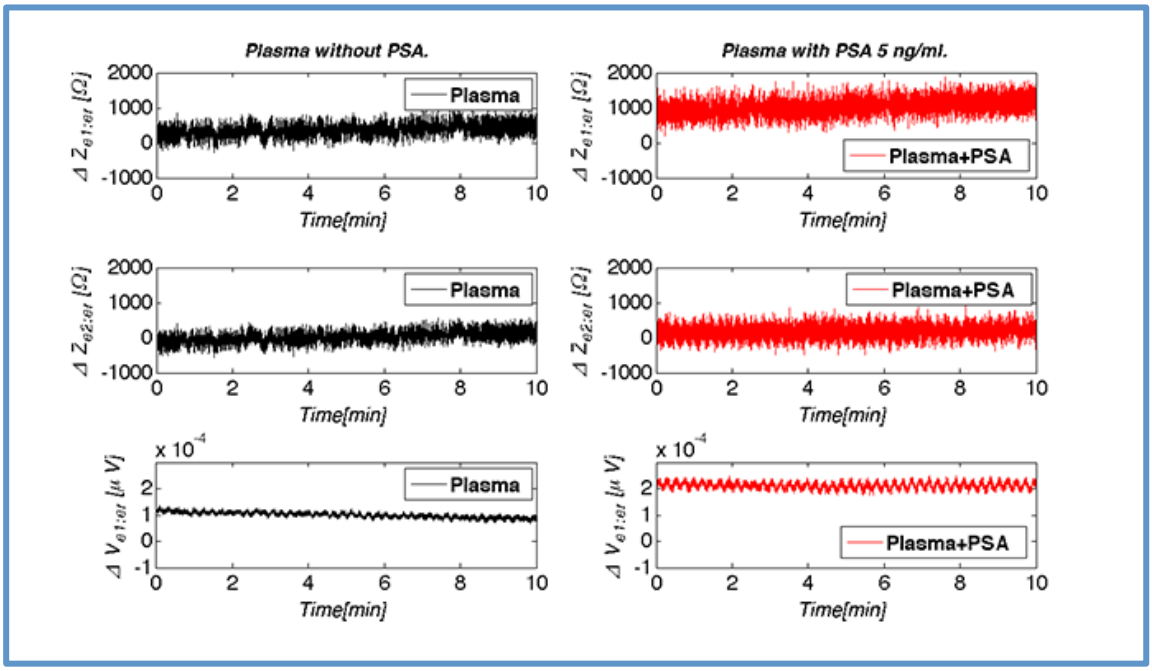

Fig. 5. 17 Tests with human plasma. The impedance modulus did not changed after the flowing of plasma without PSA (black plots) while the impedance modulus increased only for the functionalized electrode (red plots) $Z_{e1:er}$ and therefore we detect PSA on plasma.

The system saturated for PSA concentrations over 10 ng/ml which is much higher than the cutoff clinical value of 4ng/ml [11]. LOD and LOQ, when evaluating PSA concentration, were around 3-fold for Δα when compared to $\Delta|Z_{e1:er}|$ measurements (Table 5.1). The parameter α is closely related to voltage changes in the electrodes ($V_{e1:er}$ and $V_{e2:er}$) and is affected by the behavior of the blocking. Variability among samples at the same PSA concentration was also higher when evaluating Δα instead of $\Delta|Z_{e1:er}|$. We hypothesized that these results could be due non-perfect PEGylation of the reference electrodes e_2 and e_r. Both LOD values are in the range of other microfluidic immunosensors for the detection of PSA that are between 10 pg/ml [29] and 2 ng/ml [30]

Finally a test with real human serum was also performed. Three aliquots of the serum sample were first tested using three chips out of the shell that had their electrodes functionalized with anti-PSA and PEG in situ. No significant changes of $|Z_{e1:er}|$ or α values were monitored. Three other aliquots of the serum were then prepared to contain 5 ng/ml of PSA. The detected values after using three new chips for $\Delta|Z_{e1:er}|$ and Δα were in the range of the previously calibrated curves for this PSA concentration.

5.4 Conclusions

We performed an in-situ blocking of the two electrodes (e_r and e_2) that worked as reference to improve the voltage output. A PEG-based solution was used to do the blocking. The differential voltage response was improved by 50% after changing the times and concentrations of the PEG-based solution.

We were able to test the adjustability of the system. We compared the impedance change at different deposition times of PSA and performed the biosensing analysis and characterization. We achieve sensitivity almost 2.5 higher after 60 minutes of deposition compared with the first 10 minutes of deposition and 1.5 higher at the middle of the test. And the LOD and LOQ had a better response after 30 minutes of deposition and two concentrations with a difference of almost 118 pg/ml can be detected. This analysis helped to define a dynamic and adjustable sensitivity. Depending on the application, we can choose to have a greater sensitivity, only by changing the detection times. The statistical analysis helped us to define the relation between concentration and time and when we can find a significant difference. The instrumentation noise is almost 23 Ω at most therefore the LOD and LOQ is 1 ng/ml for the times when the sensitivity is smaller than the noise (before 20 minutes). When the sensitivity is higher than the noise (after 20 minutes) the LOD and LOQ are the same as the ones that were calculated and presented on the results (Table 4. 1).

With the improvement of blocking and filtering, the device was characterized for the detection of prostate specific antigen. The impedance and voltage results showed a linear behavior on the range of interest (1ng/ml-10ng/ml) of PSA. Impedance measurements showed a better sensitivity for the detection of PSA, almost 2.2 times larger than the voltage measurements. However, impedance measurements showed a 30% better LOD and LOQ response in comparison to voltage measurements. The factor α also showed a response in LOD and LOQ, similar to the voltage analysis, since it's also affected by the not complete blocking of the electrodes. The blocking helped to improve the voltage statistical analysis, since at low concentrations the p-values had a significant statistical difference. Tests with human serum didn't showed non-specific adsorption and the voltage and impedance measurements were on the range of the previous characterization, with this results we can suggest that the proposed protocol

has a high specificity for PSA and there is no cross-talk of the different proteins presented on the plasma.

5.5 References

1. J. A. Gabriel, *The Biology of Cancer*, Wiley, 2007.
2. M. Kondo, A. J. Wagers, M. G. Manz, S. S. Prohaska, D. C. Scherer, G. F. Beilhack, J. A. Shizuru and I. L. Weissman, *Annual review of immunology*, 2003, **21**, 759-806.
3. G. J. Spangrude, S. Heimfeld and I. L. Weissman, *Science*, 1988, **241**, 58-62.
4. M. D. Abeloff, J. O. Armitage and J. E. Niederhuber, *Abeloff's Clinical Oncology*, Churchill Livingstone/Elsevier, 2008.
5. J. Ferlay, H. R. Shin, F. Bray, D. Forman, C. Mathers and D. M. Parkin, *Int J Cancer*, 2010, **127**, 2893-2917.
6. R. Siegel, D. Naishadham and A. Jemal, *CA: A Cancer Journal for Clinicians*, 2013, **63**, 11-30.
7. M. Malvezzi, P. Bertuccio, F. Levi, C. La Vecchia and E. Negri, *Annals of Oncology*, 2013.
8. C. Porth, *Essentials of Pathophysiology: Concepts of Altered Health States*, Wolters Kluwer/Lippincott Williams & Wilkins, 2011.
9. M. O. Ripple, G. Wilding, W. F. Henry and R. P. Rago, *Journal of the National Cancer Institute*, 1997, **89**, 40-48.
10. S. P. Balk, Y.-J. Ko and G. J. Bubley, *Journal of Clinical Oncology*, 2003, **21**, 383-391.
11. R. E. S. El-Galley, J. A. Petros, W. H. Sanders, T. E. Keane, N. T. M. Galloway, W. H. Cooner and S. D. Graham Jr, *Urology*, 1995, **46**, 200-204.
12. A. P. Berger, C. Cheli, R. Levine, H. Klocker, G. Bartsch and W. Horninger, *Urology*, 2003, **62**, 840-844.
13. D. S. Smith and W. J. Catalona, *J Urol*, 1994, **152**, 1163-1167.
14. M. Dörr, A. Schlesinger-Raab and J. Engel, *Epidemiology of Prostate Cancer*, 2013.
15. J. H. Choi, H. S. Kim, J.-W. Choi, J. W. Hong, Y.-K. Kim and B.-K. Oh, *Biosensors and Bioelectronics*, 2013, **49**, 415-419.
16. C. S. Thaxton, R. Elghanian, A. D. Thomas, S. I. Stoeva, J.-S. Lee, N. D. Smith, A. J. Schaeffer, H. Klocker, W. Horninger, G. Bartsch and C. A. Mirkin, *Proceedings of the National Academy of Sciences*, 2009, **106**, 18437-18442.
17. J. Wang, *Analyst*, 2005, **130**, 421-426.
18. X. Luo and J. J. Davis, *Chem Soc Rev*, 2013, **42**, 5944-5962.
19. Y. Wan, Y. Su, X. Zhu, G. Liu and C. Fan, in *Biosens Bioelectron*, 2013 Elsevier B.V, England, 2013, vol. 47, pp. 1-11.
20. A. Kim, C. S. Ah, H. Y. Yu, J.-H. Yang, I.-B. Baek, C.-G. Ahn, C. W. Park, M. S. Jun and S. Lee, *Applied Physics Letters*, 2007, **91**, -.
21. C. Li, M. Curreli, H. Lin, B. Lei, F. N. Ishikawa, R. Datar, R. J. Cote, M. E. Thompson and C. Zhou, *Journal of the American Chemical Society*, 2005, **127**, 12484-12485.
22. J. Okuno, K. Maehashi, K. Kerman, Y. Takamura, K. Matsumoto and E. Tamiya, *Biosensors and Bioelectronics*, 2007, **22**, 2377-2381.
23. M. S. Chiriaco, E. Primiceri, A. Montanaro, F. de Feo, L. Leone, R. Rinaldi and G. Maruccio, *Analyst*, 2013, **138**, 5404-5410.

24. K. N. Han, C. A. Li and G. H. Seong, *Annu Rev Anal Chem (Palo Alto Calif)*, 2013, **6**, 119-141.
25. E. Prats-Alfonso, F. García-Martín, N. Bayo, L. J. Cruz, M. Pla-Roca, J. Samitier, A. Errachid and F. Albericio, *Tetrahedron*, 2006, **62**, 6876-6881.
26. D. A. Armbruster and T. Pry, *Clin Biochem Rev*, 2008, **29**, S49-52.
27. A. Shrivastava and V. B. Gupta, *Chronicles of Young Scientists*, 2011, **2**, 21.
28. C. Parra-Cabrera, C. Sporer, I. Rodriguez-Villareal, R. Rodriguez-Trujillo, A. Homs-Corbera and J. Samitier, *Lab on a Chip*, 2012.
29. N. Triroj, P. Jaroenapibal, H. Shi, J. I. Yeh and R. Beresford, *Biosensors and Bioelectronics*, 2011, **26**, 2927-2933.
30. A. Fragoso, D. Latta, N. Laboria, F. von Germar, T. E. Hansen-Hagge, W. Kemmner, C. Gartner, R. Klemm, K. S. Drese and C. K. O'Sullivan, *Lab on a Chip*, 2011, **11**, 625-631.

CHAPTER 6 Application of LOC to multiple biomarkers detection: prostate-specific antigen and Spondin-2

6.1 Introduction

The use of prostate-specific antigen test as a screening tool in diagnosing prostate cancer is controversial. The Prostate, Lung, Colorectal and Ovarian Cancer Screening Trial (PLCO), in the United States, claims that PSA test plus a digital rectal examination has no mortality reduction benefit [1]. In contrast, the European Randomized Study of Screening for Prostate Cancer (ERSPC), says that PSA screening reduces the mortality in a 20% [2]. Therefore, novel biomarkers are being studied for diagnose, staging and treatment of prostate cancer.

There had been several attempts to detect multiple cancer biomarkers towards developing point-of-care devices. A multiplex suspension array technology with microbeads was developed to detect simultaneously PSA, prostate stem cell antigen, prostatic acid phosphatase and prostate-specific membrane antigen; the biomarkers levels were quantified by fluorescent intensities showing no significant cross-talk among biomarkers [3]. Another approach was the development of a piezoelectric biosensor, where two ceramic resonators were connected in parallel for the multiplexed detection of PSA and α-fetoprotein, showing high sensitivity and fast detection [4]. Also, microfluidics had helped to developed devices for detection of cancer biomarkers. An electrochemiluminescence immunoarray with a microfluidic module was developed for the detection of PSA along with IL-6, the technology used a ultrasensitive approach by using silica nanoparticles [5].

In this chapter, the second device designed was tested for the detection of two cancer biomarkers as a proof-of-concept. The selected biomarker were PSA and Spondin-2 (SPON2), since recent works showed that this biomarkers are helpful when diagnosis prostate cancer [6, 7]. We obtained the sensitivity, LOD and LOQ of the system for SPON2. Since a previous characterization of PSA was performed, we wanted to study the cross talk and therefore specificity of the system and so we kept the PSA at a fix concentration. Once again we proved the adjustability of the system, but on this time we measured the change in impedance related to the deposition of

SPON2. Also, the simultaneous and in real-time detection of PSA and SPON2 has not been reported previously in the literature,

6.1.1 Prostate cancer biomarkers

The most commonly used biomarkers for the study of PCa can be divided depending of the matrix in serum and tissue biomarkers.

Serum biomarker

Molecules founded in blood and identified by serum assays. In addition to the most used serum biomarker for prostate cancer, the *prostate-specific antigen (PSA),* already explained on chapter 3 we have:

Kallikrein-4 (KLK-4).- Is part of the kallikreins serine proteases. These proteins are excreted and have extracellular substrates. The KLK-4 is expressed by the normal prostate cells and overexpressed in prostate cancer [8]. Besides prostate cancer, KLK-4 is found on high concentrations in patients with breast, endometrial and ovarian carcinomas [9]. Therefore, KLK-4 could be used as a potential biomarker.

Steroid receptor co-activator-3 (Src-3).- Is a co-activator for nuclear hormone receptor and is part of the family p160. The Src-3 is involved in cell proliferation and decreases cell apoptosis. The Src-3 is overexpressed in prostate cancer patients [10].

Minichromosome maintenance protein (Mcm5/7).- This protein is involved in the DNA replication and chromosomal duplication; and the protein is overexpressed with prostate cancer patients and keeps a normal level with a healthy tissue or BHP [11].

E-cadherin.- Is mediator that helps to the cell-cell communication and connection with extracellular matrix; elevated levels of this mediator are involved in metastatic prostate cancer cells. The mediator changes its configuration from E-cadherin to N-cadherin when a transition between epithelial to mesenchymal is presented [11].

Early prostate cancer antigen-2 (EPCA-2).- Is a protein used as a novel biomarker with high concentrations in cancer patients and low levels in healthy men. Some studies had shown the high specificity (97%) of this protein, between patients with prostate cancer, BHP and prostatitis. Setting a cut-off of 0.5 ng/ml an epitope of this protein, EPCA-2.19, has a specificity of 94% and sensitivity of 91% [12].

Interleukin-6 (IL-6).- Is a pleiotropic cytokine related to inflammation process; however several studies had showed that IL-6 helps to the development of cancer by increasing the tumor volume, since it helps to regulate its growth and differentiation. Patients with metastatic prostate cancer show an high concentration of IL-6 in blood serum [13].

Prostate cancer gene 3 (PCA3).- Is overexpressed in primary tumors and is a non-coding RNA and could be used as a novel biomarker [11].

Spondin-2 (SPON2).- Is an extracellular matrix secreted protein part of the F-spondin family. Some studies showed that the concentration of SPON2, on prostate cancer patients, is higher in comparison with healthy men. An presents a great accuracy with healthy patients [6].

Tissue biomarkers

There is a correlation between the tumor stage and the expression of certain proteins. After a biopsy an analysis could be performed to study the tumor progression.

Urokinase-type plasminogen activator (uPA).- Helps to angiogenesis and tumor cell metastasis and its inhibition reduces the invasive ability of the cancer. A test along with the IL-6 could be useful as a prediction test [11].

Enhancer of zeste homolog 2 (EZH2).- This protein is related to embryonic development and also in cell proliferation. However, an overexpression of this protein was founded in several diseases, including prostate cancer [14].

Prostate specific stem cell antigen (PSCA).- Is an antigen found in prostate tissue and expressed on the cell surface. The increase of the PSCA levels helps to predict the stage of the cancer [15].

Androgen receptor (AR).- Is a protein that is involved in the nuclear transcription of prostate cancer cells [11].

Fatty acid synthase (FAS).- Is a lipogenic enzyme. Studies suggest that the increment of FAS is one of the first responses related with prostate cancer [16].

6.2 Materials and methods

The developed multiplexed device was characterized for the simultaneous detection of two proteins related to prostate cancer. This LOC has two sets of electrodes (e_{1A}- e_{2A}- e_{rA} and e_{1B}- e_{2B}- e_{rB}) (Fig. 6. 1). Also, it has a main channel (*In₁*), and two lateral channels *In₂* and *In₃*, being *In₂* the lateral inlet closest to the main channel (Fig. 6. 1). In both sets, electrodes e_2 and e_r worked as references and were blocked with a PEG solution. The electrode e_{1A} was functionalized for the detection of SPON2 while e_{1B} was functionalized for the detection of prostate-specific antigen; a detailed description of the protocol follows.

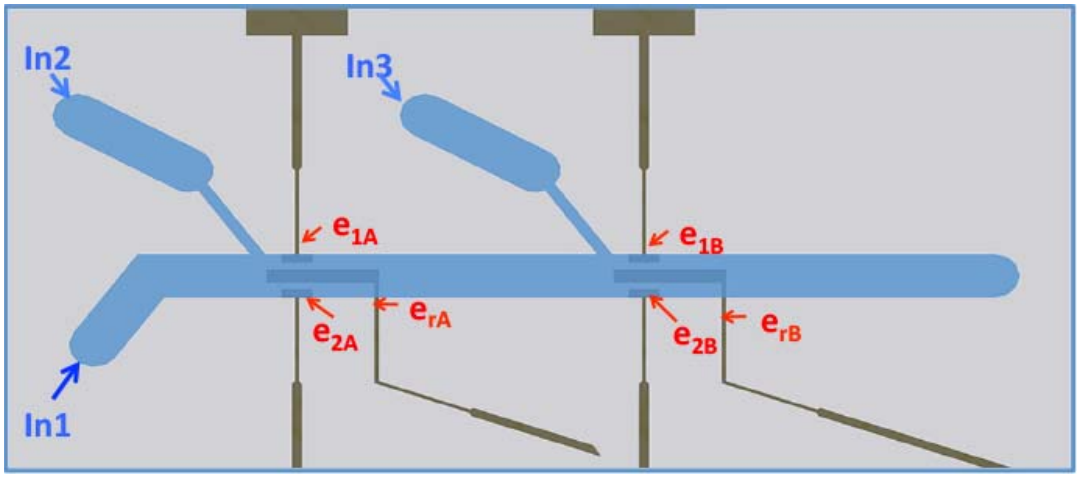

Fig. 6. 1 Layout of the microfluidic device the functionalization of the two sets of electrodes is performed through the three separated inlets.

The protocol started by cleaning the channels with PBS as performed on previous protocols. Then we proceeded with the selective blocking of the electrodes e_{2A}, e_{rA}, e_{2B} and e_{rB} (Fig. 6. 2b). A PEG-Thiol was introduced through the main channel at a flow rate of 6 µl/min, while PBS was introduced through the *In₂* at 2.5 µl/min and at 1 µl/min through the *In₃*.

The first selective functionalization started depositing a self-assembled monolayer of biotin-thiol groups over the surface of the electrode e_{1A} and e_{1B} (Fig. 6. 2c). The biotin-thiol solution was introduced at 6µl/min through the inlet *In₂*. Simultaneously, PBS buffer through the main channel was kept at a rate of 20µl/min.

The second functionalization step is meant to form a Streptavidin layer on top of the biotin layer (Fig. 6. 2d). Again, a 20 µl/min PBS is flowed into the chip through the main channel while the functionalizing solution is laterally introduced through *In₂* at 6µl/min.

Before sensing, a layer of biotinylated specific antibodies was deposited selectively over the SAV layer, as a third functionalization step. A solution of SPON2 antibody (SPON2/M spondin/Mindin antibody, antibodies-online ABIN1389055) at a concentration of 100 µg/ml was kept and introduced at 3 µl/min through the lateral channel In_2, while introducing PBS at 10 µl/min through the main channel. Simultaneously, a solution of Anti-PSA antibody (APSA, Abcam ab77310) flowed at 3 µl/min through the lateral channel In_3. This last functionalization lasted 90 minutes and a rinsing with PBS was performed later (Fig. 6. 2e).

Finally, the detection of SPON2 (Spondin 2 protein (GST tag), antibodies-online ABIN1321223) was characterized by flowing different concentrations of this analyte (1 ng/ml, 5 ng/ml and 10 ng/ml). Every SPON2 solution was mixed with a fixed concentration of PSA at 5 ng/ml, to study the cross talk between proteins. The mixed solution was introduced through the main channel at 6 µl/min during 60 minutes (Fig. 6. 2f). After each functionalization and blocking step, a rinsing was done with PBS at 20 µl/min for 30 minutes; then measurements were performed.

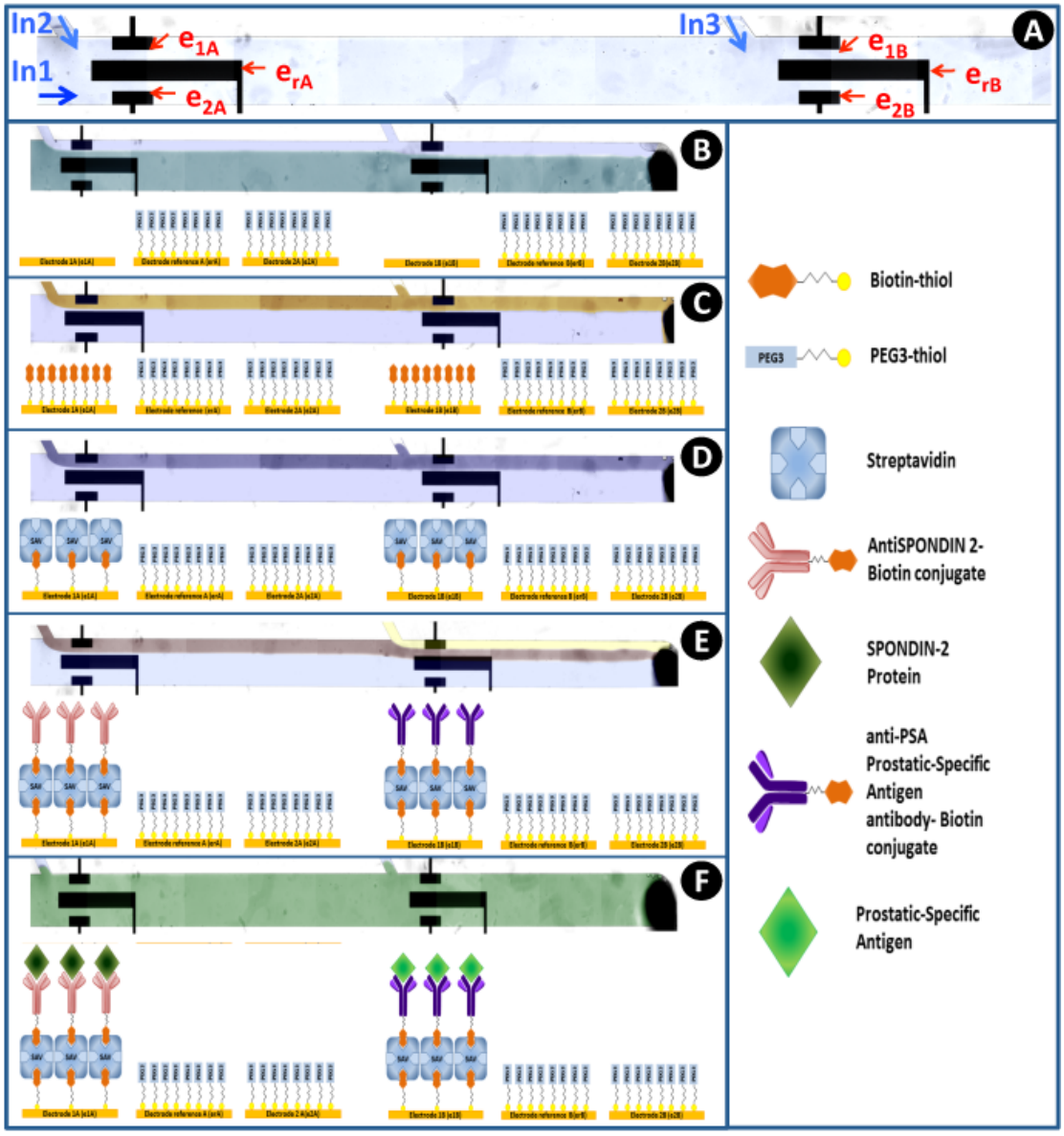

Fig. 6. 2 a) Layout of the microfluidic device the functionalization of the two sets of electrodes is performed through the three separated inlets. b-f) Protocol for the multiplexed fluidic detection of Spondin-2 and PSA. b) Selective blocking with a PEG-thiol solution, c) Electrodes surface modified with biotin-thiol, d) Addition of a layer of streptavidin, e) Simultaneous deposition of a layer biotinylated antibodies. f) Detection of Spondin-2 and PSA. The images are represented in false color.

Determination of the adjustability in the detection range for Spondin-2

The device was characterized for the real-time detection of Spondin-2 by monitoring the impedance changes, in order to get several calibration curves depending on the time. We follow the protocol presented previously on this section (Fig. 6. 2), and we compared the impedance change for all the concentrations tested every 10 minutes starting at minute 30'. Therefore, we obtained four different sets of data. A fitting analysis was used in order to get a model from the behavior of our device. We calculated the sensitivity of the system as well as the limit of detection (LOD) and

limit of quantification (LOQ). The results were analyzed with a t-Student statistical test to verify the significant differences among samples. Using this test we were aiming to prove that our novel system is adjustable in time and that the detection range can be adapted. The statistical test was done with the scientific software SigmaPlot (Systat Software, San Jose, CA).

Impedance and Voltage measurements

For the experimental set-up, the microfluidic flow at the inlets was controlled with two syringe pumps, both from KD Scientific (KDS-101) in order to control the laminar fluids co-flow, thus the selective surface functionalization inside the chip. The differential analysis of voltage was done with the Impedance Spectroscope (HF2IS by Zurich Instruments) on real-time. A Transimpedance Current Amplifier (HF2TA by Zurich Instruments) was used to monitor the electric current and perform impedance measurements.

A diagram of the set-up measurements is presented on Fig. 6. 3a. The input voltage (V_{in}) is applied between e_2 and e_1. The differential voltage of the functionalized electrode ($V_{e1:er}$), is measured directly with the HF2IS. The transimpedance current amplifier HF2TA is used to get the current flowing across the circuit ($I_{e1:e2}$). To perform the multiplexed detection we used an analog switch (DG333A from Vishay/Siliconix) to obtain the data from both sets of biosensors. The DG333A consist of four independently controlled single-pole double-throw analog switches (Fig. 6. 3b). This switch is designed to control analog signals with a high degree of accuracy. Therefore, with only one DG333A chip we were able to applied to voltage input and measure the voltage and current output.

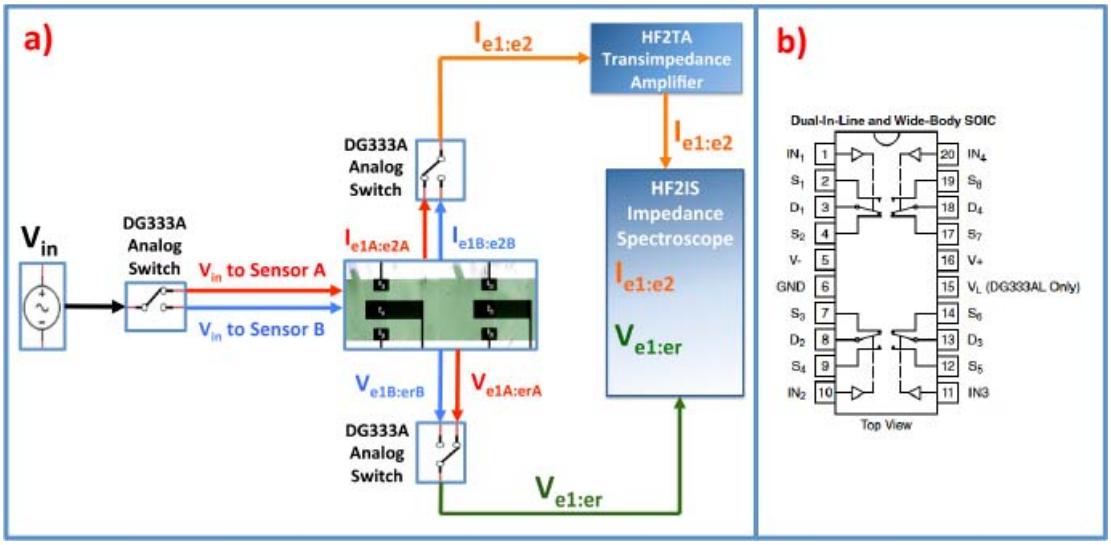

Fig. 6. 3 a) Set-up diagram, the DG333A helps to multiplex the measurements between sensor A (red path) and B (blue path). b) DG333A functional block diagram, the chip consists in 4 analog switches independently controlled.

As mention on chapter 4, we have a system that behaves as a voltage divider (Fig. 4. 9). However, since we have two sets of electrodes, we had to control and multiplex input and output from both sets of biosensors. The measurements started by applying the input V_{in} to the first set (e_{1A}, e_{2A} and e_{rA}) and getting the output from these electrodes (Fig. 6. 3a red path). Subsequently, with the help of the DG333A, the input V_{in} changed to the second set of biosensors (e_{1B}, e_{2B} and e_{rB}) and we got the output data (Fig. 6. 3a red path). The detection of both proteins was done on real time.

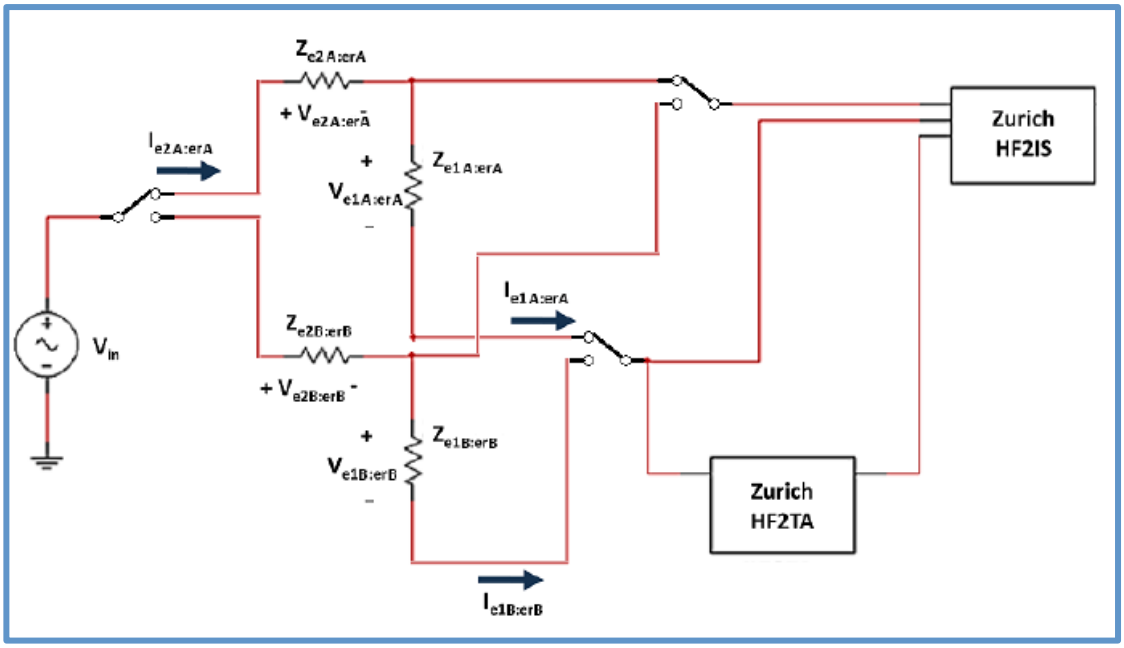

Fig. 6. 4 Electrical schematics of the voltage measurements. Voltage and impedance equivalency of the microfluidic system.

6.3 Results and discussions

6.3.1 Determination of the adjustability in the detection range for Spondin-2

The device was then characterized for different concentrations of SPON2 (1 ng/ml, 5 ng/ml and 10 ng/ml) for a real-time monitoring. The voltage input applied was 0.1 V at 1 kHz, between e_{1A} and e_{2A}. Impedance measurements were performed with the Zurich devices (HF2IS and HF2TA). The impedance modulus ($|Z_{e1A:erA}|$ and $|Z_{e2A:erA}|$) was obtained by following the same acquisition method used for the detection of PSA. Each concentration was tested with three devices. The test lasted 60 minutes since at this point we notice an impedance change in the smallest concentration. The results of one of the three tests performed on the real-time monitoring of the impedance are shown on Fig. 5. 7.

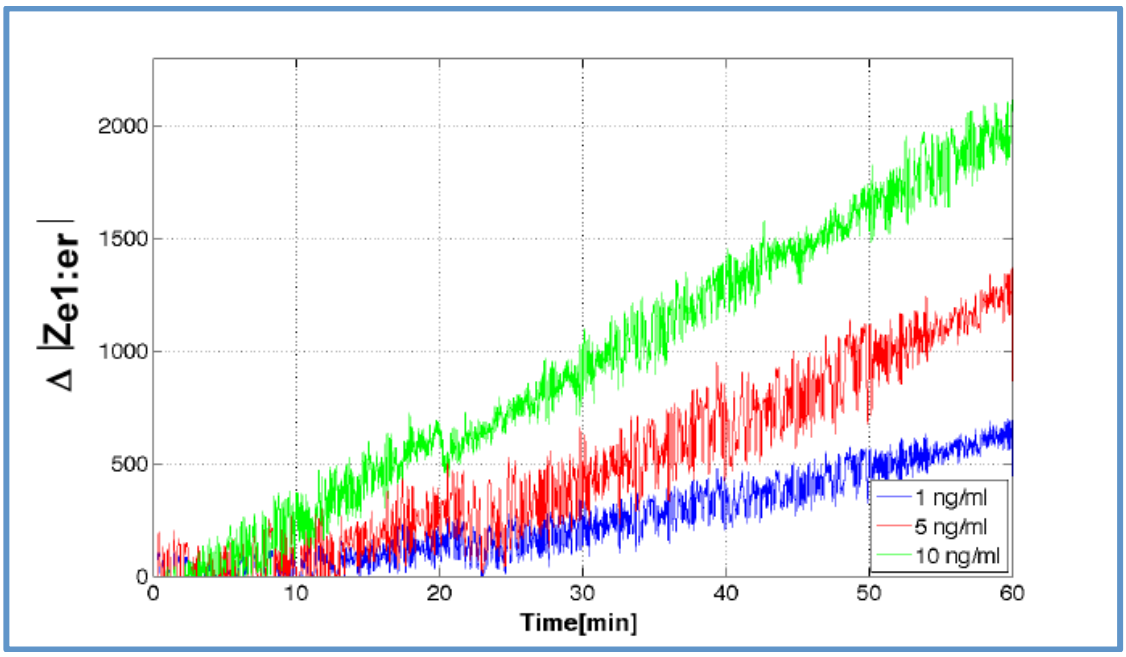

Fig. 6. 5 Real-time monitoring of impedance magnitude (o module) change for different concentrations of SPON2

The value of the impedance modulus for each concentration was taken every 10 minutes, starting at 30' minutes since we observed a greater difference after that time. The values were plotted and a fitting analysis was performed (Fig. 5. 11). The standard deviation was taken under consideration when the fitting was done.

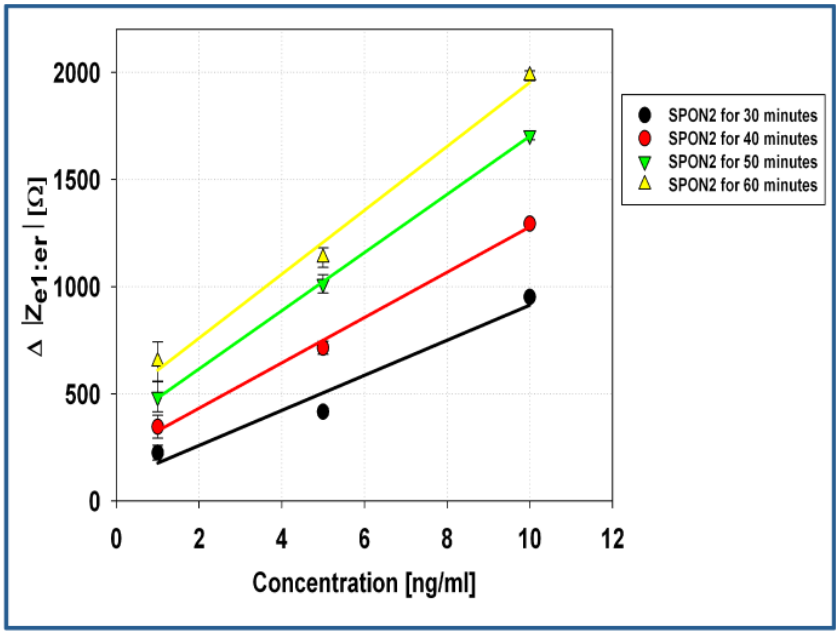

Fig. 6. 6 Sensitivity adjustment of the microfluidic system. Linear behavior of the fitting in the SPON2 concentrations.

The linear regression analysis follows the simple formula:

$$y = y_0 + b * x \qquad \text{(Eq. 6. 1)}$$

Where b is the slope of the linear regression and represent the sensitivity of the system, also with the slope and the standard deviation of the fitting we obtained the LOD and LOQ for each calibration curve.

A t-student test was performed to compare the different concentrations at specific experiment running times. Significant differences ($p<0.01$) were found in all the cases between 1ng/ml and 5ng/ml or 5ng/ml and 10ng/ml. This result indicated that the sensor surface was not saturated.

The LOD is the lowest analyte concentration likely to be reliably distinguished between each sample, while LOQ is the lowest concentration at which the analyte can not only be reliably detected but at which some predefined goals for bias and imprecision are met [17]. Both parameters can be obtained with a linear regression with the next equations [18]:

$$LOD = \frac{3.3 * SD}{b} \qquad \text{(Eq. 6. 2)}$$

$$LOQ = \frac{10 * SD}{b} \qquad \text{(Eq. 6. 3)}$$

Where, SD is the standard deviation of the linear regression and *b* is the slope of the linear regression. With all the processed data now we can obtain the sensitivity, LOD and LOQ of our system for different times, and having an adjustable method for the detection of a biomolecule of interest, in this case Spondin-2.

The sensitivity, LOD and LOQ of the system were plotted and a fitting analysis was performed in order to characterize the adjustability of this parameter. The sensitivity increases with time as shown on Fig. 6. 7a and has a linear tendency. The LOD (Fig. 6. 7b) and LOQ (Fig. 6. 7c) have an exponential decreasing behavior.

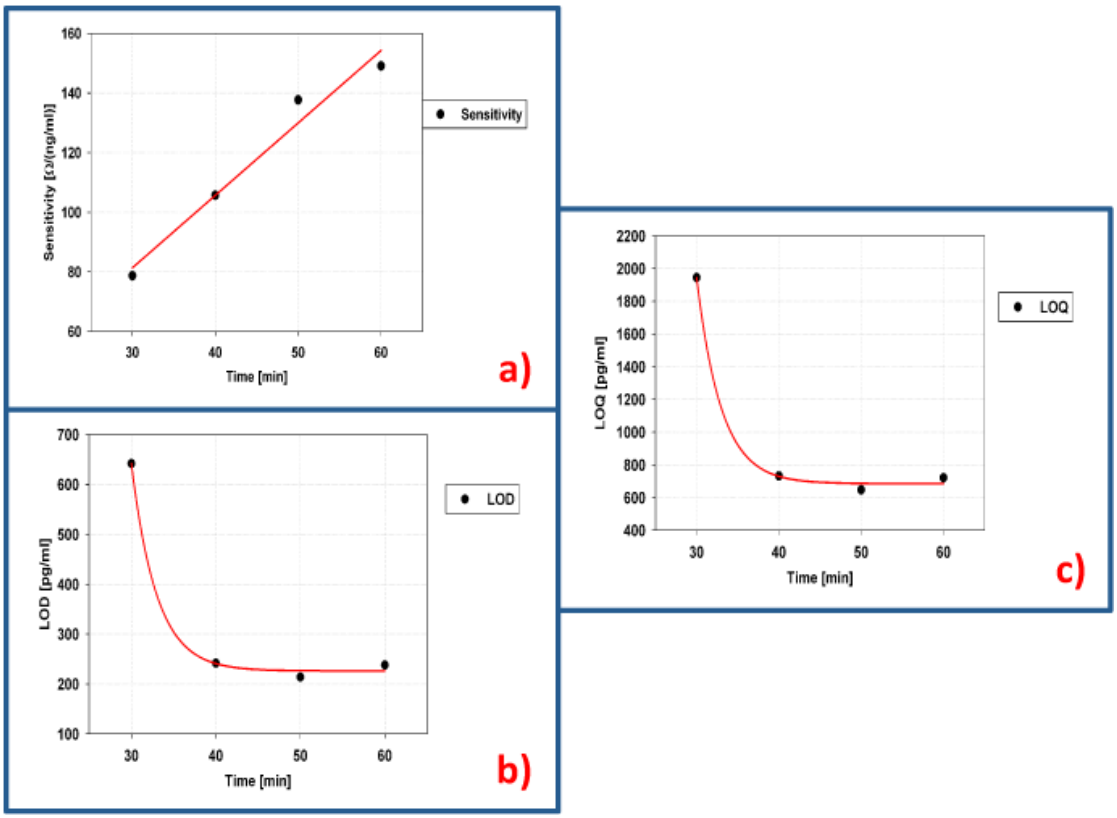

Fig. 6. 7 Adjustability of the sensing parameters of our device. a) Linear fitting of the sensitivity with the experimental data for different detection times. b) Exponential fitting for LOD with experimental data and different detection times. c) Exponential fitting for LOQ with experimental data and different detection times.

The linear behavior of the sensitivity, LOD and LOQ are represented by the next equations:

$$Sensitivity(t) = (8.48 + 2.43 * (t))[\Omega / (ng / ml)] \quad \text{(Eq. 6. 4)}$$

$$LOD(t) = (226.15 + 9.26x10^{6} * \exp(-0.3337 * t))[pg / ml] \quad \text{(Eq. 6. 5)}$$

$$LOQ(t) = (685.37 + 2.84x10^{7} * \exp(-0.3341 * t))[pg / ml] \quad \text{(Eq. 6. 6)}$$

The sensitivity can be improved using larger volumes of samples, as observed on the obtained results. LOD and LOQ improved in a similar way. However, these two parameters seem to reach a plateau and diminish significantly their improvement in our system, when used for SPON2 detection at 6 µl/min flow rate, for detection times higher than 40 minutes. Larger sample flowing times, or sample volumes, had no significant effect ($p>0.05$) on LOD and LOQ. When compared to 30 minutes detection, sample flowing times over 60 minutes improved these two parameters up to 2.6 and 2.8 times respectively.

In order to improve sensitivity and evaluate the performance of our sensor when acting in voltage measurement mode we chose to use the 60 minutes sample flow setup. This biosensor with these parameters would provide a sensitivity of 149 Ω·ng/ml, and a LOD of 238 pg/ml, without saturating the biosensors. It is important to notice that the SPON2 study working principle of the overall biosensor could be extrapolated to different biomarkers depending on the application of interest.

6.3.2 Detection of Spondin-2

The device was characterized for different concentrations of Spondin-2 (1 ng/ml, 5 ng/ml and 10 ng/ml) and keeping the concentration of PSA at 5 ng/ml. The PSA was kept fixed in order to study the cross talk between proteins or its effect with the biosensing elements. The measurements were done in two steps; first the voltage input of 0.1 V at 1 kHz was applied, between e_{1A} and e_{2A}. Impedance and voltage measurements were performed with the Zurich devices (HF2IS and HF2TA). The impedance modulus ($|Z_{e1A:erA}|$ and $|Z_{e2A:erA}|$) and the voltage drop ($V_{e1A:erA}$ and $V_{e2A:erA}$) were obtained. With the values of impedance and voltage related to the Spondin-2 (SPON2) detection, we started the measurement of the second sets of electrodes. Using the analog switch, we now applied the input between e_{1B} and e_{2B}. Once again, with the Zurich device, we got the impedance modulus ($|Z_{e1B:erB}|$ and $|Z_{e2B:erB}|$) and voltage drop ($V_{e1B:erB}$ and $V_{e2B:erB}$). The second set of electrodes was functionalized for the detection of PSA. Each concentration was tested with three devices.

We measured both, impedance and voltage, after the deposition of the antibodies (ASPON2 and APSA) and after the detection of the proteins (SPON2 and

PSA). We expected an increase of impedance and voltage after the deposition of both proteins; we calculated the increment to later plot the results:

$$\begin{aligned}\Delta\left|V_{e1A:erA}\right| &= \left|V_{e1A:erA}(SPON2)\right| - \left|V_{e1A:erA}(ASPON2)\right| \\ \Delta\left|V_{e1B:erB}\right| &= \left|V_{e1B:erB}(PSA)\right| - \left|V_{e1B:erB}(APSA)\right|\end{aligned} \quad \text{(Eq. 6. 7)}$$

$$\begin{aligned}\Delta\left|Z_{e1A:erA}\right| &= \left|Z_{e1A:erA}(SPON2)\right| - \left|Z_{e1A:erA}(ASPON2)\right| \\ \Delta\left|Z_{e1B:erB}\right| &= \left|Z_{e1B:erB}(PSA)\right| - \left|Z_{e1B:erB}(PSA)\right|\end{aligned} \quad \text{(Eq. 6. 8)}$$

We suggested that any change on the voltage drop is equivalent to a change in the impedance modulus [19]:

$$\alpha = \frac{V_{e1:er}}{V_{e2:er}} \approx \frac{\left|Z_{e1:er}\right|}{\left|Z_{e2:er}\right|} \quad \text{(Eq. 6. 9)}$$

The factor α was defined considering an ideal performance: same electrodes area, totally blocked surface on the reference electrodes, zero non-specific adsorption. Therefore, the impedance modulus of the reference electrode ($|Z_{e2:er}|$) must remain without any change after each functionalization. Now, considering a functionalization ($|Z'_{e1:er}|$) and a detection ($|Z''_{e1:er}|$) both increments (Δ|Z| and Δα) must be theoretically equivalent:

$$\Delta\left|Z\right| \cong \left(\left|Z'_{e1:er}\right| - \left|Z''_{e1:er}\right|\right) \cong \left(\alpha' - \alpha''\right)\left|Z_{e2:er}\right| = \Delta\alpha\left|Z_{e2:er}\right| \quad \text{(Eq. 6. 10)}$$

We also expected an increase of factor α after the deposition of both proteins; we calculated the increment to later plot the results:

$$\begin{aligned}\Delta\alpha_A &= \alpha\left(SPON2\right) - \alpha\left(ASPON2\right) \\ \Delta\alpha_B &= \alpha\left(PSA\right) - \alpha\left(APSA\right)\end{aligned} \quad \text{(Eq. 6. 11)}$$

The detection range graphs show an increasing linear tendency for SPON2. For the PSA, there is also an increment on the sensitivity, but we were expecting that the increment on PSA was small and no statistical relevant. The tendency of the detection range was analyzed with a linear regression in order to calculate the characterization parameters (Fig. 6. 8, Fig. 6. 9 and Fig. 6. 10).

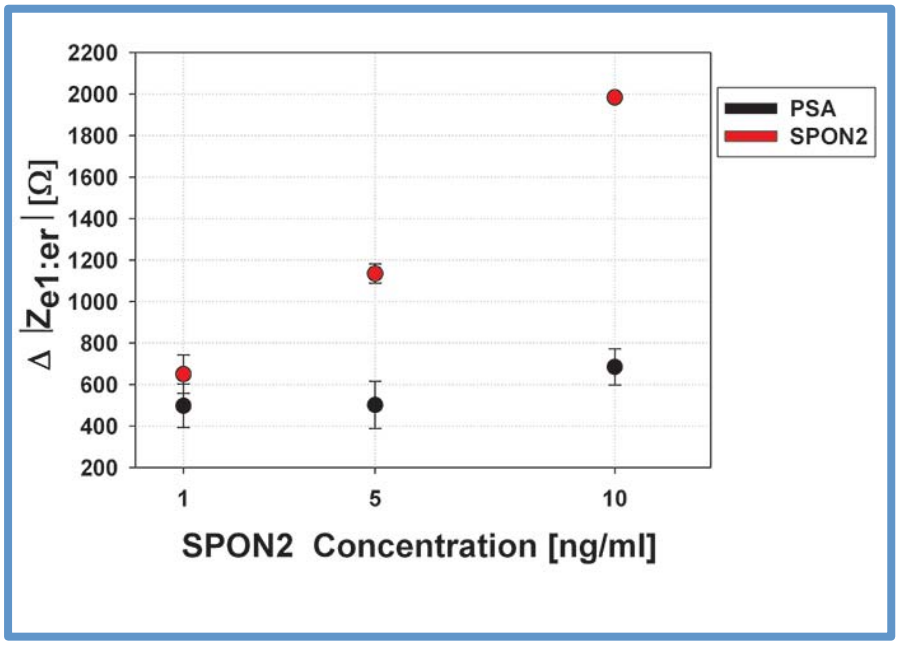

Fig. 6. 8 Detection range of impedance measurements for both biomarkers. The test 1 has a SPON2 concentration of 1 ng/ml, the test 2 had a SPON2 concentration of 5 ng/ml and the test 3 had a SPON2 concentration of 10 ng/ml. The PSA was kept at 5 ng/ml for all the tests.

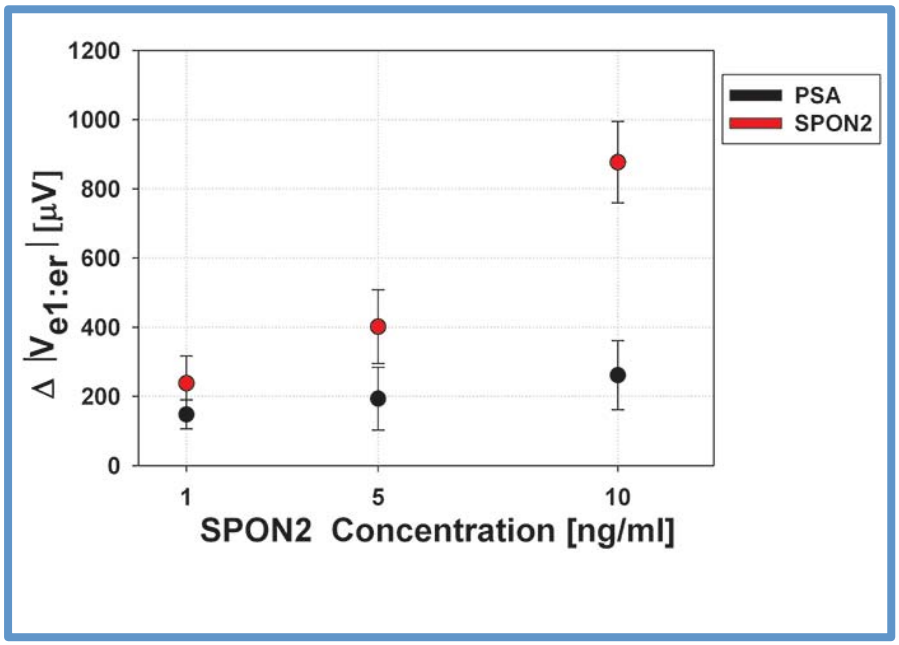

Fig. 6. 9 Detection range of voltage measurements for both biomarkers. The test 1 has a SPON2 concentration of 1 ng/ml, the test 2 had a SPON2 concentration of 5 ng/ml and the test 3 had a SPON2 concentration of 10 ng/ml. The PSA was kept at 5 ng/ml for all the tests.

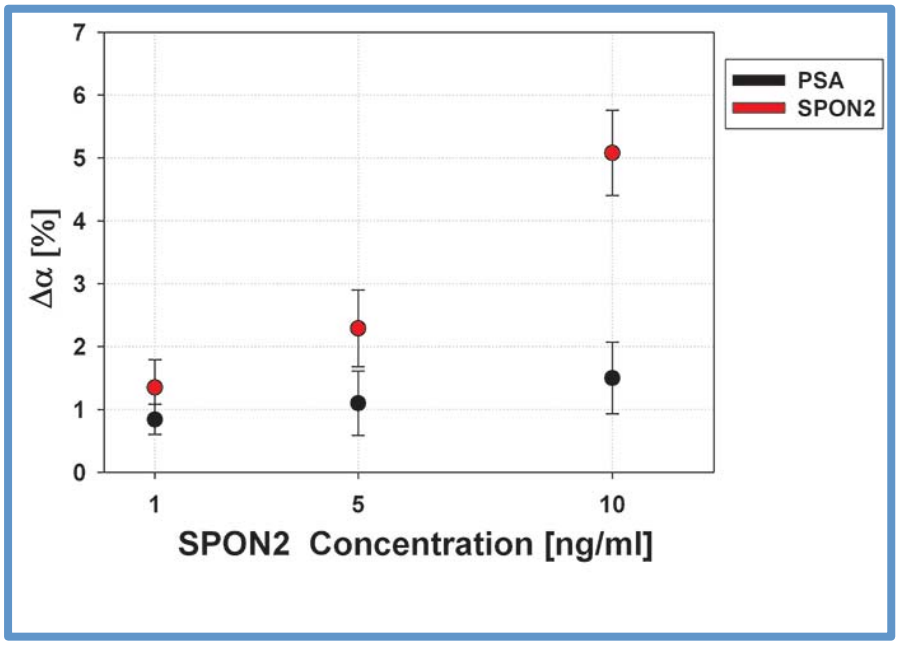

Fig. 6. 10 Detection range of factor α measurements for both biomarkers. The test 1 has a SPON2 concentration of 1 ng/ml, the test 2 had a SPON2 concentration of 5 ng/ml and the test 3 had a SPON2 concentration of 10 ng/ml. The PSA was kept at 5 ng/ml for all the tests.

The LOD and LOQ depend on the standard deviation and slope of the linear regression. With all the processed data now we can obtain the sensitivity, LOD and LOQ of our system for the detection of SPON2 with the different measurement methods. Table 4. 1 summarizes the obtained results.

Table 6. 1 LOD, LOQ and sensitivity for the different electrical measurements for SPON2

Measurement	LOD [pg/ml]	LOQ [pg/ml]	Sensitivity
$\Delta \mid Z_1 \mid$	238	721	149.1 [Ω*(ng/ml)$^{-1}$]
$\Delta \mid V_1 \mid$	841	2540	72 [μV*(ng/ml)$^{-1}$]
Factor α	856	2590	0.4206 [%*(ng/ml)$^{-1}$]

A t-student test was performed among $\Delta|Z_{e1A:erA}|$ and $\Delta\alpha_A$ values at different SPON2 concentrations: 1ng/ml, 5ng/ml and 10ng/ml. Very significant differences ($p<0.01$) were found when comparing the $\Delta|Z_{e1A:erA}|$ results obtained for any of these solution pairs with SPON2 concentrations. Results were similar for $\Delta\alpha_A$ values showing only a slightly lower significance ($p<0.05$) for the 1ng/ml and 5ng/ml pair. Oppositely, when comparing the outcomes of PSA concentrations for all the tests, using either $\Delta|Z_{e1B:erB}|$ or $\Delta\alpha_B$, no significant differences were found ($p>0.1$). Thus the system was sensitive to PSA concentration without having a crosstalk of SPON2.

LOD and LOQ, when evaluating SPON2 concentration, were around 3.5 times higher for $\Delta\alpha$ when compared to $\Delta|Z_{e1:er}|$ measurements (Table 6.1). The parameter α is closely related to voltage changes in the electrodes ($V_{e1A:erA}$ and $V_{e2A:erA}$) and is affected by the behavior of the blocking. Variability among samples at the same SPON2 concentration was also higher when evaluating $\Delta\alpha$ instead of $\Delta|Z_{e1:er}|$. We hypothesized that these results could be due non-perfect PEGylation of the reference electrodes e_l and e_r. However, we proved that there is an equivalent behavior between both methods, detection with $\Delta|Z_{e1:er}|$ and the method proposed $\Delta\alpha$. The $\Delta\alpha$ method opens the door to develop a cheap point-of-care device, for a multiple detection of biomarkers, based on a simple real-time voltage read-out strategy, supported by our electrodes configuration and system. As mention, the PSA concentration was kept fixed and no significant changes were observed when the SPON2 concentration increased. We think that the specificity of both antibodies avoid crosstalk among proteins.

6.4 Conclusions

We have used two protein biomarkers for prostate cancer detection to develop a multiplexed biosensor proof of concept based on our previous development. The multiple depositions of the proteins were monitored on real-time by checking simultaneously the impedance and voltage changes.

We were able to initially test the adjustability of the system for the detection of SPON2. We compared the variations of impedance module at different deposition times of SPON2 and performed the biosensing analysis and characterization. We achieved sensitivity almost 2 times higher after 60 minutes of deposition compared with the first 30 minutes. And when using 60 minutes as deposition time the LOD and LOQ had a better response, with a LOD as low as 250 pg/ml. This analysis helped to define a dynamic and adjustable sensitivity. Depending on the application, we can choose to have a better sensitivity, a better LOD or LOQ, only by changing the detection times. The statistical analysis helped us to define the relation between concentration and time and verify detectability through significant differences.

To prove simultaneous detection of SPON2 and PSA, we compared the variations of impedance module at different concentrations of SPON2 and a fix concentration of PSA. In parallel, these results were compared to an equivalent parameter (alpha)

based on a single voltage measurement exploiting our particular three-electrodes sensor design and voltage divider configuration. With the impedance measurements we got a LOD as low as 238 pg/ml. On the other hand, the LOD of detection for the voltage-based system was almost 850 pg/ml; this is probably due to the imperfections on the PEG-blocked electrodes of both proteins. The results lead us to conclude that our system can use the voltage differential detection method in order to simplify the read-out but with a lower performance if blocking is not improved through longer or higher concentration PEGylation.

The simultaneous detection of SPON2 and PSA showed no cross talk between both proteins. The concentration of PSA was kept at 5 ng/ml and p-values showed no significant statistical differences between PSA measurements done at different concentrations of SPON2 concluding that the antibody functionalized biosensor is specific of its own target protein.

6.5 References

1. G. L. Andriole, E. D. Crawford, R. L. Grubb, S. S. Buys, D. Chia, T. R. Church, M. N. Fouad, E. P. Gelmann, P. A. Kvale, D. J. Reding, J. L. Weissfeld, L. A. Yokochi, B. O'Brien, J. D. Clapp, J. M. Rathmell, T. L. Riley, R. B. Hayes, B. S. Kramer, G. Izmirlian, A. B. Miller, P. F. Pinsky, P. C. Prorok, J. K. Gohagan and C. D. Berg, *New England Journal of Medicine*, 2009, **360**, 1310-1319.
2. F. H. Schröder, *New England Journal of Medicine*, 2011, **365**, 1953-1955.
3. N. Liu, W. Liang, X. Ma, X. Li, B. Ning, C. Cheng, G. Ou, B. Wang, J. Zhang and Z. Gao, *Biosensors and Bioelectronics*, 2013, **47**, 92-98.
4. L. Su, L. Zou, C.-C. Fong, W.-L. Wong, F. Wei, K.-Y. Wong, R. S. S. Wu and M. Yang, *Biosensors and Bioelectronics*, 2013, **46**, 155-161.
5. N. Sardesai, K. Kadimisetty, R. Faria and J. Rusling, *Analytical and Bioanalytical Chemistry*, 2013, **405**, 3831-3838.
6. G. Lucarelli, M. Rutigliano, C. Bettocchi, S. Palazzo, A. Vavallo, V. Galleggiante, S. Trabucco, D. Di Clemente, F. P. Selvaggi, M. Battaglia and P. Ditonno, *J Urol*, 2013, **190**, 2271-2277.
7. X. Qian, C. Li, B. Pang, M. Xue, J. Wang and J. Zhou, *PLoS ONE*, 2012, **7**, e37225.
8. Z. Xi, T. I. Klokk, K. Korkmaz, P. Kurys, C. Elbi, B. Risberg, H. Danielsen, M. Loda and F. Saatcioglu, *Cancer Research*, 2004, **64**, 2365-2370.
9. Y. Dong, A. Kaushal, L. Bui, S. Chu, P. J. Fuller, J. Nicklin, H. Samaratunga and J. A. Clements, *Clinical Cancer Research*, 2001, **7**, 2363-2371.
10. H.-J. Zhou, J. Yan, W. Luo, G. Ayala, S.-H. Lin, H. Erdem, M. Ittmann, S. Y. Tsai and M.-J. Tsai, *Cancer Research*, 2005, **65**, 7976-7983.
11. S. K. Martin, T. B. Vaughan, T. Atkinson, H. Zhu and N. Kyprianou, *Oncol Rep*, 2012, **28**, 409-417.

12. E. S. Leman and R. H. Getzenberg, *Journal of Cellular Biochemistry*, 2009, **108**, 3-9.
13. W. Lou, Z. Ni, K. Dyer, D. J. Tweardy and A. C. Gao, *The Prostate*, 2000, **42**, 239-242.
14. O. R. Saramäki, T. L. J. Tammela, P. M. Martikainen, R. L. Vessella and T. Visakorpi, *Genes, Chromosomes and Cancer*, 2006, **45**, 639-645.
15. R. E. Reiter, Z. Gu, T. Watabe, G. Thomas, K. Szigeti, E. Davis, M. Wahl, S. Nisitani, J. Yamashiro, M. M. Le Beau, M. Loda and O. N. Witte, *Proceedings of the National Academy of Sciences*, 1998, **95**, 1735-1740.
16. J. V. Swinnen, T. Roskams, S. Joniau, H. Van Poppel, R. Oyen, L. Baert, W. Heyns and G. Verhoeven, *International Journal of Cancer*, 2002, **98**, 19-22.
17. D. A. Armbruster and T. Pry, *Clin Biochem Rev*, 2008, **29**, S49-52.
18. A. Shrivastava and V. B. Gupta, *Chronicles of Young Scientists*, 2011, **2**, 21.
19. C. Parra-Cabrera, C. Sporer, I. Rodriguez-Villareal, R. Rodriguez-Trujillo, A. Homs-Corbera and J. Samitier, *Lab on a Chip*, 2012.

General conclusions and discussion

Self-functionalized biosensing lab-on-a-chip devices were designed and fabricated following standard photolithographic and replication techniques. The concept exploited the laminar co-flow principle. The physics involved in microfluidic devices were studied prior the fabrication of the devices and the diffusion phenomenon was also avoided with the selected flows. The fluid dynamics was simulated and results were comparable with experimental tests and analytical calculations.

The device also included a sensing concept based on real-time direct monitoring impedance changes due to biomolecules deposition. The tests helped to select the suitable functionalization times for a complete saturation of the electrode surface with biotin-thiol and streptavidin solutions. The tests also were useful to analyze the electrical drift of the device.

Electrical and optical methods were successfully used to study and proof the selective functionalization "in situ" of the integrated biosensor. Different biomolecules, such as biotin-thiol, streptavidin, and QDs, were selectively deposited onto electrode surface and the layers formed have be monitored and detected using the two methods.

The sensitivity of the system was characterized by means of HSA detection impedance change measurements. Sensitivity of -6.6×10^{-3} $[\%*(\mu g/ml)^{-1}]$ was achieved with this proof-of-concept. A differential voltage and impedance measurements were done with the chip, which also included a real time analysis. The statistical analysis told us that the impedance measurements are the most reliable samples due to its differences in p-values. The equivalence, and the restrictions, between impedance variations and voltage variations were established and verified

The device was characterized for the detection of human serum albumin as a proof of concept. Impedance measurements showed a higher sensitivity for the detection of HSA, in comparison with voltage measurements, almost 2.2 times higher. The LOD and LOQ showed a similar response for voltage and impedance measurements.

We performed an in-situ blocking of the two electrodes (e_r and e_2) that worked as reference to improve the voltage output measurements. A PEG-based solution was used

to do the blocking. The voltage output was improved by 50% after changing the times and concentrations of the PEG-based solution.

We were able to test the adjustability of the system. We compared the impedance change at different deposition times of PSA and performed the biosensing analysis and characterization. This analysis helped to define a dynamic and adjustable sensitivity and LOD and LOQ. The statistical analysis helped us to define the relation between concentration and time and when we can find a significant difference.

With the improvement of blocking, the device was characterized for the detection of prostate specific antigen PSA. The impedance and voltage results showed a linear behavior on the range of interest (1ng/ml-10ng/ml).. Impedance measurements showed a 30% better LOD and LOQ response in comparison to voltage measurements.

We have introduced an adimensional factor α that also showed a response in LOD and LOQ, similar to the voltage analysis, and this showed that this factor is closely related to the voltage changes and is greatly affected by the blocking of the electrodes. Tests with human serum didn't showed non-specific adsorption.

We have also used two protein biomarkers PSA and SPON2 for prostate cancer. The multiple depositions of the proteins were monitored on real-time by checking simultaneously the impedance and voltage changes. The test showed no cross talk between both proteins.

We compared the impedance change at different deposition times of SPON2 and performed the biosensing analysis and characterization. The system sensitivity was similar to the results obtained with PSA, we had a impedance sensitivity of 149.1 $[\Omega*(ng/ml)^{-1}]$ and a voltage sensitivity of 72 $[\mu V*(ng/ml)^{-1}]$.

Results indicate that the systems can be easily adapted to detect different biomolecules and it could be very advantageous since it eases fabrication and long-term storage of these biosensing devices by making it possible to keep the different biomolecules stored individually before the cartridge use and biosensors-use specification. The systems have a top limit of detection that depends on the saturation of the biosensor surface.

Comparing the results obtained with the specific objectives established in this thesis, we can conclude that the main objective " study and exploit microfluidics physics, self-

assembled molecular monolayers, proteins interactions and electronic detection techniques to design, develop and fabricate a versatile biosensing novel lab-on-a-chip device suitable for point of care applications with multiplexing capabilities, and adjustable sensitivity and range of detection depending on the application" has been achieved.

Concerning the specific objectives we can conclude that, as shown on Chapter 1, we were able to fabricate and characterize lab-on-chip microdevices by photolithographic and molding techniques, also we characterize and adjust the fluid dynamics of our novel microfluidic devices.

With the results obtained on Chapter 2, we achieve the objectives of developed a self-functionalizing protocol for the detection of a biomolecule by means of laminar co-flow and study the impedance changes of the integrated biosensors after the deposition of a layer. Furthermore, we were able to study the impedance changes produced by the interaction between biotin and streptavidin on the formation of different monolayers over the surface of the biosensors.

On Chapter 3 we completed the objectives of performing an optical and impedance analysis of quantum dots after its selective deposition and detection. Besides, as one of our specific objectives, we developed custom made software to do the voltage and impedance measurements.

On Chapter 4 we achieved to objective of characterize the device for the detection of human serum albumin, by a real time voltage and impedance measurements.

We were able to complete the objectives of improving the blocking protocol to get a better response with the voltage measurements and characterizing the microfluidic LOC for the detection of prostate-specific antigen as explained on Chapter 5.

Finally, we succeeded with the last specific objective, fabricating and testing a device with multiple biosensors for the detection of two cancer biomarkers, as explained on Chapter 6.

Future work

So far we tested our system for the detection of two prostate cancer biomarkers (PSA and SPON-2) proving the concept; however more tests could be performed in order to fully characterize the behavior of the system and the suitability for a full panel of all the relevant prostate cancer,

i) Several tests must be performed with human serum in order to fully characterized and confirm that the device has no non-specific adsorption.

ii) The same set-up could be used for the detection of several prostate cancer biomarkers. We chose PSA and SPON2 but different combinations could be tested in order to study the cross talk between biomarkers and so select the best combination for the detection of prostate cancer.

iii) The system is flexible enough to be tested with biomarkers from different diseases.

Annex 1 Characterization of impedance spectroscope (HF2TA)

The response of the transimpedance current amplifier was characterized. We found out that an error was presented during the first tests. Therefore that error due to the device was corrected. Two resistances were connected as a voltage divider and the value of the resistance was measured with the Zurich instruments Fig. 4. 10. The resistance number 2 (Z_2) was fixed while the resistance number 1 changed (Z_1). The values of Z_1 were between: 120Ω and 470kΩ. The values of Z_2 were: 1kΩ, 10kΩ, 22kΩ, 47kΩ and 100kΩ.

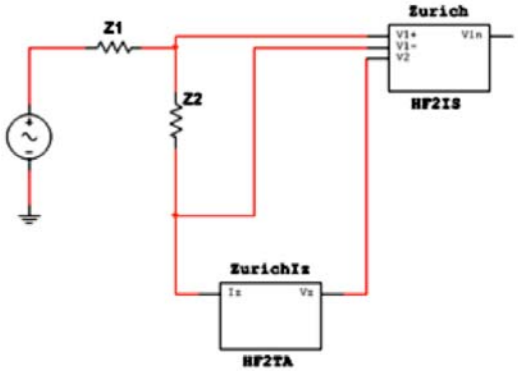

Fig. A1. 1 Schematics of the characterization set-up.

Both resistances were measure with the HF2TA and with a multimeter (real values). And the values were compared (Fig. A1. 2).

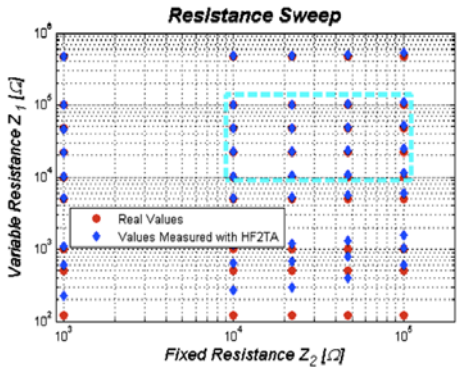

Fig. A1. 2 Comparison between HF2TA and multimeter measurements.

The percentage error of the HF2TA was calculated and plotted:

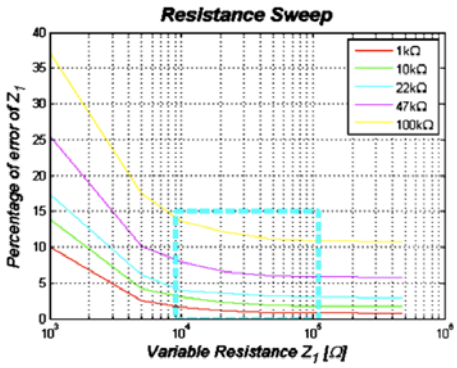

Fig. A1. 3 Characteristic curves for the percentage error of HF2TA measurements.

With the results we characterized the error and performed a correction, the correction was applied to the software and the measurements were performed again.

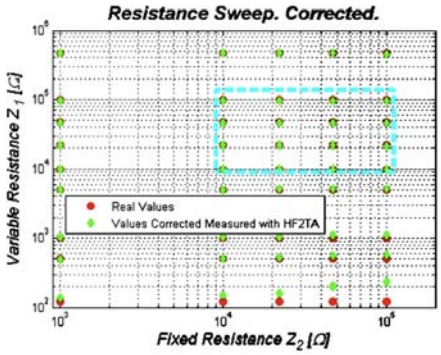

Fig. A1. 4 Corrected measurements.

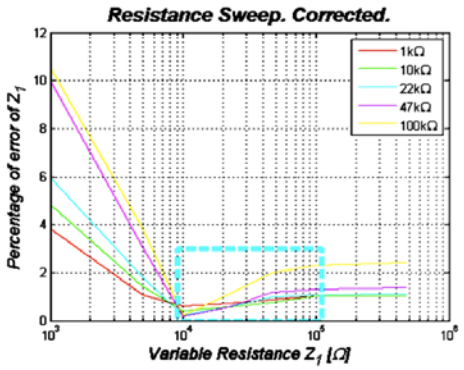

Fig. A1. 5 Characteristic curves for the percentage error after the correction.

After the correction on the software we were able to reduce the percentage error up to 2.5% in the region of interest (10 kΩ - 100kΩ). And up to 10% in the whole range. The error was reduced almost 4 times.

Annex 2 Development of custom-made software

Three different custom made software were developed. Each version was done for a different purpose. The first one was used for the experiments done with HSA and only voltage measurements were acquired. The software was programmed to configure the Zurich impedance spectroscope with three frequencies and different amplitudes. The user can choose the name of the output file and the plotting of the voltage was performed on real-time. A stopping flag was added if a problem is presented during measurements. The code for the *gui* is:

```
% --- Executes on button press in pushbutton1.
function pushbutton1_Callback(hObject, eventdata, handles)
% hObject    handle to pushbutton1 (see GCBO)
% eventdata  reserved - to be defined in a future version of
MATLAB
% handles    structure with handles and user data (see GUIDATA)
clc

% Inicializacion de variables
a1 = 0;a2 = 0;a3 = 0;a4 = 0;a5 = 0;a6 = 0;
canal1 = 1;
canal2 = 2;
osc1 = 1;
osc2 = 3;
osc3 = 5;
osc4 = 2;
osc5 = 4;
osc6 = 6;
segs=0.1;  % Tiempo de actulizacion de la medida
rate=450;
tc = 0.001;
freq1 = get(handles.frec1, 'String');
freq1 = str2num(freq1);
freq2 = get(handles.frec2, 'String');
freq2 = str2num(freq2);
freq3 = get(handles.frec3, 'String');
freq3 = str2num(freq3);
diff1 = get(handles.diferencial, 'Value');
volt1 = get(handles.volt, 'String');
volt1 = str2num(volt1);
volt2 = get(handles.volt2, 'String');
volt2 = str2num(volt2);
volt3 = get(handles.volt3, 'String');
volt3 = str2num(volt3);
ciclos = get(handles.duracion, 'String');
ciclos = 60*str2num(ciclos);
axes(handles.axes1);cla;
axes(handles.axes2);cla;
axes(handles.axes3);cla;
axes(handles.axes4);cla;
axes(handles.axes5);cla;
axes(handles.axes6);cla;

% Funcion para iniciar el Zurich
[dispositivo]=iniciar_zurich;

% Función para configurar al Zurich
config_zurich(dispositivo,canal1);

% Función para configurar al Zurich primera frecuencia Canal
diferencial
 config_entradas(dispositivo,canal1,rate,freq1,volt1,tc,osc1,diff1);

% Función para configurar al Zurich segunda frecuencia Canal
diferencial
 config_entradas(dispositivo,canal1,rate,freq2,volt2,tc,osc2,diff1);

% Función para configurar al Zurich tercera frecuencia Canal
diferencial
 config_entradas(dispositivo,canal1,rate,freq3,volt3,tc,osc3,diff1);

% Función para configurar al Zurich primera frecuencia Canal NO
diferencial
 config_entradas2(dispositivo,canal2,rate,freq1,tc,osc4,0);

% Función para configurar al Zurich segunda frecuencia Canal NO
diferencial
 config_entradas2(dispositivo,canal2,rate,freq2,tc,osc5,0);

% Función para configurar al Zurich tercera frecuencia Canal NO
diferencial
 config_entradas2(dispositivo,canal2,rate,freq3,tc,osc6,0);

% Pause to get a settled lowpass filter
pause(10*tc);

set(handles.tiemp,'String',num2str(0));
set(handles.tdiff,'String',num2str(0));

tactualiza = 1;
tstart =tic;
tvisual= clock;
for i=1:ciclos
   ylim1 = get(handles.ylim1, 'String');
   ylim1 = str2num(ylim1);
   ylim2 = get(handles.ylim2, 'String');
   ylim2 = str2num(ylim2);

   t1 = clock;
   % Función para configurar al Zurich primera frecuencia Canal
diferencial

%config_entradas(dispositivo,canal1,rate,freq1,volt1,tc,osc1,diff1);

   [x1,y1,f1] = medir_zurich(dispositivo,segs,osc1,tc);
   b1 = length(x1);
   minutos1 = i-1+1/b1:1/b1:i;
   minutos1 = minutos1 / 60;
   r1 = sqrt(x1.^2 + y1.^2);
   if i == 1
      rf1 = r1;
      min1 = minutos1;
   else
       min1 = [min1 minutos1];
       rf1 = [rf1 r1];
   end
   axes(handles.axes1);
   plot(min1,rf1)
   title(['Voltaje de Entrada,',num2str(f1(1)),'Hz'])
   xlabel('Tiempo [min]')
   ylabel('Voltaje [V]')
   a1 = a1+b1;

   % Función para configurar al Zurich segunda frecuencia Canal
diferencial

%config_entradas(dispositivo,canal1,rate,freq2,volt2,tc,osc1,diff1);

   [x2,y2,f2] = medir_zurich(dispositivo,segs,osc2,tc);
   b2 = length(x2);
   minutos2 = i-1+1/b2:1/b2:i;
   minutos2 = minutos2 / 60;
   r2 = sqrt(x2.^2 + y2.^2);
   if i == 1
      rf2 = r2;
      min2 = minutos2;
```

```
    else
        min2 = [min2 minutos2];
        rf2 = [rf2 r2];
    end
    axes(handles.axes2);
    plot(min2,rf2)
    title(['Voltaje de Entrada,',num2str(f2(1)),'Hz'])
    xlabel('Tiempo [min]')
    ylabel('Voltaje [V]')
    a2 = a2+b2;

    % Función para configurar al Zurich tercera frecuencia Canal
diferencial

%config_entradas(dispositivo,canal1,rate,freq3,volt3,tc,osc1,diff1);

    [x3,y3,f3] = medir_zurich(dispositivo,segs,osc3,tc);
    b3 = length(x3);
    minutos3 = i-1+1/b3:1/b3:i;
    minutos3 = minutos3 / 60;
    r3 = sqrt(x3.^2 + y3.^2);
    if i == 1
        rf3 = r3;
        min3 = minutos3;
    else
        min3 = [min3 minutos3];
        rf3 = [rf3 r3];
    end
    axes(handles.axes3);
    plot(min3,rf3)
    title(['Voltaje de Entrada,',num2str(f3(1)),'Hz'])
    xlabel('Tiempo [min]')
    ylabel('Voltaje [V]')
    a3 = a3+b3;

    % Función para configurar al Zurich primera frecuencia Canal
NO diferencial
    %config_entradas2(dispositivo,canal2,rate,freq1,tc,osc1,0);

    [x4,y4,f4] = medir_zurich(dispositivo,segs,osc4,tc);
    b4 = length(x4);
    minutos4 = i-1+1/b4:1/b4:i;
    minutos4 = minutos4 / 60;
    r4 = sqrt(x4.^2 + y4.^2);
    if i == 1
        rf4 = r4;
        min4 = minutos4;
    else
        min4 = [min4 minutos4];
        rf4 = [rf4 r4];
    end
    alarma = get(handles.alarma, 'Value');
    media = mean(rf4);
    media2 = mean(r4);
    if alarma == 1
        set(handles.media_total,'String',num2str(media));
        set(handles.media_local,'String',num2str(media2));
        porcent = get(handles.Porcen, 'String');
        porcent1 = str2num(porcent);
        if i>180
            if media2< (100- porcent1)/100*media || media2 >
(100+porcent1)/100*media
                [y, Fs, nbits, readinfo]  = wavread('alarma2.wav');
                sound(y,2*Fs)
                sound(y,2*Fs)
                pause(10)
            end
        end
    end
    axes(handles.axes4);
    plot(min4,rf4)
    if ylim1 ~= ylim2
        ylim([ylim1 ylim2])
    else
        ylim('auto')
    end
    title(['Voltaje de Salida,',num2str(f1(1)),'Hz'])
    xlabel('Tiempo [min]')
    ylabel('Voltaje [V]')
    a4 = a4+b4;

    % Función para configurar al Zurich segunda frecuencia Canal
NO diferencial
    %config_entradas2(dispositivo,canal2,rate,freq2,tc,osc1,0);

    [x5,y5,f5] = medir_zurich(dispositivo,segs,osc5,tc);
    b5 = length(x5);
    minutos5 = i-1+1/b5:1/b5:i;
    minutos5 = minutos5 / 60;
    r5 = sqrt(x5.^2 + y5.^2);
    if i == 1
        rf5 = r5;
        min5 = minutos5;
    else
        min5 = [min5 minutos5];
        rf5 = [rf5 r5];
    end
    axes(handles.axes5);
    plot(min5,rf5)
    title(['Voltaje de Salida,',num2str(f2(1)),'Hz'])
    xlabel('Tiempo [min]')
    ylabel('Voltaje [V]')
    a5 = a5+b5;

    % Función para configurar al Zurich tercera frecuencia Canal
NO diferencial
    %config_entradas2(dispositivo,canal2,rate,freq3,tc,osc1,0);

    [x6,y6,f6] = medir_zurich(dispositivo,segs,osc6,tc);
    b6 = length(x6);
    minutos6 = i-1+1/b6:1/b6:i;
    minutos6 = minutos6 / 60;
    r6 = sqrt(x6.^2 + y6.^2);
    if i == 1
        rf6 = r6;
        min6 = minutos6;
    else
        min6 = [min6 minutos6];
        rf6 = [rf6 r6];
    end
    axes(handles.axes6);
    plot(min6,rf6)
    title(['Voltaje de Salida,',num2str(f3(1)),'Hz'])
    xlabel('Tiempo [min]')
    ylabel('Voltaje [V]')
    a6 = a6+b6;

    if (etime(clock,tvisual)/60)> 5*tactualiza
    set(handles.tiemp,'String',num2str(etime(clock,tvisual)/60));
    tactualiza = tactualiza +1;
    end

    t2 = etime(clock,t1);
    while t2 < 1
        if t2 < 1
            t2 = etime(clock,t1);
        end
    end
    seleccion = get(handles.detener, 'Value');
    if  seleccion == 1
        break
    end


end
telapsed = toc(tstart);
telapsed = telapsed/60;
tselec = ciclos/60;
tdiff = tselec - telapsed;
tdiff = tdiff;
set(handles.tiemp,'String',num2str(telapsed));
set(handles.tdiff,'String',num2str(tdiff));

% Apagar el Zurich
apagar_zurich(dispositivo,canal1);

[y, Fs, nbits, readinfo]  = wavread('Ding.wav');
sound(y,2*Fs)
sound(y,2*Fs)
sound(y,Fs/2)

nombre1 = get(handles.nombre, 'String');
archivo1 =
sprintf(['C1_',nombre1,'_',num2str(freq1/1000),'k.mat']);
archivo2 =
sprintf(['C1_',nombre1,'_',num2str(freq2/1000),'k.mat']);
archivo3 =
sprintf(['C1_',nombre1,'_',num2str(freq3/1000),'k.mat']);

archivo4 =
sprintf(['C2_',nombre1,'_',num2str(freq1/1000),'k.mat']);
```

```
archivo5 =
sprintf(['C2_',nombre1,'_',num2str(freq2/1000),'k.mat']);
archivo6 =
sprintf(['C2_',nombre1,'_',num2str(freq3/1000),'k.mat']);

direc = sprintf([datestr(now, 7),datestr(now, 5),datestr(now, 10)]);
mkdir(direc)
cd(direc)
save(archivo1,'rf1')
save(archivo2,'rf2')
save(archivo3,'rf3')
save(archivo4,'rf4')
save(archivo5,'rf5')
save(archivo6,'rf6')
cd ..
```

And the final image is:

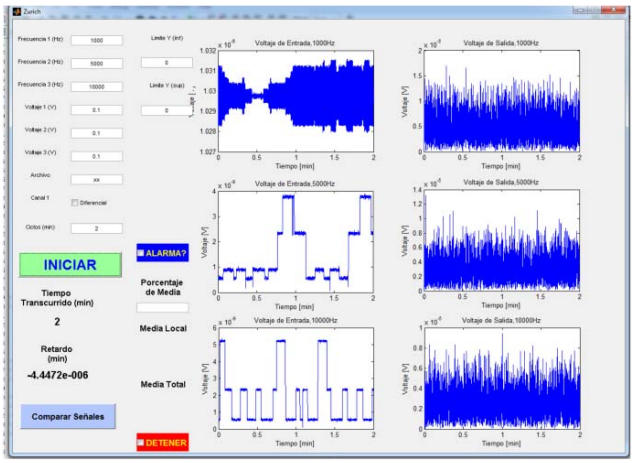

Fig. A2. 1 Custom-made software first version, voltage measurements only.

The second version included the measurement of impedance and current, along with the voltage. This one was an upgrade of the first version. The software also was able to configure the Zurich transimpedance amplifier. The correction of the error was applied also. The code for this version is:

```
% --- Executes on button press in pushbutton1.
function pushbutton1_Callback(hObject, eventdata, handles)
% hObject    handle to pushbutton1 (see GCBO)
% eventdata  reserved - to be defined in a future version of
MATLAB
% handles    structure with handles and user data (see GUIDATA)
clc

% Inicializacion de variables
a1 = 0;a2 = 0;a3 = 0;a4 = 0;a5 = 0;a6 = 0;
canal1 = 1;
canal2 = 2;
osc1 = 1;
osc2 = 2;
osc3 = 3;
osc4 = 4;
osc5 = 5;
osc6 = 6;
osc7 = 7;
osc8 = 8;
segs=0.5;  % Tiempo de medida
rate=450;
tc = 0.01;
freq1 = get(handles.frec1, 'String');
freq1 = str2num(freq1);
freq2 = get(handles.frec2, 'String');
freq2 = str2num(freq2);
freq3 = get(handles.frec3, 'String');
freq3 = str2num(freq3);
volt1 = get(handles.volt, 'String');
volt1 = str2num(volt1);
Act_f1 = get(handles.Act_F1, 'Value');
Act_f2 = get(handles.Act_F2, 'Value');
Act_f3 = get(handles.Act_F3, 'Value');
ciclos = get(handles.duracion, 'String');
ciclos = 60*str2num(ciclos);
axes(handles.axes1);cla;
axes(handles.axes2);cla;
axes(handles.axes3);cla;
axes(handles.axes4);cla;
axes(handles.axes5);cla;
axes(handles.axes6);cla;
axes(handles.axes7);cla;
axes(handles.axes8);cla;
axes(handles.axes9);cla;
axes(handles.axes10);cla;
axes(handles.axes11);cla;
axes(handles.axes12);cla;

% Funcion para iniciar el HF2TA_gui
[dispositivo]=iniciar_zurich_HF2TA;

% Función para configurar al HF2TA_gui
config_zurich_HF2TA(dispositivo,canal1);

% Función para configurar al HF2TA_gui primera frecuencia
Canal diferencial
if Act_f1 == 1
config_entradas_HF2TA(dispositivo,canal1,rate,freq1,volt1,tc,osc1
,1);
end

% Función para configurar al HF2TA_gui segunda frecuencia
Canal diferencial
if Act_f2 == 1
config_entradas_HF2TA(dispositivo,canal1,rate,freq2,volt1,tc,osc3
,1);
end
```

```
% Función para configurar al HF2TA_gui tercera frecuencia Canal
diferencial
if Act_f3 == 1
config_entradas_HF2TA(dispositivo,canal1,rate,freq3,volt1,tc,osc5
,1);
end

% Función para configurar al HF2TA_gui primera frecuencia
Canal NO diferencial
if Act_f1 == 1
config_entradas2_HF2TA(dispositivo,canal2,rate,freq1,tc,osc2,0);
end

% Función para configurar al HF2TA_gui segunda frecuencia
Canal NO diferencial
if Act_f2 == 1
config_entradas2_HF2TA(dispositivo,canal2,rate,freq2,tc,osc4,0);
end

% Función para configurar al HF2TA_gui tercera frecuencia Canal
NO diferencial
if Act_f3 == 1
config_entradas2_HF2TA(dispositivo,canal2,rate,freq3,tc,osc6,0);
end

% Función para configurar Ganancias
current = get(handles.CurrentG, 'Value');
switch current
   case 1
      current = 100;
   case 2
      current = 1000;
   case 3
      current = 10e3;
   case 4
      current = 100e3;
   case 5
      current = 1e6;
   case 6
      current = 10e6;
   case 7
      current = 100e6;
end
   voltage = get(handles.VoltageG, 'Value');
switch voltage
   case 1
      voltage = 1;
   case 2
      voltage = 10;
end
   ganancias_HF2TA(dispositivo,current,voltage);

set(handles.tiemp,'String',num2str(0));
%set(handles.tdiff,'String',num2str(0));

correct = get(handles.correct, 'Value');
if correct == 1


   fvoltc1 = 0;
   fvoltc2 = 0;
   for i=1:30;
      t1 = clock;
      [voltc1] =
medir_Vin(dispositivo,segs,current,voltage,volt1,Act_f1,Act_f2,Ac
t_f3,correct);
      fvoltc1 = [fvoltc1 voltc1];
      t2 = etime(clock,t1);
      while t2 < 1
         if t2 < 1
            t2 = etime(clock,t1);
         end
      end
   end
   for i=1:30;
      t1 = clock;
      [voltc2] =
medir_Vin2(dispositivo,segs,current,voltage,volt1,Act_f1,Act_f2,
Act_f3,correct);
      fvoltc2 = [fvoltc2 voltc2];
      t2 = etime(clock,t1);
      while t2 < 1
         if t2 < 1
            t2 = etime(clock,t1);
         end
      end
   end
   voltc = mean(fvoltc1)+mean(fvoltc2)
   pause(1)
else
   voltc = volt1/sqrt(2);
   % Función para configurar al HF2TA_gui primera frecuencia
Canal diferencial
   if Act_f1 == 1

config_entradas_HF2TA(dispositivo,canal1,rate,freq1,volt1,tc,osc1
,1);
   end

   % Función para configurar al HF2TA_gui segunda frecuencia
Canal diferencial
   if Act_f2 == 1

config_entradas_HF2TA(dispositivo,canal1,rate,freq2,volt1,tc,osc3
,1);
   end

   % Función para configurar al HF2TA_gui tercera frecuencia
Canal diferencial
   if Act_f3 == 1

config_entradas_HF2TA(dispositivo,canal1,rate,freq3,volt1,tc,osc5
,1);
   end
end

tactualiza = 1;
tstart =tic;
tvisual= clock;
tcontrol = clock; % Reloj que controlará la duración de la medida

tpausa = 0;
tdur = 0;
for i=1:ciclos


   ylim1 = get(handles.ylim1, 'String');
   ylim1 = str2num(ylim1);
   ylim2 = get(handles.ylim2, 'String');
   ylim2 = str2num(ylim2);

   t1 = clock;

   % Funcion de obtencion de medidas
   correct = get(handles.correct, 'Value');


[f1,f2,f3,f4,f5,f6,r1,r2,r3,r4,r5,r6,Z1,Z2,Z3,Vz21,Vz22,Vz23,Z21,
Z22,Z23] =
medir_zurich_HF2TA_all(dispositivo,segs,current,voltage,voltc,Ac
t_f1,Act_f2,Act_f3,correct);

   if i == 1
      rf1 = r1;
      rf2 = r2;
      rf3 = r3;
      rf4 = r4;
      rf5 = r5;
      rf6 = r6;
      Zf1 = Z1;
      Zf2 = Z2;
      Zf3 = Z3;
      Vzf21 = Vz21;
      Vzf22 = Vz22;
      Vzf23 = Vz23;
      Zf21 = Z21;
      Zf22 = Z22;
      Zf23 = Z23;
   else
      rf1 = [rf1 r1];
      rf2 = [rf2 r2];
      rf3 = [rf3 r3];
      rf4 = [rf4 r4];
      rf5 = [rf5 r5];
      rf6 = [rf6 r6];
      Zf1 = [Zf1 Z1];
      Zf2 = [Zf2 Z2];
      Zf3 = [Zf3 Z3];
      Vzf21 = [Vzf21 Vz21];
      Vzf22 = [Vzf22 Vz22];
      Vzf23 = [Vzf23 Vz23];
      Zf21 = [Zf21 Z21];
```

```
    Zf22 = [Zf22 Z22];
    Zf23 = [Zf23 Z23];
end
tactual = etime(clock,tcontrol);
tactual = tactual/60;
periodo = tactual/length(rf1);
periodo2 = tactual/length(rf3);
periodo3 = tactual/length(rf5);

minutos = periodo:periodo:tactual;
minutos2 = periodo2:periodo2:tactual;
minutos3 = periodo3:periodo3:tactual;

axes(handles.axes1);
plot(minutos,rf1)
%if ylim1 ~= ylim2
%   ylim([ylim1 ylim2])
%else
   ylim('auto')
%end
title(['Voltaje Z1,',num2str(f2(1)),'Hz'])
xlabel('Tiempo [min]')
ylabel('Voltaje [V]')
axes(handles.axes2);
plot(minutos2,rf3)
%if ylim1 ~= ylim2
%   ylim([ylim1 ylim2])
%else
%   ylim('auto')
%end
title(['Voltaje Z1,',num2str(f4(1)),'Hz'])
xlabel('Tiempo [min]')
ylabel('Voltaje [V]')
 axes(handles.axes3);
plot(minutos3,rf5)
%if ylim1 ~= ylim2
%   ylim([ylim1 ylim2])
%else
%   ylim('auto')
%end
title(['Voltaje Z1,',num2str(f6(1)),'Hz'])
xlabel('Tiempo [min]')
ylabel('Voltaje [V]')

axes(handles.axes4);
plot(minutos,Zf1)
if ylim1 ~= ylim2
   ylim([ylim1 ylim2])
else
   ylim('auto')
end
title(['Impedancia Z1,',num2str(f2(1)),'Hz'])
xlabel('Tiempo [min]')
ylabel('Impedancia [\Omega]')
axes(handles.axes5);
plot(minutos2,Zf2)
if ylim1 ~= ylim2
   ylim([ylim1 ylim2])
else
   ylim('auto')
end
title(['Impedancia Z1,',num2str(f4(1)),'Hz'])
xlabel('Tiempo [min]')
ylabel('Impedancia [\Omega]')
axes(handles.axes6);
plot(minutos3,Zf3)
if ylim1 ~= ylim2
   ylim([ylim1 ylim2])
else
   ylim('auto')
end
title(['Impedancia Z1,',num2str(f6(1)),'Hz'])
xlabel('Tiempo [min]')
ylabel('Impedancia [\Omega]')

axes(handles.axes7);
plot(minutos,rf2)
title(['Voltaje HF2TA,',num2str(f2(1)),'Hz'])
xlabel('Tiempo [min]')
ylabel('Voltaje [V]')

axes(handles.axes8);
plot(minutos2,rf4)
title(['Voltaje HF2TA,',num2str(f4(1)),'Hz'])
xlabel('Tiempo [min]')
ylabel('Voltaje [V]')

axes(handles.axes9);
plot(minutos3,rf6)
title(['Voltaje HF2TA,',num2str(f6(1)),'Hz'])
xlabel('Tiempo [min]')
ylabel('Voltaje [V]')

axes(handles.axes10);
plot(minutos,Zf21)
title(['Impedancia Z2,',num2str(f2(1)),'Hz'])
xlabel('Tiempo [min]')
ylabel('Impedancia [\Omega]')

axes(handles.axes11);
plot(minutos2,Zf22)
title(['Impedancia Z2,',num2str(f4(1)),'Hz'])
xlabel('Tiempo [min]')
ylabel('Impedancia [\Omega]')

axes(handles.axes12);
plot(minutos3,Zf23)
title(['Impedancia Z2,',num2str(f6(1)),'Hz'])
xlabel('Tiempo [min]')
ylabel('Impedancia [\Omega]')

if (etime(clock,tvisual)/60)> tactualiza
set(handles.tiemp,'String',num2str(etime(clock,tvisual)/60));
tactualiza = tactualiza +1;

end

t2 = etime(clock,t1);
while t2 < 1
   if t2 < 1
      t2 = etime(clock,t1);
   end
end
seleccion = get(handles.detener, 'Value');

if  seleccion == 1
   break
end

tbreak = etime(clock,tcontrol);
if tbreak > ciclos
   break
end

current = get(handles.CurrentG, 'Value');
switch current
   case 1
      current = 100;
   case 2
      current = 1000;
   case 3
      current = 10e3;
   case 4
      current = 100e3;
   case 5
      current = 1e6;
   case 6
      current = 10e6;
   case 7
      current = 100e6;
end
voltage = get(handles.VoltageG, 'Value');
switch voltage
   case 1
      voltage = 1;
   case 2
      voltage = 10;
end
ganancias_HF2TA(dispositivo,current,voltage);

pausa = get(handles.pausa,'Value');

if  pausa == 1
   ziDAQ('unsubscribe',['/' dispositivo '/demods/*/sample']);
   ziDAQ('flush');
   tpini = clock;

   while pausa ==1
         pausa = get(handles.pausa,'Value');
         pause(1)
   end
```

```
      tdur = etime(clock,tpini);
      tpausa = tpausa + tdur;
   end
end


telapsed = toc(tstart);
telapsed = telapsed/60;
tselec = ciclos/60;
tdiff = tselec - telapsed;
tdiff = tdiff;
set(handles.tiemp,'String',num2str(telapsed));
%set(handles.tdiff,'String',num2str(tdiff));

% Apagar el HF2TA_gui
apagar_zurich_HF2TA(dispositivo,canal1);



nombre1 = get(handles.nombre, 'String');
archivo1 =
sprintf(['V1_',nombre1,'_',num2str(freq1/1000),'k.mat']);
archivo2 =
sprintf(['V1_',nombre1,'_',num2str(freq2/1000),'k.mat']);
archivo3 =
sprintf(['V1_',nombre1,'_',num2str(freq3/1000),'k.mat']);

archivo4 =
sprintf(['Z1_',nombre1,'_',num2str(freq1/1000),'k.mat']);
archivo5 =
sprintf(['Z1_',nombre1,'_',num2str(freq2/1000),'k.mat']);
archivo6 =
sprintf(['Z1_',nombre1,'_',num2str(freq3/1000),'k.mat']);

archivo7 =
sprintf(['V2_',nombre1,'_',num2str(freq1/1000),'k.mat']);
archivo8 =
sprintf(['V2_',nombre1,'_',num2str(freq2/1000),'k.mat']);
archivo9 =
sprintf(['V2_',nombre1,'_',num2str(freq3/1000),'k.mat']);

archivo10 =
sprintf(['Z2_',nombre1,'_',num2str(freq1/1000),'k.mat']);
archivo11 =
sprintf(['Z2_',nombre1,'_',num2str(freq2/1000),'k.mat']);
archivo12 =
sprintf(['Z2_',nombre1,'_',num2str(freq3/1000),'k.mat']);

archivo13 =
sprintf(['VIz_',nombre1,'_',num2str(freq1/1000),'k.mat']);
archivo14 =
sprintf(['VIz_',nombre1,'_',num2str(freq2/1000),'k.mat']);
archivo15 =
sprintf(['VIz_',nombre1,'_',num2str(freq3/1000),'k.mat']);

direc = sprintf([datestr(now, 5),datestr(now, 7),datestr(now, 10)]);
mkdir(direc)
cd(direc)
save(archivo1,'rf1')
save(archivo2,'rf3')
save(archivo3,'rf5')

save(archivo4,'Zf1')
save(archivo5,'Zf2')
save(archivo6,'Zf3')

save(archivo7,'Vzf21')
save(archivo8,'Vzf22')
save(archivo9,'Vzf23')

save(archivo10,'Zf21')
save(archivo11,'Zf22')
save(archivo12,'Zf23')

save(archivo13,'rf2')
save(archivo14,'rf4')
save(archivo15,'rf6')
cd ..

[y, Fs, nbits, readinfo]  = wavread('Ding.wav');
sound(y,2*Fs)
sound(y,2*Fs)
sound(y,Fs/2)
```

The user interface was the next one:

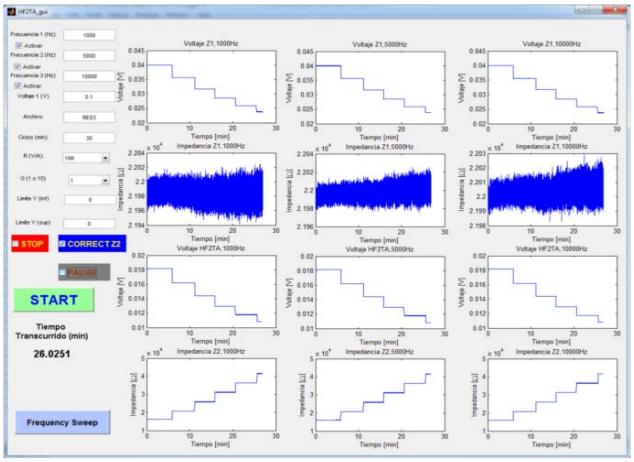

Fig. A2. 2 Custom-made software second version, impedance and voltage simultaneous measurements.

Finally a last version of the software was developed. The upgrades included a control of an analog switch with the serial port of the PC, a multiplexed signal with the same switch and the measurements of two devices with three different frequencies and amplitudes. The code is the next:

```
% --- Executes on button press in pushbutton1.
function pushbutton1_Callback(hObject, eventdata, handles)
% hObject    handle to pushbutton1 (see GCBO)
% eventdata  reserved - to be defined in a future version of
MATLAB
% handles    structure with handles and user data (see GUIDATA)
clc

if isempty(instrfind)==1
else
fclose(instrfind)
end

s1 = serial('COM1');
fopen(s1)
s1.RequestToSend = 'on';
s1.DataTerminalReady = 'on';

% Inicializacion de variables
a1 = 0;a2 = 0;a3 = 0;a4 = 0;a5 = 0;a6 = 0;
canal1 = 1;
canal2 = 2;
osc1 = 1;
osc2 = 2;
osc3 = 3;
osc4 = 4;
osc5 = 5;
osc6 = 6;
osc7 = 7;
osc8 = 8;
segs=0.5;  % Tiempo de medida
rate=450;
tc = 0.01;
freq1 = get(handles.frec1, 'String');
freq1 = str2num(freq1);
freq2 = get(handles.frec2, 'String');
freq2 = str2num(freq2);
freq3 = get(handles.frec3, 'String');
freq3 = str2num(freq3);
volt1 = get(handles.volt, 'String');
volt1 = str2num(volt1);
Act_f1 = get(handles.Act_F1, 'Value');
Act_f2 = get(handles.Act_F2, 'Value');
Act_f3 = get(handles.Act_F3, 'Value');

ciclos = get(handles.duracion, 'String');
ciclos = 60*str2num(ciclos);
ciclos2 = get(handles.ciclos2, 'String');
ciclos2 = 60*str2num(ciclos2);

axes(handles.axes1);cla;
axes(handles.axes2);cla;
axes(handles.axes4);cla;
axes(handles.axes5);cla;
axes(handles.axes7);cla;
axes(handles.axes8);cla;
axes(handles.axes10);cla;
axes(handles.axes11);cla;

% Funcion para iniciar el HF2TA_gui
[dispositivo]=iniciar_zurich_HF2TA;

% Función para configurar al HF2TA_gui
config_zurich_HF2TA(dispositivo,canal1);

% Función para configurar al HF2TA_gui primera frecuencia
Canal diferencial
if Act_f1 == 1
config_entradas_HF2TA(dispositivo,canal1,rate,freq1,volt1,tc,osc1
,1);
end

% Función para configurar al HF2TA_gui segunda frecuencia
Canal diferencial
if Act_f2 == 1
config_entradas_HF2TA(dispositivo,canal1,rate,freq2,volt1,tc,osc3
,1);
end

% Función para configurar al HF2TA_gui tercera frecuencia Canal
diferencial
if Act_f3 == 1
config_entradas_HF2TA(dispositivo,canal1,rate,freq3,volt1,tc,osc5
,1);
end

% Función para configurar al HF2TA_gui primera frecuencia
Canal NO diferencial
if Act_f1 == 1
config_entradas2_HF2TA(dispositivo,canal2,rate,freq1,tc,osc2,0);
end

% Función para configurar al HF2TA_gui segunda frecuencia
Canal NO diferencial
if Act_f2 == 1
config_entradas2_HF2TA(dispositivo,canal2,rate,freq2,tc,osc4,0);
end

% Función para configurar al HF2TA_gui tercera frecuencia Canal
NO diferencial
if Act_f3 == 1
config_entradas2_HF2TA(dispositivo,canal2,rate,freq3,tc,osc6,0);
end

% Función para configurar Ganancias
current = get(handles.CurrentG, 'Value');
switch current
   case 1
      current = 100;
   case 2
      current = 1000;
   case 3
      current = 10e3;
   case 4
      current = 100e3;
   case 5
      current = 1e6;
   case 6
      current = 10e6;
   case 7
      current = 100e6;
end
   voltage = get(handles.VoltageG, 'Value');
switch voltage
   case 1
      voltage = 1;
   case 2
      voltage = 10;
end
   ganancias_HF2TA(dispositivo,current,voltage);

set(handles.tiemp,'String',num2str(0));
%set(handles.tdiff,'String',num2str(0));

correct = get(handles.correct, 'Value');
if correct == 1


   fvoltc1 = 0;
   fvoltc2 = 0;
   for i=1:30;
      t1 = clock;
      [voltc1] =
medir_Vin(dispositivo,segs,current,voltage,volt1,Act_f1,Act_f2,Ac
t_f3,correct);
      fvoltc1 = [fvoltc1 voltc1];
      t2 = etime(clock,t1);
      while t2 < 1
         if t2 < 1
            t2 = etime(clock,t1);
         end
      end
   end
   for i=1:30;
      t1 = clock;
      [voltc2] =
medir_Vin2(dispositivo,segs,current,voltage,volt1,Act_f1,Act_f2,
Act_f3,correct);
      fvoltc2 = [fvoltc2 voltc2];
      t2 = etime(clock,t1);
      while t2 < 1
         if t2 < 1
            t2 = etime(clock,t1);
         end
      end
   end
   voltc = mean(fvoltc1)+mean(fvoltc2)
   pause(1)
else
   voltc = volt1/sqrt(2);
   % Función para configurar al HF2TA_gui primera frecuencia
Canal diferencial
```

```
   if Act_f1 == 1

config_entradas_HF2TA(dispositivo,canal1,rate,freq1,volt1,tc,osc1
,1);
   end

   % Función para configurar al HF2TA_gui segunda frecuencia
Canal diferencial
   if Act_f2 == 1

config_entradas_HF2TA(dispositivo,canal1,rate,freq2,volt1,tc,osc3
,1);
   end

   % Función para configurar al HF2TA_gui tercera frecuencia
Canal diferencial
   if Act_f3 == 1

config_entradas_HF2TA(dispositivo,canal1,rate,freq3,volt1,tc,osc5
,1);
   end
end


%-------------------------------------------------------------------------
%-------------------------------------------------------------------------
%----------------------MULTIPLEXING CHANNEL1----------------
-------------
%-------------------------------------------------------------------------
%-------------------------------------------------------------------------


mux1 = get(handles.mux1, 'Value');

if mux1 == 1
tactualiza = 1;
tstart =tic;
tvisual= clock;
tcontrol = clock; % Reloj que controlará la duración de la medida

tpausa = 0;
tdur = 0;
for i=1:ciclos


   ylim1 = get(handles.ylim1, 'String');
   ylim1 = str2num(ylim1);
   ylim2 = get(handles.ylim2, 'String');
   ylim2 = str2num(ylim2);

   t1 = clock;

   % Funcion de obtencion de medidas
   correct = get(handles.correct, 'Value');


[f1,f2,f3,f4,f5,f6,r1,r2,r3,r4,r5,r6,Z1,Z2,Z3,Vz21,Vz22,Vz23,Z21,
Z22,Z23] =
medir_zurich_HF2TA_all(dispositivo,segs,current,voltage,voltc,Ac
t_f1,Act_f2,Act_f3,correct);

   if i == 1
      rf1 = r1;
      rf2 = r2;
      rf3 = r3;
      rf4 = r4;
      rf5 = r5;
      rf6 = r6;
      Zf1 = Z1;
      Zf2 = Z2;
      Zf3 = Z3;
      Vzf21 = Vz21;
      Vzf22 = Vz22;
      Vzf23 = Vz23;
      Zf21 = Z21;
      Zf22 = Z22;
      Zf23 = Z23;
   else
       rf1 = [rf1 r1];
       rf2 = [rf2 r2];
       rf3 = [rf3 r3];
       rf4 = [rf4 r4];
       rf5 = [rf5 r5];
       rf6 = [rf6 r6];
       Zf1 = [Zf1 Z1];
       Zf2 = [Zf2 Z2];
       Zf3 = [Zf3 Z3];
       Vzf21 = [Vzf21 Vz21];
       Vzf22 = [Vzf22 Vz22];
       Vzf23 = [Vzf23 Vz23];
       Zf21 = [Zf21 Z21];
       Zf22 = [Zf22 Z22];
       Zf23 = [Zf23 Z23];
end
tactual = etime(clock,tcontrol);
tactual = tactual/60;
periodo = tactual/length(rf1);
periodo2 = tactual/length(rf3);
periodo3 = tactual/length(rf5);

minutos = periodo:periodo:tactual;
minutos2 = periodo2:periodo2:tactual;
minutos3 = periodo3:periodo3:tactual;

axes(handles.axes1);
plot(minutos,rf1)
%if ylim1 ~= ylim2
%    ylim([ylim1 ylim2])
%else
   ylim('auto')
%end
title(['Voltaje Z1,',num2str(f2(1)),'Hz'])
xlabel('Tiempo [min]')
ylabel('Voltaje [V]')

axes(handles.axes4);
plot(minutos,Zf1)
if ylim1 ~= ylim2
   ylim([ylim1 ylim2])
else
   ylim('auto')
end
title(['Impedancia Z1,',num2str(f2(1)),'Hz'])
xlabel('Tiempo [min]')
ylabel('Impedancia [\Omega]')

axes(handles.axes7);
plot(minutos,rf2)
title(['Voltaje HF2TA,',num2str(f2(1)),'Hz'])
xlabel('Tiempo [min]')
ylabel('Voltaje [V]')

axes(handles.axes10);
plot(minutos,Zf21)
title(['Impedancia Z2,',num2str(f2(1)),'Hz'])
xlabel('Tiempo [min]')
ylabel('Impedancia [\Omega]')

if (etime(clock,tvisual)/60)> tactualiza
set(handles.tiemp,'String',num2str(etime(clock,tvisual)/60));
tactualiza = tactualiza +1;

end

t2 = etime(clock,t1);
while t2 < 1
   if t2 < 1
      t2 = etime(clock,t1);
   end
end
seleccion = get(handles.detener, 'Value');

if  seleccion == 1
   break
end

tbreak = etime(clock,tcontrol);
if tbreak > ciclos
   break
end

current = get(handles.CurrentG, 'Value');
switch current
   case 1
      current = 100;
   case 2
      current = 1000;
   case 3
      current = 10e3;
   case 4
      current = 100e3;
   case 5
```

```
            current = 1e6;
        case 6
            current = 10e6;
        case 7
            current = 100e6;
    end
    voltage = get(handles.VoltageG, 'Value');
    switch voltage
        case 1
            voltage = 1;
        case 2
            voltage = 10;
    end
    ganancias_HF2TA(dispositivo,current,voltage);

    pausa = get(handles.pausa,'Value');

    if  pausa == 1
        ziDAQ('unsubscribe',['/' dispositivo '/demods/*/sample']);
        ziDAQ('flush');
        tpini = clock;

        while pausa ==1
              pausa = get(handles.pausa,'Value');
              pause(1)
        end

        tdur = etime(clock,tpini);
        tpausa = tpausa + tdur;
    end
end


telapsed = toc(tstart);
telapsed = telapsed/60;
tselec = ciclos/60;
tdiff = tselec - telapsed;
tdiff = tdiff;
set(handles.tiemp,'String',num2str(telapsed));
%set(handles.tdiff,'String',num2str(tdiff));

nombre1 = get(handles.nombre, 'String');
archivo1 =
sprintf(['M1_V1_',nombre1,'_',num2str(freq1/1000),'k.mat']);
archivo2 =
sprintf(['M1_V1_',nombre1,'_',num2str(freq2/1000),'k.mat']);
archivo3 =
sprintf(['M1_V1_',nombre1,'_',num2str(freq3/1000),'k.mat']);

archivo4 =
sprintf(['M1_Z1_',nombre1,'_',num2str(freq1/1000),'k.mat']);
archivo5 =
sprintf(['M1_Z1_',nombre1,'_',num2str(freq2/1000),'k.mat']);
archivo6 =
sprintf(['M1_Z1_',nombre1,'_',num2str(freq3/1000),'k.mat']);

archivo7 =
sprintf(['M1_V2_',nombre1,'_',num2str(freq1/1000),'k.mat']);
archivo8 =
sprintf(['M1_V2_',nombre1,'_',num2str(freq2/1000),'k.mat']);
archivo9 =
sprintf(['M1_V2_',nombre1,'_',num2str(freq3/1000),'k.mat']);

archivo10 =
sprintf(['M1_Z2_',nombre1,'_',num2str(freq1/1000),'k.mat']);
archivo11 =
sprintf(['M1_Z2_',nombre1,'_',num2str(freq2/1000),'k.mat']);
archivo12 =
sprintf(['M1_Z2_',nombre1,'_',num2str(freq3/1000),'k.mat']);

archivo13 =
sprintf(['M1_VIz_',nombre1,'_',num2str(freq1/1000),'k.mat']);
archivo14 =
sprintf(['M1_VIz_',nombre1,'_',num2str(freq2/1000),'k.mat']);
archivo15 =
sprintf(['M1_VIz_',nombre1,'_',num2str(freq3/1000),'k.mat']);

direc = sprintf([datestr(now, 5),datestr(now, 7),datestr(now, 10)]);
mkdir(direc)
cd(direc)
save(archivo1,'rf1')
save(archivo2,'rf3')
save(archivo3,'rf5')

save(archivo4,'Zf1')
save(archivo5,'Zf2')
save(archivo6,'Zf3')

save(archivo7,'Vzf21')
save(archivo8,'Vzf22')
save(archivo9,'Vzf23')

save(archivo10,'Zf21')
save(archivo11,'Zf22')
save(archivo12,'Zf23')

save(archivo13,'rf2')
save(archivo14,'rf4')
save(archivo15,'rf6')
cd ..
ziDAQ('unsubscribe',['/' dispositivo '/demods/*/sample']);
      ziDAQ('flush');
end
%-------------------------------------------------------------------
%-------------------------------------------------------------------
%--------------------MULTIPLEXING CHANNEL2--------------------
-------------
%-------------------------------------------------------------------
%-------------------------------------------------------------------

mux2 = get(handles.mux2, 'Value');

if mux2 == 1

   if isempty(instrfind)==1
   else
      fclose(instrfind)
      s1 = serial('COM1');
      fopen(s1)
      s1.RequestToSend = 'on';
   end

s1.DataTerminalReady = 'off'

medir_zurich_HF2TA_all(dispositivo,segs,current,voltage,voltc,Ac
t_f1,Act_f2,Act_f3,correct);


tactualiza = 1;
%tstart =tic;
tvisual= clock;
tcontrol = clock; % Reloj que controlará la duración de la medida

tpausa = 0;
tdur = 0;
for i=1:ciclos2


   ylim1 = get(handles.ylim1, 'String');
   ylim1 = str2num(ylim1);
   ylim2 = get(handles.ylim2, 'String');
   ylim2 = str2num(ylim2);

   t1 = clock;

   % Funcion de obtencion de medidas
   correct = get(handles.correct, 'Value');


[f1,f2,f3,f4,f5,f6,r1,r2,r3,r4,r5,r6,Z1,Z2,Z3,Vz21,Vz22,Vz23,Z21,
Z22,Z23] =
medir_zurich_HF2TA_all(dispositivo,segs,current,voltage,voltc,Ac
t_f1,Act_f2,Act_f3,correct);

   if i == 1
      rf1 = r1;
      rf2 = r2;
      rf3 = r3;
      rf4 = r4;
      rf5 = r5;
      rf6 = r6;
      Zf1 = Z1;
      Zf2 = Z2;
      Zf3 = Z3;
      Vzf21 = Vz21;
      Vzf22 = Vz22;
      Vzf23 = Vz23;
      Zf21 = Z21;
      Zf22 = Z22;
      Zf23 = Z23;
   else
       rf1 = [rf1 r1];
```

```
    rf2 = [rf2 r2];
    rf3 = [rf3 r3];
    rf4 = [rf4 r4];
    rf5 = [rf5 r5];
    rf6 = [rf6 r6];
    Zf1 = [Zf1 Z1];
    Zf2 = [Zf2 Z2];
    Zf3 = [Zf3 Z3];
    Vzf21 = [Vzf21 Vz21];
    Vzf22 = [Vzf22 Vz22];
    Vzf23 = [Vzf23 Vz23];
    Zf21 = [Zf21 Z21];
    Zf22 = [Zf22 Z22];
    Zf23 = [Zf23 Z23];
end
tactual = etime(clock,tcontrol);
tactual = tactual/60;
periodo = tactual/length(rf1);
periodo2 = tactual/length(rf3);
periodo3 = tactual/length(rf5);

minutos = periodo:periodo:tactual;
minutos2 = periodo2:periodo2:tactual;
minutos3 = periodo3:periodo3:tactual;

axes(handles.axes2);
plot(minutos,rf1,'r')
%if ylim1 ~= ylim2
%    ylim([ylim1 ylim2])
%else
    ylim('auto')
%end
title(['Voltaje Z1,',num2str(f2(1)),'Hz'])
xlabel('Tiempo [min]')
ylabel('Voltaje [V]')

axes(handles.axes5);
plot(minutos,Zf1,'r')
if ylim1 ~= ylim2
    ylim([ylim1 ylim2])
else
    ylim('auto')
end
title(['Impedancia Z1,',num2str(f2(1)),'Hz'])
xlabel('Tiempo [min]')
ylabel('Impedancia [\Omega]')

axes(handles.axes8);
plot(minutos,rf2,'r')
title(['Voltaje HF2TA,',num2str(f2(1)),'Hz'])
xlabel('Tiempo [min]')
ylabel('Voltaje [V]')

axes(handles.axes11);
plot(minutos,Zf21,'r')
title(['Impedancia Z2,',num2str(f2(1)),'Hz'])
xlabel('Tiempo [min]')
ylabel('Impedancia [\Omega]')

if (etime(clock,tvisual)/60)> tactualiza
set(handles.tiemp,'String',num2str(etime(clock,tvisual)/60));
tactualiza = tactualiza +1;

end

t2 = etime(clock,t1);
while t2 < 1
    if t2 < 1
        t2 = etime(clock,t1);
    end
end
seleccion = get(handles.detener, 'Value');

if  seleccion == 1
    break
end

tbreak = etime(clock,tcontrol);
if tbreak > ciclos2
    break
end

current = get(handles.CurrentG, 'Value');
switch current
    case 1
        current = 100;
    case 2
        current = 1000;
    case 3
        current = 10e3;
    case 4
        current = 100e3;
    case 5
        current = 1e6;
    case 6
        current = 10e6;
    case 7
        current = 100e6;
end
voltage = get(handles.VoltageG, 'Value');
switch voltage
    case 1
        voltage = 1;
    case 2
        voltage = 10;
end
ganancias_HF2TA(dispositivo,current,voltage);

pausa = get(handles.pausa,'Value');

if  pausa == 1
    ziDAQ('unsubscribe',['/' dispositivo '/demods/*/sample']);
    ziDAQ('flush');
    tpini = clock;

    while pausa ==1
        pausa = get(handles.pausa,'Value');
        pause(1)
    end

    tdur = etime(clock,tpini);
    tpausa = tpausa + tdur;
end
end


telapsed = toc(tstart);
telapsed = telapsed/60;
tselec = (ciclos+ciclos2)/60;
tdiff = tselec - telapsed;
tdiff = tdiff;
set(handles.tiemp,'String',num2str(telapsed));
%set(handles.tdiff,'String',num2str(tdiff));

nombre1 = get(handles.nombre, 'String');
archivo1 =
sprintf(['M2_V1_',nombre1,'_',num2str(freq1/1000),'k.mat']);
archivo2 =
sprintf(['M2_V1_',nombre1,'_',num2str(freq2/1000),'k.mat']);
archivo3 =
sprintf(['M2_V1_',nombre1,'_',num2str(freq3/1000),'k.mat']);

archivo4 =
sprintf(['M2_Z1_',nombre1,'_',num2str(freq1/1000),'k.mat']);
archivo5 =
sprintf(['M2_Z1_',nombre1,'_',num2str(freq2/1000),'k.mat']);
archivo6 =
sprintf(['M2_Z1_',nombre1,'_',num2str(freq3/1000),'k.mat']);

archivo7 =
sprintf(['M2_V2_',nombre1,'_',num2str(freq1/1000),'k.mat']);
archivo8 =
sprintf(['M2_V2_',nombre1,'_',num2str(freq2/1000),'k.mat']);
archivo9 =
sprintf(['M2_V2_',nombre1,'_',num2str(freq3/1000),'k.mat']);

archivo10 =
sprintf(['M2_Z2_',nombre1,'_',num2str(freq1/1000),'k.mat']);
archivo11 =
sprintf(['M2_Z2_',nombre1,'_',num2str(freq2/1000),'k.mat']);
archivo12 =
sprintf(['M2_Z2_',nombre1,'_',num2str(freq3/1000),'k.mat']);

archivo13 =
sprintf(['M2_VIz_',nombre1,'_',num2str(freq1/1000),'k.mat']);
archivo14 =
sprintf(['M2_VIz_',nombre1,'_',num2str(freq2/1000),'k.mat']);
archivo15 =
sprintf(['M2_VIz_',nombre1,'_',num2str(freq3/1000),'k.mat']);

direc = sprintf([datestr(now, 5),datestr(now, 7),datestr(now, 10)]);
mkdir(direc)
```

```
cd(direc)
save(archivo1,'rf1')
save(archivo2,'rf3')
save(archivo3,'rf5')

save(archivo4,'Zf1')
save(archivo5,'Zf2')
save(archivo6,'Zf3')

save(archivo7,'Vzf21')
save(archivo8,'Vzf22')
save(archivo9,'Vzf23')

save(archivo10,'Zf21')
save(archivo11,'Zf22')
sound(y,Fs/2)
save(archivo12,'Zf23')

save(archivo13,'rf2')
save(archivo14,'rf4')
save(archivo15,'rf6')
cd ..
end

% Apagar el HF2TA_gui
apagar_zurich_HF2TA(dispositivo,canal1);

[y, Fs, nbits, readinfo]  = wavread('Ding.wav');
sound(y,2*Fs)
sound(y,2*Fs)
```

The user interface is presented next:

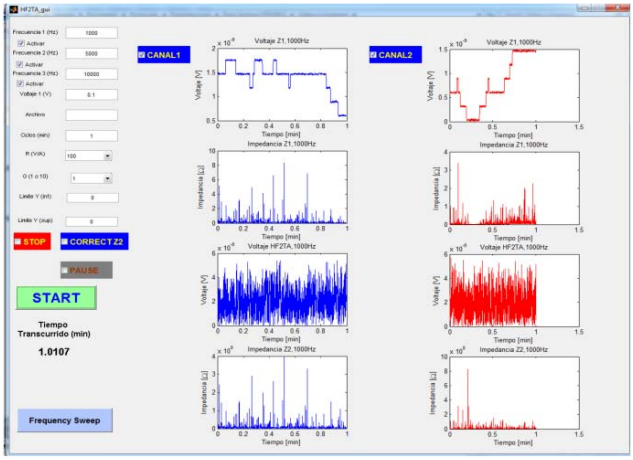

Fig. A2. 3 Custom-made software third version, multiplexed measurements.

Annex 3 Surface characterizations of OSTE polymer measurements

Materials and methods

An off-stoichiometric thiol–ene (OSTE) polymers were fabricated at different concentrations of thiol excess (20, 40, 60 and 80), and the excess was characterized with 5′-Dithiobis(2-nitrobenzoic acid) (D8130, Sigma Aldrich) reagent, also known as Ellman's reagent. Then with the calibration curve we started the fabrication of a gradient.

The samples of OSTE-thiol (20, 40, 60 and 80) were fabricated as follows. The OSTE pre-polymer was prepared with 1.8 : 1, 1.6:1, 1.4:1 and 1.2:1 ratio of Tris[2-(3-mercaptopropionyloxy)ethyl] isocyanurate (731250, Sigma Aldrich) and Tetra(allyloxy)ethane (T0030, Tokyo chemical Industry CO., LTD.). To the mixture, 0.3% of a UV initiator, ethyl-2, 4, 6-trimethylbenzoylphenylphosphinate (Lucirin TPO-L, BASF AG) was added. The components were then mixed and degassed. The pre-polymeric solution was spun over a glass slide in two spinning steps: 5 seconds at 500 rpm and 30 seconds at 700 rpm. The polymer was cured with an UV light for 60 seconds at 13 mW/cm^2.

The thiol concentration of the surface was characterized with Ellman's reagent. The sample was immersed into the reagent at a concentration of 80 μg/ml during 20 minutes. The absorbance of the solution was measured with an UV-VIS spectrophotometer (V-630, Jasco) from a wavelength of 200 to 550 nm, focusing on the 412 nm wavelength, since the reagent reach a peak. With all measured data a calibration curve was obtained.

Then a gradient of off-stoichiometric thiol–ene (OSTE) polymers was fabricated; and the concentration of the thiol-ene surface was measured indirectly by following the protocol designed by Ellman[1].

The fabrication started with a layer of OSTE-thiol (80) with an excess of benzophenone. The OSTE pre-polymer was prepared with 1.8 : 1 ratio of Tris[2-(3-mercaptopropionyloxy)ethyl] isocyanurate and Tetra(allyloxy)ethane. To the mixture, 0.3% of a UV initiator, ethyl-2, 4, 6-trimethylbenzoylphenylphosphinate and 2% of a second UV initiator benzophenone (B9300, Sigma Aldrich) were added. The

components were then mixed and degassed. The pre-polymeric solution was spun over a glass slide in two spinning steps: 5 seconds at 500 rpm and 30 seconds at 700 rpm. The polymer was cured with an UV light for 60 seconds at 13 mW/cm^2, using a 400 nm filter to avoid the reaction of the benzophenone.

A second OSTE-thiol (80) was prepared but without photoinitiators. The solution was poured over the first cured layer of OSTE-thiol (80) and keeping a tilt between 0 and 150 µm along the glass slide. The second layer was exposed to UV light for 60 seconds at 13 mW/cm^2. The glass slide was rinsed with toluene (244511, Sigma Aldrich) for 4 minutes to eliminate the uncured excess of pre-polymeric solution.

The thiol concentration of the second layer was characterized with 5,5′-Dithiobis(2-nitrobenzoic acid) reagent. The sample was cut into 4 pieces of the same size and each piece was immersed into 10 ml of Ellman's reagent at a concentration of 80 µg/ml during 20 minutes. The absorbance of the solution was measured with an UV-VIS spectrophotometer (V-630, Jasco) from a wavelength of 200 to 550 nm, focusing on the 412 nm wavelength. The protocol is summarized on Fig. A3. 1.

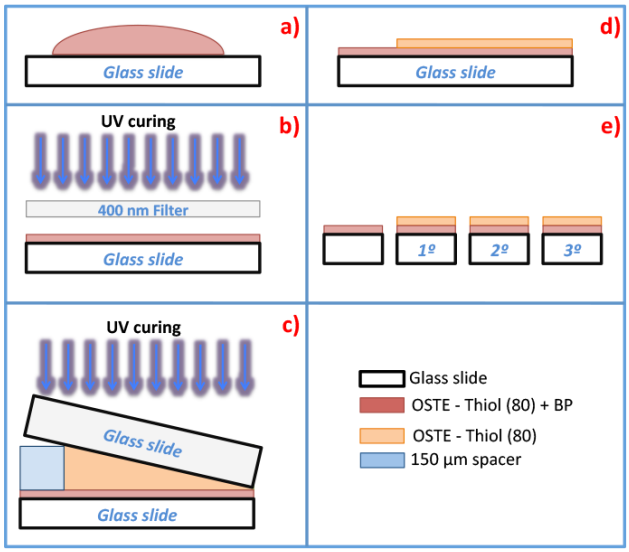

Fig. A3. 1 Protocol for the fabrication of an OSTE-thiol gradient. a) The OSTE-thiol (80)+BP is spun over a glass slide, b) The polymer is UV cured, c) The second solution of OSTE-thiol (80) is poured over the first layer with a tilt and UV cured, d) After the sample is rinsed in toluene a second layer is formed on top of the first OSTE, e) The sample is cut into 4 pieces and immerse on Ellman's reagent to estimate the thiol concentration.

Results and discussions

Prior the fabrication of a gradient, the thiol concentration of the surface was characterized, for different samples and concentrations. Ellman's reagent (5,5'-Dithio-

Bis(2-Nitrobenzoic Acid), DTNB) was used to evaluate the thiol density at the surface of different OSTE-thiol slides. The OSTE-thiol was prepared at different concentrations: 20, 40, 60 and 80% excess of thiols. The pre-polymeric solutions were spun on top of glass slides. Then, the slides were cured with UV light.

The reagent was prepared at a concentration of 80 µg/ml in sodium phosphate buffer (pH = 8.0)[2]. Every slide was immersed separately in 30 ml of Ellman's solution for 20 minutes (Fig. A3. 2). The solution reacted with the thiols on the surface of the samples and changed its color (Fig. A3. 2). The slides were removed and the absorbance of the solution was measured between the wavelengths 200 a 550 with an UV-VIS spectrophotometer (V-630, Jasco). The absorbance of a sample of un-reacted Ellman's reagent was also measured, in order to know the absorbance of the DTNB.

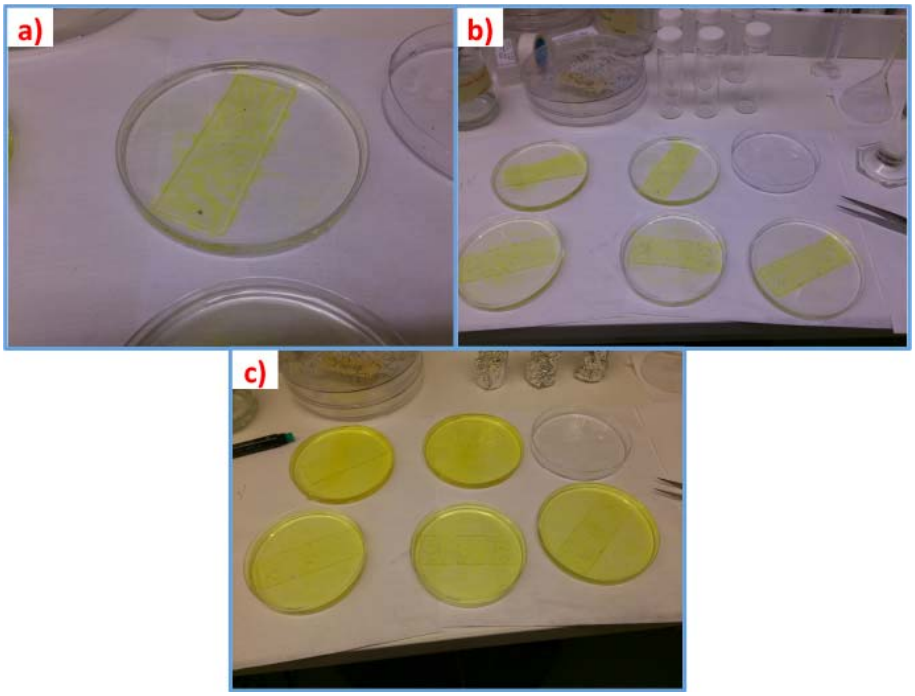

Fig. A3. 2 OSTE-thiol samples immersed in Ellman's reagent. a) Each sample was immerse in 30 ml, b) Different concentrations were characterized, c) The absorbance of the reacted solution was measured.

The relative absorbance of each sample is the contribution of the OSTE-thiol plus the DTNB (Fig. A3. 3a), and can be expressed as:

$$A_{sample} = A_{OSTE\text{-}thiol} + A_{DTNB} \qquad \text{(Eq. A3. 1)}$$

Therefore, the absolute absorbance of every OSTE-thiol sample can be calculated with the measured data (Fig. A3. 3b):

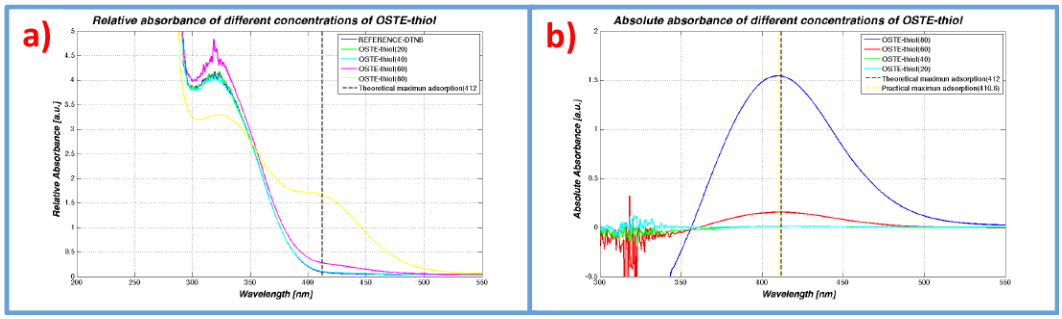

Fig. A3. 3 a) Relative absorbance of the OSTE-thiol samples, b) Absolute absorbance.

The calibration curve was obtained with the maximums of every OSTE-thiol concentrations. Ellman defined a maximum at 412 nm [1], while Riddles et al claimed that the maximum was at 410 nm [3]. We followed the original protocol and used the wavelength of 412 nm to get our calibration curve (Fig. A3. 4).

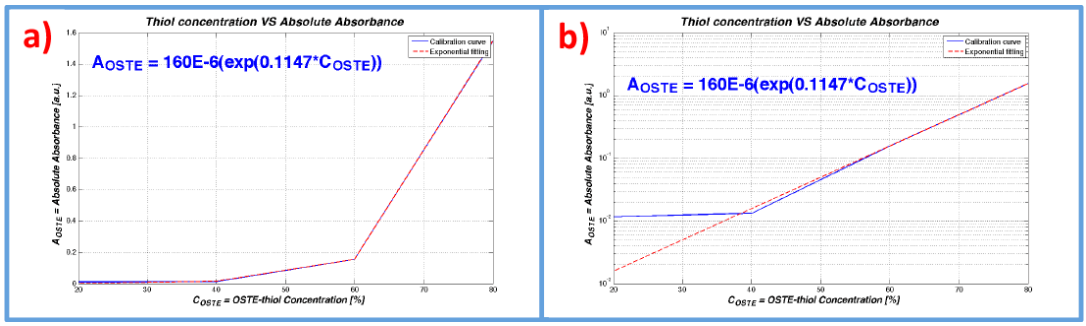

Fig. A3. 4 Calibration curve for different OSTE-thiol concentrations.

The absorbance shows an exponential behavior for the OSTE-thiol samples:

$$A_{OSTE} = 160x10^{-6}\left(e^{0.1147*C_{OSTE}}\right) \qquad \text{(Eq. A3. 2)}$$

Once we had the calibration curve, we started to tests the fabricate gradients. First, over the layer of OSTE-thiol(80) with an excess of benzophenone, we poured a pre-polymeric solution of OSTE-thiol(80), and used a 150 µm tilt to generate the gradient over the surface of the sample. Each slide was cut into four pieces of 1.9 cm. However, the piece that was cover by the spacer was not analyzed. The results are showed on Fig. A3. 5.

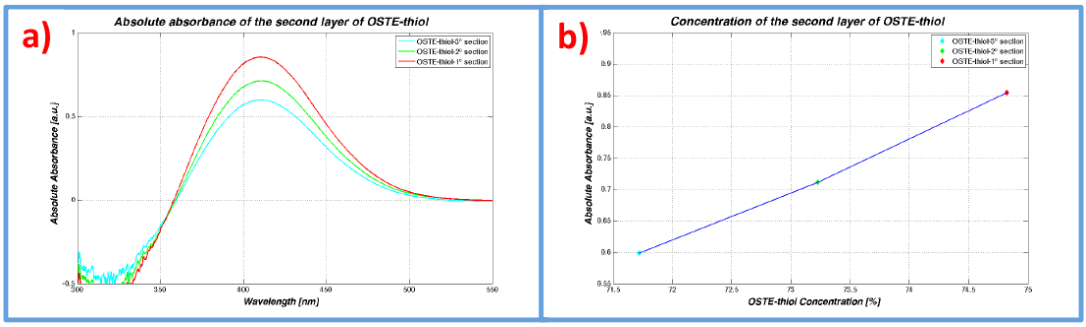

Fig. A3. 5 First test with a gradient. a) Absorbance of the three sections, b) Absorbance of each section at 412 nm.

The red curve represents the piece closest to the spacer, with a tilt between 150 and 100 µm. The green line corresponds to the middle piece, with an inclination between 100 and 50 µm. And, the cyan line is related to the last piece with a tilt between 50 and 0 µm. The approximated angle of inclination is 1.5074º (Fig. A3. 6).

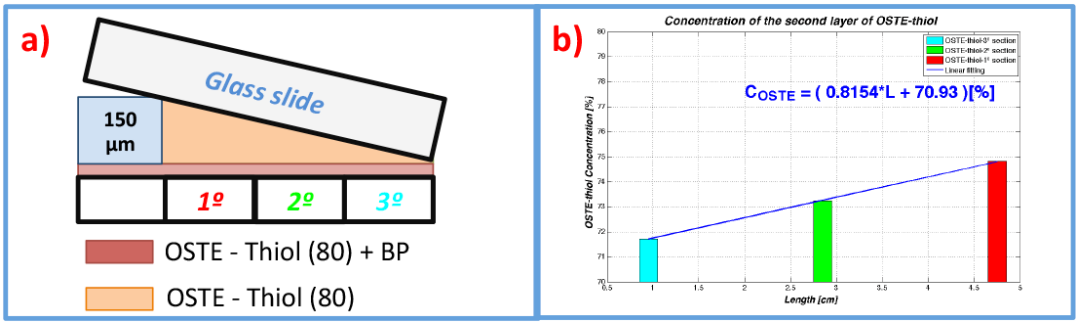

Fig. A3. 6 a) Diagram of the first gradient, b) Concentration as a function of distance.

We can relate the thiol concentration with the length of the sample (L), we are considering that the initial point is where the tilt is 0 and the final is the 150 µm inclination (Fig. A3. 6b). The concentration showed a linear response:

$$C_{OSTE} = (70.93 + 0.8154 * L)\% \qquad \text{(Eq. A3. 3)}$$

We fabricated a second layer with a gradient, however the range is small, approximately 5% of difference. In order to improve this difference we changed the second solution and used a Tetra(allyloxy)ethane. The results are showed on the next figures (Fig. A3. 7).

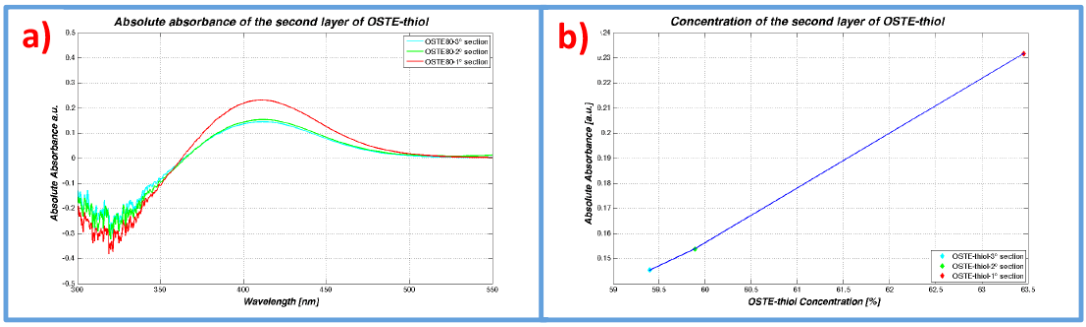

Fig. A3. 7 Second test, an allyl solution was used as second layer.

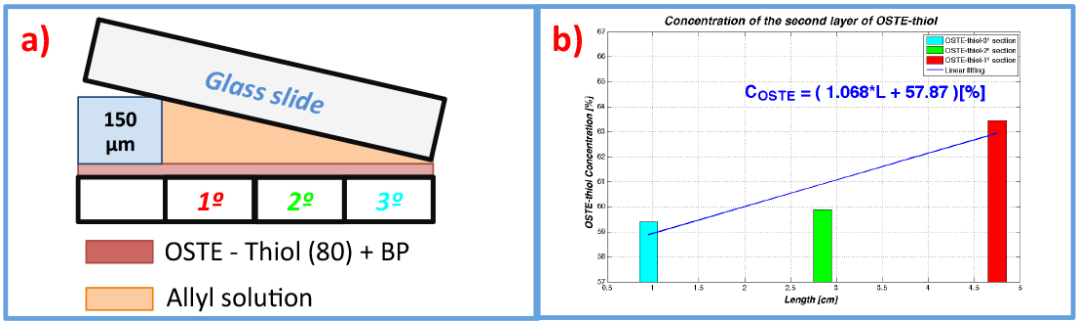

Fig. A3. 8 a) Diagram of the first gradient, b) Concentration as a function of distance.

We could fabricate a gradient, once again, but the difference remained the same, about 5%. However, the concentration was smaller, between 58 and 63% of thiol concentration, in comparison with the concentration of 70-75% of the first test. A liner fitting was calculated:

$$C_{OSTE} = (57.87 + 1.068 * L)\% \qquad \text{(Eq. A3. 4)}$$

Finally, we change increased the height of the spacer (1 mm), and fabricated the second layer using an OSTE-thiol(80) solution (Fig. A3. 9).

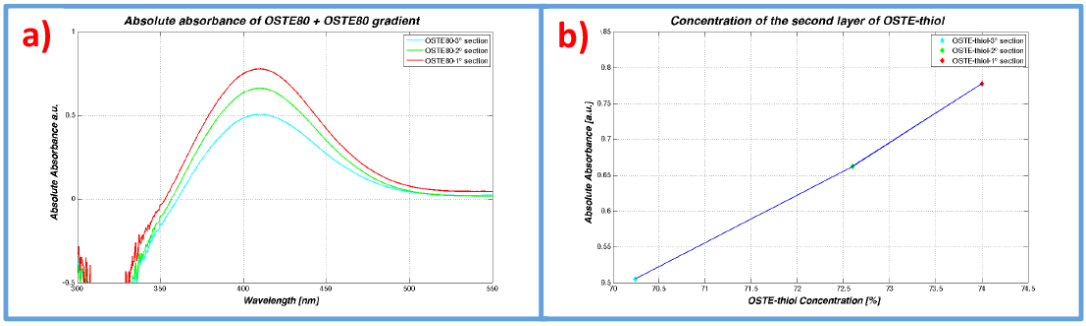

Fig. A3. 9 Third test of fabrication. The height of the tilt was increased.

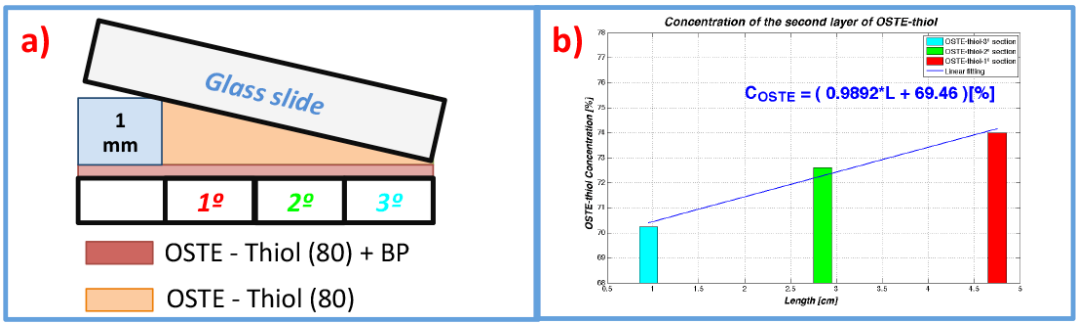

Fig. A3. 10 a) Diagram of the first gradient, b) Concentration as a function of distance.

The results obtained showed a similar response as the first test. The gradient was also 5% and the concentration was between 70 and 75%. The linear approximation of the data is:

$$C_{OSTE} = (69.46 + 0.9892 * L)\% \qquad \text{(Eq. A3. 5)}$$

So far, we were able to fabricate a gradient with a novel technique; however the range of the gradient must to be improve. When working with surface functionalization one key factor is the oxygen contribution [4]. The oxygen inhibits the free-radical photo-polymerization of different monomers [5], including OSTE-thiol polymers. When the sample has a greater oxygen concentration, the pieces with a higher tilt, then the polymerization reaction was inhibited. Therefore, the thiol concentration is higher in comparison with the pieces with small tilt and oxygen contribution. The next step on the fabrication of a gradient could be to diminish the effect of the oxygen, and fabricate the samples in an "oxygen-free" environment. With a greater gradient a protein functionalization could be performed. A solution of biotin could be used to react with the thiols and a second block of streptavidin could be added next. And so, finally a biotinylated protein could be added to react with the SAV layer to form a protein gradient. This technique could be useful to create fast gradients and be tested on cell differentiations.

Conclusions

A novel fabrication method was developed for creating a surface gradient. Prior the fabrication of the gradient, the thiol concentration of OSTE-thiol samples was characterized. An adsorption curve was obtained and related to the concentrations of thiols on the surface of a polymer samples. Different solutions and heights for the tilt gradient were tested. However, the first results lead us to think that the effect of the oxygen plays a key role during the fabrication process. The maximum gradient obtained

so far was 5% of difference. An "oxygen-free" environment is suggested for getting better results. If the gradient is improved, a cell differentiation test can be done.

References

1. G. L. Ellman, *Arch Biochem Biophys*, 1959, **82**, 70-77.
2. J. P. Lafleur, R. Kwapiszewski, T. G. Jensen and J. P. Kutter, *Analyst*, 2013, **138**, 845-849.
3. P. W. Riddles, R. L. Blakeley and B. Zerner, *Methods Enzymol*, 1983, **91**, 49-60.
4. C. Decker and A. D. Jenkins, *Macromolecules*, 1985, **18**, 1241-1244.
5. T. Y. Lee, C. A. Guymon, E. S. Jönsson and C. E. Hoyle, *Polymer*, 2004, **45**, 6155-6162.